UNIVERSITY OF
BIRMINGHAM

ROLL COMPACTION OF PHARMACEUTICAL EXCIPIENTS

by

SHEN YU

A thesis submitted to The University of Birmingham for the degree of

DOCTOR OF PHILOSOPHY

School of Chemical Engineering

College of Engineering

The University of Birmingham

October 2012

UNIVERSITY OF
BIRMINGHAM

University of Birmingham Research Archive

e-theses repository

This unpublished thesis/dissertation is copyright of the author and/or third parties. The intellectual property rights of the author or third parties in respect of this work are as defined by The Copyright Designs and Patents Act 1988 or as modified by any successor legislation.

Any use made of information contained in this thesis/dissertation must be in accordance with that legislation and must be properly acknowledged. Further distribution or reproduction in any format is prohibited without the permission of the copyright holder.

ABSTRACT

Roll compaction is commonly used as a dry granulation technique in the pharmaceutical industry to produce tablets in secondary manufacturing with formulations sensitive to heat and moisture. In particular, roll compactors are generally used in combination with milling systems to produce granules with enhanced flowability and increased bulk density, ready for die compression. However, the process is not well understood due to its complexity and strong dependence on the properties of the feed powders. This thesis reports systematic studies on the behavior of pharmaceutical excipients in associated unit operations (*i.e.* roll compaction, milling, tabletting), as well as their correlations.

Roll compaction of pharmaceutical excipients (*i.e.* microcrystalline cellulose, di-calcium phosphate dihydrate, mannitol and lactose) was carried out using an instrumented roll compactor with a gravity feeding system. The maximum pressures were measured experimentally and the nip angles which describe the extent of the compact zone were determined from pressure gradients using a robust method developed on the basis of the theory for granular solids proposed by Johanson (1965). They were considered key factors for describing roll compaction behavior. The influence of the process parameters (*i.e.* roll gap and roll speed), material properties (*i.e.* frictional properties and flowability) and powder conditioning (*i.e.* lubrication and moisture) were investigated. It was found that roll compaction was greatly affected by the flowability of the feed powders when a gravity feed was used, especially at large roll gaps and high roll speeds. The incorporation of a lubricant resulted in a reduction in the nip angle and maximum pressure. However, the effects depended on the surface area and mechanical strength of the feed particles. It was also found that water didn't affect the compaction behaviour at relativelow water contents (*i.e.* $\leq$ 5%), but as a binder at relative high water contents (*i.e.* > 5 %).

Ribbons produced in roll compaction were granulated using an oscillating mill to investigate the milling process. A first order kinetics equation was introduced to describe the mass throughput of the granules. The experimental results revealed that the mass throughput and granule size depended upon the milling conditions (*i.e.* milling frequency and screen size) and material property (*i.e.* ribbon fracture energy). Using positron emission particle tracking technique, which provided a measurement of instantaneous velocity and the location of the ribbons, two milling regions (*i.e.* impact and abrasion) involving distinct fracture mechanisms were identified.

Tabletting of the granules was performed using a universal test machine. An evaluation of the viability of the methods capable of determining the compressibility of granular solids (*i.e.* Heckel equation, Kawakita equation, Johanson model, Adams equation) was performed, showing that the Adams equation has the advantages on determining the compressibility through all stress range. A reduction in the compressibility and compactibility of the granules compared to the feed powders, due to work hardening, was also observed.

Based on an improved understanding of the unit operations, a process design applicable for the current system was proved to be achievable. A method was introduced to determine the optimized process conditions for roll compaction and milling through a close examination of the correlation between the unit operations.

I dedicate this thesis to

My Grandfather

Prof. Shaojin Yu

ACKNOWLEDGEMENT

I would like to express my deepest gratitude and appreciation to all supervisors: Dr. ChuanYu Wu, Prof. Mike Adams, Dr. Bindhumadhavan Gururajan, Dr. Ron Roberts and Dr. Gavin Reynolds for their supervision, invaluable guidance and support through the PhD, without which this thesis would not have been possible.

I would like to thank Dr. James Bowen for his generous help on material characterisation experiments; Dr. Thomas Leadbeater and Dr. Joseph Gargiuli for their technical support on PEPT; Mrs. Theresa Morris for her help on SEM. I would also like to thank the technical support staff at the University of Birmingham.

I am grateful to all the past and current members of particulate group for their help and companionship. I wish to express my appreciation to Dr. James Andrews for his suggestions on mathematics.

I would like to convey my thanks to School of Chemical Engineering, University of Birmingham for administrative support and laboratory facilities, as well as AstraZeneca for the financial assistance.

Finally, I would like to express my heartfelt thanks and love to my family for their encouragement, support and understanding.

TABLE OF CONTENTS

List of Figures

LIST OF TABLES

NOMENCLATURE

A	Constant in Johanson's equation
A_H	Constant in Heckel equation
A_J	Cross-section area of Jenike shear cell
A_R	Cross section area of powder bed in ring shear cell tests
a_K	Constant in Kawakita equation
b_c	Constant determined by the minimum compression pressure to produce a tablet for powder materials
b_K	Constant in Kawakita equation
C_K	Constant in Kawakita equation
C_p	Dimensionless compactibility
C_u	Constant related to the powder deformation at relative low stress
c	Cohesion
D	Diameter of the roll in roll compaction
D_{punch}	Displacement of the punches
D_r	Relative density
D_t	Diameter of a tablet
d	Pocket size on the roll surfaces
d_{die}	Internal diameter of the die
d_{50}	Mean diameter of the particles
F_A	Counterbalance force applied in ring shear cell tests

F_{crush}	Diametric force applied to crush a tablet
F_N	Normal force in Jenike shear cell tests
F_{NR}	Normal force in ring shear cell tests
F_S	Shear force in Jenike shear cell tests
F_{SR}	Friction force in ring shear cell tests
F_1, F_2	Tangential forces applied in ring shear cell tests
f_a	Inter-particle adhesive force
ff_c	Flow function
f_{mill}	Milling frequency
H	Deformation hardness of a tablet
$H_{\max}$	Theoretical maximal possible deformation hardness
h	Thickness of the slab in the slab method for roll compaction
h_i	Initial height of the powder bed in uniaxial compression
h_p	Current height of the powder bed in uniaxial compression
h_t	Height of a tablet
k_H	Constant in Heckel equation
k_{RD}	Constant in Ryshkewitch-Duckworth equation, representing the bonding capacity of the material
k_s	Constant for shear stress calculation in roll compaction
m_{powder}	Mass of powder in die compression
N_b	Number of milling cycles for breakage

N_c	Characteristic number of milling cycles
P	Pressure
P_{mu}	Maximum compression pressure during uniaxial compression
p	Normal pressure acting on the layer in the slab method for roll compaction
p_R	Normal stress acting on the roll in the model proposed by Schönert and Sander (2002)
R	Roll radius
R_a	Surface roughness
R_{Blade}	Radius of the milling impeller
S	Minimum roll gap
S_a	3D roughness
SCS	Specific crushing strength of a tablet
t	Time
u	Roll speed
V_{blade}	Speed of the blade
V_α	Volume of the powder for a given arc-length segment ΔL at nip angle in roll compaction
V_θ	Volume of the powder for a given arc-length segment ΔL at angular position θ in roll compaction
ν	Acute angle
W	Width of the roll in roll compaction
α	Nip angle in roll compaction
α_i	Instantaneous angle for the slab in the slab method for roll compaction
β	the compressibility factor in Adams'

	equation
γ	Compression susceptibility
ΔL	Arc-length segment in roll compaction
ε	current compressive natural stain
ε_i	initial compressive natural stain
θ	Angular position in roll compaction
θ_{mp}	angular position where the maximum pressure occurs in roll compaction
κ	Compressibility factor
λ	Horizontal load ratio
μ	Coefficient of friction
μ_w	wall friction coefficient
$\mu(\rho)$	Coefficient of friction varied with angular position between the rolls
$v(\rho)$	Poisson's ratio of the powder
ρ	Density of the powder assemble
ρ_{ini}	Initial bulk density in tablet compression
ρ_P	apparent density at a pressure P
ρ_t	True density
ρ_u	Apparent density in uniaxial compression
ρ_α	Density of the powder at nip angle α in roll compaction
ρ_θ	Density of the powder at an angular position θ
Σ_α	a fitting parameter referring to the nip pressure
σ	Normal stress
σ_a	Applied stress

σ_c	Unconfined yield strength
σ_{con}	Consolidated stress
σ_{pre}	Pre-defined normal stress in ring shear cell tests
σ_{sh}	Normal stress on 'shear point' in ring shear cell tests
σ_t	Tensile strength of compacts
σ_u	Apparent normal stress in uniaxial compression
σ_w	Normal stress corresponding to wall shear stress
σ_x	Stress along the *x* direction in the slab method for roll compaction
σ_y	Stress along the *y* direction in the slab method for roll compaction
σ_α	Nip pressure in roll compaction
σ_θ	Normal stress of the powder at an angular position θ
$\overline{\sigma}$	Tensile strength at zero porosity
σ_1	Major principal stress
σ_2	Minor principal stress
τ	Shear stress
τ_f	Frictional stress in the slab method for roll compaction
τ_R	Shear stress on the roll surfaces in the model proposed by Schönert and Sander (2002)
τ_{sh}	Shear stress on 'shear point' in ring shear cell tests
τ_w	Wall shear stress

$Y(\rho)$	Effective shear stress in the slab method for roll compaction
ϕ_e	Effective frictional angle
ϕ_w	wall friction angle
φ	Powder porosity
φ_P	Powder porosity at pressure P
ω	Rotation rate of the roll

CHAPTER 1 INTRODUCTION

Roll compaction is a dry granulation method widely used in industries such as chemical, mineral, ceramic and pharmaceutical. It generates high pressure and compresses particles in small sizes into large agglomerates. In pharmaceutical manufacturing, this technique is employed to produce flake-like compacts, ribbons or briquettes ready for subsequent milling and tabletting processes. Roll compaction is considered as an effective method to provide pre-densification and improve the flowability of the primary powders. The objective of this chapter is to introduce the roll compaction process, classification of the instrument design and its utility in pharmaceutical industry. The research objectives are also discussed, and the overview of the thesis is explained.

1.1 Roll compaction

1.1.1 Fundamentals of roll compaction technique

During roll compaction, the feed powders pass through the gap between two counter-rotating rolls under gravity or feeding forces. The powders are gripped in the decreasing gap by the friction forces on the roll surfaces. In the region close to the minimum roll gap, the powders are compressed into high density compacts.

A simplified model developed by Johanson (1965) assumed that the space between the two rolls was divided into three different regions (as shown in Fig. 1.1): slip, nip and release regions. The slip region is the zone close to the feeding of the powders. The powders slip along the roll surfaces and are rearranged in this region, but only small roll pressures are developed. The location where the velocity of the powder between the rolls equals to that of the roll surfaces is defined as the boundary of the nip region. In this zone, the powder is dragged to the smallest gap and compressed by the increasing pressure developed during the process. Powder densification primarily takes place in this region. The compacts then enter the release region after passing the smallest gap in which elastic recovery could take place.

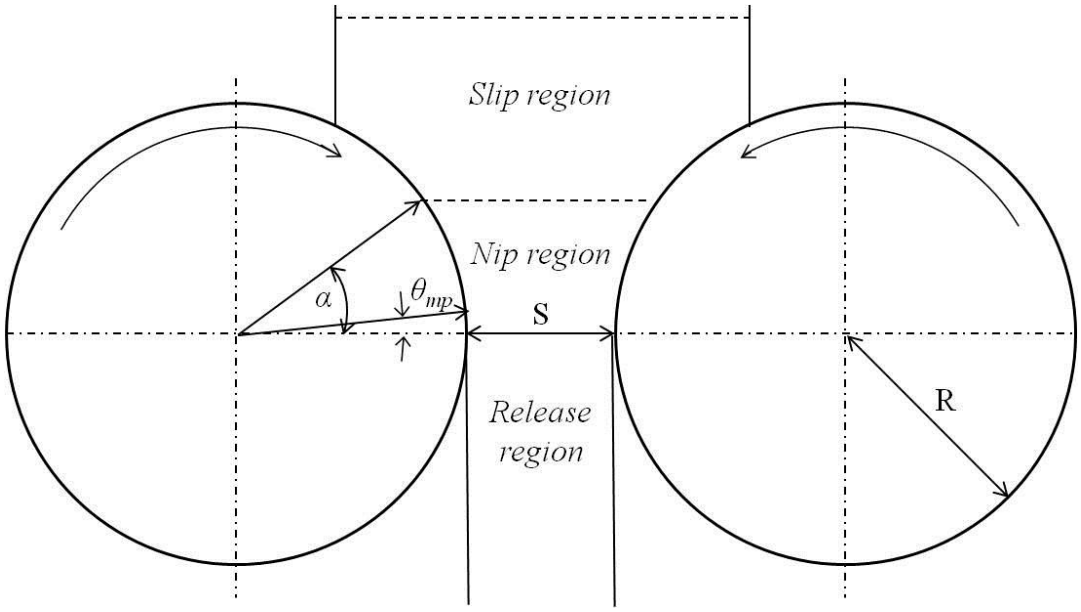

Figure 1.1 Schematic diagram of roll compaction showing the slip, nip and release regions defined by Johanson's theory (1965), *R* is the roll radius, *S* is the minimum roll gap, and α and θ_{mp} are the nip angle and angular position where the maximum pressure occurs, respectively.

1.1.2 Roll compaction equipment

There are a wide range of roll compactors that are used in the pharmaceutical industry. The instruments could be classified by roll assembly, sealing systems (Funakoshi *et al*., 1977), feeding methods (Miller, 1994), roll layouts (Shlieout *et al*., 2000), roll surface conditions, and powder de-aeration method (Guigon and Simon, 2003). Generally, they may be classified by:

- Roll assembly: fixed rolls or floating (movable) rolls
- Sealing systems: side cheek plates or rim sealed rolls
- Feeding methods: gravity fed and force fed (with one or two screws)
- Roll layout: vertical, horizontal and inclined
- Roll surface conditions: smooth, knurled or pocketed rolls
- Powder de-aeration system (for example, vacuum de-aeration in slip region)

1.2 Application of roll compaction in pharmaceutical manufacturing

1.2.1 Utility of roll compaction

As an option for dry granulation, roll compaction is adopted in secondary pharmaceutical manufacturing of tablets (as shown in Fig. 1.2) in which the blends of active ingredients and excipients were transformed to dosage forms. Roll compaction is used to achieve the required increase in bulk density and uniformity of the tablets. In practice, the roll compactor is normally combined with an oscillating mill. The ribbons or briquettes produced are forwarded to the mill and granulated to attain the granules with desired sizes, which are ready for tablet manufacture (Bennett and Cole, 2003).

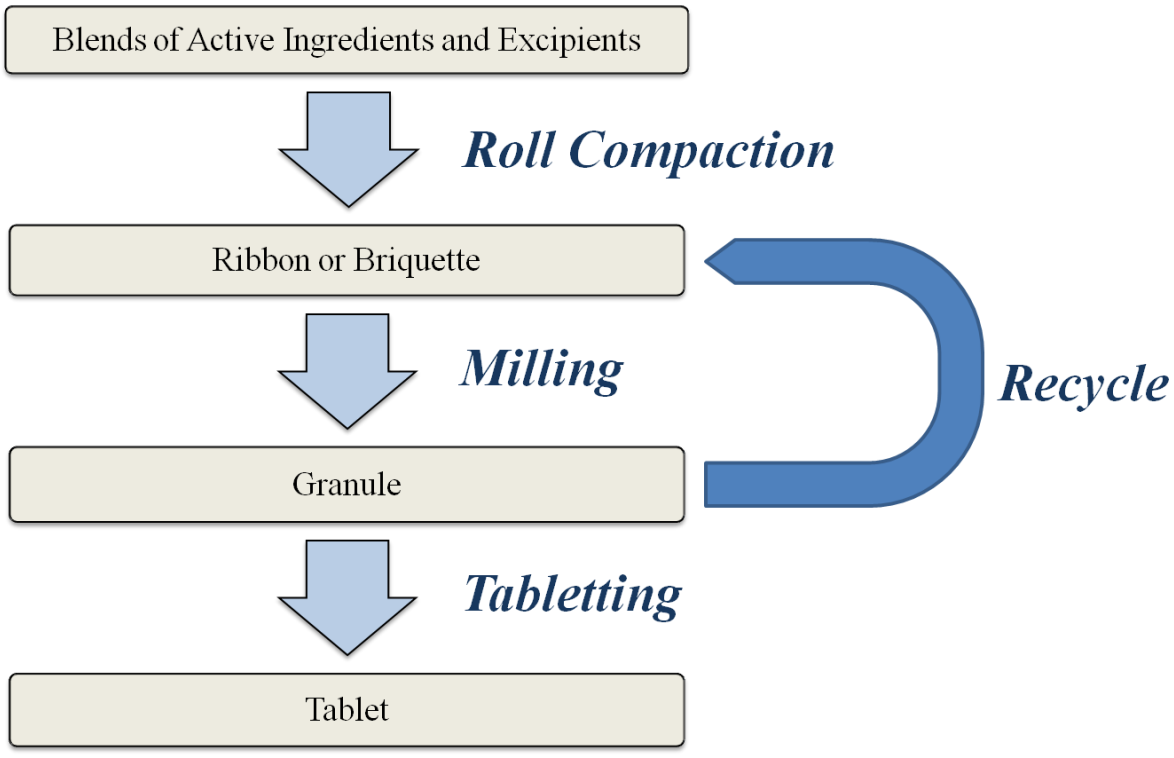

Figure 1.2 Illustration of secondary manufacturing in pharmaceutical industry.

1.2.2 Advantages and limitation of roll compaction

Compared with other granulation techniques, roll compaction has significant advantages that have led to its widespread adoption in industry. This process produces free flowing, dust free granules with improved bulk density. The technique is remarkable for its good performance at reducing the processing costs, energy saving, equipment simplification, and ease operation. Specifically, in pharmaceutical applications, accessible process control, high mass throughput, and produced compacts with desired density and strength (Parikh, 1997) make the roll compaction an outstanding option for dry granulation. The technique shows great advantages in handling materials sensitive to moisture or heat, because no liquid or drying steps are required.

However, the limitations of the technique cannot be ignored. Firstly, the roll compaction process results in 'loss in reworkability'. The tablets produced using roll compaction technique show inferior tensile strength comparing to those produced using wet granulation or direct compact due to work hardening (Herting and Kleinebudde, 2008). A second disadvantage of the technique is the existence of non-compacted powder. A high amount of fines remain is obtained due to the lack of liquid binders, and therefore require recycle units to be used. In addition, some types of powders (*e.g.* calcium carbonate, magnesium carbonte) cannot be easily roll compacted (Parrot, 1981), and an addition of powdered binder (*e.g.* cellulose) is required for successful process (Freitag and Kleinebudde, 2003).

The most challenging problem in using the technique is the design of the instrument and the determination of the optimal processing conditions for a given feed powder formulation.

1.3 Challenges and research needs

The roll compaction process is complex and sample sensitive. Although roll compaction has been investigated intensively in the last few decades, it is still not well understood primarily

due to the diversity in the controlling factors and material properties. The lack of the process understanding results in difficulties in process design. Currently, the trial-and-error method is the routine for new materials because there is no complete scientific theory or universal model that is suitable for all powders. The time and cost consumption in trial-and-error study for industrial application is a driving force to undertake fundamental research in order to understand the process better and to develop applicable theories to meet the practical needs.

1.4 Objectives

The objective of this study is to understand the relationship between feeding powder properties, roll compaction parameters (*i.e.* roll gap and roll speed) and the process performances, and to investigate the influence of roll compaction on the downstream manufacturing processes (*i.e.* milling and tabletting) and characteristics of the final products (*i.e.* tablets). The research is dedicated to provide improved understanding of the roll compaction in pharmaceutical manufacturing, in a comprehensive perspective.

Pharmaceutical excipients with distinctive properties were employed to explore the sensitivity of the roll compaction on the feeding powder properties. The fully characterised powders (see Chapter 4) were compressed using an instrumented roll compactor to understand the effects of powder properties (*i.e.* particle size, frictional and flow properties, content of mixtures). Experiments at various roll gaps and roll speeds were also carried out to investigate the effects of roll compaction parameters.

The milling experiments were carried out using an oscillating mill. The dependency of mass throughput on milling parameters such as milling frequency and screen size, and ribbon strength were investigated. The motions of ribbons were tracked using Positron Emission Particle Tracking (PEPT) technique to understand the milling kinematics involved in granulation. Tabletting experiments for primary powders and granules illustrated how the roll compaction and milling process affect the final tablet properties (*i.e.* strength and density).

1.5 Overview of thesis

An overview of this thesis is summarised:

Chapter 2 Brief reviews on the powder theory relevant to roll compaction are presented in this chapter. The survey covers knowledge of particle density and size distribution. The friction model, compressibility and compactibility that describe the powder behaviour in roll compaction are explained.

Chapter 3 Previous works in roll compaction of pharmaceutical powders are reviewed in this chapter. This chapter introduces the major theoretical models proposed, including Johanson's model, the slab model, Finite element model and discrete element model. The publications on experimental work investigating the influence of various material properties, different system layouts and process parameters are also discussed.

Chapter 4 This chapter describes the materials and methods used in this study. The methodologies used for sample preparations, characterisation of the feeding powders are explained. The instruments and experimental operations are introduced in detail. The calculation and data analysis on process parameters and products are also discussed.

The results presented in this thesis are divided into three chapters which concern the investigation on the roll compaction and two corresponding downstream processes (*i.e.* milling and tabletting) in pharmaceutical manufacturing.

Chapter 5 -7 report the results obtained in this work. And the consequent discussions are addressed in detail in **Chapter 8.**

Chapter 5 This chapter describes the key results on roll compaction experiments. The methods used to determine the factors describing the process performances (*i.e.* nip angle, pressure profile and transaction angle) are explained. In order to provide solid evidence for improving the understanding of the roll compaction process, the experiments concerning sample materials with distinct properties (*i.e.* flowabilities, frictional properties), and various process parameters are (*i.e.* roll gap, roll speed) detailed.

Chapter 6 This chapter covers the investigation on milling of the roll compacted ribbons. A first order kinetic model is introduced to illustrate the mass throughput of the granules during the milling process. In addition, the motion of the ribbons in the milling chamber is tracked using Positron Emission Particle Tracking technique.

Chapter 7 In this chapter, the results of tabletting on primary powders and granules produced using roll compaction are presented. The stress-strain relationship obtained from uniaxial compression is analysed. The measurements of tablet density and strength which are used for product qualification are presented.

Chapter 8 This chapter discuss the experimental results obtained. The influences of feeding powder properties and process parameters on the roll compaction behaviour are discussed. The correlation between the roll compaction and downstream milling, tabletting processes are explored. The key factors affecting the quality of final product are analysed and explained as well.

Chapter 9 An overall summary of the experiments completed and the results obtained are presented in this chapter, followed by the future work.

CHAPTER 2 POWDER THEORY

As a collection of fine solid particles, a powder shows remarkable flowability, compressibility and resistance to deformation comparing to solid substances. The behaviour of the powder depends on basic properties of the particles such as density, size distribution, flow and frictional characteristics, and moisture content. In the pharmaceutical industry, manufacturing processes, especially roll compaction, greatly depend on the powder properties due to the complexity of the drug formulations. This chapter introduces fundamental powder theories used to describe the powder properties (*i.e.* Coulomb model, flowability, compressibility and compactibility) relevant to roll compaction.

2.1 Powders in pharmaceutical industry

More than 80 % of medicines in the pharmaceutical market are in tablet dosage form (Bennett and Cole, 2003). Various processes such as crushing, grinding, blending, granulation, drying and compression are involved in making the final products. Generally, blends of active ingredients and excipients in powder form are employed in the manufacturing processes. The qualities of the final product (*i.e.* homogeneity and dissolution rate) greatly depend on the properties of the feed materials (*i.e.* particle size, compressibility, flowability and frictional properties) and compaction processes (*e.g.* roll compaction, recycle).

Pharmaceutical formulations are obtained by mixing active ingredients and diverse excipients which are normally pharmacologically inactive additives used as diluents and carriers. The homogeneity of the blends is affected by the particle size, density and particle shape of the powders. Differences in particle size, particle shape and density of the compositions can lead to segregation, and therefore inhomogeneous mixing which results in the inhomogeneous dosage. On the other hand, irregular particle shapes may increase the difficulty of mixing, but the mixtures are not likely to separate during subsequent processing. In contrast, the mixing

of spherical particles is easily accessible but unstable because the minimal particle interaction and inferior filling of the gaps between the particles (Wong and Pilpel, 1990).

The dissolution rate of the dosage form is not only affected chemically by the solubility of the materials, but physically influenced by the surface area of the drug. The surface area is determined by the particle size and morphology of the drug powders, or the particles generated after disintegration for tablet dosage form. Thus, the release of the drug can be affected by the particle size of the powders.

Generally, the tablets are made from a mixture of powder materials. In order to achieve the final product with the desired qualities, processes are normally adopted to enhance the processing window of the parameters for the powders.

The powder properties that influence pharmaceutical manufacturing, mainly tabletting, will be discussed in the following sections, including powder density, particle size and shape, and flow and frictional properties. The effects of powder properties on roll compaction will be discussed in Chapter 3.

2.2 Powder properties relevant to roll compaction

Roll compaction and milling were widely employed as an option for dry granulation, aiming to increase the density and optimize the processability of the powders (*i.e.* flowability). Powder materials are processed in roll compaction in order to produce granules with enhanced flowability.

The Mohr-Coulomb criterion (Coulomb, 1776, Mohr, 1900) is often used to describe the yielding of a powder, acting as the fundamental of the measurement for frictional and flow properties. This criterion is briefly introduced in the following sections.

Compressibility, which is defined as ability measure of the volume change of a bulk powder (*i.e.* volume reduction) as a response to the change of pressure, and compactibility, which is defined as the ability of a powder to be compressed into a tablet with a specific strength (Leuenberger, 1982, Leuenberger and Jetzer, 1984), are two important parameters to describe the behaviour of a powder in a compression process. The determinations of the two parameters are reviewed, and their dependencies on other powder properties are discussed in Chapter 3.

2.2.1 Frictional and flow properties

The Mohr-Coulomb criterion (Coulomb, 1776, Mohr, 1900) is the most commonly used shear failure criterion for describing the response of a solid to a normal and shear stresses. Coulomb (1776) proposed that failure occurs in compression occurs when the shear stress is sufficient to overcome the cohesion and the frictional force along the failure plane. The mathematical expression can be written as follows:

$$\tau = \mu\sigma + c \qquad \text{Eq (2.1)}$$

where μ is the coefficient of friction, which is equivalent to the tangent of the angle of friction ϕ (see Fig. 2.1), and c is the cohesion, τ and σ are the shear and normal stresses, respectively.

Mohr (1900) suggested that the correlation between the normal and shear stress across the failure plane at failure can be written as:

$$\tau = f(\sigma) \qquad \text{Eq (2.2)}$$

Agreement with the Coulomb criterion is obtained when a linear form function f is applied. Thus, the criterion shown as Eq. (2.1) is known as the Mohr-Coulomb criterion. A graphical expression of the yield criterion is shown on the (σ, τ) diagram by a Mohr stress circle (Fig. 2.1)

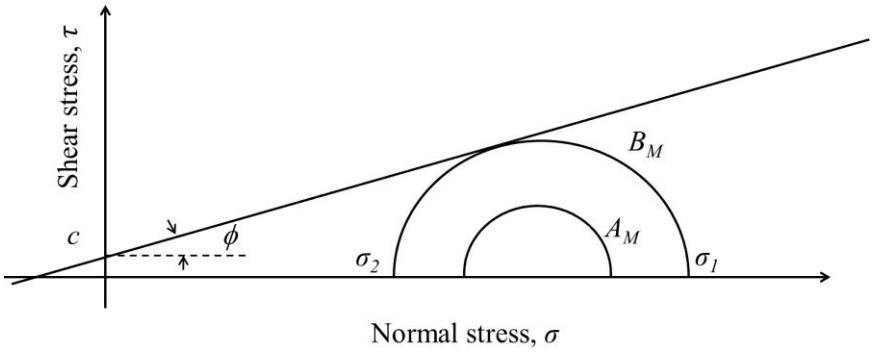

Figure 2.1 Representation of the Mohr Coulomb yield criterion.

According to the yield criterion (Mohr, 1900), it is clear that states of stress with the Mohr circle A_M below the Coulomb line causes no plastic deformation and the states of stress with Mohr circles that cut the Coulomb line are physically impossible. States of stress presented by the Mohr circle B_M, which is tangential to the Coulomb line, cause yielding. A correlation between the major principal stress σ_1, the minor principal stress σ_2 and angle of friction ϕ can be obtained by simple geometrical analysis:

$$\sigma_1 = \sigma_2 \frac{1 + \sin\phi}{1 - \sin\phi} + 2c \frac{\cos\phi}{1 - \sin\phi} \quad \text{Eq (2.3)}$$

Assume the material is cohesionlessl, with $c = 0$, the relationship can be written as:

$$\frac{\sigma_1}{\sigma_2} = \frac{1 + \sin \phi}{1 - \sin \phi} \qquad \text{Eq (2.4)}$$

Jenike (1961) modified Mohr-Coulomb yield criteria and applied it to bulk solids. For a powder material, the yield behaviour depends on the existing state of consolidation when it is caused to flow or yield under normal and shear stresses. The yield behaviour can be measured using shear cell tests (*i.e.* Jenike shear cell or ring shear cell test), as presented schematically in Fig. 2.2.

As shown in Fig 2.2a, the Jenike shear cell consists of a lower ring, an upper ring and a lid. The lid is loaded centrally with a normal force, F_N. The upper part of the shear cell is displaced horizontally against the fixed bottom ring at a shear force, F_S. From a knowledge of the cross-section area of the shear cell, A_J, the normal and the shear stresses can be determined. For the measurement of a point of a yield locus, the shear cell is filled with the powder. After a manual pre-consolidation the sample is pre-sheared and then sheared to failure as outlined in the previous section. For the next point of the yield locus, a sample has to be prepared and sheared. In ring shear cell tests, a normal force, F_{NR}, is exerted to the crossbeam in the rotational axis of the shear cell and transmitted through the lid to the sample. Thus a normal stress is applied to the sample. The counterbalance force, F_A, also acts in the centre of the crossbeam to counteract the gravity force. The bottom of the shear cell and the lower side of the lid are rough in order to prevent the sample sliding relative to these surfaces. The rotation of the lower ring creates a shear deformation within the sample. The shear stress proportional to the tangential forces F_1 and F_2 is measured.

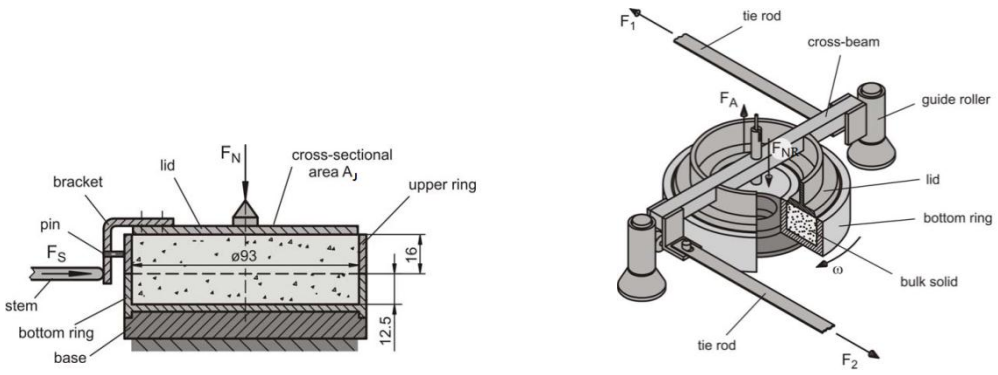

a) b)

Figure 2.2 Schematic diagram of a) Jenike shear cell tester and ((EFCE), 1989, Andrew W. Jenike, 1964) b) ring shear cell tester (Schulze, 2008) for internal friction measurement.

The test procedure for ring shear cell tests is shown in Fig. 2.3. In ring shear cell tests, pre-shear and shear are applied to obtain the yield locus (Schulze, 2006). The powder is consolidated with a pre-defined normal stress σ_{pre}. The sample then shears under a constant normal stress. Once the shear stress reaches a constant value, this is taken as a point on the yield locus. When the powder is sheared under the normal stress $\sigma_{sh} < \sigma_{pre}$, it will start to flow when a sufficiently large shear force, or shear stress, is attained. At that point particles start to move over each other. The maximum shear stress characterizes incipient flow. The corresponding pair of values (σ_{sh}, τ_{sh}) is a point on the yield limit of the consolidated specimen in the σ, τ -diagram (Fig. 2.3). Such a point is called a 'shear point' or a 'point of incipient flow'. A complete yield locus is measured with a given sample by repeating the measurement procedure (see Fig. 2.4).

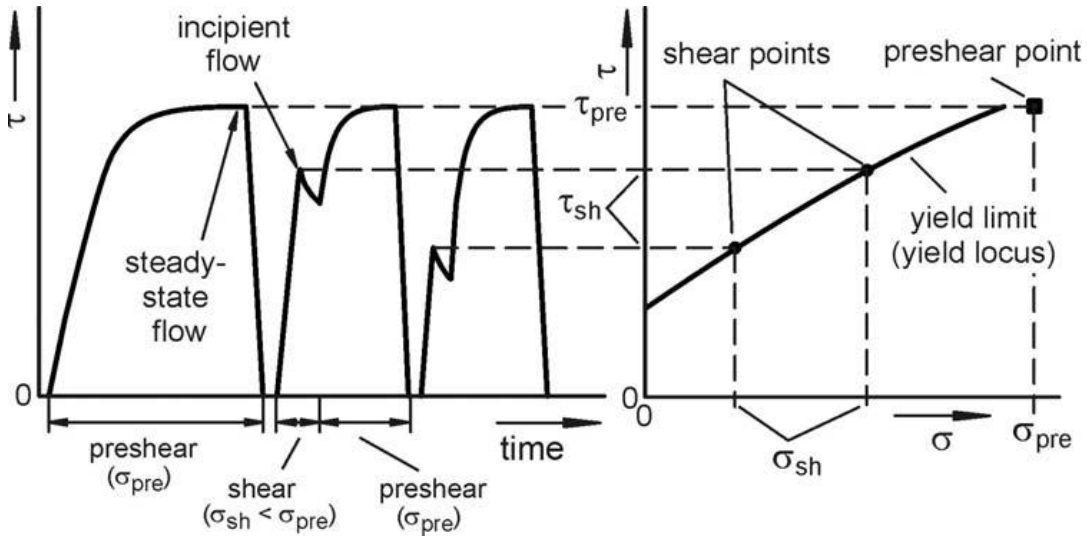

Figure 2.3 Test procedure of a ring shear cell tester (Schulze, 2008).

The parameters that describe the internal friction and flow properties of the powders can be determined from the yield locus. As shown in Fig. 2.4, the principal stresses (σ_1 and σ_2) and unconfined yield strength (σ_c) can be determined. In addition, the effective yield locus through the origin which represents an extremely simple and convenient physical law for steady state flow is obtained (Jenike, 1961). Thus, the effective angle of internal friction, ϕ_e , which is related to the internal friction at steady state flow, can be measured from the gradient of the effective yield locus (Schulze, 2006).

The flowability of a powder can be characterised by the unconfined yield strength, σ_c, and consolidation stress, σ_{con} ,by the flow function, ff_c , which is defined as the ratio of consolidation stress to unconfined yield strength. Since the consolidation stress σ_{con} is equal to the major principal stress σ_1 of the Mohr stress circle which is tangential to the yield locus and intersects at the point of steady state flow (σ_{pre}, τ_{pre}) (Schulze, 2006), ff_c can be obtained by:

$$ff_c = \frac{\sigma_1}{\sigma_c} \qquad \text{Eq (2.5)}$$

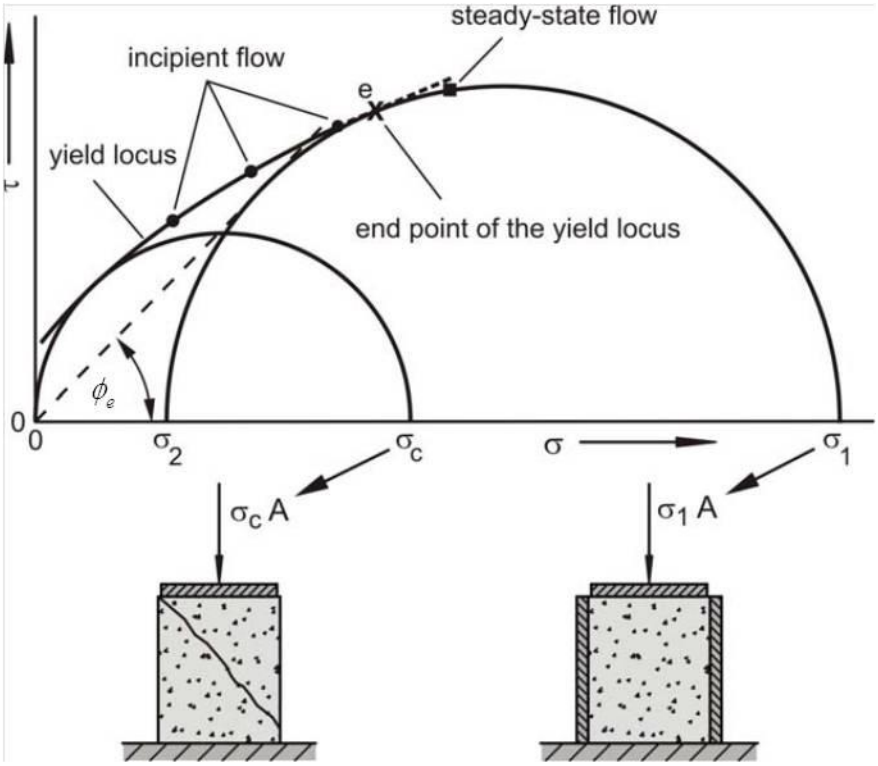

Figure 2.4 yield locus obtained from ring shear cell tests (Schulze, 2008).

The wall shear stress τ_w is proportional to the normal stress, σ_w, following a Coulomb relation:

$$\frac{\tau_w}{\sigma_w} = \mu_w = \tan \phi_w \qquad \text{Eq (2.6)}$$

where μ_w and ϕ_w is the wall friction coefficient and wall friction angle, respectively. Thus, the wall friction properties of a powder can be measured in a similar manner as the measurement for internal friction. As shown in Fig. 2.5, the normal stress, σ_w, and shear stress, τ_w, can be obtained from the normal and tangential forces (see in Fig. 2.5).

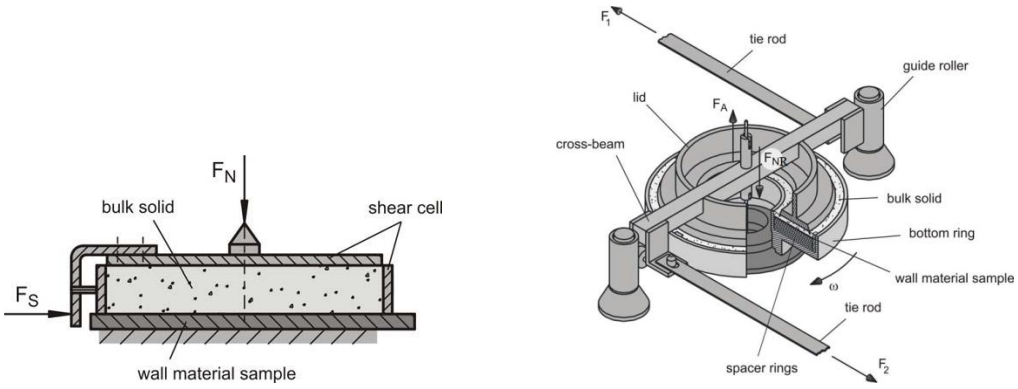

a) b)

Figure 2.5 Schematic diagram of a) Jenike shear cell tester ((EFCE), 1989, Andrew W. Jenike, 1964) and b) ring shear cell tester (Schulze, 2008) for wall friction measurement.

2.2.2 Compressibility

There are several models that can be used to evaluate the compressibility of powders, such as the Heckel equation (1961), Kawakita equation (1970), pressure-density relationship adopted by Johanson (1965), and Adams equation based on the micromechanical analysis of the pressure-volume relationship (Adams and McKeown, 1996). The theories are introduced in this section.

Heckel analysis

Heckel (1961) introduced an equation for the densification of powders using first order kinetics. The equation is:

$$\ln\left(\frac{1}{1-D_r}\right) = k_H P + A_H \qquad \text{Eq (2.7)}$$

where k_H and A_H are constants, D_r is the relative density of a powder column at a pressure P. The parameter k_H provides a measure of the plasticity of a compressed sample, while A_H is related to the volume reduction during die filling and powder rearrangement before the deformation of the powder.

The relative density of a powder column is given as

$$D_r = \frac{\rho_b}{\rho_t} \qquad \text{Eq (2.8)}$$

where ρ_t is the true density of the powder that can be measured using a pycnometer as introduced in Chapter 4 and ρ_b is the bulk density. ρ_b is obtained from the ratio of the mass and instantaneous volume of the powder which is calculated from the measured geometry of the powder bed.

Kawakita analysis

An equation was introduced by Kawakita (1970) to describe the relationship between volume reduction of powders and the pressure as follows:

$$\frac{P}{C_K} = \frac{P}{a_K} + \frac{1}{a_K b_K} \qquad \text{Eq (2.9)}$$

where a_K and b_K are constants. The constant a_K can be used describe the compressibility of a powder, while b_K represents the tendency for volume reduction. The factor C_K corresponds to the extent of volume reduction, and is given by:

$$C_K = 1 - \frac{\rho_{ini}}{\rho_P} = \frac{\varphi - \varphi_P}{1 - \varphi_P} \quad \text{Eq (2.10)}$$

where ρ_{ini} is the initial bulk density of a powder column, ρ_P is the apparent density at a pressure P. φ and φ_P are the porosities which are defined as the ratio of the volume of all the pores in a powder material to the volume of the whole at these conditions, equalling to $1 - D_r$.

Johanson's approach

The compressibility of a powder can be defined as the variation of the relative density with the applied pressure (A. W. Jenike and Shield, 1959). Johanson (1965) introduced a compressibility factor κ and proposed the following pressure-density relationship for application to roll compaction:

$$\sigma_\theta / \sigma_\alpha = (\rho_\theta / \rho_\alpha)^\kappa \quad \text{Eq (2.11)}$$

where σ_θ and ρ_θ are normal stress and density of the powder at an angular position θ. Accoring to the work by Johanson (1965), θ equals 0 at the minimum roll gap S and has positive values in the slip ang nip region, as shown in Chapter 3 (Fig. 3.1) σ_α was defined as the nip pressure by Johanson (1965) but is actually a fitting parameter defining the lower limit for which this relationship describes the data (Patel *et al.*, 2010) and ρ_α is the corresponding density.

The compressibility factor κ was obtained in terms of the continuity of the powders defined by Eq (2.11). Assuming that the lower bound of the equation is known, Eq (2.11) can be hence written as:

$$\log \sigma_\theta - \log \sigma_\alpha = \kappa\left(\log \rho_\theta - \log \rho_\alpha\right) \quad \text{Eq (2.12)}$$

Therefore, the relationship can be described by the following equation:

$$\log \rho_u = \frac{1}{\kappa} \log \sigma_u + C_u \quad \text{Eq (2.13)}$$

where ρ_u and σ_u presents the instantaneous apparent density and normal stress in uniaxial compression, C_u is a constant related to the powder deformation at relative low stress ($< \sigma_\alpha$). However, this relationship is only applicable to the region where the stress and density follow a logarithmic relationship. Thus it is not applicable at small strains.

Adams' equation

Patel *et al.* (2010) analysed uniaxial compression data for powders adopting a microscopic analysis (Adams, 1994) and derived a modified equation for the compressibility factor calculation, which can be applied to all strains of uniaxial compression, and thus achieve more precise results:

$$\ln \sigma = \ln\left[1 - \exp\left(-\beta\varepsilon\right)\right] + \ln \Sigma_\alpha + \beta\varepsilon \quad \text{Eq (2.14)}$$

where Σ_α is a fitting parameter referring to the nip pressure in Johanson theory (1965), β is the compressibility factor, ε is the current compressive natural stain, and can be obtained from the initial height, h_i, and current height, h_p, of the powder bed as:

$$\varepsilon = \frac{h_i - h_p}{h_p} \qquad \text{Eq (2.15)}$$

2.2.3 Compactibility

The compactibility of a powder system is another critical factor determining their compression behaviour in addition to the compressibility. Leuenberger (1982) introduced an approach to describe the deformation hardness of a tablet H as a function of the applied stress σ_a and the relative density D_r:

$$H = H_{\max}\left[1 - \exp\left(-\gamma\sigma_a D_r\right)\right] \qquad \text{Eq (2.16)}$$

where H_{max} is the theoretical maximal possible deformation hardness at $\sigma_a D_r \rightarrow \infty$, which can be used to describe the compactibility of the feeding powder. The term γ is defined as the compression susceptibility, and describes indirectly the compressibility.

Sonnergaard (2006) carried out uniaxial compression experiments on pharmaceutical powders and made attempts to quantify the compactibility of the samples. The analysis was performed on the basis of the maximum normal stress during the compression and the specific crushing strength of the produced tablets. The specific crushing strength (SCS) is defined as (Sonnergaard, 2006):

$$SCS = \frac{F_{crush}}{D_t h_t} \qquad \text{Eq (2.17)}$$

where F_{crush} is the force applied to diametrically crush a cylindrical tablet with a diameter D_t and height h_t.

Sonnergaard (2006) showed that the maximum compression pressure P_{mu} during uniaxial compression and the specific crushing strength (*SCS*) have a linear relationship, which can be written as:

$$SCS = C_p P_{mu} + b_c \qquad \text{Eq (2.18)}$$

where b_c is a constant determined by the minimum compression pressure to produce a tablet for powder materials. Thus, the dimensionless compactibility, C_p, which corresponds to the strength of a tablet produced at a given maximum pressure, can be obtained from the regression line of *SCS* data as a function of P_m,. This method has been adopted due to the ease to use and potential to compare the compactibility of different powders (Bacher *et al*., 2008, Caillard and Subirade, 2011, C. Q. Sun, 2008).

2.3 Conclusions

This chapter introduced the utilization of powders in pharmaceutical manufacturing, highlighting their application in tablet production. The Mohr-Coulomb yield criterion and the model modified by Jenike, which is the theoretical background of the measurements for the frictional and flow properties, of a powder were discussed. Shear cell testing was introduced as well. This chapter also includes the definition and fundamental theories of compressibility and compactibility that are essential to describe the compression behaviour of powders.

CHAPTER 3 LITERATURE REVIEW

3.1 Introduction

Roll compaction technique is widely used in many fields such as the food industry, metallurgical processing, the chemical industry, ceramic manufacturing, semi-conductor and waste recycling (Balicki, 2003). The application of roll compaction in pharmaceutical manufacturing was first reported in 1966 (Cohn *et al.*, 1966, Jaminet and Hess, 1966). The technique has been used in the pharmaceutical industry for more than 50 years (Kleinebudde, 2004), to produce granules with acceptable flowability, compaction properties, compositional uniformity and chemical stability. In the past several decades, increasing attention was paid to the technique and researches were conducted both theoretically and experimentally. Theoretical models were developed to predict the magnitude of densification during roll compaction and to provide information for the process design, according to the properties of the feeding powders and the process parameters such as dimension of the instruments and roll pressure. However, the capability of the developed models is limited due to the complexity of the process. Experimental work covered the influences of the processing parameters and the effects of the properties of materials. Nevertheless, the mechanisms of the process and the influences of the material properties are not fully understood yet.

In the pharmaceutical industry, milling and tabletting processes are down-line processes to produce final dosage form (*i.e.* tablets). The quality of the final products is not only affected by roll compaction, but these downstream processes as well. Therefore, understanding of these processes is also necessary for process design and quality control.

This chapter introduces a literature review of the application of roll compaction, milling and tabletting.

3.2 Theoretical models for roll compaction

Many theoretical models have been developed to investigate the mechanics of roll compaction and to predict the quality of the produced compacts (John C. Cunningham *et al.*, 2010, Dec *et al.*, 2003, Inghelbrecht *et al.*, 1997, Johanson, 1965, Katashinskii, 1966, Michrafy *et al.*, 2011a, Michrafy *et al.*, 2011b, Muliadi *et al.*, 2012, Odagi *et al.*, 2001, Turkoglu *et al.*, 1999). Johanson (1965) proposed a one-dimensional rolling theory for granular solids. It was the first mathematical model for predicting the extent of the compression region and the pressure distribution after the powder are gripped by the rolls. Katashinskii (1986) produced an analytical model for the roll compaction of powder materials using the slab method adopted from metal working. The model predicts the pressure distribution and separating forces on the rolls.

Besides analytical models, numerical methods have been introduced to simulate roll compaction. In 1997, Inghelbrecht *et al.* (1997) analysed roll compaction using a neural network. A Multilayer Feed-Forward neural network (MLF) was used to evaluate the effects of the roll compaction parameters on the friability of the produced granules which describes the ability of the granules to withstand the breakage due to mechanical shocks. Neural networks and genetic algorithms were used by Turkoglu *et al* (1999) to model the roll compaction process, predicting the effects of the addition of a binder and the number of compaction revolutions on the properties of final tablets. Dec *et al.* (2003) employed finite element method to predict the behaviour of powder materials in the nip region using the commercial software, ABAQUS. They showed a capability for predicting relative densities, material flow, deformation energy, shear stress, pressure distribution, position of nip angle and neutral angle, failure of the compact during release. Odagi *et al.* (2001) developed a two-dimensional roll compaction model using discrete element methods. They evaluated the effects of an adhesive force and roll speed on the compressive flow property of particles.

These modelling methods for roll compaction will be described in more detail in the following section.

3.2.1 Johanson's model

Johanson (1965) proposed a theory of roll compressing for granular solids. This is the first model allowing the calculation of the roll forces and pressures and the prediction of the performance of the materials during the process. The model assumes that:

- The material is isotropic, frictional and cohesive;
- The rolls are rigid;
- The material undergoes continuous shear deformation between the rolls;
- It is a plane strain problem in the nip region;
- The contact area is much smaller than the size of the rolls, so that the curvature of the powder-roll interface is negligible;
- The Coulomb frictional law is valid between the material and the roll surfaces;
- The effect of the gravity is negligible when forced feeding is used.

Based on the above assumptions, Johanson divided the zone between the rolls into two regions: i) a slip region where the slip occurring along the roll surface and ii) a nip region where a no slip boundary condition applies, as shown in Fig. 1.1: The zone beyond the minimum roll gap is usually defined as the release region in which the stresses are relieved and the compacts were extruded from the system.

In the nip region, the model assumes that no slip exists and the powder between the rolls could be treated as solid elements which are eventually compacted to a dense form equal to the dimension of the minimum roll gap. An empirical pressure-density relationship obtained from uniaxial compression (A. W. Jenike and Shield, 1959) was adopted. The compression behaviour of the powder was described by a compressibility factor and the pressure distribution in the nip region could be obtained provided that the nip angle and pressure at the position are known.

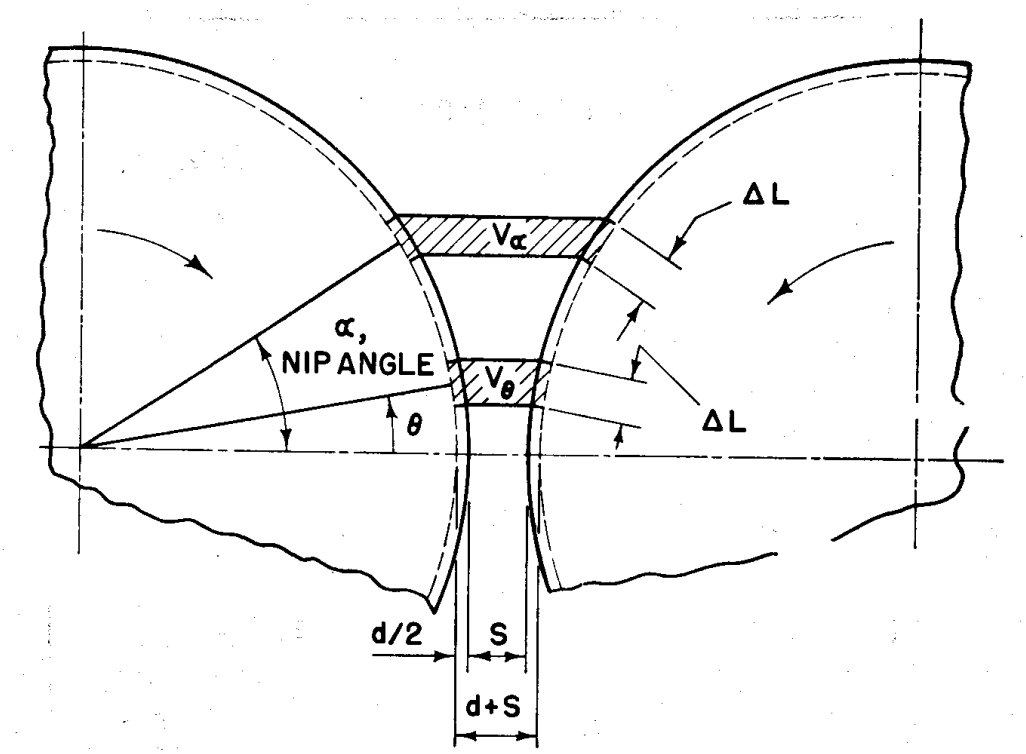

Figure 3.1 Schematic diagram of the deformation of a solid element in nip region (Johanson, 1965), d and s represent the pocket size and minimum roll gap, respectively.

Since the powder in the nip region does not experience slip along the roll surface, it must be compressed to the final roll gap dimension. This means a volume V_α (see Fig. 3.1) must be compressed to a volume V_θ between the same arc-length segments. Continuity requires that the bulk densities ρ_α and ρ_θ in the volumes V_α and V_θ are related by:

$$\frac{\rho_\alpha}{\rho_\theta} = \frac{V_\alpha}{V_\theta} \qquad \text{Eq (3.1)}$$

The pressure σ_θ at any angle $\theta < \alpha$ can be determined as a function of the pressure σ_α at an angle $\theta = \alpha$ by adopting the pressure-density relationship introduced in Section 2.2.2. Substituting Eq (3.1) in to Eq (2.11), we have

$$\frac{\sigma_\alpha}{\sigma_\theta} = \left(\frac{V_\alpha}{V_\theta}\right)^\kappa \qquad \text{Eq (3.2)}$$

For smooth roll surface ($d = 0$), the volume of powder V_θ between the arc-lengths segment ΔL is

$$V_\theta = \Delta L W\left[S + D\left(1 - \cos\theta\right)\right]\cos\theta \qquad \text{Eq (3.3)}$$

where D is the diameter of the rolls and W is the roll width. Combining Eq (3.2) and Eq (3.3) leads to:

$$\sigma_\theta = \sigma_\alpha \left[\frac{\left(1+\frac{S}{D}-\cos\alpha\right)\cos\alpha}{\left(1+\frac{S}{D}-\cos\theta\right)\cos\theta}\right]^\kappa \quad \text{for } \theta \le \alpha \qquad \text{Eq (3.4)}$$

Thus, the pressure distribution between the rolls can be obtained provided that the nip angle and the pressure there are known.

The nip angle was defined as the angular position where no relative motion occurs between the granular material and the rolls. Johanson suggested that pressure gradient in the slip region is larger; and a no slip analysis provides lower values of pressure gradient in the nip region. Thus, the nip angle could be determined at the point where the slip and nip pressure gradient coincide.

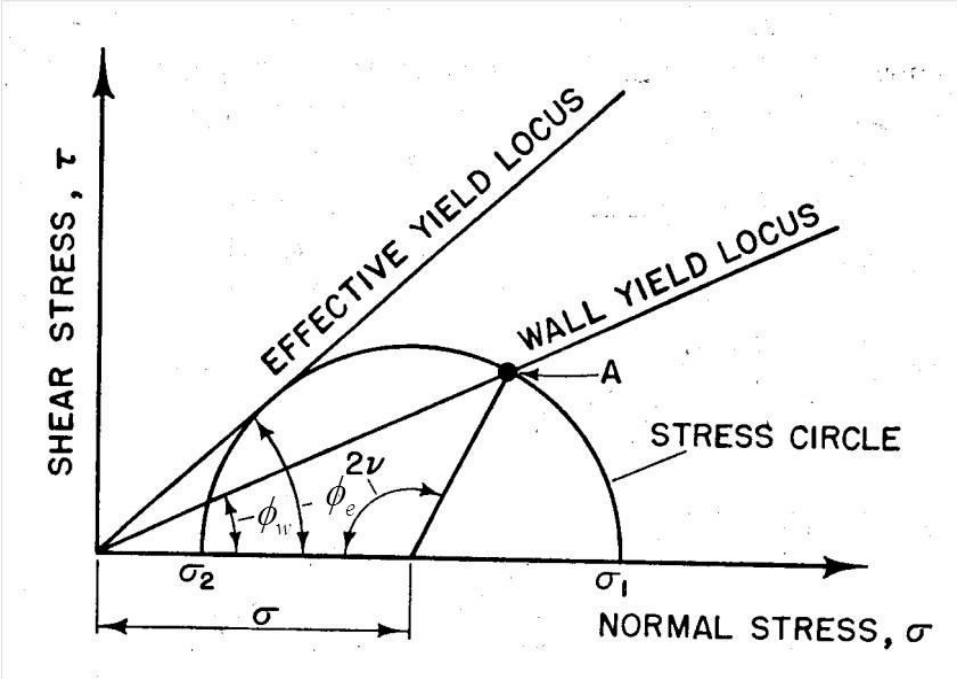

Figure 3.2 Effective and wall yield loci (Johanson, 1965).

The powder material is assumed to obey the effective yield function proposed by Jenike and Shield (1959), as represented in Fig. 3.2, in which ϕ_e is the effective angle of friction, ϕ_w is the angle of wall friction and v is the acute angle given by:

$$2v = \pi - \arcsin\frac{\sin\phi_w}{\sin\phi_e} - \phi_w \qquad \text{Eq (3.5)}$$

A hyperbolic system of partial differential equations was obtained by combining the equation of the effective yield locus with the equations of equilibrium. By combining the chosen top boundary at $\theta = \frac{\pi}{2} - v$, and the friction condition along the roll surface in the slip region, the pressure gradient $\frac{d\sigma}{dx}$ can be determined by the acute angle and the yield criterion as follows:

$$\frac{d\sigma}{dx} = \frac{4\sigma\left(\frac{\pi}{2} - \theta - \nu\right)\tan\phi_w}{\frac{D}{2}\left(1 + \frac{S}{D} - \cos\theta\right)\left[\cot(A - \mu) - \cot(A + \mu)\right]} \qquad \text{Eq (3.6)}$$

where the x coordinate corresponds to the centre of the gap between the rolls with an origin at the minimum roll gap such that positive values are against the direction of powder flow, A is a function of the effective internal friction angle ϕ_e and the wall friction angle ϕ_w and defined as:

$$A = \frac{\theta + \nu + \frac{\pi}{2}}{2} \qquad \text{Eq (3.7)}$$

The pressure gradient in nip region is obtained from Eq (3.4), as:

$$\frac{d\sigma}{dx} = \frac{\kappa\sigma(2\cos\theta - 1 - S/D)\tan\theta}{\frac{D}{2}\left[(1 + S/D - \cos\theta)\cos\theta\right]} \qquad \text{Eq (3.8)}$$

This expression is zero for $\theta = 0$ and $\theta \approx 60°$.

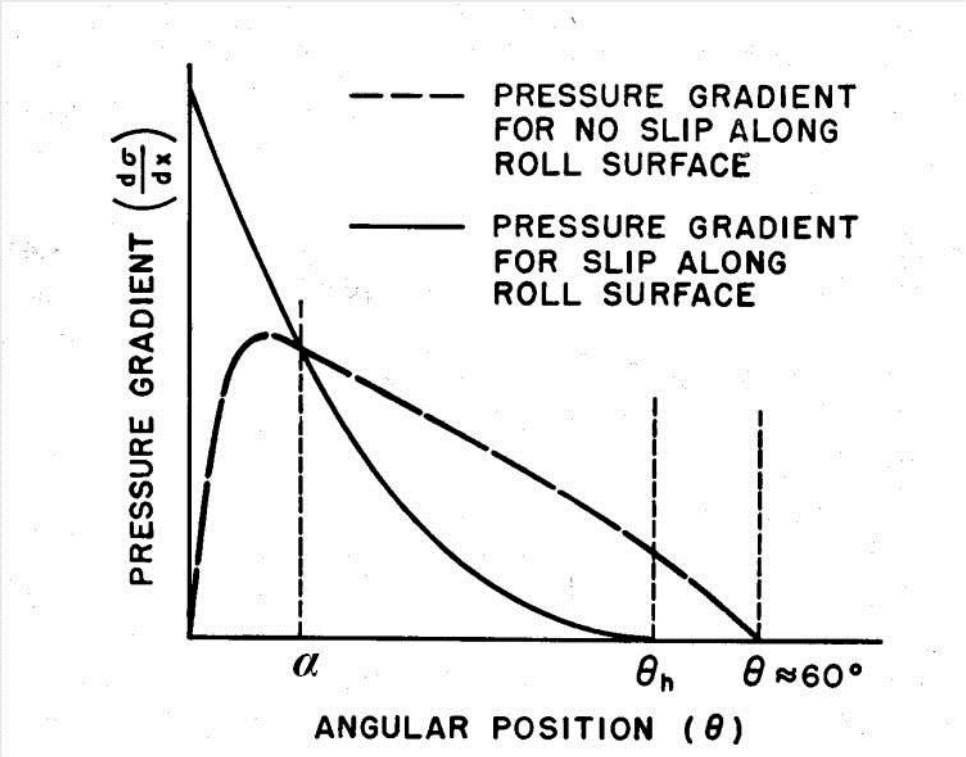

Figure 3.3 Vertical pressure gradient versus angular position between the rolls (Johanson, 1965)

The solid line in Fig 3.3 is a typical pressure gradient profile given by Eq (3.6) for the condition of slip along the roll surface. When $\theta=\theta_h$, which represents the upper boundary of the slip region, the pressure gradient $d\sigma/dx$ is zero. However when slip does not occur along the roll surface, the pressure gradient is given by Eq (3.8), shown as the dashed line. This expression is zero for angles $\theta = 0^o$ and for $\theta \approx 60^o$. Johanson (1965) proposed that the intersection of the two pressure gradient curves is a point at which the nip angle occurs ($\theta = \alpha$).

Johanson theory provided a method for calculating the parameters of the roll compaction such as the roll force, the roll torque, the roll gap and the feed pressure necessary to achieve the required maximum pressure. As the first complex model, it has made a major contribution in equipment design and operation and process understanding. It is considered to be a valuable tool for process prediction and design. The model has been used in experimental investigations as a common analysis model. Yusof *et al.* (2005) carried out roll compaction

experiments on maize powder and used Johanson's model to predict roll force and the roll torque by incorporating measured powder properties obtained using uniaxial compression. The predicted values showed reasonable agreements with experimental results. Bindhumadhavan *et al.* (2005) made an attempt to validate the sensitivity of Johanson's model to peak pressure by undertaking measurements with an instrumented roll compactor. Their results showed that the model could predict the peak pressure accurately for microcrystalline cellulose.

However, there are limitations due to the simplification of the powder behaviour in the nip region. Discrepancies might be relatively large when cavities are cut into the working surfaces of the rolls, high compaction pressures (> 100MPa) are applied or materials are very compressible, or changes in the roll speed during the processes since Johanson theory did not consider the effects of the roll speed which might result in insufficient feeding and inferior bulk density and strength of the produced compacts (Dec *et al*., 2003). Furthermore, the proposed model allows the nip angle to be determined only if the frictional properties and compressibility κ are accurately measured using techniques such as shear tests and uniaxial compression. Since the wall friction angle is a parameter for a powder in contact with a given wall surface and depends significantly on the wall material, exactly the same wall material with the same surface finish as the roll surface should be used to measure the wall friction angle. In practice, this is difficult to achieve. Furthermore, it is still questionable whether shear cell tests give accurate values of the wall friction as it generally varies with the applied normal stresses. Moreover, the effects of roll speed are not considered in Eqs 3.6 and 3.8, so that the method cannot be used to explore the effect of this parameter.

3.2.2 The slab method

A model termed 'slab method' was initially used to predict the pressure distribution and roll separating force in the rolling process of metal sheets. In order to overcome the issues arising from the simplifications of the powder behaviour in the nip region, Katashinskii (1966) introduced the slab method for the roll compaction of metal powder. In the analysis, the concept of yield criterion for fully dense metal powders proposed by Kuhn and Downey

(1971) was adopted for the material model. Similarly to Johanson theory (1965), the powder materials are assumed to be solid elements and remain in plane strain as they pass through the rolls. The deformation zone between the rolls (*i.e.* nip region) was divided into trapezoidal slabs as shown in Fig. 3.4 (Dec *et al*., 2003).

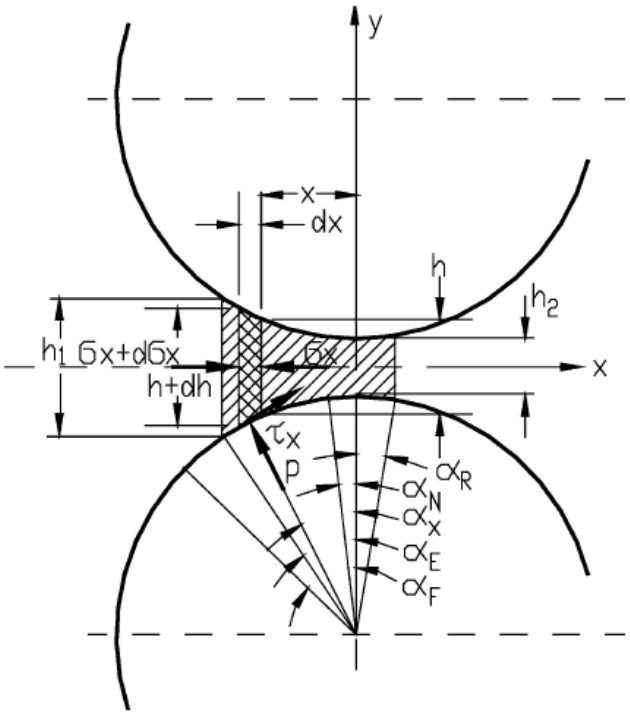

Figure 3.4 Stress acting on a slab element in roll nip region. (Dec *et al*., 2003)

A force balance on the slab leads to the equilibrium equation in the feeding direction (*i.e.* the *x* direction):

$$\frac{\partial(h\sigma_x)}{\partial x} + 2(p\tan\alpha_i - \tau_f) = 0 \qquad \text{Eq (3.9)}$$

where σ_x is the stress along the *x* direction (as shown in Fig. 3.4), *h* is the thickness of the slab, *p* is the normal pressure acting on the layer, α_i is the instantaneous angle, τ_f is the frictional stress. The friction stress is expressed as:

$$\tau_f = Y(\rho) \quad \text{for } \mu(p)p \geq Y(\rho) \qquad \text{Eq (3.10)}$$

$$\tau_f = \mu(p)p \quad \text{for } \mu(p)p < Y(\rho) \qquad \text{Eq (3.11)}$$

where $Y(\rho)$ is the effective shear stress, and $\mu(\rho)$ is the coefficient of friction varied with angular position between the rolls.

Assuming that principal stresses act in direction *x* and *y*, the following equilibrium equation is obtained:

$$\left[\sigma_x^2 + \sigma_y^2 - 2\nu(\rho)\sigma_x\sigma_y\right]^{\frac{1}{2}} = Y(\rho) \qquad \text{Eq (3.12)}$$

where σ_y=-*p*, $\nu(\rho)$ is the Poisson's ratio of the powder which is defined as is the ratio of transverse contraction strain to longitudinal extension strain in the direction of stretching force, the effective shear stress $Y(\rho)$ is a function of the density of the slab element. The calculation was carried out with the assumption of the initial stresses and density, provided that the nip angle and the position of the neutral plane were obtained experimentally. The density of the compacts was determined from compression test data for a corresponding mean stress at each step of calculation. The calculation was repeated until the ribbon density results coincided with the measured values.

The model is more complex than the Johanson model and allows more parameters and their effects to be evaluated. The advantage of this model is that it provides information about the two principal stresses unlike the Johanson model that only describes the mean stress. It also has potential to include characteristics of powders such as cohesion and global friction between particles (Balicki, 2003).

Nevertheless, the model depends on the experimental inputs of processing data such as nip angle and neutral angle at the which the shear stress on the roll surface changes the direction. The model is not applicable to predict these parameters based on the other inputs. And the initial stress conditions and density of the materials need to be known. The calculation procedure from the entry to the compression zone was repeated until the results agree with the density of the compacted strip. The experimentally measured nip angle values were used for the calculation and results were forced to match the output density to achieve the agreement with experimental roll force and torque. Hence, the capability of the prediction for the model is limited.

3.2.3 Finite element method (FEM)

The finite element method (FEM) has been applied to roll compaction by Dec *et al.* (2003) who developed a 2D model using the commercially available ABAQUS code. The work focused on evaluating the effects of the wall friction coefficient and the feed pressure on process parameters such as roll force, roll torque, nip angle and neutral angle. They used microcrystalline cellulose as the model powder. The constitutive model of the powder was based on a pressure-dependent yielding plasticity model with linear elasticity. This plasticity rate-independent model was calibrated by a series of mechanical tests, which were diametrical compression, simple compression and compaction in an instrumented die. The internal friction angle between the particles was determined to be 65^{o} and the cohesion of the powder was assumed to be zero for the simplification. The wall friction was assumed to follow the Coulomb friction law with a constant friction coefficient in a range of 0.35 to 0.5. The simulation was conducted until steady state conditions at which the values of roll force and roll torque are constant were achieved.

The results were consistent with Johanson's analytical model (1965) on the slip/stick behaviour of the powder materials in slip and nip regions. They concluded that the performance of the powder during roll compaction was greatly affected by the wall friction

and feed pressure at which the powders driven into the roll compactor by a screw feeding system. It was reported that, at a constant feed pressure, increasing wall friction coefficient resulted in a larger nip angle and maximum roll pressure. Generally, an increase in the density of the compacted ribbon could be achieved by increasing the wall friction coefficient and the feed pressure. As expected, increases in roll force and roll torque were observed in this case.

Dec *et al.* (2003) argued that the FEM modelling showed advantages for process design and prediction compared to Johanson's model and the slab method. It can predict relative densities, material flow, deformation energy, shear stress (roll torque), pressure distribution (roll force), position of nip angle and neutral angle, and failure of the compact during release. Further analysis can be performed to solve realistic manufacturing problems by including feeding process and forming tool geometry (*i.e.* geometry of the counter-rotating rolls). Thus, the model has potential for improved process design and scaling by providing reliable prediction for specific processes. They also pointed out that the key problem affecting the implementation is the input of more accurate material models and appropriate friction models (Dec *et al*., 2003).

Cunningham (2005) roll compacted mixtures consisting of microcrystalline cellulose (MCC, Avicel PH 102), mannitol (Pearlitol 200DS) and magnesium stearate (MgSt) using a instrumented roll compactor with smooth rolls and simulated the process using a FEM approach. He found that the nip angle is strongly affected by the wall friction between the powder and the roll surface, but approximately independent on other process parameters (*i.e.* feed stress, roll gap, initial density of the powder and entry angle). It was reported the feed process, which was dominated by the feed stress and entry angle, might cause pre-densification in the entry and slip regions, which significantly affected the density of the ribbon produced. In addition, it was noted that the peak pressure occurred slightly before the minimum roll gap. He also developed a 3D model based on the 2D plane strain model and examined the effects of the side seal friction and uniformity of the feeding. He concluded that the side seal friction due to the resistance of the cheek plates which are plastic plates allocating on the edges of the rolls to prevent the leakage of the powders resulted in a reduction in the maximum roll pressure in the area adjacent to the cheek plate. In addition, it

was found that non-uniform feeding, which was caused by non-uniform feed stress and the side friction, resulted in non-uniform maximum roll pressure distribution.

Cunningham *et al.* (2010) carried out roll compaction experiments on the mixture of MCC (Avicel PH 102) and MgSt using a roll pair with textured roll surfaces. One of the rolls was instrumented with 3 embedded load cells through the width of the roll (see Fig. 3.5) capable of measuring the contact stresses (*i.e.* normal stress and shear stress), following the design used by Schönert and Sander (2002). They simulated the process using 2D and 3D FEM models on the basis of the experiments. Their simulation showed that the maximum pressure occurred slightly before reaching the minimum roll gap, similar to the observations obtained for smooth rolls (2005). However, the maximum density of the compacts was achieved at the minimum roll gap suggesting that the location of the peak pressure and the maximum density do not coincide. They also observed significant variation of the powder feeding through the thickness (see Fig. 3.5) at entry angle and slip region. By comparing the local speed of the powder pattern against the roll speed, they suggested a second slip region at the exit of the rolls where powder moves faster than the roll in an extrusion-like fashion.

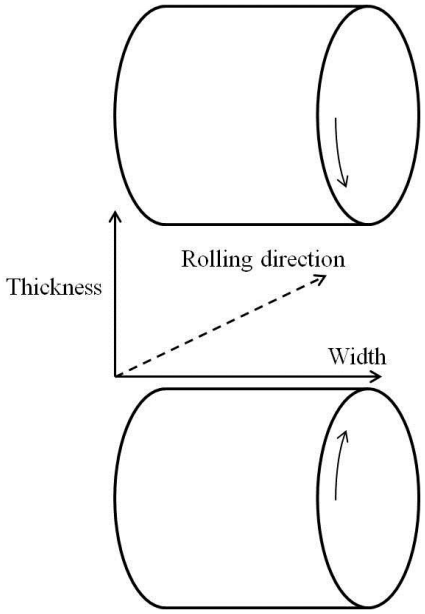

Figure 3.5 Schematic diagram of the thickness, width and rolling direction in roll compaction.

Michrafy *et al.* (2011b) modelled the roll compaction of MCC (Avicel PH 102) using a 2D FEM model. Their results revealed that 1) the maximum pressure was achieved before the minimum roll gap, 2) there was a slip region following the nip region, consistent with the observation of Cunningham *et al.* (2010). However, the results from Michrafy *et al.* (2011b) showed that the ribbon density also reached its maximum before the neutral angle at which the shear stress is zero, identical to the maximum pressure.

Michrafy *et al.* (2011a) also examined the uniformity of the pressure and density across roll compacted MCC ribbons using 3D FEM. They examined the pressure and density distribution of the ribbons with two conditions: constant feed pressure and constant feed velocity. In terms of the simulation results, they reported that a uniform pressure and density distribution could be achieved using the constant feed pressure. However, using a constant feed velocity led to the observation that the pressure was higher at the centre of the ribbon but lower at the edges. The density distributed in the same manner as the pressure across the ribbon width.

Recently, Muliadi *et al.* (2012) compared the predicted nip angle, normal pressure at the minimum roll gap and maximum material relative density using Johanson theory (1965) and 2D FEM approach. The material model based on MCC (Avicel PH 102) was employed for the calculation. They found that the predicted parameters obtained from FEM followed similar trends to those using Johanson approach, except that the nip angles obtained using FEM decreases with increasing effective friction angle, contrary to Johanson's results. In addition, the values of relative density and normal pressure obtained from Johanson theory varied more significantly than those predicted using FEM. The authors pointed out that the relative densities predicted by Johanson's model are greater than unity regardless of the processing conditions and material model used. They argued that this unrealistic result was ascribed to the velocity gradient in nip region, which was not considered in Johanson theory.

3.2.4 Discrete element method (DEM)

The discrete element method has also been employed in roll compaction studies. Based on Tsuji's DEM code (1992), which used Hertz and Mindlin (Hertz, 1881, Mindlin and Deresiewicz, 1953) theories to describe the particle-particle normal contacts and particle interactions in the tangential direction respectively, Odagi *et al*. (2001) developed a 2D DEM simulation of powder flow in the roll compaction process. The particles were assumed to be mono-sized and spherical. By introducing an inter-particle adhesive force f_a that describes the cohesion of the powder, the roll compaction behaviour was simulated. The values of the adhesive force were obtained from experimental measurements of the tensile strength of roll compacted ribbons, using Rumpf's (1970) correlation for agglomerate composed of mono-sized spheres:

$$\sigma_{tr} = \left(\frac{1-\varphi}{\varphi}\right)\frac{f_a}{d_{50}^{\ 2}} \qquad \text{Eq (3.13)}$$

where σ_{tr} is the tensile strength of the ribbon, d_{50} is the mean diameter of the particles, φ is the porosity of the agglomerate.

The experimental results showed that the adhesive force largely depends on the compression pressure used to produce the ribbons. To simplify the numerical work, a constant value of f_a was employed for all the particles in the whole simulation. The simulations were conducted with and without the adhesive force. The flow behaviour and densification of the powders was not able to be efficiently simulated without adhesive forces, with the particles failing to be compressed into a ribbon. On the other hand, in the presence of the adhesive force, the mass throughput showed a linear relationship with roll speed, which is comparable with the experimental results. However, the pressure profile from the simulation was quite different from experimental results even for those with adhesion. This was attributed to the fact that the influence of air which might result in aeration and hence the reduction in the compaction pressure generated was neglected and the particles were assumed to be spherical. The

validation of the model was carried out by comparing the numerical results with the experimental data obtained by Michel's (1994).

3.2.5 Artificial Neural Network Modelling

Artificial neural networks (ANNs) are biologically inspired computer programs designed to simulate the way in which the human brain processes information. ANNs gather their knowledge by detecting the patterns and relationships in data and learn (or be trained) through experience, not from programming (Agatonovic-Kustrin and Beresford, 2000). The connection of hundreds of artificial neurons results in a system with significant computational capability. The system is able to be trained and optimise the connections between neurons to minimise the error, and predict the output when the input information is given, once it has been trained and validated.

McCulloch and Pitts (McCulloch and Pitts, 1943) modelled the biological neuron, and proposed the unification of neuro-physiology with mathematical logic, which was the basis of the method. A learning rule, known as the Hebbian learning rule, was derived from a model based on synaptic connections between nerve cells responsible for biological associative memory (Hebb, 1949), and refined by Rosenblatt in the perceptron model (Rosenblatt, 1958). In 1976, Willshaw and von der Malsburg proposed the self-organising map architecture based on competitive learning (Willshaw and von der Marlsburg, 1976).

Artificial neural network (ANN) systems have been used for data analysis by pharmaceutical researchers since the 1980s and it was shown that the ANN methodology performs well and it was a good candidate to replace multiple regression methods (Turkoglu *et al*., 1999). The system showed good reliability for the development of pharmaceutical formulations (Bourquin *et al*., 1997). The application of the system in the study of the roll compaction has also been considered. Inghelbrecht *et al*. (1997) studied the influence of the velocity of the rolls, the speed of the horizontal and the vertical screw and the air pressure and the interrelation of these parameters on the compact and granule quality using multilayer feed-

forward neural network . They also reported the advantage of ANNs to describe nonlinear correlations between input and output. They concluded that the horizontal feed screw speed and the air pressure influenced the granule quality (*i.e.* friability). The available range of this screw speed was determined by the roll speed and the vertical screw speed. Mansa *et al*. (2008) employed INForm software utilising ANNs, genetic algorithms and fuzzy logic to predict the roll compaction processing conditions necessary to produce ribbons with specific properties. They used *FormRules* to reveal the rules that described the relationships between the powder properties (*i.e.* frictional properties, compressibility), process conditions (*i.e.* roll gap and roll speed) and outputs (*i.e.* maximum pressure, average nip angle and porosity of the produced ribbon). With complete training of the software, they attempted to predict the process conditions required for compacting di-calcium phosphate anhydrous (DCPA) and MCC powders into ribbons with desired porosity. Despite the acceptable results given by the calculations, discrepancies between the porosity of the ribbons produced experimentally followed the process conditions suggested by the ANN and the target values were observed. This was attributed to the fact that the training data did not cover the region of the experiments which indicated that a sufficient data base is required for accurate prediction using ANN.

3.3 Experimental studies of roll compaction

Experimental investigations of roll compaction of pharmaceutical powders were established in 1960s (Cohn *et al*., 1966, Jaminet and Hess, 1966). Cohn *et al.* (1966) attempted to optimise the roll compaction process to prepare granules to which other drugs could be added and directly compressed into tablets using a Fitzpatrick roll compactor. They investigated the effects of the oil pressure on the amperage of roll compaction, amount of non-compacted powder and the hardness of the tablets. They found that there were not simple relationships between the input (*i.e.* oil pressure) and output variables (*i.e.* amount of non-compacted material and hardness of the tablet) due to the complexity of the process. However, they suggested optimal settings of the output variables could be achieved.

A trial and error system was employed to solve specific design problems in manufacturing due to the complicated nature of the roll compaction technique. Limitations of the process such as material bypass, insufficient feeding and inhomogeneous compaction were observed. In order to optimise the process, various system layouts were introduced and investigations were carried out to achieve better understanding of the process. With improved knowledge, the research has focused on the effects of process parameters and feeding powder properties (Parrot, 1981, Inghelbrecht and Remon, 1998, Schönert and Sander, 2002, Simon and Guigon, 2003, Bindhumadhavan *et al.*, 2005, Lecompte *et al.*, 2005, Mansa *et al.*, 2006). More attempts have been made recently to explore the mechanism of the roll compaction (Miguélez-Morán, A.M. *et al.*, 2008, 2009, Cunningham *et al.*, 2010, Wu *et al.* 2010b, Michrafy *et al.* 2011a,b Nesarikar *et al.*, 2012). In the following section, a literature review of experimental work on roll compaction is presented.

3.3.1 System layouts

Sealing system

In order to minimise leakage during roll compaction, stationary side seals termed cheek plates have been added to block the bypassing powder (Miller, 1997). However, an adequate supply of powder was not delivered to the compaction zone even with screw feeding system because the check plate acted as a resistance to the powder flow (Parrot, 1981). In addition, the compaction pressure was greater toward the middle of the width of the rolls compared to the edges (Funakoshi *et al.*, 1977). Funakoshi *et al.* (1977) designed a concavo-convex roll pair to seal the material leakage and improve the uniformity of the pressure across the width of the roll surfaces. In the design, there are rims on one of the rolls and notches on the other to ensure a mutually fix of the rolls. The authors indicated that the design provided an adequate supply of powder to the compaction zone, and the powder was fully conveyed into the minimum roll gap. In addition, a uniformity index P_{max}/P_{min} given by the maximum and minimum pressures across the roll surface width was combined with the amount of leaked powder to evaluate the efficiency of the sealing system. They examined these factors at various rim wall slope angles, and found that 65 °was the optimal of the concavity.

Deaeration

Air aeration was believed to be another reason causing inhomogeneous compaction and therefore limited the quality of the compacts. Spinov and Vinogradov (1967) carried out roll compaction using an instrumented roll compactor to investigate the effect of air aeration. The rolls were 120 mm in diameter. The roll speed was maintained constant at 17.5 mm/min throughout all the experiments. The sample material was a copper powder with a mean particle size smaller than 40 μm. It was fed into the gap using a hopper with a length of 80 mm and inclination of 48 º. The initial height of the powder bed was 70 mm for all the experiments.

The authors anticipated two types of air flow affecting the compaction behaviour. First is the air flow passing between the particles, which limited the amount of powder fed into the area near the roll gap causing pore formation and low bulk density. To minimise the influence of this type of air flow, it is essential to optimise the roll speed and roll gap. The second type of air flow is that passing along the powder-roll interface. To evaluate the influence of this type of air flow, a vacuum deaeration facility was combined with the roll compactor close to the minimum roll gap. It was found that the pores in the ribbons were reduced and the qualities of the ribbons were improved. The bulk density and porosity of the ribbons were constant in this case, which suggested that the formation of the pores and unstable densification were caused by aeration, as expected.

Feeding system

In roll compaction, powders are fed by either gravity or by means of screws (Guigon and Simon, 2003, Miller, 1997). Feeding is problematic when using a gravity feed system, especially for fine powders (Simon and Guigon, 2000). The problem is attributed to the poor de-aeration ability and insufficient flowability of such powders. Therefore, a screw feed system is employed. In this case, the roll compaction behaviour is not only affected by the roll parameters such as roll speed and roll gap but also by the feed conditions (*e.g.* feed speed).

Inghelbrecht and Remon (1998) investigated roll compaction of 4 different types of lactose powder with distinct particle size, bulk density and morphology using a Fitzpatrick L83 Chilsonator (The Fitzpatrick Company, Elmhurst, USA). The powder was fed into the compaction zone by a feeding system consisting of a vertical and horizontal screw. The roll compaction behaviour and granule friability were investigated in order to evaluate the effects of the process parameters such as roll pressure, roll speed and screw speed. They argued that the pressure was the most important parameter followed by the roll speed and the horizontal screw speed. The products with highest tensile strengthswere obtained at a high pressure and a low horizontal screw speed at any roll speeds.

Simon and Guigon (2003) carried out roll compaction of lactose, alumina and sodium chloride on a B100 QC laboratory scale roll compactor (Komarek®). The vertically arranged rolls with a diameter of 130 mm and width of 50 mm were initially separated 0.8 mm from each other. A single screw feeder was used to drive the powders into the compaction zone. In order to determine the influence of powder properties and feeding conditions on the compaction, the distribution of the effective applied stress in the roll gap during the process was measured by two flush-mounted piezoelectric transducers fitted on the upper roll. It was observed that the measured pressure fluctuated and was not homogeneous along the roll width during the roll compaction. A variation of density and strength on the compacted strip according to the fluctuations of the screw feeding rate was also observed. They indicated that the heterogeneity of the compact properties was caused by the heterogeneity of the feeding pressure, which was primarily due to the powder packing occurred in the last flight of the screw feeder, and the local pressure in the feeding zone varied with time at the same rate as the screw feed rate.

Michrafy *et al.* (2011a) performed roll compaction experiments on MCC (Avicel PH 102) using a vertical-layout roll compactor combined with a horizontal feeding screw. Cheek plates were installed on both sides of the roll assemble to prevent the leakage. They analysed the density homogeneity of the ribbons using light transmission and mercury porosimetry measurements. Both approaches resulted in heterogeneity of the density across ribbon width: the light transmission revealed periodic heterogeneity shown by darker and lighter zones of

the compacted strip, whereas the mercury porosimetry showed higher densities at the central part of the compact and lower densities at the sides.

Nevertheless, Lecompte *et al*. (2005) showed that a homogeneous pressure distribution along the roll width could be obtained using a single screw feeder. They roll compacted organic powders with an instrumented roll compactor, combined with a horizontal screw feeder. In order to obtain an accurate pressure distribution along the roll width, three pressure sensors were used. The first sensor was located at the centre of the roll width, the second at one-third and the third at two-thirds of the roll half width. The sensors were located at the roll surface, 120 ^{o}apart from each other. In contrast to the work of Simon and Guigon (2003), they showed that a homogeneous pressure distribution was achievable with a single screw feeder at a high feeding rate and low roll speed. Correspondingly, ribbons of better quality (*i.e.* higher density and mechanical strength) with reduced porosity were produced.

3.3.2 Effects of powder properties and process parameters

Inghelbrecht and Remon (1998) evaluated the influence of particle size on the range of the processing parameters (*i.e.* vertical and horizontal screw speed, roll speed) available for a success roll compaction. For lactose, with a smaller particle size with a poor flowability but reasonable binding properties, the range in which the value of the horizontal screw speed could be varied was larger than that for lactose, which had a relatively larger particle size. It was also reported that there were difficulties in roll compacting spray dried lactose, which were observed due to the leakage caused by the excellent flowability.

Mansa *et al.* (2006) performed roll compaction on pharmaceutical powders using a roll compactor with rolls of width 45 mm and diameter 200 mm. The roll speed was varied between 0.5 and 9 rpm, and the roll gap was adjusted between 0.5 and 5 mm. The roll compaction behaviour of powder formulations such as MCC (Comprecel M101) and DCPA (Anhydrous Emcompress) and mixtures of these two powders with various ratios was investigated. It was found that an increase in the effective friction angle and cohesion of the

feed powder resulted in an increase of the nip angle. On the other hand, increasing the roll speed led to a reduction in the nip angle. It was observed that the relative densities of the ribbons increased with the average maximum pressure generated during roll compaction at lower roll speed (1 – 3 rpm). The trend was particularly pronounced for pure MCC. The authors ascribed the observation to a combination of particle size effects and mechanical properties for MCC. They argued that the wide particle size distribution of MCC resulted in a greater capacity for pore filling and the particles were more easily able to yield and deform under the compression. In addition, the needle shape of the particles contributed to a stable compacted form.

Bindhumadhavan *et al.* (2005) carried out roll compaction experiments on MCC (Avicel PH 102) using a instrumented gravity-fed roll compactor. The roll gap was adjusted in a range of 0.9 to 2 mm at a roll speed of 2 rpm. MCC powders were lubricated to vary the wall frictional properties. A Peschl® rotational split level shear tester was used to provide the accurate values of effective internal friction angle and the wall friction angle of the feeding powders. They found that the maximum pressure was quite sensitive to the variation of the flow properties of the feed powders, and increased with increasing wall friction at the interface between the powders and stainless steel roll surfaces.

Miguélez-Morán *et al.* (2008) examined the effect of lubrication during the roll compaction of microcrystalline cellulose using an instrumented roll compactor. A common used pharmaceutical lubricant magnesium stearate (MgSt) was employed as the lubricant. In order to investigate the influence of lubricant, no lubricant, bulk lubricant and wall lubricant cases were considered. The ribbons produced were sectioned to evaluate the variation of the bulk density along the roll width. It was observed that wall lubrication did not affect the roll compaction behaviour and ribbon density. On the other hand, bulk lubrication caused a reduction in both the nip angle and maximum pressure, but a smaller variation across the ribbon width. They suggested that the nip angle, maximum pressure and variation in density across the ribbon width increase as the friction increases. The authors argued that that the homogeneity of the ribbon density was dominated by the way that the powders were fed into the roll compactor. A term ‘drag angle’, which denoted the angle formed between the centre and the edges of the roll when the powder was dragged into the roll gap, was introduced to

describe the uniformity of the powder feeding. It was suggested that the larger difference between the powder flow in the middle of the roll width and those at the edges leads to a smaller drag angle. A drag angle of 180 ºindicated a uniform feeding of the powder.

von Eggelkraut Gottanka *et al.* (2002) conducted roll compaction on dry extracts of a plant *H. perforatum* L., containing magnesium stearate as a lubricant, using a GMP Mini-Pactor (Gerteis, Switzerland). The instrument consisted of a feed hopper system, a pair of counter-rotating rolls and a granulation unit. A constant powder flow was fed into the roll compactor. The roll speed was varied between 0.5 and 30 rpm. The compaction force was controlled by a hydraulic pressure system, between 0.5 and 20 kN/cm (force per cm of the roll width). The roll gap was maintained by the feeding rate, varying between 0.8 and 6 mm. It was reported that the roll compaction yielded granules with a reduced amount of fines and improved flowability. It was also found that the mean particle sizes of the granules increased with increasing compaction forces. In addition, they suggested that the poor flowability of the feed powders with a small particle size might result in the fluctuation of the powder filling even when a screw feeder was used. This phenomenon might cause aeration during roll compaction, which could facilitate the formation of pores in compacted ribbons and therefore limited densification as reported in Spinov and Vinogradov (1967).

Parrot (1981) carried out roll compaction of several common pharmaceutical powders using a concavo-convex roll compactor. An oscillating granulator in which ribbons could be broken by oscillating impellers over a screen of selected mesh was combined to produce granules. The particle size, flowability and density of unprocessed powders and compacts produced by roll compaction were analysed to evaluate the effects of the process. It was found that for most powders, the particle size, flowability and bulk density increased after the roll compaction except for lactose and dibasic calcium phosphate. The author argued that this observation might be due to the brittle nature of these two materials. Moreover, it was reported that the density of the compacts increased as the compaction pressure increased. Moreover, a linear relationship between the bulk density and the logarithm of the compaction pressure was observed.

Wu *et al.* (2010b) roll compacted MCC (Avicel PH 102) powder with different amount added water to evaluate the effects of the moisture content. The cohesion, frictional properties (*i.e.* internal frictional angle) and angle of repose were measured to characteristic the moist powders. The process outputs (*i.e.* pressure distribution and nip angle) were recorded to describe the process. It was found that the internal friction angle and flowability for MCC decreased with increasing moisture content, while the cohesion increased. The maximum pressure was approximately constant at moisture content < 10%, but increased sharply when the moisture content was greater than 10%. The authors argued that this could be attributed to the increase in cohesion and the decrease in the flowability and internal friction, which led to a larger amount of powder fed into the compaction zone and compressed. They suggested that the maximum pressure was directly related to the powder flow properties (*i.e.* cohesion, flowability and internal friction). It was also reported that the nip angle decreased sharply when the moisture content was greater than 10%, which was also ascribed to the variation in powder flow properties.

3.3.3 Shear-driven observations

Asymmetric neutral angle

Lecompte *et al*. (2005) found that the compaction of a powder mainly occurred along the centre line of the roll width when the ratio of feeding rate to roll speed was small enough (say < 1). In addition, they found that the maximum pressure generated in roll compaction did not always occur at the minimum roll gap, but up to 3 °away from it. Furthermore, the maximum pressure was further from the minimum roll gap when the feeding-rolling ratio increased.

This was consistent with the observation first reported by Chekmarev *et al.* (1963) that the pressure profiles in roll compaction are asymmetrical and not always centred on the smallest roll gap. Radchenko (1974) suggested that a neutral angle *i.e.* the angular distance between the maximum pressure and the minimum gap, could be introduced to represent this phenomenon.

Experimental work on the shear stress and pressure distribution also suggested that the neutral angle does not coincide with the maximum pressure. Schönert and Sander (2002) investigated the shear stresses and material slip in a high pressure roll mill using a lab-scale instrument with smooth rolls of 200 mm in diameter and 100 mm in width. A sensor with a two-legged cross section having a separating angle of 90 ° was designed for measuring the normal and shear stresses simultaneously. Their results showed that the measured maximum pressure and zero shear stress did not occur at the same angular position. This suggested that the maximum pressure is not obtained at the neutral angle in the roll compaction of powder materials according to the definition of the neutral angle (Vinogradov *et al*., 1970).

In addition, Schönert and Sander (2002) attempted to explore the relationship between the normal pressure and shear stress in roll compaction. By assuming proportionality between the transversal pressure in the powder bed and the normal pressure on the roll, an equation relating the shear stress to the normal pressure was obtained according to the force balance on a differential strip:

$$\tau_R = -k_s\left(\frac{\lambda dp_R}{d\theta} - \frac{p_R d\lambda}{d\theta}\right) + (1-\lambda)p_R\theta \qquad \text{Eq (3.14)}$$

where τ_R is the shear stress on the roll surfaces, p_R is the normal stress acting on the roll, θ is the current angular position. k_s is a factor determined by angular position θ, minimuim roll gap S and roll diameter D , equal to $\frac{S}{D}+\frac{\theta^2}{2}$. λ is a horizontal load ratio with values between the Poisson's ratio of the material and 1; $\lambda = 1$ indicates that the material behaves like a fluid.

They found that material slip only existed near the outlet of the release region, which caused a 'tensile force' on the material above the smallest roll gap and increased due to the shear on the rolls. This 'tensile force' acted in the rolling direction and created an additional tangential

force on the rolls. This force could explain the increase in maximum pressure just above the smallest gap. In terms of the comparison between predicted and experimental results, it was argued that there were two regions: 1) the calculated and measured shear stress agreed well and 2) the calculated and measured shear stress showed substantial divergence. The authors suggested that the divergence in the second region was due to material slip close to the minimum roll gap.

Inhomogeneous distribution along the roll width

Cunningham *et al.* (2010) observed that the pressure distribution through the roll width was not uniform. The lowest pressure was found at the edge of the roll and the highest pressure did not occurred at the centre of the roll, but the area between the edge and the centre. These observations were ascribed to the nature of side friction and the nature of the screw feeder. Although the screw feeder was placed in the centre of the roll gap, the pressurisation was not symmetric around its axis of rotation because of the helical geometry. They found that the variation of the pressure along the width was determined by the feeding rate at the local position. In addition, they suggested that the frictional resistance at the side seal further reduced the flow to the edge, and hence the pressure at that position.

Nesarikar *et al.* (2012) carried out roll compaction experiments on blends of excipients (*i.e.* MCC Avicel PH 102 and anhydrous lactose at 1:1 ratio with sodium croscarmellose, colloidal silicon dioxide, and MgSt) and active ingredient using an instrumented roll compactor. Three force transducers were installed linearly along the width of the roll, with one in the centre and the other two on sides. It was found that normal pressure recorded by the side sensors were lower than those recorded by the central sensor. The data from the side sensors showed greater variability than of the central sensor. In addition, it was found that the normal pressure was directly proportional to hydraulic pressure and inversely to screw speed/ roll speed ratio.

Miguélez-Morán, A.M. *et al.* (2009, 2008) examined the density distribution of MCC ribbons using a sectioning approach, micro-indentation, and X-ray micro-computed tomography. It was shown that all three techniques could produce comparable results provided that proper calibration was performed. They found that the densities in the middle of the ribbon width were higher than those at edges due to non-uniform powder feeding caused by the friction on the side cheek plates. Wu *et al.* (2010b) analysed the SEM images of the ribbons made from moist MCC (*i.e.* moisture content in a range of 4 to 15 %, w/w) and reported that the powder was compressed to a denser state in the middle of the ribbon compared to the edges, which indicated that a higher density was achieved in the middle of the ribbon width, consistent with the observation by Miguélez-Morán, A.M. *et al.* (2009, 2008). Furthermore, they found that the ribbons split into two halves at the central line due to the reduction in the mechanical strength of ribbons with sufficiently high moisture content > 10%.

3.3.3 Process prediction

A method for simulating the roll compaction process using a laboratory scale compaction simulator was proposed by Zinchuk *et al.* (2004). A mathematical expression based on a sine function of roll speed in roll compaction (Eq 3.16) was proposed to model the motion of a point on the circumference of the roll:

$$D_{punch} = R \sin[\omega t] \qquad \text{Eq (3.15)}$$

where D_{punch} is the displacement of the punches, R is the radius of the real roll, ω is the rotation rate of the roll in sec^{-1} and t is time in sec. The upper and lower punch displacement profiles were defined using Eq (3.16), so that the powder was compressed at the same strain rate as in an actual roll compactor. Once the punches reached the minimum separation, the compact was decompressed before the ejection to simulate the release in the roll compaction process. Thus, a continuous roll compaction process was able to be simulated by a controlled batch process of die compression.

The method was evaluated using microcrystalline cellulose, and ribbon relative density and tensile strength were taken as the key ribbon properties. The tensile strengths of the real and simulated ribbons with the same relative density were measured using the 3-point bend approach. The results showed that the ribbons produced using the compaction simulator had tensile strengths equivalent to those produced using a roll compactor, which indicated that the method is valid for evaluating roll compaction behaviour.

The simulated results showed good agreement for the compression pressure of a simulated roll compaction process at equivalent roll speeds. The authors argued that the model enabled prediction and scale up studies for a roll compaction process in terms of the key parameters. However, the simulation could not account for non-homogeneous ribbon density and material leakage. Furthermore, the shear stress on the roll-powder interface could not be considered in the model. Hence, the capability of the model is doubtful, especially in the case of feed powders for which the shear stress plays a more important role in roll compaction than microcrystalline cellulose.

Patel *et al.* (2010) predicted the roll compaction behaviour for MCC (Avicel PH 102) using Johanson's theory (1965) according to the compressibility factor determined in confined uniaxial compression. They pointed out that the definition of the nip angle in Johanson's model was actually the upper bound at which the empirical pressure-density relationship was valid. In addition, they introduced the Adams' equation (Adams and McKeown, 1996) which was derived based on a microscopic analysis as an alternative to the pressure-density relationship used to evaluate the compressibility of the powder material. Thus, the modified approach was able to describe the compression behaviour of a powder even in the lower strain region unlike Johanson's model. The predicted nip angles and pressure distributions were compared to those obtained experimentally using an instrumented roll compactor. It was found that the nip angle was underestimated at lower roll speeds ($\leq$ 5 rpm), but overestimated at relative high roll speeds (> 5 rpm). The values of the compaction pressure were underestimated for all the processing conditions considered. The authors suggested that this

was due to the fact that the uniaxial compression was only a first order representation of the roll compaction and did not consider the shear component.

3.3.4 Compactibility reduction

Bultman (2002) investigated the effects of multiple roll compactions using microcrystalline cellulose (Avicel PH 101, Lehmann and Voss and Co, D-Hamburg) as a model substance. The granules were re-compacted using a Gerteis 3 W-Polygran roll compactor (GMP Gerteis Maschinen 1 Process engineering AG, CH-Jona) up to 10 times. The process condition was fixed at a roll speed of 2 rpm, a roll gap of 3mm and a 'compaction pressure' of 7 kN/cm. The particle size distribution, flowability and tabletting properties of the granules were examined.

It was reported that multiple compaction resulted in a reduction of fines of the granules, improved flow properties and increased granule sizes. On the other hand, the tensile strength of the subsequent tablets reduced. The author argued that the plastic deformability of MCC led to a significant loss of the dry binding potential by each re-compaction step.

Herting and Kleinebudde (2007) roll compacted binary mixtures of MCC and theophylline with various mixing ratios. The granules were compressed to tablets in order to investigate the effects of flowability and particle size of the feed powders and granules on the tensile strength of the tablets. The results showed that the tensile strength of the tablets was only determined by the particle size of the feed powder or granules fed into the die even after roll compaction. In addition, it was reported that the feed powders with smaller particle sizes led to larger granules with better flowability.

Sun and Himmelspach (2006) investigated the reduced compactibility of roll compacted granules made from different grades of microcrystalline cellulose. The ribbons were produced using a Freund roll compactor (Model TF mini, Vector Corporation, Marion, IA) at

2 rpm roll speed and 39 Kgf/cm^2 roll pressure. The ribbons were then milled into granules using a Quadro CoMil (Model 193AS, Quadro Engineering, Inc., Waterloo, OT, Canada) with an opening size of 229 μm. The corresponding granules were then lubricated by MgSt and tableted using a tableting emulator (Presster, Model 252, Metropolitan Computing Corporation, East Hanover, NJ). They used the term 'compactibility' to describe the capability of a feed to form a tablet. They found that 1) roll compacted granules of smaller size exhibited greater compactibility than a feed with a larger size from the same batch; 2) the compactibility of granules was comparable to to the primary powder with similar particle size; 3) roll compacted granules with sizes smaller than the feed powder showed better compactibility; 4) multiple roll compaction had no effect on the compactibility of the granules provided that the particle size distribution is constant. Therefore, the authors argued that the reduction in compactibility of roll compacted granules was caused by granule-size enlargement.

Herting and Kleinebudde (2008), however, gave a different explanation of the phenomenon. They carried out similar experiments on microcrystalline cellulose. In this study, an instrumented roll compactor (Mini-Pactor, Gerteis, Switzerland) with 25 cm roll diameter and 2.5 cm roll width was used to prepare the ribbons, at a roll gap of 3 mm and roll speed of 1 rpm. The ribbons were granulated using a pocket mould grooved granulator with a 1.25mm screen mesh. They suggested that the compactibility reduction was caused by work hardening, which was a combination of particle size enlargement and hardening of the material as proposed by Malkowska and Khan (1983). The observation that tablets of higher tensile strengths were obtained from raw materials with smaller particle size was viewed as evidence to support the argument. There were still uncertainties since the experimental conditions in the two studies were not identical. Despite the differences in the feed powders and processing parameters, the presence of magnesium stearate might result in a reduction in the bonding properties for the host particles and therefore decreasing compactibility. For this reason, the conclusion from Herting and Kleinebudde (2008) seems more reliable for a single component formulation (*i.e.* microcrystalline cellulose). The results from Sun and Himmelspach (2006) and Herting and Kleinebudde's previous work (2007) indicated that an apparent granule size enlargement correlation was obtained for simple binary mixtures. Nevertheless, this explanation might not be applicable to other powder materials and realistic mixture formulations.

Kuntz *et al.* (2011) produced tablets from roll compacted acetames granules. The surface area of the feed powders and roll compacted granules were measured using nitrogen adsorption. Crushing forces were measured using a hardness tester (HT1, Sotax, Basel, Switzerland) at a constant speed of 1 mm/s to evaluate the compactibility of the granules. It was reported that the roll compaction induced an increase in compactablity for a specific material, contrary to most investigated pharmaceutical powders. This observation was consistent with the increase in specific surface area arising from the roll compaction process

3.4 Milling

In practise, oscillating granulators are commonly combined with a roll compactor to produce the desired granules (M. G. Herting and Kleinebudde, 2007, Kleinebudde, 2004, Miller, 1997). An oscillating granulator is able to granulate compacted materials (roll compacted ribbons) into granules capable to pass through a wire mesh screen using an oscillating rotor (Vendola and Hancock, 2008). A schematic diagram of the instrument is shown in Fig. 3.6. Wired screens form a milling chamber, in which a milling blade acts a reciprocating movements with a fixed rotating angle to fracture the feeding materials. The size of the milled granules is controlled by the mill-screen size, the rotor speed, and the rotation angle of the rotor (Lantz, 1990).

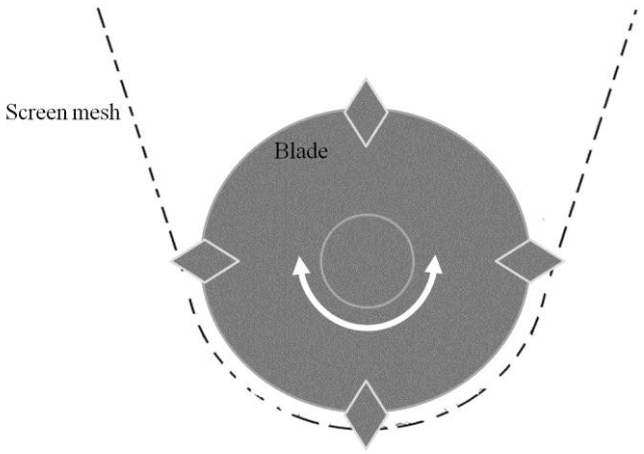

Figure 3.6 Schematic diagram of an oscillating mill.

Abraham and Cunningham (2008) reported that an oscillating granulator could be used as a downstream granulator to provide a composition with improved flow characteristics and a reduced amount of fine particles. Their data showed that an oscillating granulator produced coarser granules comparing to comil or flitzmil with the same mesh size.

Sakwanichol *et al.* (2012) evaluated the granule properties obtained from an oscillating granulator and roll mill. They varied four oscillating-granulator parameters *i.e.* rotor speed, oscillating angle, aperture of mesh screen and rotor type, and six roll-mill parameters, *i.e.* throughput, speed ratio in both first and second stages, gap between roll pair in both stages and roll-surface texture. They compared the granules with similar median particle size from both mills. For an oscillating mill, they concluded that all the examined parameters affected significantly the granule size distribution. However, the rotor types of the oscillating granulator did not affect the amount of fine particles.

3.5 Tabletting

In practical pharmaceutical manufacturing, the roll compaction produces flake-like compacts which are milled to granules ready for tablet compression (Bennett and Cole, 2003). Therefore, the properties of the ribbons greatly affect the tableting process (*i.e.* filling, compression) and properties (*i.e.* tablet strength, density, and dissolution rate) of the final tablet. The effects of the properties of the feeding powder/granules on the tabletting are introduced in the following sections.

3.5.1 Density

Xie and Puri (2012) investigated the die filling process using a pressure deposition tester. They evaluated the pressure distribution of powders during filling with various densities in a multiple die system. The results showed that low bulk density of the feed leads to irregular pressure profiles that are complicated and irreproducible. Essentially, the small values of the

particle density may lead to non-uniform powder filling and therefore inhomogeneous of final products. Guo *et al.* (2010) conducted an investigation of the density – induced segregation using numerical methods. The segregation behaviour of a binary mixture of particles with same size but distinct densities was studied. It was reported that difference in densities resulted in segregation in gravity feeding systems *i.e.* particles with small densities tended to settle on the top of the final powder pattern while denser particles at the bottom. It was also found that this tendency was enhanced in the presence of air.

3.5.2 Particle size and shape

The shape and size of particles may greatly affect the die filling behaviour of feed powders in tabletting. Previous research suggested that the influence of particles shape and size are mainly reflected in the interaction with air (Guo *et al*., 2009, Wu *et al*., 2010a, 2012, Yaginuma *et al*., 2007).

Yaginuma *et al.* (2007) explored the flow behaviour of a powder during high-speed tabletting. They reported excellent die filling properties of needle shape MCC which was suggested to be suitable for high-speed tabletting due to the particle shape which held air uniformly in a powder bed when agitated during feeding. Xie and Puri (2012) reported that powder deposition was affected by the physical properties (*i.e.* particle size and shape). It was found that powders with various particle sizes and shapes behaved differently when filled in E-shaped dies, as indicated by the pressure distribution. The denser powder with larger-size and less spherical particles had the highest pressure close to the back, but the smaller spherical particles with lower density had the highest pressure in the middle.

Wu *et al.* (2010a) performed a quantitative investigation of powder flow during die filling for two grades of spherical microcrystalline cellulose (MCC). The velocities of individual particles were monitored using Positron Emission Particle Tracking (PEPT) technique. The results showed that higher falling velocities were achieved for larger particles in a gravity forced system, which resulted in improved efficiency. Wu *et al.* (2010a) explained that the

observations were caused by the presence of air in the die that significantly inhibited the flow of small particle but only showed limited effects on large particles. The previous numerical simulation work obtained using a coupled discrete element method and computational fluid dynamics (DEM/CFD) model (Guo *et al*., 2009) implied similar results. Guo *et al*. (2009) modelled the die filling process and concluded that the presence of air limited the flow of particles with smaller size and density. In contrast, there were no differences in the mass flow between particles with various densities and sizes in a vacuum system. Conclusively, experimental and simulation works both verified that the impact of air on the particle shape and sizes.

3.5.3 Flow and frictional properties

Flow and frictional properties play considerably important roles in the production of tablets. Specifically, the feeding behaviour shows a strong dependency on the flowability of a powder. The friction generates resistance to relative motion between the powder and tool surface, and therefore affects the compression behaviour and tablet properties.

Yaginuma *et al.* (2007) explored the correlation between powder behaviour in tabletting and powder flowability. This involved a mixture of microcrystalline cellulose and spray-dried lactose whose static and dynamic flowability were experimentally measured by an angle of repose tester and a powder rheometer, respectively. They indicated that the behaviour of the powder in a gravity feeding system was dominated by the static flowability, and the critical factor is the dynamic flowability in force feeding cases. Xie and Puri (2012) explained that the difficulty of die filling of powders with smaller particles was due to poor flowability as a result of a small mean particle size. However, contrary arguments which suggested the independence of the filling behaviour on the powder flowability have been published. Felton *et al.* (2002) investigated capsule filling using a tamping-tape encapsulation apparatus. Formulations containing microcrystalline cellulose (MCC) and silicified microcrystalline cellulose (SMCC) were used to explore the influence of the flowability of the powders. It was reported that higher fill weights and a lower variation in the fill weights were achieved with SMCC formulations, which has better flowability. However, the values of fill weights and the

weight variation were not significantly different from those for MCC samples. Therefore, Felton *et al.* (2002) suggested that the powder flow did affect the weight uniformity during encapsulation using a tamping-type system, but it may not be a critical parameter. This observation might be ascribed to the similarity of the powder nature of MCC and SMCC, and the specification of the tamping-type system since the powder patterns were affected by the tapping and the influence of air was minimised.

Sinka *et al.* (2003) investigated the compression of tablets with curved faces and explored the impact of internal friction and wall friction. It was reported that increasing the internal friction resulted in a significant enhancement in the density of the tablets due to the improved binding properties of the particles. Increasing the wall friction gave the same trend, although the magnitude of the increase was relatively small. In addition, the density distribution of the tablets was determined by the magnitude of the wall friction. The peak density was found on the edge of the tablets (close to the die wall) and the smallest values at the centre when there was significant wall friction. However, an opposite trend was observed when lubrication was applied on the die wall to reduce the wall friction.

3.6 Conclusions

This chapter discussed the application of roll compaction in the pharmaceutical industry. The major theoretical models proposed to describe the process and the experimental work exploring the underlying mechanisms were reviewed. Although many attempts have been made to understand the process, the knowledge of the roll compaction is still limited due to the complex nature of the process and diversity of the feed powders. It was concluded that roll compaction behaviour is greatly affected by the feeding conditions (*i.e.* feeding speed), system layout (*i.e.* sealing system and aeration), processing parameters (*i.e.* roll pressure, roll gap and roll speed) and properties of the feeding powders (*i.e.* particle size, flowability and frictional properties). Thus, a general model describing the performance of the process that can provide reliable prediction and guidance on process design is still not achievable.

Roll compaction is commonly combined with oscillating milling and tabletting to produce a final dosage form. Hence, an understanding of these two downstream processes is necessity for the design and control of roll compaction. The dominating parameters in oscillating granulation and the effects of roll compaction on tabletting were also discussed in this section.

Limited work has been reported on the different behaviour of pharmaceutical powders with distinct properties. The information about mechanisms in milling processes and the dependence of the tabletting on roll compaction have received only limited attention. Therefore, an attempt will be made to explore roll compaction and downstream process for different feed powders, and provide a guiding tool for manufacturing design and control. This includes the investigation of effects of powder properties and process parameters on roll compaction, mechanisms in milling and tabletting processes and correlations between them, as to be discussed in this thesis.

CHAPTER 4 MATERIALS AND METHODS

Roll compaction greatly depends on the properties of the feed powders. To understand the influence of their properties, common pharmaceutical excipients with distinctive properties were used in this work, which are introduced in Section 4.1. The preparation of the powders and techniques used to characterise the samples are presented in Section 4.2. The measurement of typical powder properties such as particle size, density, frictional and flow properties are discussed. An instrumented roll compactor was employed for roll compression. Section 4.3 introduces the experimental layout and procedure, including ribbon characterisation. In section 4.4 and 4.5, the methodologies used to carry out the investigations on milling and tableting are discussed.

4.1 Materials

Commonly used pharmaceutical excipients were used as sample materials in this work, including microcrystalline cellulose (MCC), di-calcium phosphate dihydrate (DCPD), mannitol, lactose.

4.1.1 Microcrystalline cellulose (MCC)

Microcrystalline cellulose (MCC) is a form of cellulose derived from wood pulp by treating fibrous plants with mineral acids. The commercial form of MCC is disintegrated cellulose consisting of purified, depolymerised cellulose particles with a needle shape (Fig. 4.1) It is insoluble in water, dilute acid, common organic solvents and oils. It is widely used in pharmaceutical industry as ideal filler due to its excellent compactibility under a wide range of compaction pressures and its resistance to organic and non-organic contaminants. In this work, MCC of grades Avicel PH 101 (Fig, 4.1a) and Avicel PH102 (Fig. 4.1b) were used for direct compression. They are white, odourless and tasteless powders with excellent flow properties. These two grades have similar compressiblity but different particle sizes (mean

particle size d_{50} (volume diameter which indicates the diameter of the sphere with the same volume as the particle) of ~ 60 µm for MCC Avicel PH 101, and ~ 100 µm for MCC Avicel PH 102).

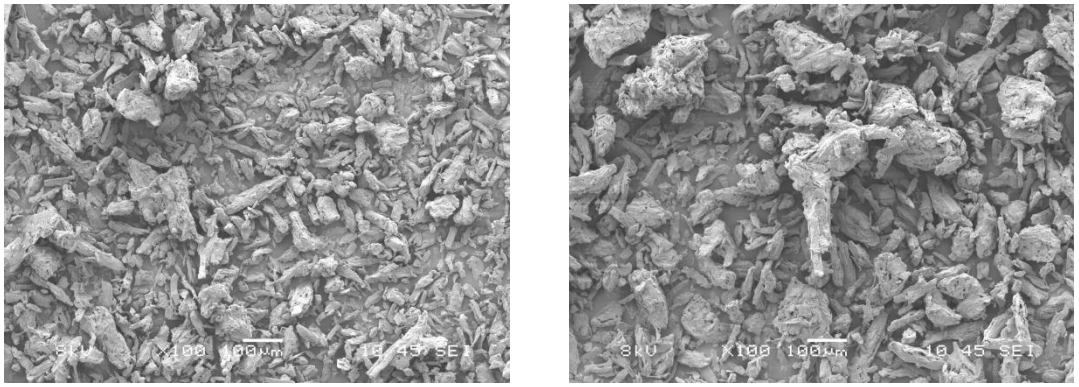

a) b)

Figure 4.1 SEM images of a) MCC Avicel PH 101 and b) MCC Avicel PH 102

4.1.2 Di-calcium phosphate dihydrate (DCPD)

Di-calcium phosphate is an inorganic monohydrogen phosphate, normally in the form of dihydrate. It is produced commercially by reaction between calcium carbonate and phosphoric acid. Di-calcium phosphate dihydrate (DCPD) is partially soluble in alcohol and soluble in dilute mineral acidsIn tablet manufacturing, DCPD is employed as a diluent or a source of calcium and phosphorus for nutritional purposes. In this work, DCPD of grade Calipharm D (Rhodia, France) was selected. It is an odourless, tasteless, white crystalline powder with shale-like shape and small particle size (d_{50} ~ 8 µm), as shown in Fig. 4.2. DCPD (Calipharm D) is brittle in nature so that it tends to fracture under pressure.

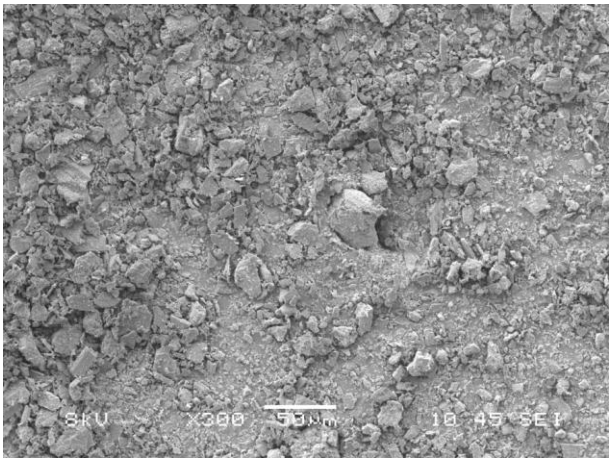

Figure 4.2 SEM image of DCPD (Calipharm D)

4.1.3 Mannitol

Mannitol is a naturally occurring sugar alcohol. It shows high stability to chemical reactions and low hygroscopicity. The substance is soluble in organic solvents, partially insoluble in water, but very slightly soluble in ethanol. In medical applications, mannitol is used as a drug for treating acute glaucoma, cystic fibrosis and bronchiectasis, and as a carrier for transporting active ingredients directly into the brain. In pharmaceutical manufacturing, it has been adopted for the protection of active ingredients and to enhance dissolution. As an excipient, mannitol is suitable for both wet and dry granulation depending on the physical form (powder or granule) and particle size. In this work, mannitol of grade Mannogem powder (SPI Pharma Group, UK) was used. The material is a powder consisting of crystalline particles with a d_{50} of ~ 110 µm (Fig. 4.3).

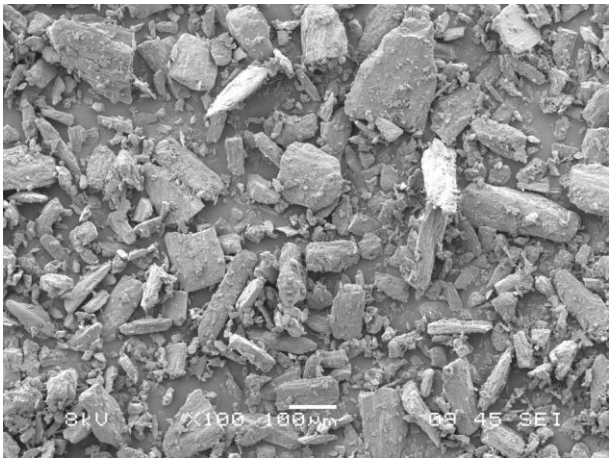

Figure 4.3 SEM image of mannitol

4.1.4 Lactose

Lactose is a disaccharide sugar, produced from extracting sour whey. It is soluble in water, but insoluble in organic solvents. Lactose has been used in pharmaceutical formulation for a long time due to its high stability, low hygroscopicity and relative low cost. Various grades of lactose are available for direct compression, such as spray-dried lactose, beta-anhydrous lactose and alpha-monohydrate lactose crystals (Jivray *et al.*, 2000). In this work, lactose in the form of a spray dried powder (Grade D.C., FMC, USA) was used. It is prepared by spray-drying a suspension of fine α-lactose monohydrate particles in a saturated aqueous solution of lactose. It was the first excipient used as the binder in the direct compression of tablets (Rowe and Roberts, 1996) and is still widely used in pharmaceutical manufacturing. Spray dried lactose is an odourless, white powder with a sweet taste that consists of particles containing 85% α-monohydrate crystals and 15% amorphous lactose (Fig. 4.4).

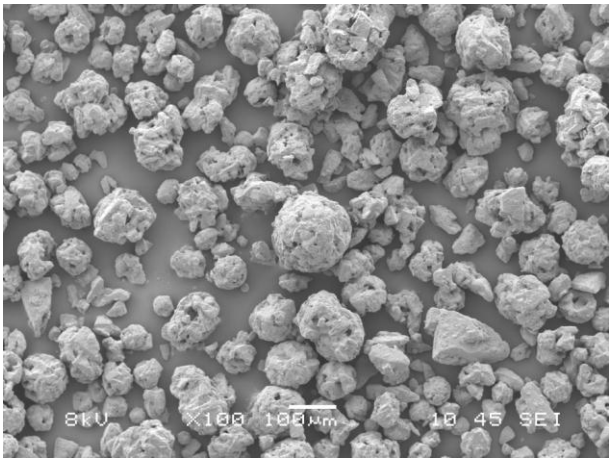

Figure 4.4 SEM image of Lactose

4.1.5 Magnesium Stearate

In pharmaceutical manufacturing, a lubricant is generally required to improve flowability and to prevent adherence to the tool surfaces for processing the most cohesive feed powders. Magnesium stearate (MgSt) is widely used as the lubricant for this purpose. It is a common boundary lubricant and such materials reduce solid-solid friction by forming a film with an interfacial shear strength that is smaller than that of the underlying surfaces. As the most commonly used pharmaceutical lubricant, magnesium stearate (MgSt) is used mainly to prevent a tablet from sticking to the die and punches and, in addition, it minimizes the wear of the tools (Zuurman *et al.*, 1999). Moreover, during uniaxial compression, it allows the feed particles to compact more tightly and homogeneously since the lubricant reduce both the internal and wall friction (Doelker and Massuelle, 2004).

MgSt is produced by the reaction of sodium stearate and magnesium sulphate. It is a white odourless flake-like powder (see Fig. 4.5), which is insoluble in water. The substance is widely used in the pharmaceutical industry since it is considered safe for human consumption at relatively low levels (< 2500 mg/kg per day). Generally, MgSt is added to the system during dry granulation by applying bulk lubrication (Strickland. *et al.*, 1956).

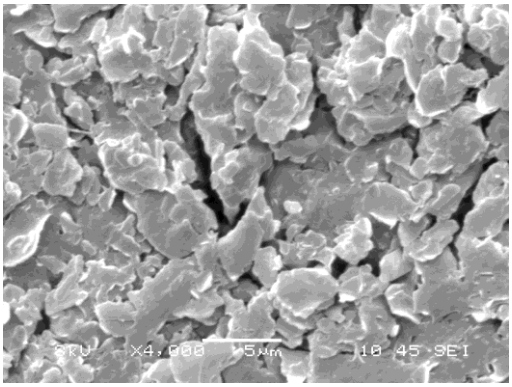

Figure 4.5 SEM image of magnesium stearate.

4.2 Powder Preparation and Characterisation

This section presents the sample preparation involved in the experiments. The measurement of the properties of sample powders such as particle size and shape, true density, frictional and flow properties are also introduced.

4.2.1 Particle size, densities and SEM, surface area

Particle size distribution

A SympaTec laser particle size distribution analyser with (HELOS model, SympaTec, Germany, shown in Fig. 4.6) was used to measure the particle size distribution. The measurement was based on the different diffraction of the laser light by particles of various sizes. The instrument provided a measurement range from 0.1 to 875 μm.

Figure 4.6 Laser particle size analyser (HELOS mode, SympaTec, Germany).

In order to measure the size distribution of granules with larger size (> 875 μm) and shapes of particles and granules, a Qicpic model (Fig. 4. 7) using image analysis was used.

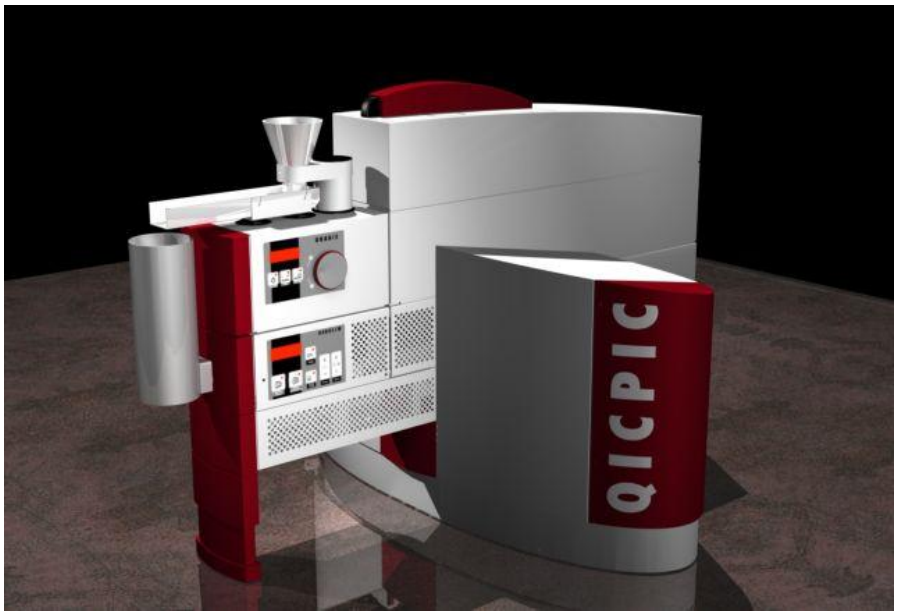

Figure 4.7 Size and shape analyser (Qicpic, SympaTec, Germany).

True density measurement

To measure the true densities of the powders, a helium pycnometer (AccuPycII 1340, Micromeritics USA) was used (Fig. 4.8). The measurements were performed using a chamber with a volume of 1.3327 cm^3, at a temperature of 22 ± 0.5 ℃. The measurements were repeated three times to ensure the reproducibility of the results.

Figure 4.8 Helium pycnometer (AccuPycII 1340, Micromeritics USA).

Surface area

The surface areas of the particles were measured by BET analysis. The term BET was derived from the first initials of Burnauer, Emmett and Teller, and refers to the method of measuring the surface area and porosity of solid materials using the principles of physical adsorption and de-sorption of a gas. An ASAP BET surface area analyser (Micrometrics, USA) using Nitrogen as an adsorptive was employed. The system performs automatic single-point and multi-point BET surface area measurements.

4.2.2 Frictional and flow properties

The effective angle of internal friction was measured using an RST-XS ring shear cell tester (Dietmar Schulze, Germany, Fig. 4.9) with normal stresses in the range of 4 - 10 kPa. This instrument was also used to measure the angles of wall friction against a smooth stainless steel plate (surface roughness R_a ~ 0.3 μm) with normal stresses in the range of 1.1 to 20 kPa.

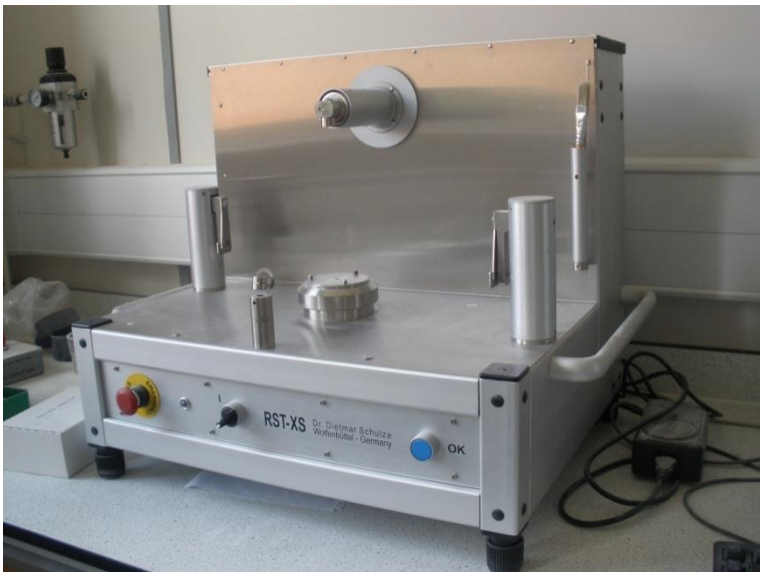

Figure 4.9 The RST-XS ring shear tester.

4.2.3 Powder preparation

Water content control

In order to evaluate the effects of moisture content of powders on roll compaction behaviour, water with a weight concentration of 2.5 to 15 % was added to the powders (*i.e.* MCC 102 powder with initial moisture content of 6.3 ± 0.4% (w/w), DCPD powder with intial moisture content of 5.6 ± 0.2% (w/w)) by gradually spraying on the powder bed while it was agitating in a rotating drum for 30 min to ensure distribution uniformity.

Lubrication

The influence of bulk and wall lubrication was investigated. In order to investigate the influence of bulk lubrication, MgSt in a range of 0.15 to 1.5 % (w/w) was mixed with the sample powders. In the case of wall lubrication, the roll surfaces were lubricated with ethanol suspensions of MgSt with weight concentrations of 0.25 and 1%.

Mixing

In this work, binary mixtures and lubricated powders were used to investigate the influence of powder properties on the behaviour of roll compaction and subsequent processing. For sample preparation, powders and the lubricant were mixed using a double-cone blender at a speed of 72 rpm. The properties (*i.e.* wall friction coefficient and adhesion) of the mixture were sensitive to the mixing time and hence the influence of varying this parameter was investigated (Figs 4.10 and 4.11).

The effects of the mixing time on the wall friction coefficient (μ_w) against the stainless steel surface were measured using ring shear cell tests, as shown in Fig. 4.10. It can be seen that the value reaches the asymptotic value after 1 min.

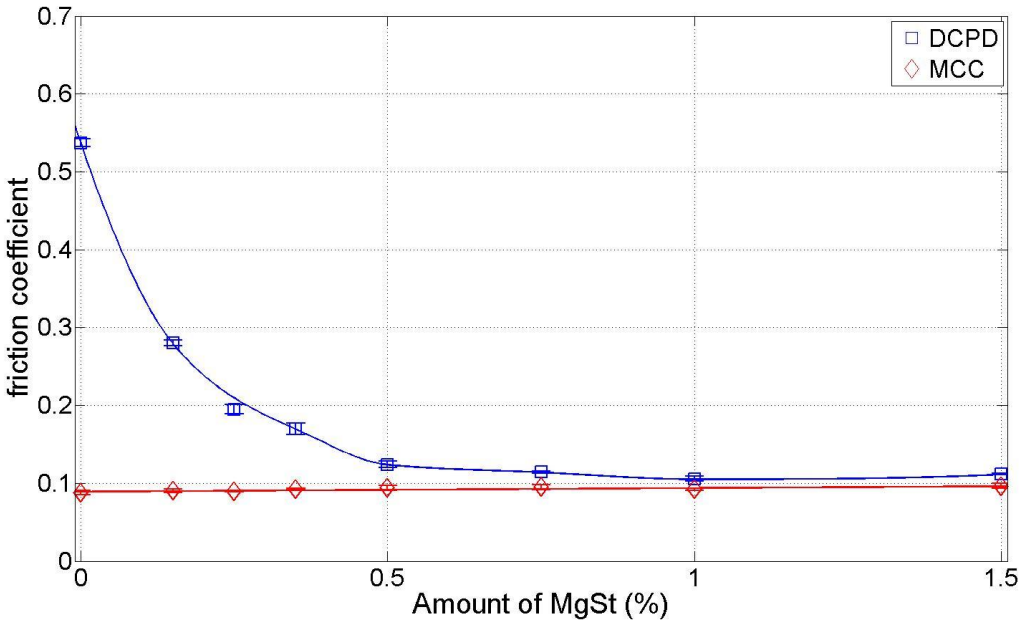

Figure 4.10 Friction coefficient against stainless steel as a function of mixing time.

Figure 4.11 shows the variation of adhesion indicating the attractive force between the particles and the wall surface, which is determined from the correlation of normal force and friction force measured in ring shear cell tests (Appendix 1), with the mixing time. It can be seen that the value for DCPD decreases sharply in the first minute of mixing and reaches 0.1 after 10 min since the layer of MgSt on the particle surface would lead to great reduction in attractive force even at small mixing time. Prolonged mixing time which produced more uniform coating of MgSt resulted in decreasing amount of the uncoated particles, and hence further reduction in adhesion. In contrast, the initial value of the adhesion for MCC is smaller (*i.e.* ~ 0.5) and decreases gradually with the mixing time. It was noted that the experimental error for the adhesion measurement using ring shear cell tests was relatively large (see Fig. 4.11) due to the sensitivity of the adhesion value to the lubrication on the wall surface, which is affected by the mixing time and possibile segregation occurs when feeding the powders into the cell.

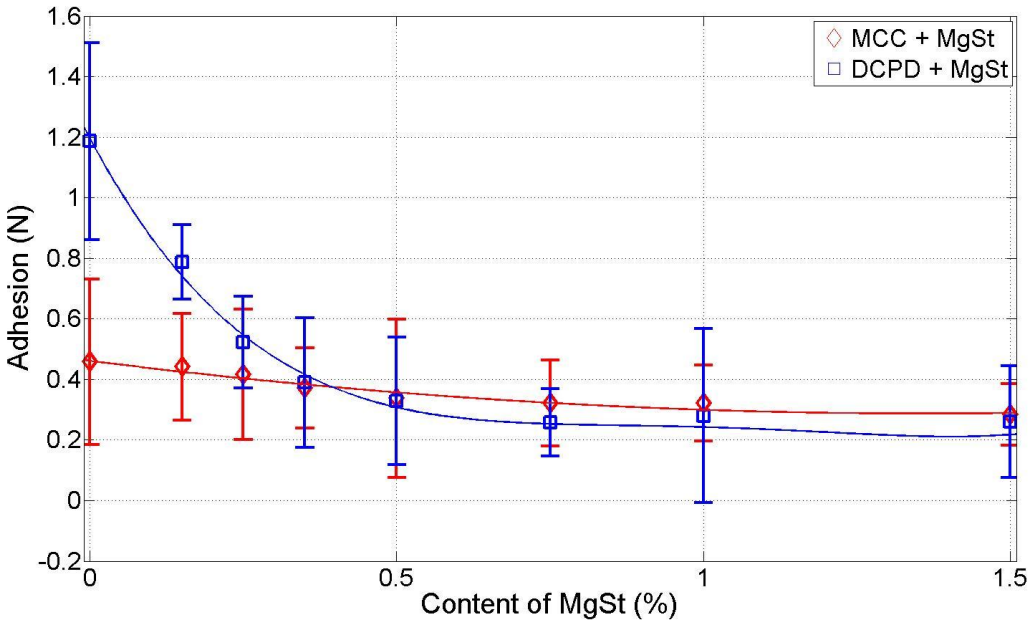

Figure 4.11 The variation of adhesion with mixing time.

The studies revealed that the frictional and flow properties of the powders did not change for mixing times longer than 5 min for MCC, 10 min for DCPD. Thus, these time periods was selected as the mixing time for the preparation of the binary mixture and lubricated powders.

4.3 Ribbon Characterisation

The roll compaction instrument and approaches used to analyse the data are introduced in this section. The characterisation techniques used to measure the densities, surface morphologies and strength of the ribbon compacts are also discussed.

4.3.1 Ribbon production – roll compaction

Roll compaction process

The powders were compacted using a laboratory scale instrumented roll compactor (Fig. 4.12) developed at the University of Birmingham (Bindhumadhavan *et al*., 2005, Miguélez-Morán *et al*., 2008, Patel *et al*., 2010). It consists of two smooth stainless steel rolls (R_a ~ 0.3 μm) of 46 mm in width and 100 mm in radius. Gravity powder feeding was employed, which involved an initial constant volume of powder in a hopper with a rectangular cross-section that was filled manually, and the excess was levelled gently. In the current study, the minimum roll gap, *S*, was varied in the range 0.8 to 1.4 mm, and the roll speed, *u*, was varied in the range 0.5 to 5 rpm. The angular position, θ, is measured with reference to the minimum roll gap. A piezo-electric pressure sensor (PCB 105C33, Techni-Measure, Studley, UK), which is fitted in the centre of one roll, allowed the corresponding radial roll pressure, *p* to be obtained.

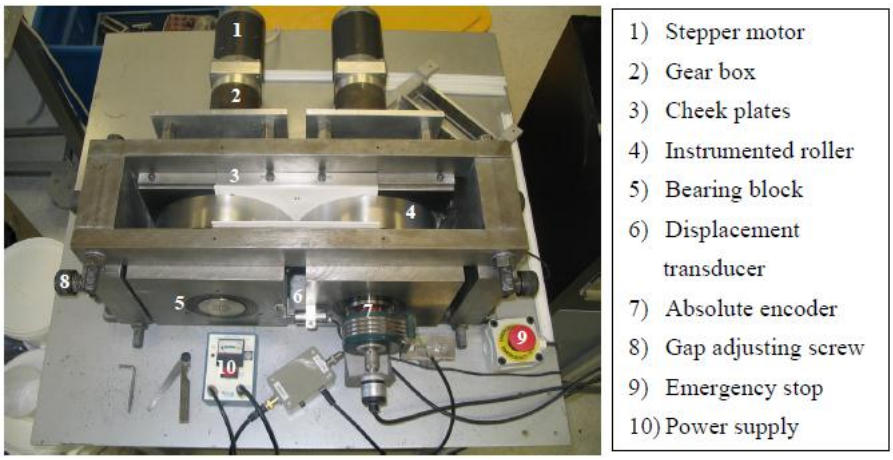

Figure 4.12 Laboratory scale instrumented roller compactor (Bindhumadhavan, 2004).

Typical pressure distributions for DCPD and MCC are presented as a function of angular position in Fig. 4.13, for which the roll speed is 1.0 rpm and the roll gap is 1 mm. It is noticed that negative values of the pressure were obtained after the minimum roll gap, due to the restoration of the pressure transducer. The pressures generated in roll compaction for DCPD were smaller than MCC, which might be ascribed to the air aeration and insufficient feeding.

From the measured pressure profiles, the maximum pressure was determined, which indicate the extent of compression and the nip angle that defines the extent of compression zone, as discussed in the next section.

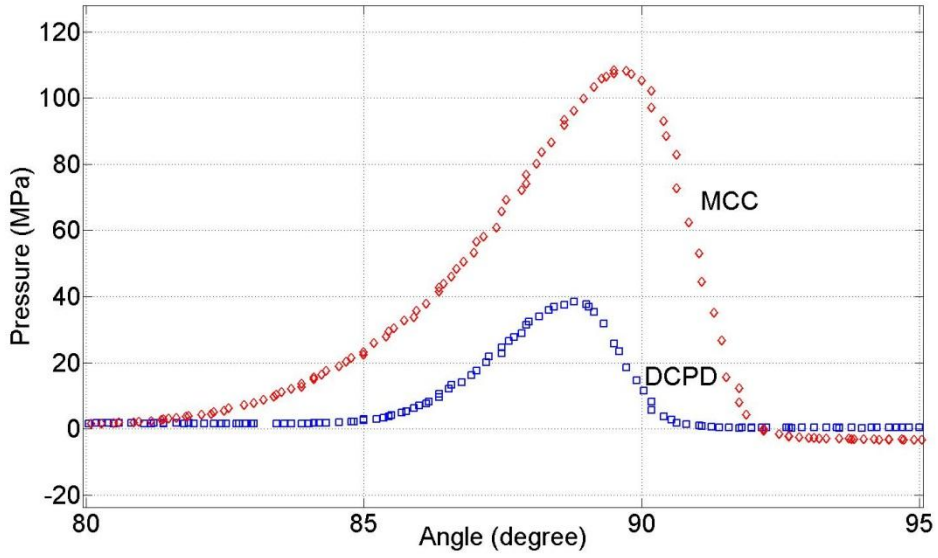

Figure 4.13 Pressure profiles as a function of angular position for MCC and DCPD (S = 1.0 mm, u = 1.0 rpm), the zero angle corresponds to the minimum roll gap.

Nip angle determination

The angular location at which the pressure starts to increase can be treated as a first order approximation to the value of the nip angle. There is a significant uncertainty in estimating the nip angle using this method due to artificial error and neglect of the physical meaning of the term. In order to obtain accurate value of the nip angle, various alternative approaches have been proposed. Johanson (1965) adopted the Jenike-Shield yield criterion and proposed a method to determine the nip angle as discussed in Chapter 3.

Using Johanson's approach (Johanson, 1965), the nip angle can be determined only if the frictional properties and compressibility, κ , are accurately measured using techniques, such as shear cell tests and uniaxial compression. Since the wall friction angle is a parameter for a

powder in contact with a given wall surface and depends significantly on the wall material, exactly the same wall material with the same surface finish as the roll surface should be used for the measurements. In practice, this is difficult to achieve. Furthermore, it is still questionable whether shear cell testers give an accurate value of the wall friction as it generally varies with the applied normal stresses. Moreover, the effects of roll speed are not considered in Johanson's approach (1965), so that it cannot be used to explore the effects of roll speed.

In order to obtain the nip angle experimentally from the pressure measurements using an instrumented roll compactor, an alternative method was developed by Bindhumadhavan *et al*. (2005). The nip angle was defined as the difference between two pre-defined angular positions in the nip and release regions of the measured circumferential roll pressure distributions. These positions were identified with a critical pressure that is relatively small compared to the maximum pressure. The method is convenient and has been used by Miguélez-Morán *et al.* (Miguélez-Morán *et al*., 2008) but the result strongly depends on the critical pressure, which was generally specified from previous experience on some well-studied powders and is consequently of very limited applicability for new powders. Moreover, the potential errors are greater when the maximum pressure is small and a small critical value that is close to zero has to be chosen. Furthermore, the underlying physical concept is somewhat confusing as it apparently defined the nip angle using the data in both the nip and release regions.

Here, a more robust approach is hence adopted for determining the nip angle directly from the measured pressure profiles. It is based on an analysis of the pressure gradient calculated using the measure pressure profiles as follows. Using experimental pressure-angular position data, the incremental pressure ($\Delta\sigma$) and corresponding pressure gradient $\partial\sigma/\partial\theta$ as a function of angular location were fitted numerically. A typical plot of $\partial\sigma/\partial\theta$ with angular position, θ, for MCC and DCPD is shown in Fig. 4.14. The origin represents the angular position at the minimum roll gap and the positive *x*-axis is directed towards the feed zone. The quantity $\partial\sigma/\partial\theta$ has a maximum value at an intermediate angular positions, which corresponds to the nip angle but there is an uncertainty of ± 1 º. However, since the

trend shown in Fig. 4.14 is similar to that predicted from Johanson's theory, the data corresponding to angles less than the maximum value of $\partial \sigma / \sigma \partial \theta$ were fitted to Eq (3.8) and those at greater angles were fitted to Eq (3.6). This involved multivariate fitting and the values of the compressibility factor, κ, which is one of the fitting parameters for the stick region. The obtained compressibility factors are in good agreement with those obtained from uniaxial compression, which will be discussed in Chapter 5.

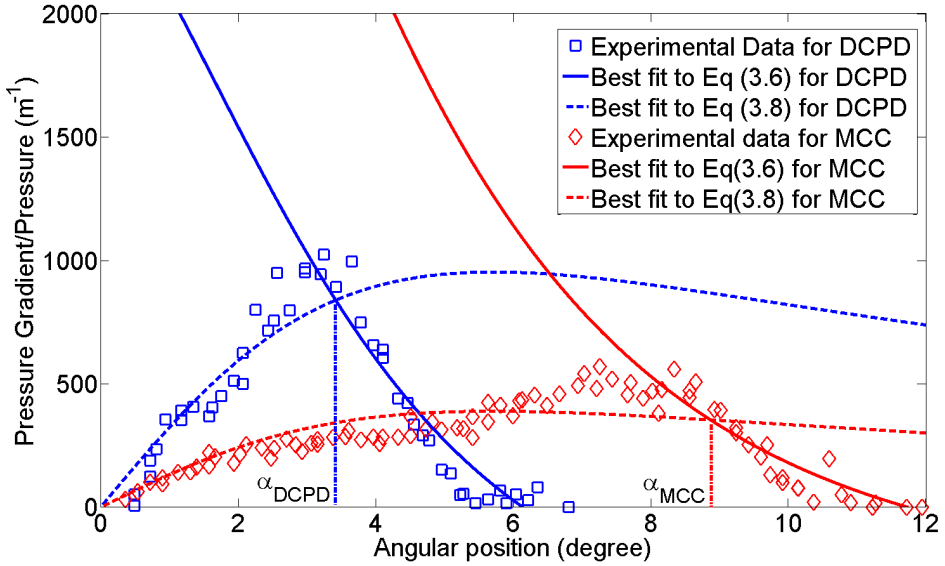

Figure 4.14 The determination of nip angle from pressure gradient data (S =1.0 mm, u =1.0 rpm), α_{DCPD} and α_{MCC} represents the nip angle for DCPD and MCC, respectively.

The main advantages of this method are that 1) it is based on the intrinsic features of slip and no-slip interactions between the powder and roll surface and is thus consistent with the physics of roll compaction, 2) it is applicable to any roll speed and 3) the nip angle can be obtained directly from the pressure profiles obtained from roll compaction experiments without resource to other complicated measurements, which have intrinsic difficulties as discussed previously.

4.3.2 Bulk density of ribbons

The compacted ribbons were cut to blocks of 8 x 40 mm across the width using a bench saw (Scheppach Basato 1, Germany); the dimensions (*i.e.* length, width and thickness) were measured accurately using a digital calliper (Mitutoyo, Hampshire, UK) to determine the volumes. The mass of the ribbons were weighed using a laboratory balance (Ohaus Explorer Precision EP213, USA). The bulk density was calculated based on the mass and dimensions of the cut blocks, following the principles of sectioning method proposed by Miguélez-Morán *et al.* (2009), a density map was obtained as well. In addition, the relative density density of the ribbons was calculated following Eq (2.8).

4.3.3 Surface topography measurement

The surface topography of the ribbons was measured using a white light interferometer (MicroXAM2, KLA Tencor, USA). In the analysis, 3-D interferometric profiling splits a beam of light, reflecting it off both the test and reference surface. The light then recombines and interference patterns are detected by a high resolution camera. This information is then interpreted to provide height information on a pixel basis, building a highly resolved 3D representation of the surface. The system performed a non-destructive analysis on the sample surface, providing information of surface texture, roughness, and 3D structures.

4.3.4 Fracture energy measurement

In order to measure the mechanical properties of the roll compacted ribbons, three point bending tests were carried out using an environmental mechanical analyser (MicroTest 5848, Instron, UK). The configuration of the experiment is shown in Fig. 4.15. The radii of the supporting beams and blade are 0.8 mm. The length of the ribbons between the centres of the supports is approximately 25 mm. The exact values of the dimensions of the ribbons were measured. The force-displacement curve was obtained, as shown in Fig 4.16.

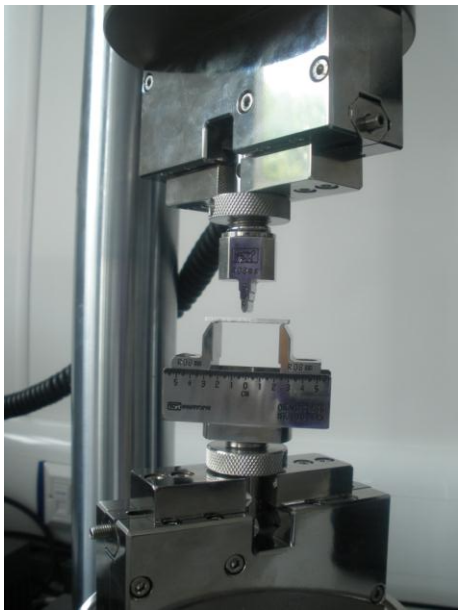

Figure 4.15 The configuration of the 3 point bending experiment.

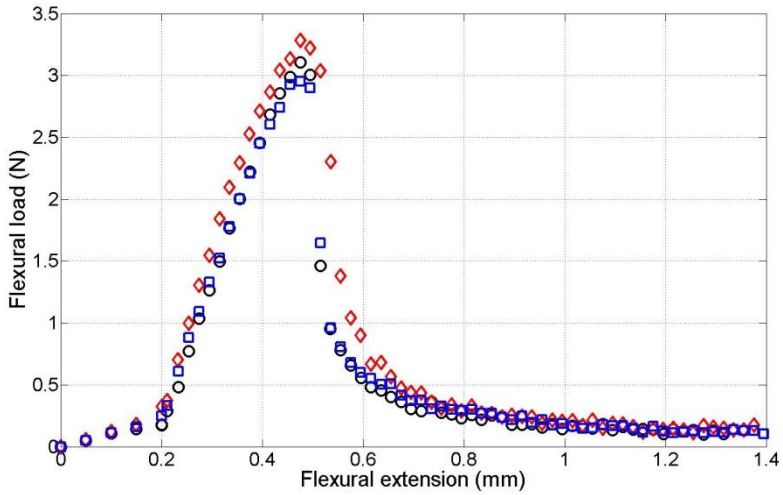

Figure 4.16 Typical 3 point bending force-displacement curves for MCC ribbons produced at S =1.0 mm, u =1.0 rpm.

A term 'fracture energy' G_f ($J \cdot m^{-2}$) that is defined as energy required to create a fracture surface of a unit area was used to describe the strength of the ribbons. The energy ΔU was obtained from the integral of the force curve. Thus, G_f can be calculated by:

$$G_f = \frac{\Delta U}{A} \qquad \text{Eq (4.1)}$$

where A is the fracture area generated in the bending.

4.4 Granulation

The experimental design of the granulation – milling of the ribbons is discussed. The background and layout of PEPT which was used to monitor the ribbon motion during milling are also introduced.

4.4.1 Granule production – oscillating milling

An oscillating granulator (AR 401, Coeply, UK, Fig. 4.17) was employed for the granulation since this type of mill is commonly combined with roll compactors in industrial manufacturing (M. G. Herting and Kleinebudde, 2007, Kleinebudde, 2004, Miller, 1997). As shown in Fig. 4.17, a milling chamber is formed by a milling blade with 4 arms and a screen mesh; both were made of stainless steel. During milling, the blade rotates reciprocally with a rotating angle of 90 º, which breaks the ribbons into granules.

The feed powders were firstly compacted to ribbons using the instrumented roll compactor (Fig. 4.12). In order to obtain coherent ribbons, MCC powder was compacted with the roll gap in a range of 0.8 – 1.4 mm at a constant roll speed of 1 rpm. For DCPD, the roll

compaction was carried out with a roll gap of 1 mm at a roll speed of 1 rpm for comparison. Segments of ribbons (100g) were cut to specific dimensions (approximately 22 x 22 mm) in order to minimise the effects of variations due to different shapes and sizes of feed materials. The milling behaviour of the ribbons at various milling frequencys (*i.e.* from 50 to 330 rpm), and screen sizes (*i.e.* from 630 to 2000 μm) were examined. The screen was sealed to prevent any leakage The mass throughput of granules as a function of time (Fig. 4.18) was measured using a computerised balance. The particle size and shape of the corresponding granules were measured using the method as described in Section 4.2.1.

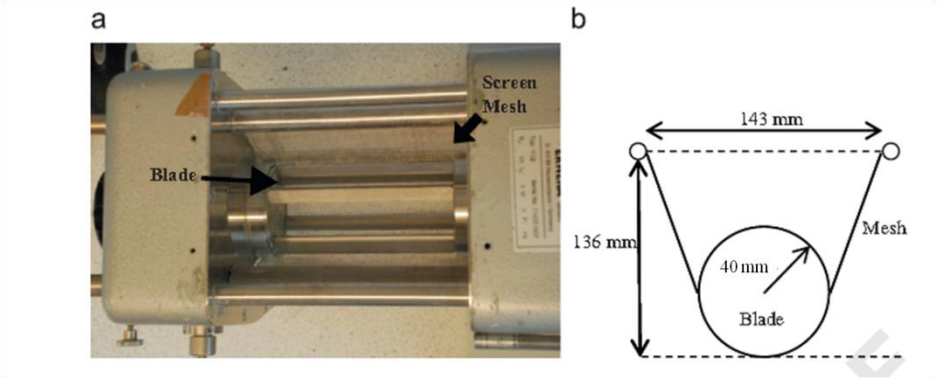

Figure 4.17 a) Photograph of the oscillating mill showing the blades and screen; b) schematic diagram of the cross-sectional geometry.

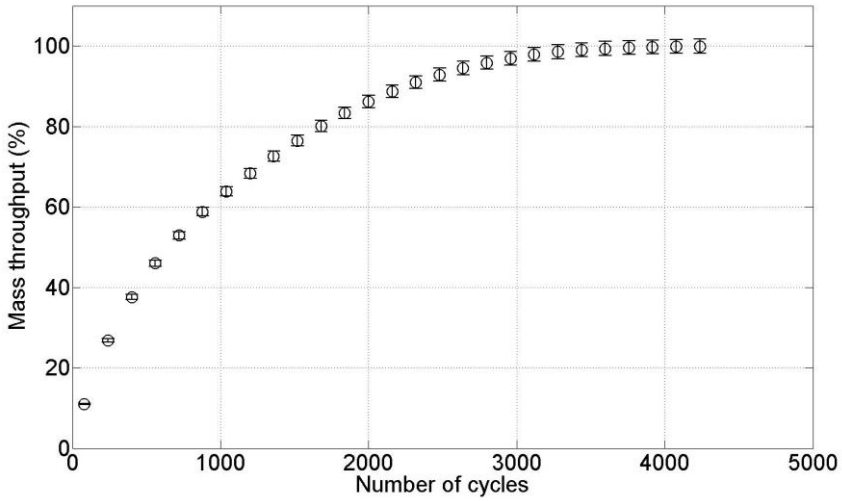

Figure 4.18 Typical milling results for roll compacted ribbons made from MCC (Avicel PH 102) powders at S =1.0 mm, u =1.0 rpm.

4.4.1 Positron emission particle tracking

PEPT technique

The basis of PEPT is the detection of the photons emitted when a positron, produced by the beta decay of an unstable nucleus, annihilates with an electron. This occurs when the positron is essentially at rest, and conservation of energy and momentum then require that two photons with an energy of 511 keV ($= m_e c^2$ where m_e is electron mass which is approximately $9.10938188 \times 10^{-31}$ kg, c is the speed of light in a vacuum) are emitted back-to-back ($180°$ apart). Simultaneously detecting both photons defines a line, and the annihilation is assumed to have occurred somewhere along this line. For the consideration of the accuracy, the particle position is determined by triangulation from pairs of γ-ray (as shown in Fig 4.19). The detection of a few such events is sufficient to locate the position of the single tracer particle.

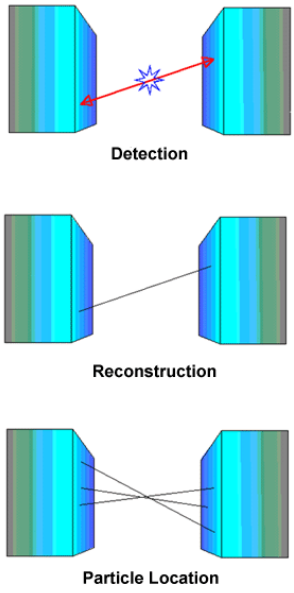

Figure 4.19 Imaging in PEPT (obtained from Positron Imaging Cenre, UoB)

The tracers are resin beads made of functionalised (by quaternary ammonium hydroxide groups) polystyrene, crosslinked with divinylbenzene (8% crosslink density) with the commercial name of Dowex SBR LC NG (OH) Strong Base Anion Exchange Resin (Sigma-

Aldrich, UK). The density of the particle is 1.08 g/cm^3, which is comparable to water and less than that of the MCC particles (1.56 g/cm^3). The activation of the beads occurs by ion exchange between the hydroxide ions from the functional groups of the highly porous beads and the F^{-18} ions (fluoride ions, F^-) diluted in the water. As the water is evaporated, the aqueous solution of the fluoride becomes more concentrated, thus driving the ion exchange process and resulting, once the beads are fully dried, in beads carrying as many fluoride ions as chemically and physically possible. The F^{-18} ions then decay over time by positron emission with a half-life of 110 min. In order to assure the radioactivity of the tracers and maximized the data collected, all the tracers were used within 1 h after labelling.

In practice, unwanted events may occur and interfere with the collected data which may lead to an inaccuracy of the positioning. Firstly, photons may be scattered prior to detection and hence arrive at the wrong point. Also, some positron emitting radionuclides (*e.g.* ^{22}Na, ^{124}I) emit γ-rays in association with the beta decay, resulting in the possibility of detecting associated γ-ray coincidences in which a gamma-ray is detected in coincidence with an annihilation photon (or another γ-ray). In order to eliminate the error caused by these factors, the tracking algorithm developed in the University of Birmingham (Parker *et al.*, 1993) was used, which selects suitable intervals for collecting the data and rejecting the unwanted events.

Experiment layout

The milling process was investigated using PEPT with a single tracer and double tracers. MCC (Avicel PH 102) was selected as the sample material for the PEPT study. The prepared tracer was placed in the layers of the feed powder in order to produce radioactive ribbons using the roll compactor. The ribbons were then sectioned and measured using a radioactivity detector to identify a particular ribbon piece with the tracer. In double tracer experiments in which one of the tracers was compressed in the ribbons and the other was adhered to one of the milling arms or another part of the tracer ribbon, which makes it possible to obtain the relative motion between the milled ribbons and/or the milling blade. In this case, the radioactivity of the tracer on the blade (ribbon) is a factor of 3 greater than the one in the ribbon, in order to discriminate the two tracers. This was controlled by the size of the tracer

particle, since larger resin beads tend to absorb more F^{-18} ions. The exact radioactivity of the tracers were measured and labelled after the preparation.

A schematic diagram of the experiment layout is shown in Fig. 4.20. The 3D location of the tracer particle was recorded as a function of time. In the current work, the algorithm proposed by Parker *et al.* (1993) and Yang *et al.* (2006) were used for single-tracer and multi-tracer PEPT tracking, respectively. The interval of the data collection was defined as 6, which means the average of every 6 data points was used to determine the location of the tracer particle. The data collected were then analysed using the 'Track' program developed by the Positron Imaging Centre to obtain the raw data for the particle location, which can be used by a MATLAB code to obtain the velocity mapping and speed distribution. For the experiments at various milling frequencies, in which the occupancy of the particle was greatly affected, the occupancy was also calculated using the 'Track' programme.

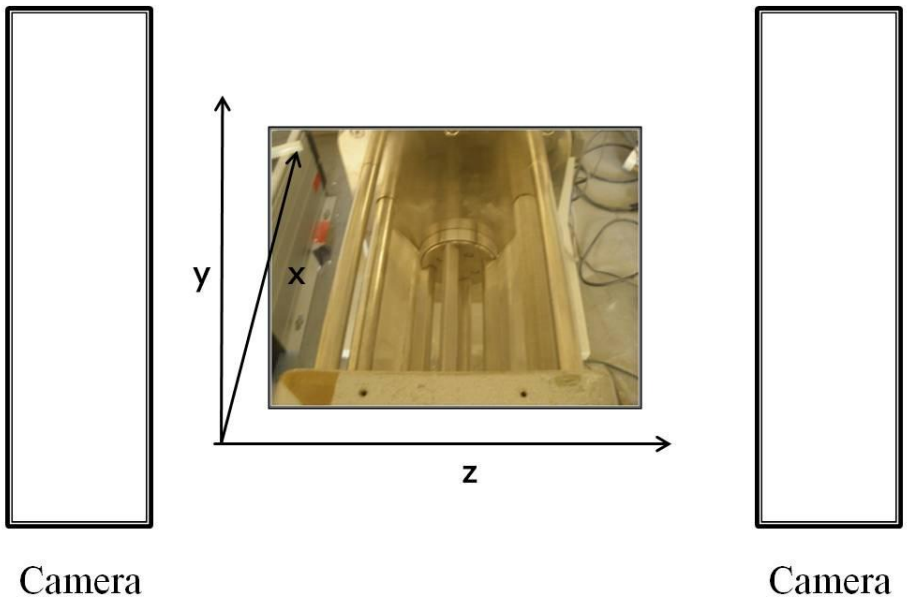

Figure 4.20 Simplified scheme of the PEPT experiment layout.

The investigation has focused on the cross-section of the milling chamber (y-z plane in Fig. 4.20), which corresponds to the motion of the ribbons along the moving direction of the blade.

The influence of both material properties and milling parameters (*i.e.* fracture energy of ribbons and milling frequency) were examined.

4.5 Tabletting

The die compression in pharmaceutical manufacturing was simulated in the laboratory. The instrument and methods used are introduced. The experiment settings are also presented.

4.5.1 Tablet production – uniaxial compression

The primary powders and granules obtained from the milling process were compressed uniaxially into tablets in a stainless steel die with an internal diameter of 13.0 mm (Specac, UK) using a universal material testing machine (Z030, Zwick Roell, Germany, Fig. 4.21). Trial experiments were first carried out to determine the feeding mass in order to ensure that tablets of approximate 5 mm height could be produced for a given compression force. The feed powders/ granules were tapped manually for 30 s before the compression in order to obtain a dense packing. The uniaxial compression tests were repeated four times for each excipient, under various maximum loads from 8 to 16 kN, that corresponds to maximum pressures of approximately 60 to 120 MPa. The compression speed was 0.5 mm/s, which is close to the effective uniaxial component (*i.e.* the horizontal speed) for the smallest roll speed (0.5 rpm) used in roll compaction. The force-displacement curves (as shown in Fig. 4.22) were recorded, and used to calculate the pressures as a function of densities. The compressibility, compactibility and porosity-pressure behaviour of the primary powders and granules were then analysed.

Figure 4.21 The universal material testing machine Z030, Zwick Roell, Germany).

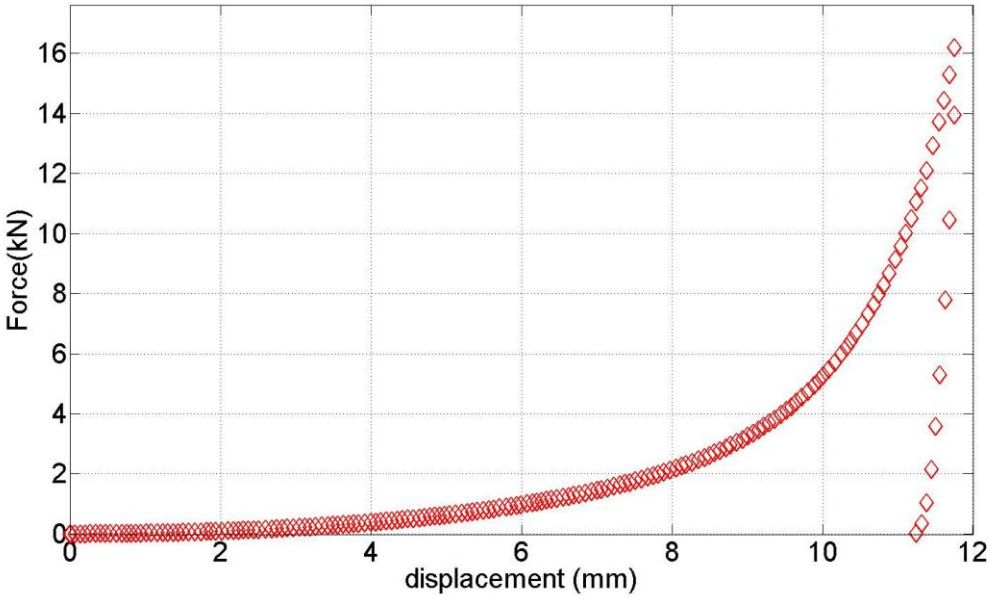

Figure 4.22 A typical force-displacement curve obtained in the uniaxial compression (MCC Avicel PH 102 at a maximum load of 16 kN).

4.5.1 Tablet characterisation

For the characterisation of the tablets, the bulk density and strength were measured. The dimensions (*i.e.* diameter, thickness) and masses of the tablets were measured after ejection so that the bulk densities could be determined. The tablets were then compressed diametrically to determine their tensile strength using the universal material testing machine (Z030, Zwick Roell, Germany).

4.6 Conclusion

This Chapter introduced the pharmaceutical excipients selected as the sample materials in this work. The properties of the powders, such as particle size and shape, true density, surface area, frictional and flow properties were fully characterised using various techniques to investigate their effects on roll compaction and subsequent processes. The experimental layout and data analysis of the roll compaction and characterisation of the ribbon (*i.e.* density measurement, surface topography and mechanical strength) were also described. In addition, the methods employed for investigation in milling and tabletting were discussed. It was concluded that the methods and data analysis procedures were satisfactory for the current application.

CHAPTER 5 POWDER CHARACTERISATION AND ROLL COMPACTION RESULTS

In this chapter, typical results of powder characterisation are presented and combined with the experimental roll compaction results to explore the influence of powder properties on roll compaction. In addition, the effects of process parameters such as roll speed and roll gap are also described. The densities and strengths of the roll compacted ribbons were also measured and the effects of the properties of the feeding powders and the processing conditions are also explored. The discussion of the results will be presented in Chapter 8.

5.1 Powder Characterisation

This section describes the characterisation of the basic properties of the powders, including the size and shape, true density, surface area, frictional and flow properties. The influence of lubrication, moisture and binary mixing on the powder characteristics are also explored.

5.1.1 Particle size, densities and surface area

Particle size distribution and shape

The cumulative distributions and mean particle sizes of the primary pharmaceutical excipients powders are shown in Figs 5.1 and 5.2, respectively. Some brittle crystal powders such as DCPD and mannitol (Mannogem powder), di-calcium phosphate anhydrous (DCPA) and mannitol of granule grade (Parteck M200) which are also commonly used in the pharmaceutical industry are considered for comparison.

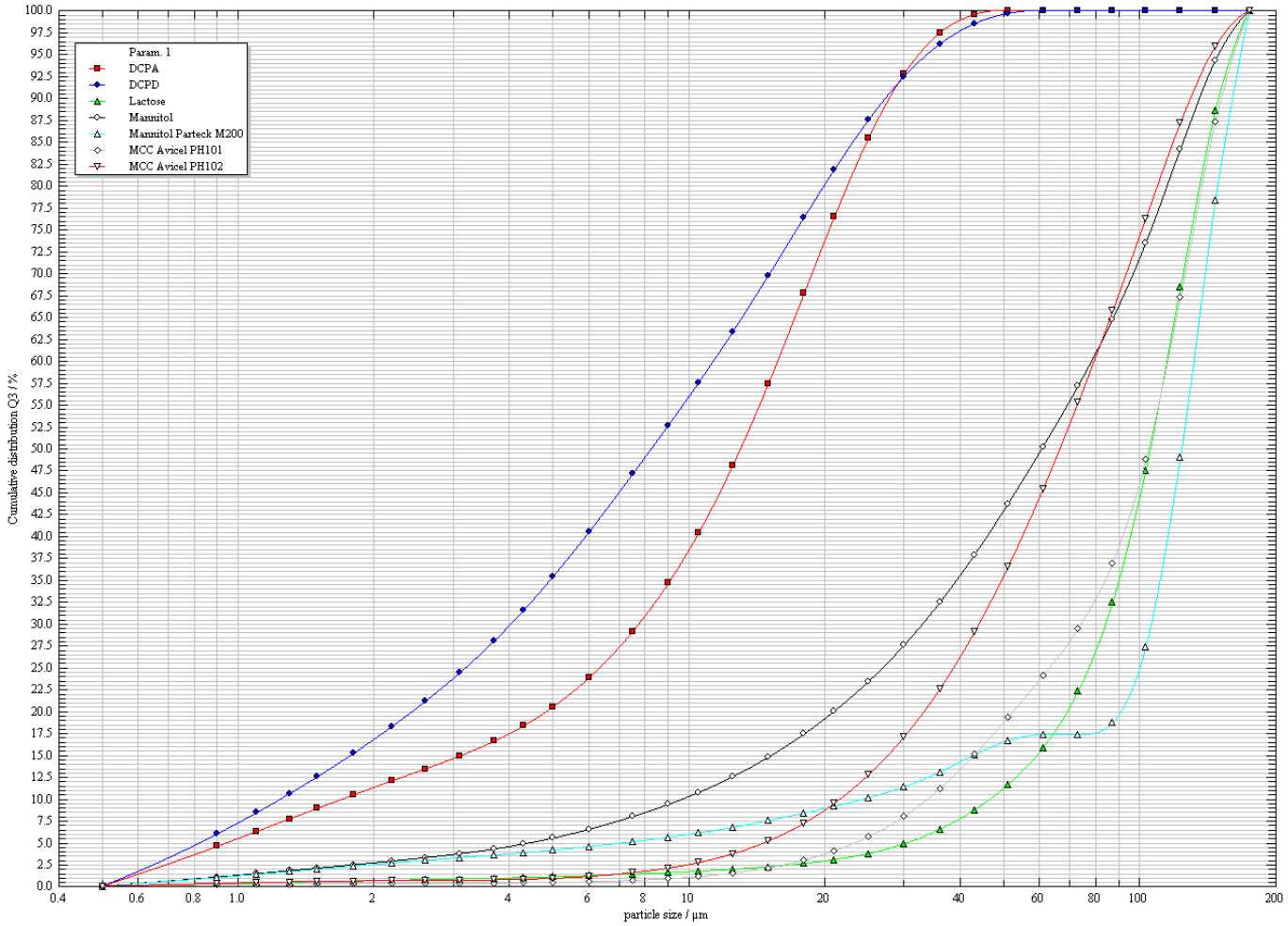

Figure 5.1 Particle size distributions of the sample powders

The particle shape described by aspect ratio and sphericity are shown in Figs 5.3 and 5.4. The results are consistent with observations from SEM. For instance, higher values of the aspect ratio and sphericity were obtained for lactose and Mannitol Parteck M200, which were nearly spherical as shown in the SEM images. For those powders consisting of irregular shaped particles, such as MCC Avicel PH 101 and 102, the values of the aspect ratio and sphericity are relatively small. However, the image analysis method has limitations on processing particles of small sizes. The approach is incapable of measuring particles of ~10 µm or smaller (*e.g.* DCPA and DCPD), because of the limited number of pixels occupied by the particles.

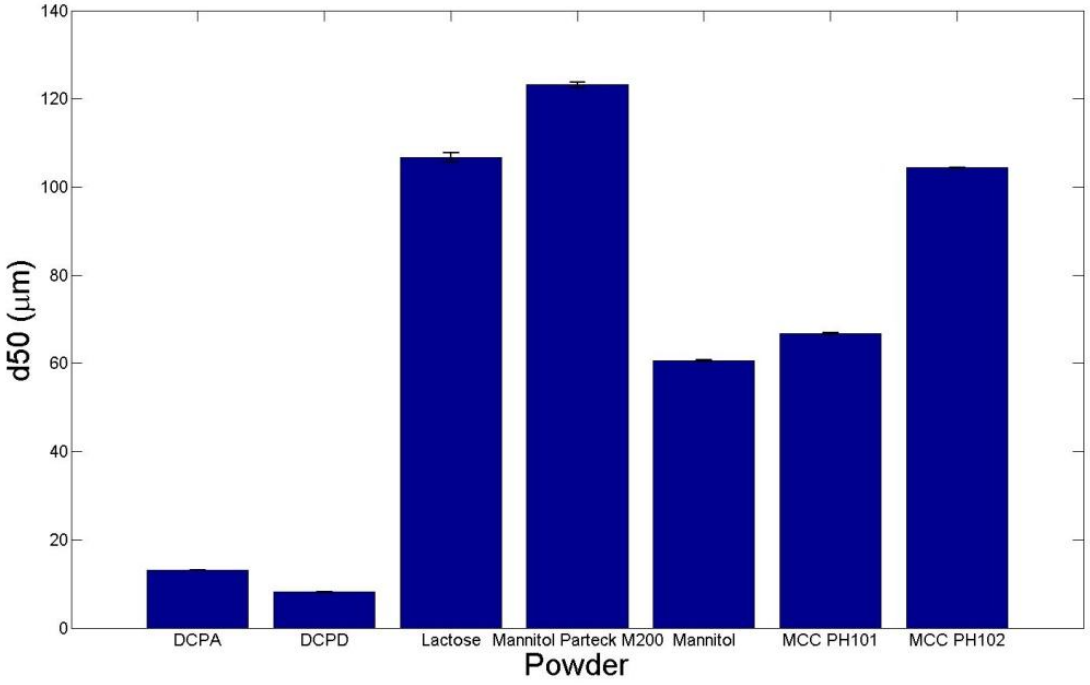

Figure 5.2 Mean particle sizes of the sample powders.

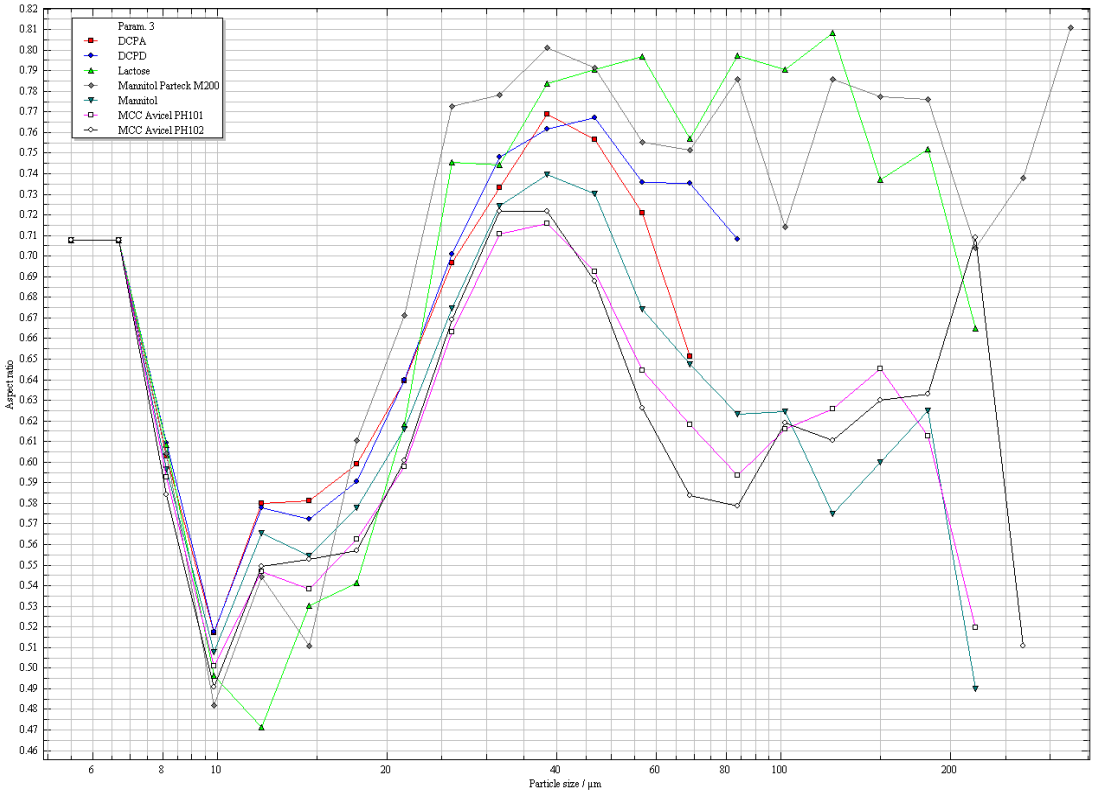

Figure 5.3 Aspect ratios of the sample powders.

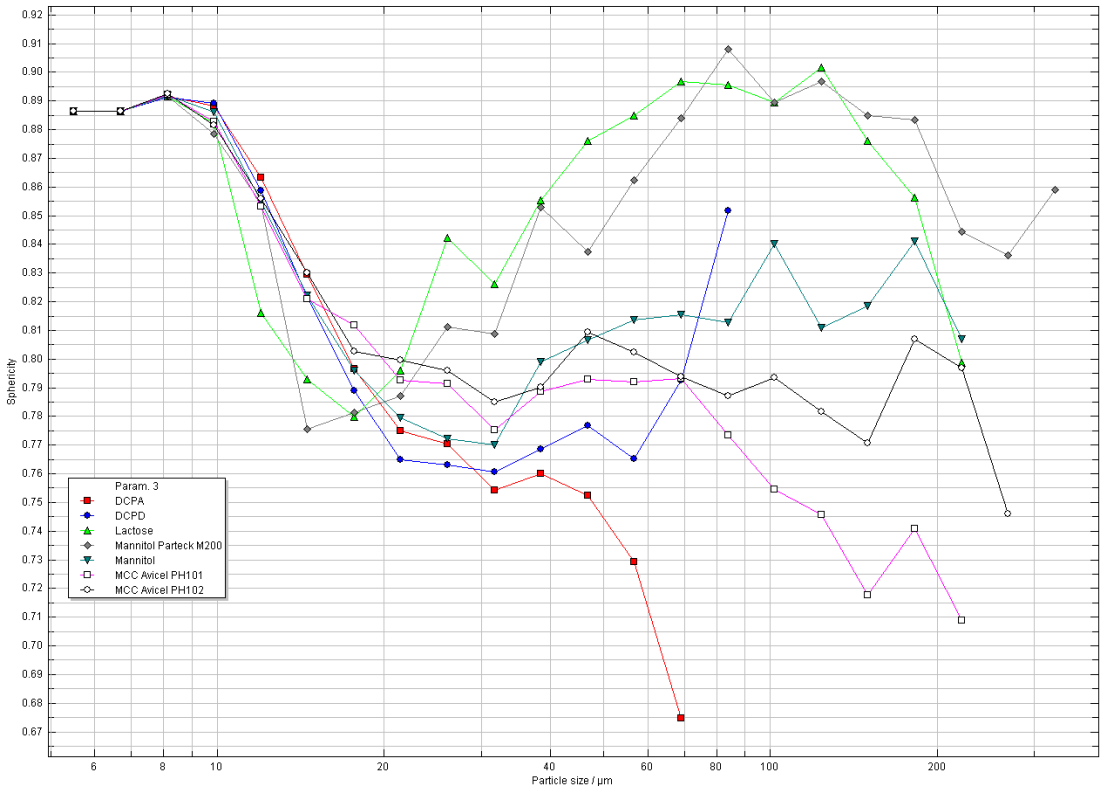

Figure 5.4 Sphericity of the sample powders.

True density and surface area

Densification is a critical factor in roll compaction. As an essential parameter to calculate relative density and evaluate the efficiency of densification, the true density is of particular interest. The surface area, on which the surface coverage of a lubricant depends, is also an important property of the powders. The true densities, ρ_t , measured using helium pycnometer and BET surface area measured using nitrogen absorption are shown in Table 5.1.

Table 5.1 The true densities and surface areas of the sample powders.

Powder	ρ_t (g/cm^3)	BET surface area (m^2/kg)
DCPD	2.58	4394
Lactose	1.62	924
Mannitol	1.53	3758
MCC (Avicel PH101)	1.56	1280
MCC (Avicel PH102)	1.57	1089

5.1.2 Frictional and flow properties – ring shear cell testing results

Typical yield loci for the powders are displayed in Fig. 5.5. The internal frictional properties of the powders, which can be described by effective friction angle, ϕ_e , and the flow function are obtained from the measurement. It is shown that, the internal friction properties of the powders are comparable, except for the lower values of DCPA and lactose. According to the flow function values, the sample powders can be divided into three groups (Table 5.2) according to Jenike's classification (1967):

Table 5.2 The flowability of the sample powders.

Flow function, ff_c	Type of flow	Powder
$2 < ff_c < 4$	Cohesive	DCPD
$4 < ff_c < 10$	Easy flowing	MCC Avicel PH 101
		MCC Avicel PH 102
		Mannitol
		DCPA
$ff_c < 10$	Free flowing	Lactose
		Mannitol Parteck M200

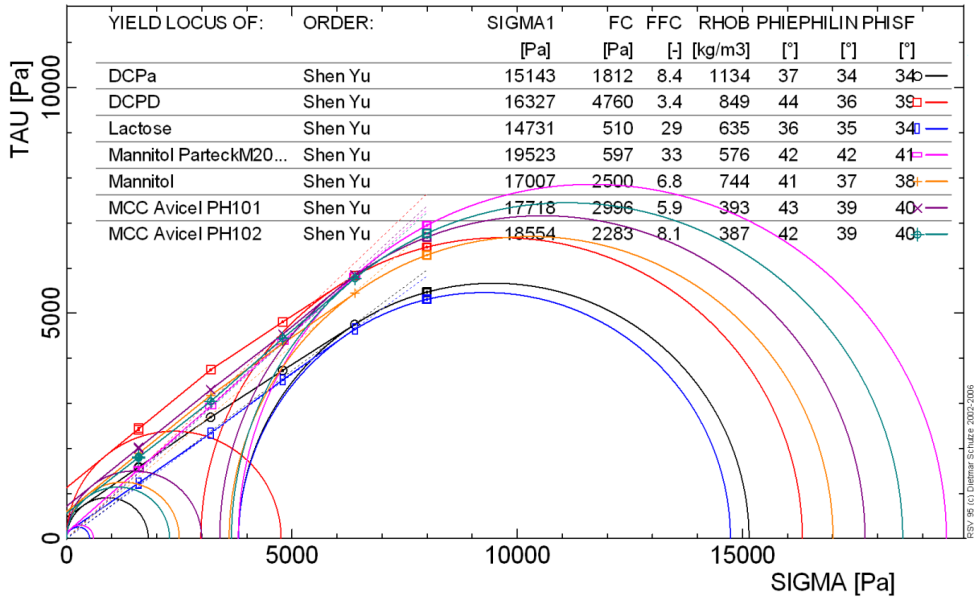

Figure 5.5 Yield loci for the sample powders under 8 kPa normal load, SIGMA1 is major principal stress, FC is the unconfined stress, FFC is the flow function, RHOB is the density of the bulk, PHIE, PHILIN, PHISF is effective friction angle, linear friction angle and friction angle for steady flow, respectively.

The shear stresses of the powders obtained in the ring shear cell tester are plotted as a function of the applied normal stresses (see in Fig 5.6). The wall friction angle, ϕ_w and corresponding coefficient, μ_w, are calculated by adopting the linear regression between shear and normal stress, as shown in Fig 5.7. It can be seen that di-calcium phosphate has the greatest friction coefficient, while MCC has the smallest.

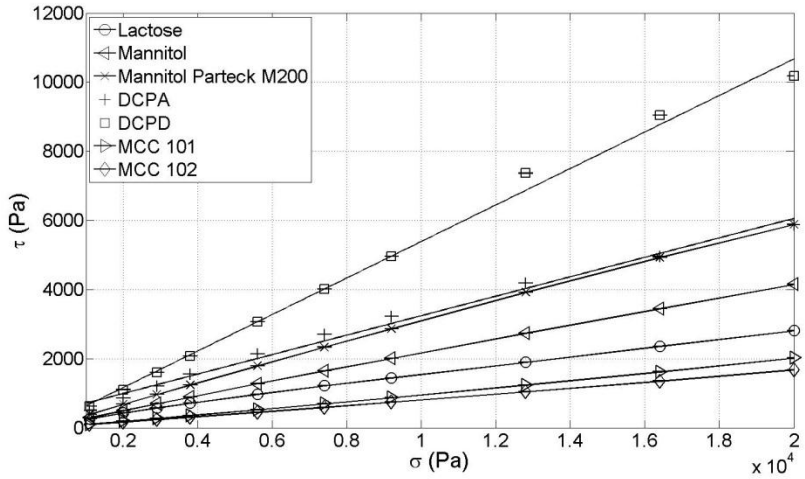

Figure 5.6 The variation of the wall shear stress with normal stress for the sample powders.

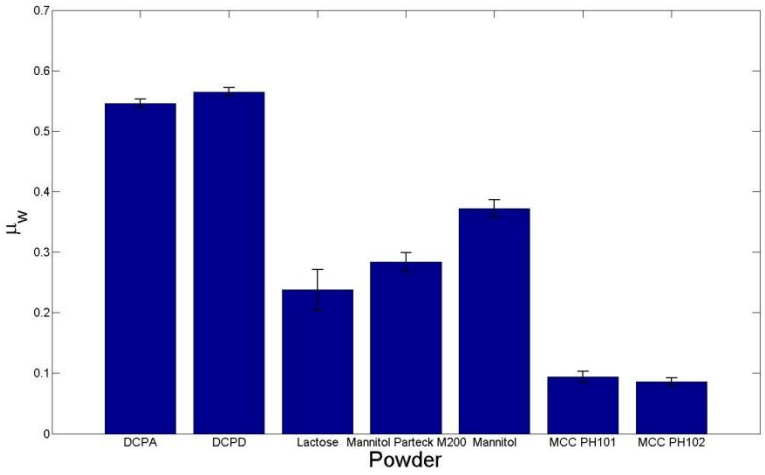

Figure 5.7 Wall friction coefficient of the sample powders again smooth stainless steel wall material with roughness of 0.31 ± 0.02 *μm*.

Effects of lubrication

MgSt (0.25 – 1.5% w/w) was added to MCC (Avicel PH102) and DCPD in order to investigate the effects of bulk lubrication on the frictional and flow properties. The variation of the flow function with increasing MgSt concentration is shown in Fig. 5.8. It can be seen that the flow function increases significantly with the amount of MgSt added for MCC, especially at small MgSt concentrations. On the other hand, the flow function of DCPD is insensitive to the lubricant.

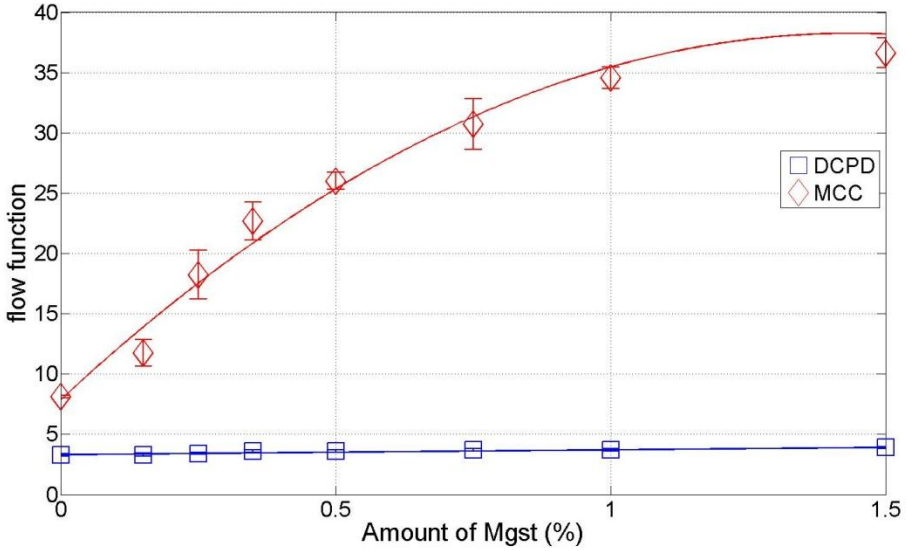

Figure 5.8 The variation of flow function of DCPD and MCC 102 as a function of the concentration of MgSt.

Figure 5.9 shows the wall shear stress as a function of the normal stress for the feed powders mixed with different amounts of MgSt; the gradients are equal to the coefficients of friction. In the case of the unlubricated powders, the gradients for DCPD and MCC are ~ 0.5 and ~ 0.09, respectively. The gradients for DCPD reduces to ~ 0.1 when 0.75% (w/w) MgSt was added to the bulk, while for MCC the values are unaffected by the addition of the lubricant. The influence of the amount of lubricant on the wall friction in terms of the angle of wall friction, ϕ_w, is shown in Fig. 5.10, together with the corresponding effective angles of friction, ϕ_e . The value of ϕ_e for unlubricated DCPD is only slightly greater than that for MCC and it does not decrease with increasing MgSt concentration unlike MCC.

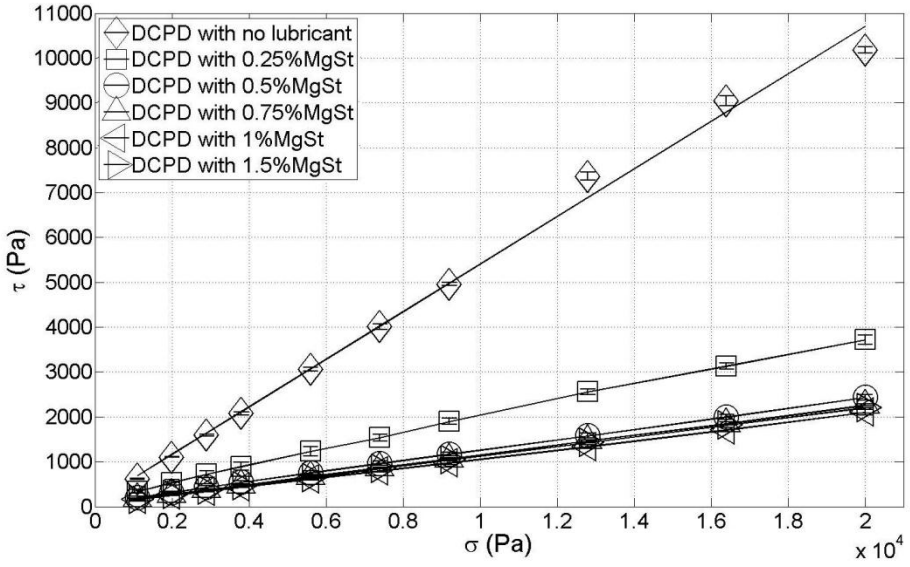

a)

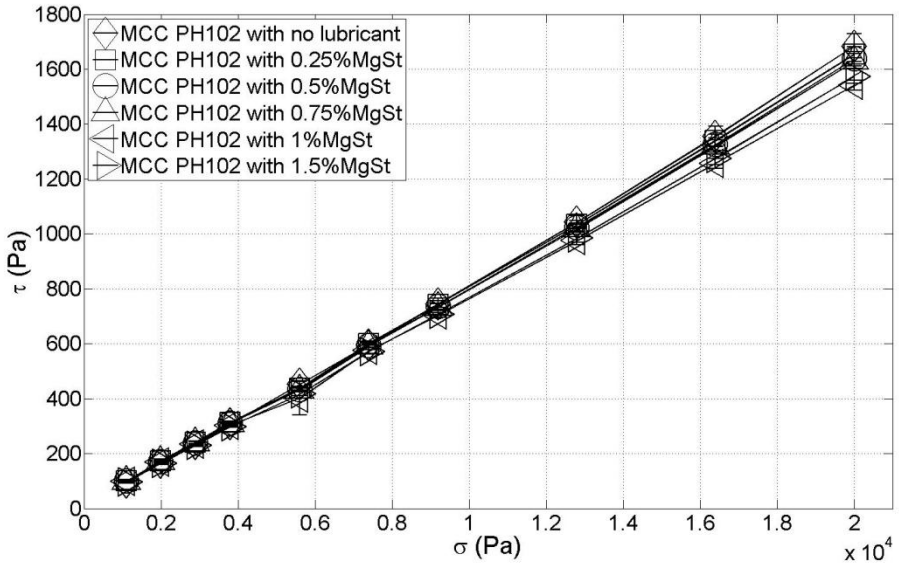

b)

Figure 5.9 The variation of the wall shear stress with normal stress for a) DCPD and b) MCC 102, with various amounts of MgSt in the bulk.

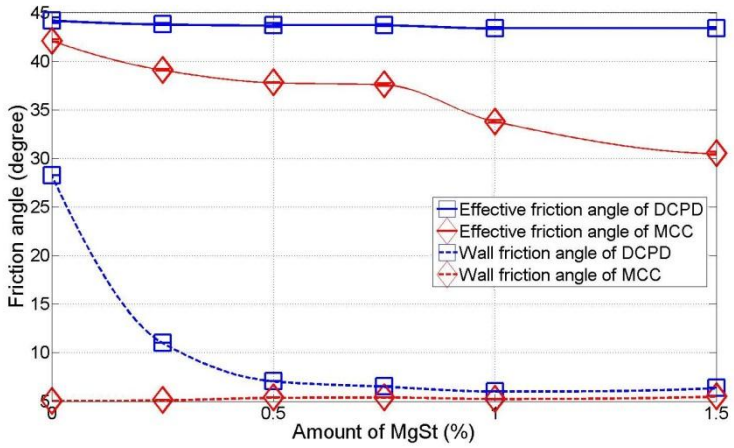

Figure 5.10 Frictional angles of MCC 102 & DCPD as a function of concentration of MgSt.

Effects of moisture content

In order to investigate the effects of moisture content, MCC (Avicel PH 102) and DCPD were mixed with water (2.5 – 15%, w/w). The actual moisture contents are measured using a moisture analyser (MA30 Goettingen, Sartorius, Germany) shown in Table 5.3. The effect of moisture content on the flow function of the powders is shown in Fig. 5.11. For both powders, the flow function is almost constant at low moisture contents (*i.e.* added water < 5% w/w), but decreases at higher moisture contents (added water > 5%). It may be noted that the variations of the flow function for both powders are not significant (*i.e.* $\Delta ff_c < 3$).

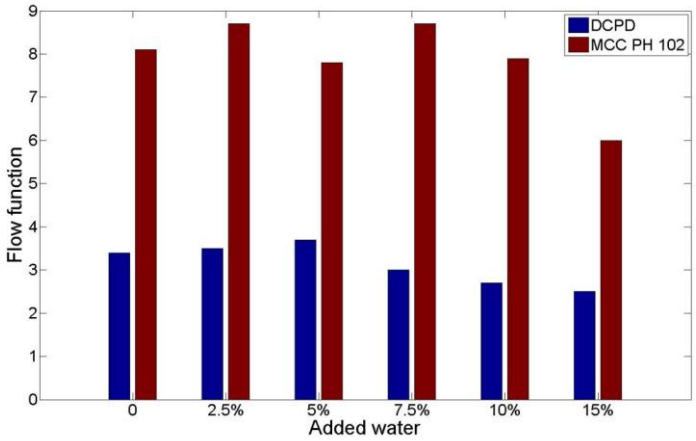

Figure 5.11 Flow function of DCPD and MCC PH 102 with various moisture contents.

Table 5.3 The moisture content of DCPD and MCC with various water contents.

Powder	Water content (w/w)	Moisture content (w/w)
DCPD	0	5.6 ± 0.2 %
	2.5%	8.4 ± 0.1%
	5%	9.6 ± 0.2 %
	7.5%	12.4 ± 0.2%
	10%	15.2 ± 0.3 %
	15%	20.4 ± 0.2 %
MCC PH 102	0	6.3 ± 0.4 %
	2.5%	9.1 ± 0.2 %
	5%	11.4 ± 0.2 %
	7.5%	14.1 ± 0.3 %
	10%	16.4 ± 0.4 %
	15%	22.0 ± 0.3%

The wall friction coefficients of the powders increases with increasing moisture content (Fig 5.12). At low moisture contents (< 2.5% added water), the wall friction coefficient of DCPD increases with the amount of added water. The influence of moisture content on the values of ϕ_e is shown in Fig. 5.13. The trends can be summarised by dividing the moisture contents into three regions with boundaries at 5 and 10% added water:

Table 5.4 The effect of moisture content on the internal effective friction angle for MCC and DCPD.

Added water (%)	Moisture content of DCPD (%)	Change in ϕ_e (DCPD)	Moisture content of MCC (%)	Change in ϕ_e (MCC)
< 5	5.6 – 9.6 %	Decrease	6.3 – 11.4 %	Decrease
5 – 10	9.6 – 15.2 %	Increase	11.4 –16.4 %	Increase
> 10	> 15.2 %	Decrease	> 16.4 %	Increase

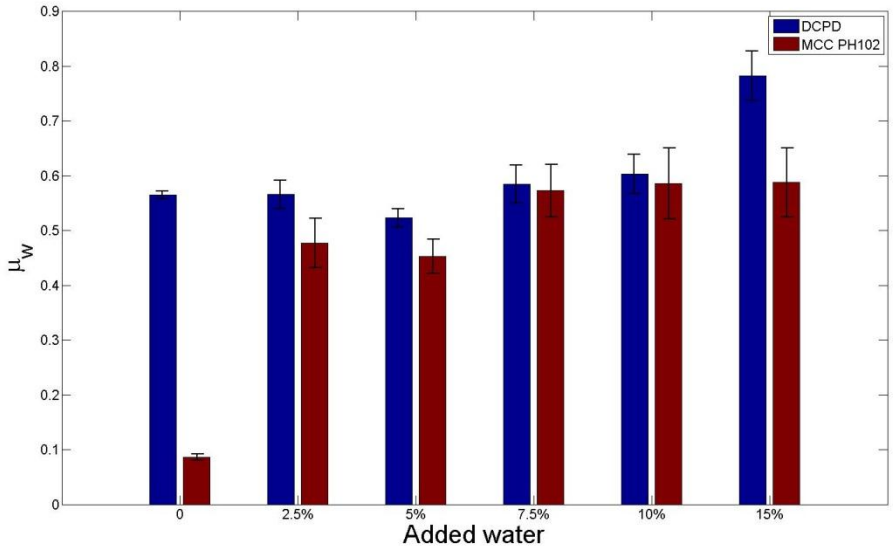

Figure 5.12 Wall friction coefficients of DCPD and MCC PH 102 at various moisture contents.

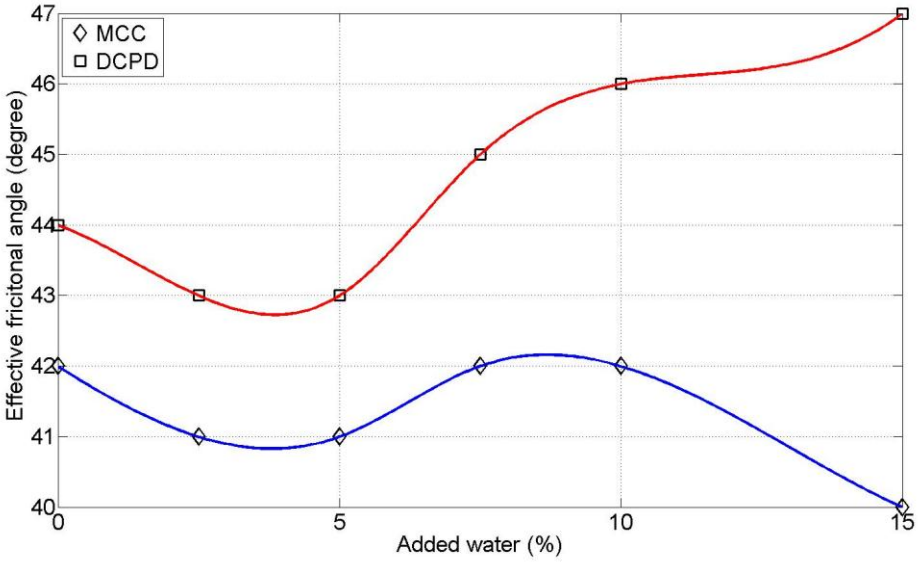

Figure 5.13 Effective internal frictional angle of DCPD and MCC with various moisture contents.

Properties of binary mixtures

In order to investigate the effects of flowability on the maximum pressure and nip angles, two binary mixtures of MCC (Avicel PH 102) and DCPD, mannitol and MCC (Avicel PH 101)

were characterised and roll compacted. The frictional and flow properties of the mixtures are shown in Figs 5.14 – 5.16. The variation of the values of ϕ_w and wall friction coefficient indicate almost ideal mixing behaviour (Figs 5.14 & 5.15). This also the case for the flow functions (Fig. 5.16) corresponding to the DCPD and MCC mixtures. For the mannitol and Avicel PH102 mixtures, the data are characterised by a relatively sharp transition region.

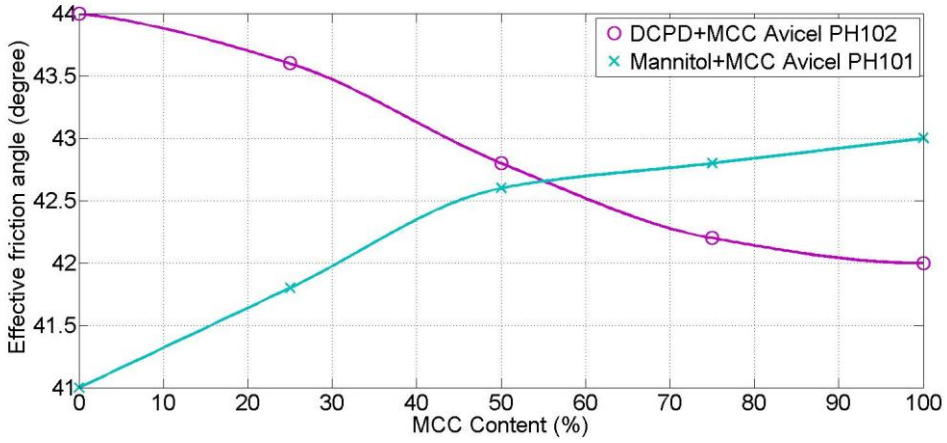

Figure 5.14 Effective friction angle of binary mixtures as a function of MCC content.

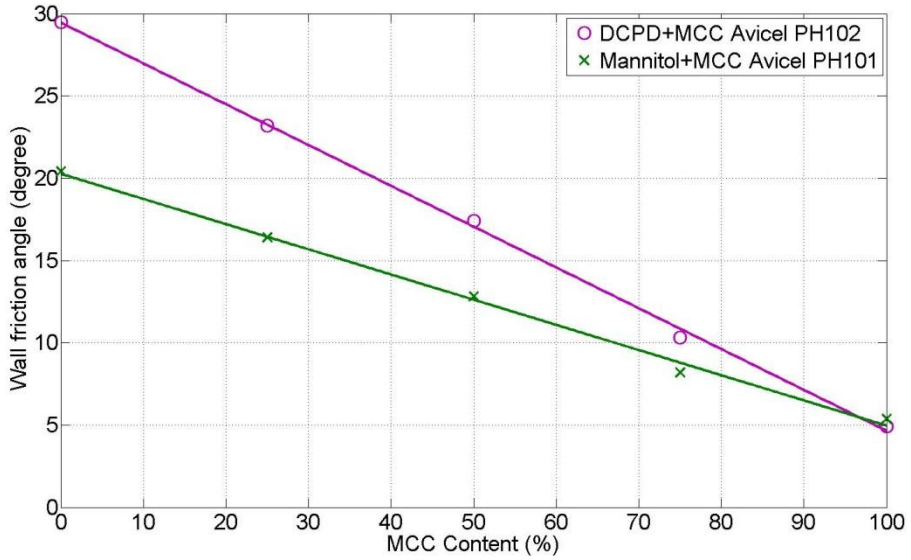

Figure 5.15 Wall friction angle of binary mixtures as a function of MCC content.

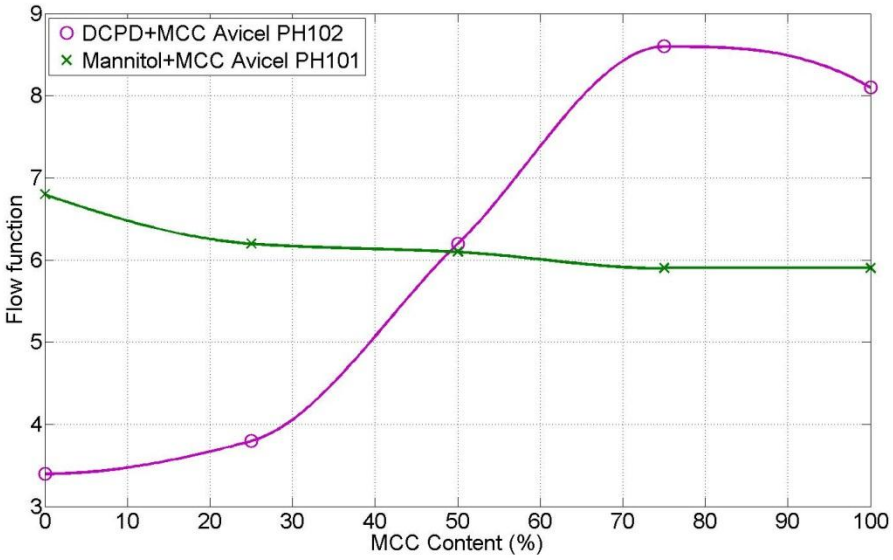

Figure 5.16 Flow function of binary mixtures as a function of MCC content.

5.2 Roll Compaction

5.2.1 Processing behaviour

Roll compaction experiments with powders of distinctive properties, and various process parameters were carried out to explore the dependency of the process behaviour and quality of the produced compacts. The maximum pressure generated, and the nip angle in roll compaction was considered as critical factors describing the process. The density and fracture energy of the ribbons that is related to the strength and fracture potential in granulation were employed to evaluate the products. In this section, the experimental results revealing the effects of process parameters (*i.e.* roll gap, roll speed), powder properties (*i.e.* lubrication, moisture content and binary mixtures) are presented.

Effects of roll gap

Roll compaction of MCC (Avicel PH 102) and DCPD were carried out with a fixed roll speed of 1 rpm. The roll gap was varied in the range 0.6 to 2.0 mm in order to evaluate the effects

on the behaviour of these two powders. It was noticed that DCPD powder could not be successfully compacted at the roll gap of 2.0 mm due to the leakage and insufficient compaction pressure generated (no compaction pressure recorded during the process). The variation of the maximum pressure and nip angle with the roll gap are shown in Figs 5.17 and 5.18. The maximum pressure reduces with increasing roll gap (see in Fig. 5.17). For the nip angle, the value increases with the roll gap for MCC, but decreases for DCPD (Fig. 5.18).

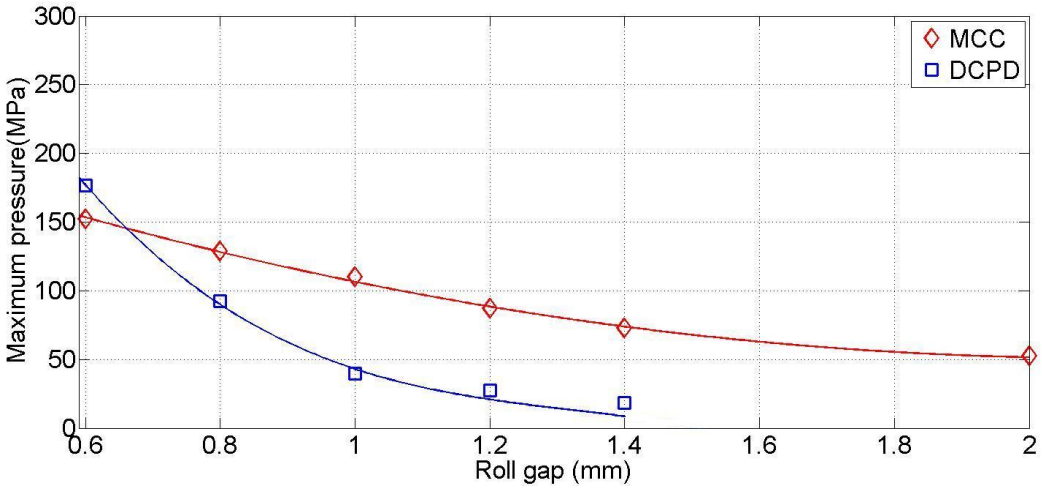

Figure 5.17 Effects of roll gap on maximum roll pressures.

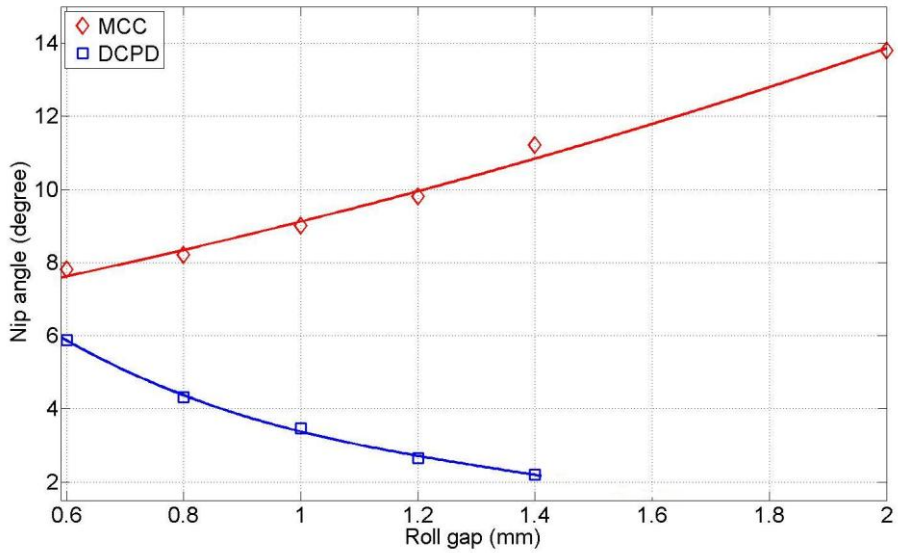

Figure 5.18 Effects of roll gap on nip angle in roll compaction.

Effects of roll speed

In order to investigate the effects of roll speed, MCC (Avicel PH 102) and DCPD were compacted at a constant roll gap S =1.0 mm with roll speeds in the range 0.5 to 5 rpm (Petit-Renaud *et al*., 1998). The maximum pressures for the powders at different roll speeds are shown in Fig. 5.19. At the lowest roll speed considered (*i.e.* 0.5 rpm), a high maximum pressure is obtained for DCPD, which has a larger effective friction angle and wall friction angle than MCC. As the roll speed increases, a rapid decrease in the maximum pressure is observed for DCPD, which is consistent with previous work (Inghelbrecht and Remon, 1998, Petit-Renaud *et al*., 1998). Ribbons could not be produced at high roll speeds because the compaction pressure was too small. For MCC, the maximum pressure decreases slightly as the roll speed increases.

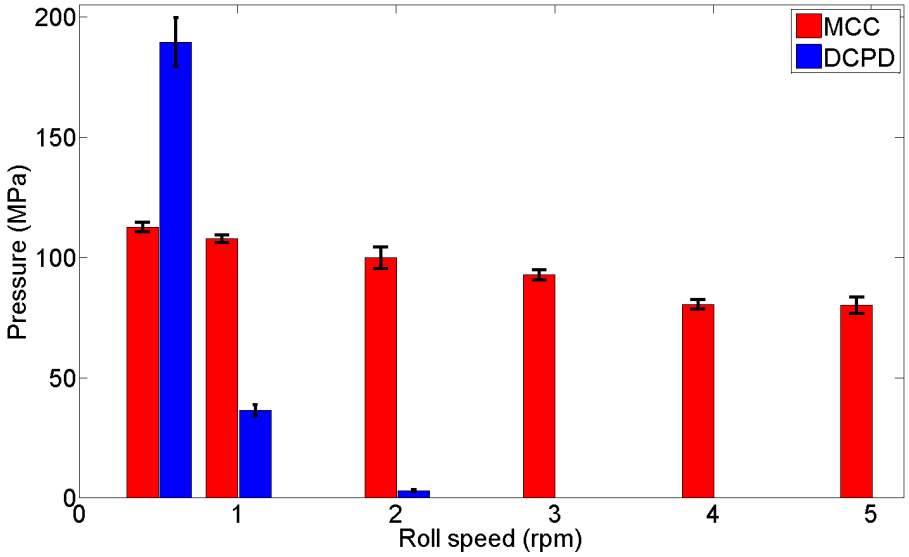

Figure 5.19 Effects of roll speed on maximum roll pressures.

The nip angles at the various roll speeds were determined using the proposed approach (Section 4.3.1) and are shown in Fig. 5.20. The values calculated using the methods employed by Johanson (1965) and Bindhumadhavan *et al.* (2005) are also superimposed. It can be seen that, for MCC (*i.e.* the easy flowing powder), the values of the nip angle were almost constant, while for DCPD they decreases sharply. Similar results were obtained using

the present method (Section 4.3.1) and that proposed by Bindhumadhavan *et al.* (2005). However, the current approach shows advantages in the measurement of the nip angle for cohesive powder like DCPD at higher roll speed (*i.e.* 3 rpm, shown in Fig. 5.20) In contrast, constant nip angles were obtained using Johanson theory (1965), as the effect of roll speed was not considered. In addition, Johanson theory (1965) slightly underestimates the nip angle for MCC but overestimate the value for DCPD.

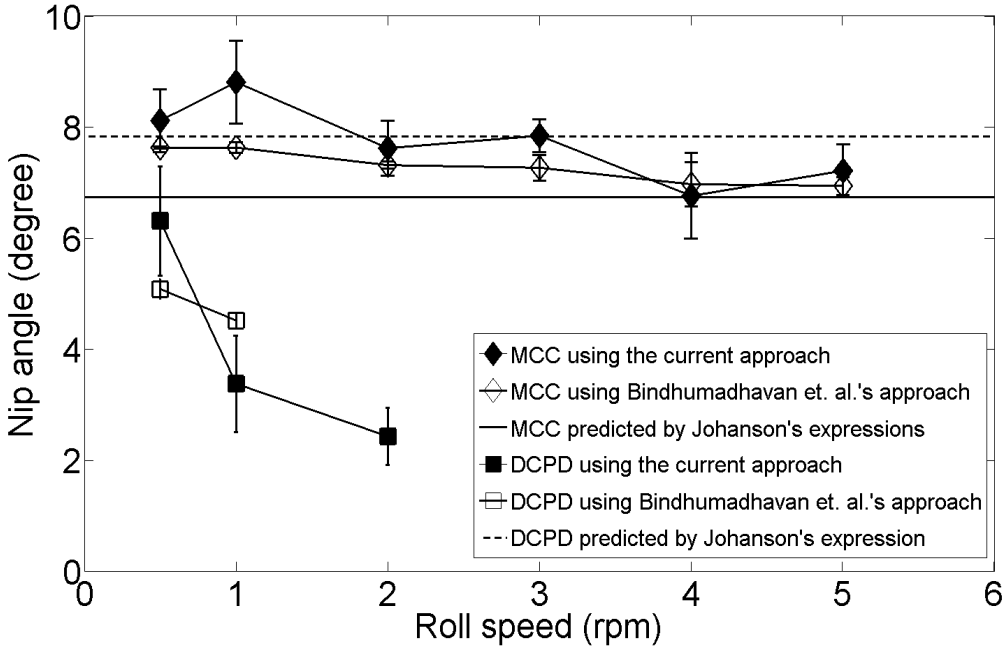

Figure 5.20 Effects of roll speed on nip angle in roll compaction.

Effects of lubrication

To explore the influence of the lubrication, two powders (DCPD, MCC Avicel PH 102) showing different sensitivity to MgSt (Vromans *et al.*, 1988, Zuurman *et al.*, 1999) were used. The powders are both commonly used pharmaceutical excipients but with distinctive particle sizes, surface topographies and sensitivities to lubrication with MgSt; it has been reported that the lubrication of DCPD with MgSt is very insensitive to the mixing conditions (Vromans *et al.*, 1988), unlike MCC (Zuurman *et al.*, 1999). MgSt of 0.25 and 1% (w/w) were employed for bulk and wall lubrication conditioning (*i.e.* lubricating the roll surfaces). The bulk lubricated powders were prepared by mixing MgSt and primary powders at 72 rpm

rotating speed in a double-cone blender (5 min mixing time for MCC, 10 min mixing time for DCPD). Wall lubrication was achieved by spraying an ethanol suspension of MgSt on the roll surfaces.

The corresponding maximum roll pressures and nip angles are shown in Figs 5.21 and 5.22. For MCC, the maximum pressure and nip angle were unaffected when the roll surfaces were lubricated but they were reduced by bulk lubrication. For DCPD, both roll and bulk lubrication resulted in reductions in the nip angle and maximum pressure. However, the values of the maximum pressure and nip angle reached a constant value at 0.25 % w/w MgSt. Provided that there is sufficient MgSt to induce the maximum possible lubrication, the reduction in the nip angle and maximum pressure values are similar.

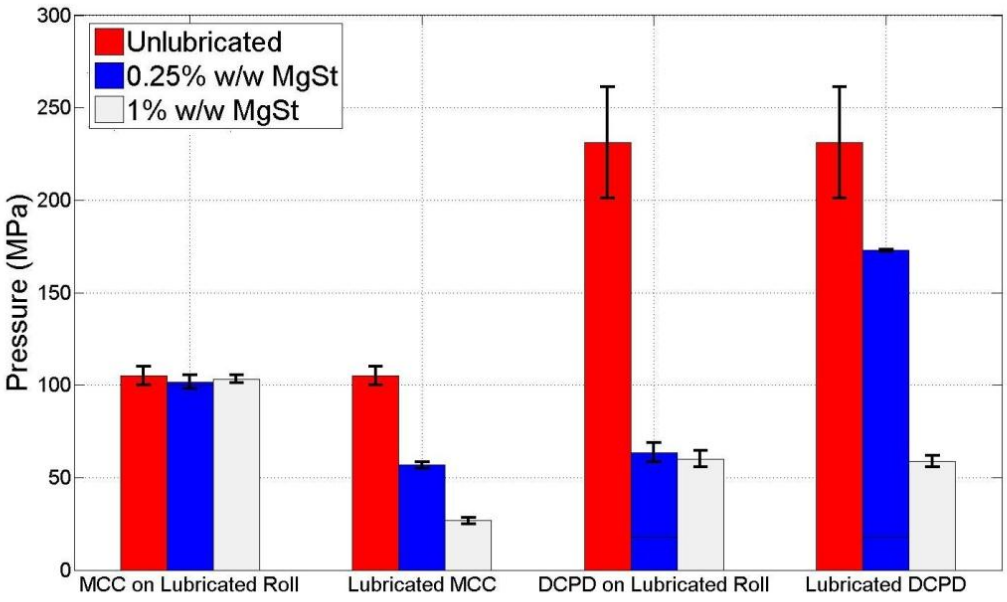

Figure 5.21 Effects of lubrication on the maximum roll pressures.

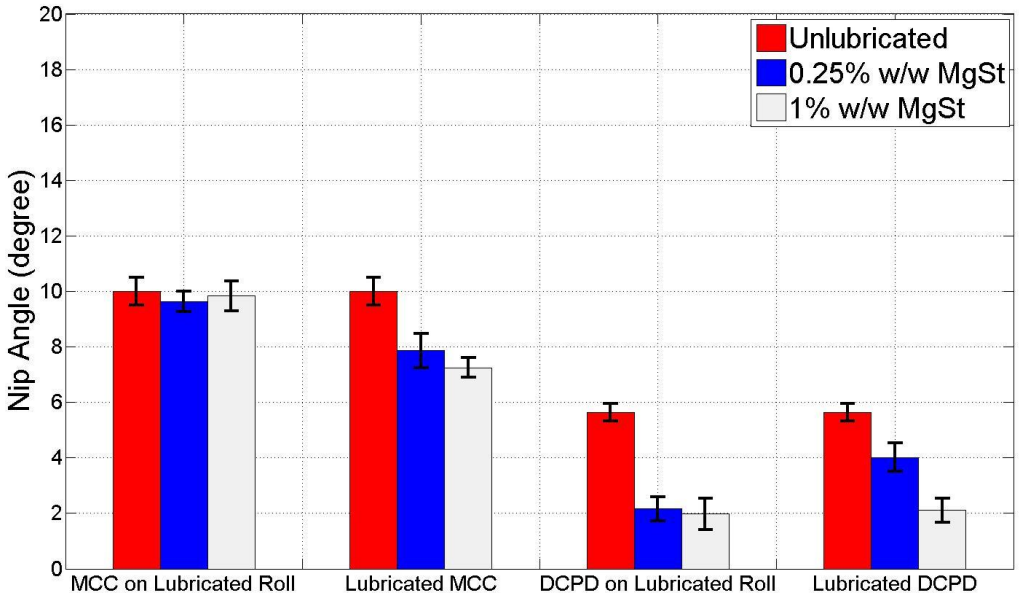

Figure 5.22 Effects of lubrication on nip angle in roll compaction.

Effects of moisture content

Attempts were also made to roll compact DCPD and MCC (Avicel PH 102) powders with additional water. It was found that jamming occurred during the processing of DCPD. Therefore, the powder could not be successfully pressed with added water. The experimental measured maximum pressure and nip angle for MCC with various amounts of added water are shown in Figs 5.23 and 5.24. Initially, with increasing amount of added water, the maximum pressure keeps constant (amount of added water < 2.5% w/w), then increases sharply (see in Fig. 5.23), consistent with the observation by Wu *et al.* (2010b). However, the results show that the maximum pressure increases with the amount of added water even at high concentration which indicates the water acting as a binder(> 10% w/w), opposite to the work by Wu *et al.* (2010b) which reported the pressure generated for most moist MCC powders decreases due to the reduction in cohesion and increase in flowability that causes powder passing through the roll gap without compaction.Despite the constant values at low amounts of added water (< 2.5% w/w), the nip angle generally decreased with increasing moisture content, similar to the results from Wu *et al.* (2010b) (see in Fig. 5.24).

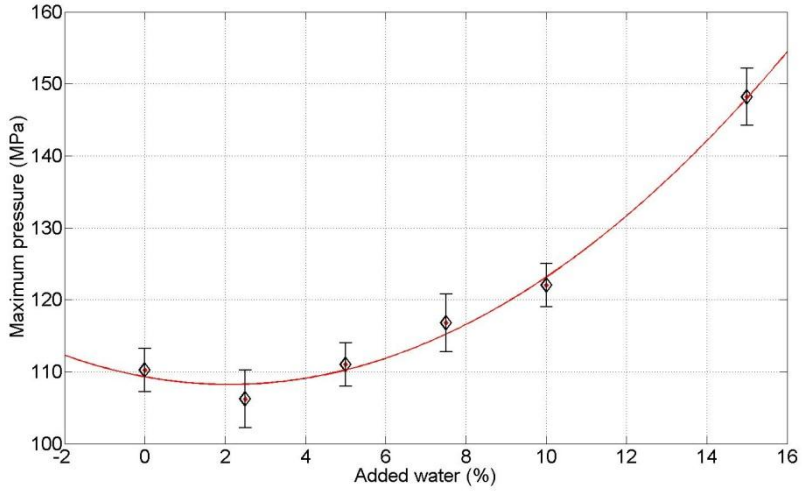

Figure 5.23 Effects of water contents on maximum roll pressures for MCC 102.

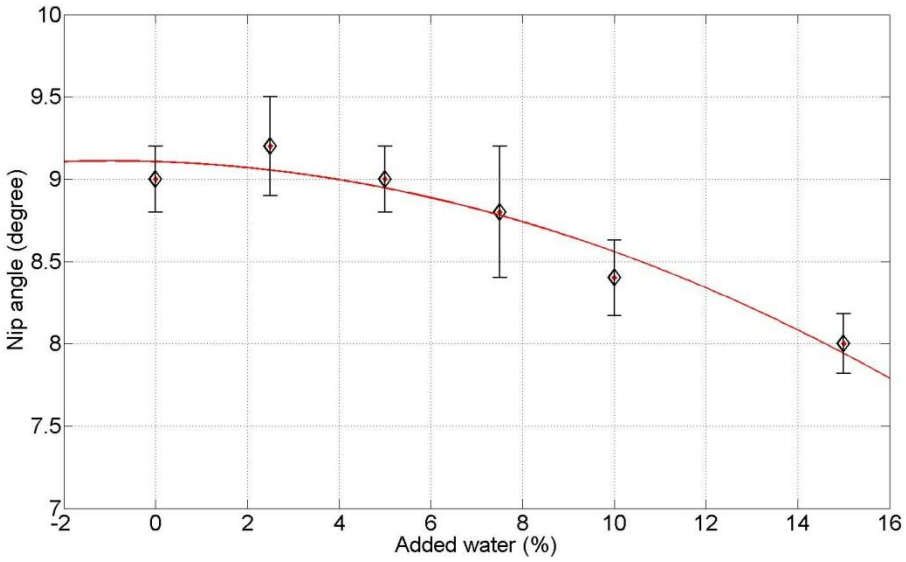

Figure 5.24 Effects of water content on nip angle in roll compaction for MCC 102.

Binary mixtures

The maximum pressure and nip angle of binary mixtures of MCC (Avicel PH 102) and DCPD are shown in Fig. 5.25. It is clear that the maximum pressure increases monotonically with increasing concentration of MCC. The addition of MCC leads to an increasing flowability of the mixture and improved feeding in roll compaction, and thus an increase of

the nip angle. However, the nip angle is primarily determined by MCC when its concentration is greater than 75%.

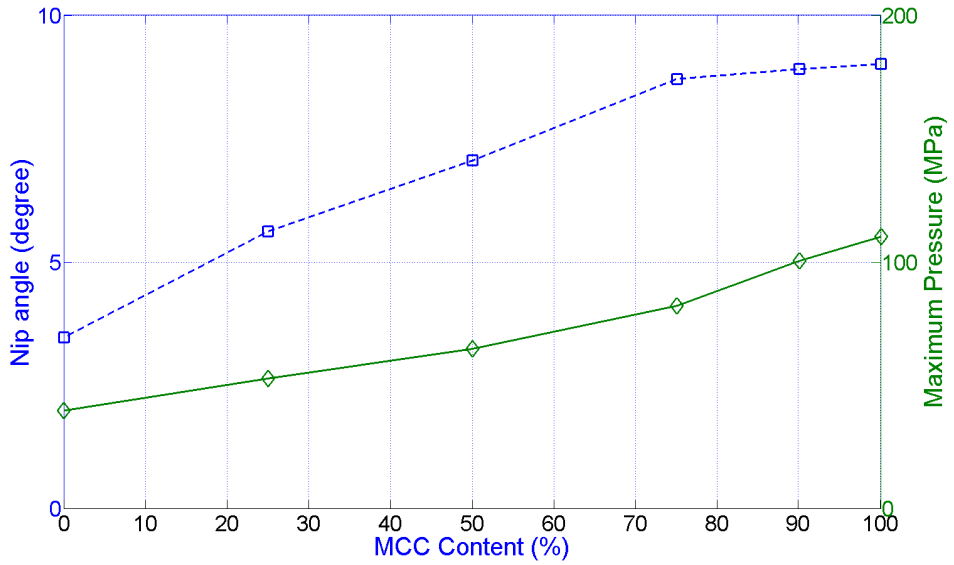

Figure 5.25 The maximum pressure and nip angle as a function of MCC content for MCC 102-DCPD mixtures (S =1.0 mm, u =1.0 rpm).

In this work, powders with constant volume were fed into the system and roll compacted as introduced in Section 4.3.1. During the compaction, the rolls rotate several loops (revolutions). The number of loops in a single run depends on the feeding of the material (*e.g.* 6 loops for MCC 102 and 12 loops for DCPD).In order to evaluate the reproducibility of the compaction results, the pressure profile from the beginning (1st loop) till the end (last loop) for a single compaction run were recorded and compared. For the binary mixtures of mannitol and MCC (Avicel PH 101), reproducible compression pressures and nip angles could not be achieved during the process. As shown in the pressure profile of the 8 loops of roll compaction (Fig. 5.26a), the compaction pressure increases gradually every loop. In addition, the corresponding nip angle increases with the processing time/loop number. In contrast, it can be seen that for pure MCC, the value of the maximum pressure remained constant after the first loop (Fig. 5.26b).

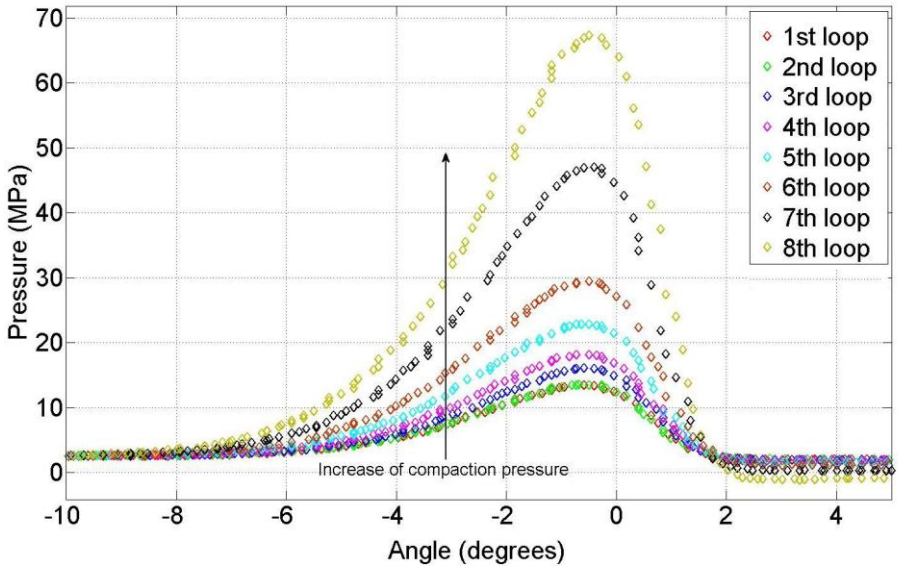

a)

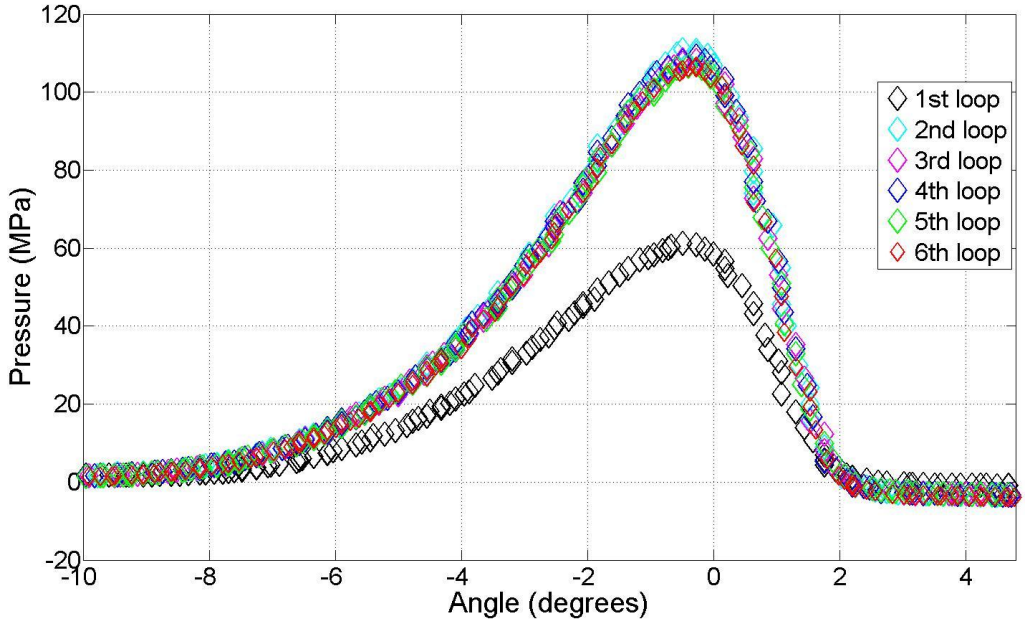

b)

Figure 5.26 Typical pressure profiles obtained for a) Mannitol-MCC 101 mixture and b) DCPD-MCC 102 in one run (S =1.0 mm, u =1.0 rpm), angle = 0 represents the minimum roll gap.

5.2.2 Ribbon properties

Ribbon properties were characterized by the densities and fracture energies. Additionally, the determination of the ribbon density using surface topography was obtained using a white light interferometer.

Effects of roll gap

It was found that the DCPD ribbons were too fragile for density and strength measurements. Therefore, only the results for MCC are presented to illustrate the effects of moisture content. For the same reason, the results for DCPD ribbons are not displayed and the investigation is based on the results for MCC.

The fracture energies, G_f , and bulk densities of the ribbons produced at various roll gaps are presented in Figs 5.27 and 5.28, referring to the maximum pressure and nip angle shown in Figs 5.17 and 5.18 . It may be observed that both parameters decrease with increasing roll gap, which is the trend for the maximum pressure. The density distributions across the width of the ribbons for those produced with roll gaps of 0.6, 1.0 and 1.4 mm are compared in Fig. 5.29. From the density distribution curves, it is seen that the differences between the central section and edge sections reduce with decreasing roll gap.

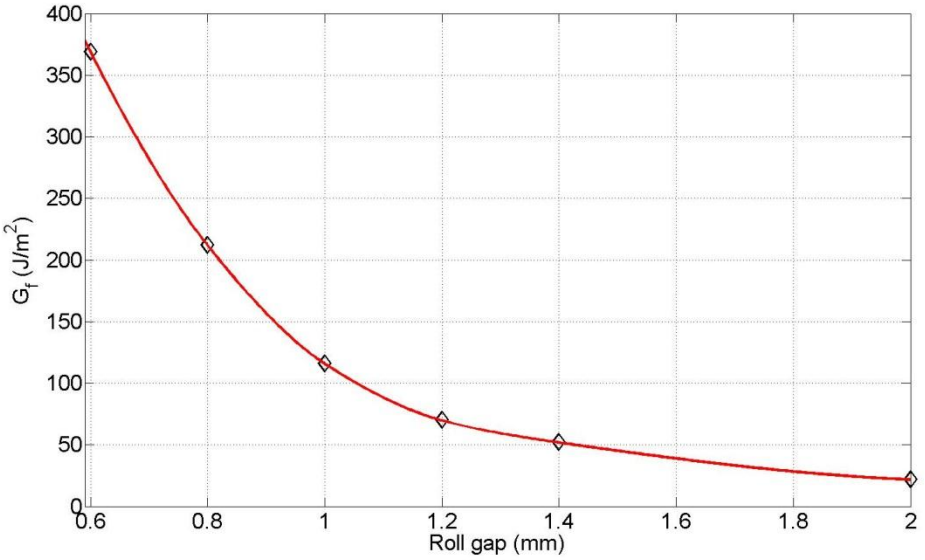

Figure 5.27 The fracture energy of the ribbons as a function of roll gap.

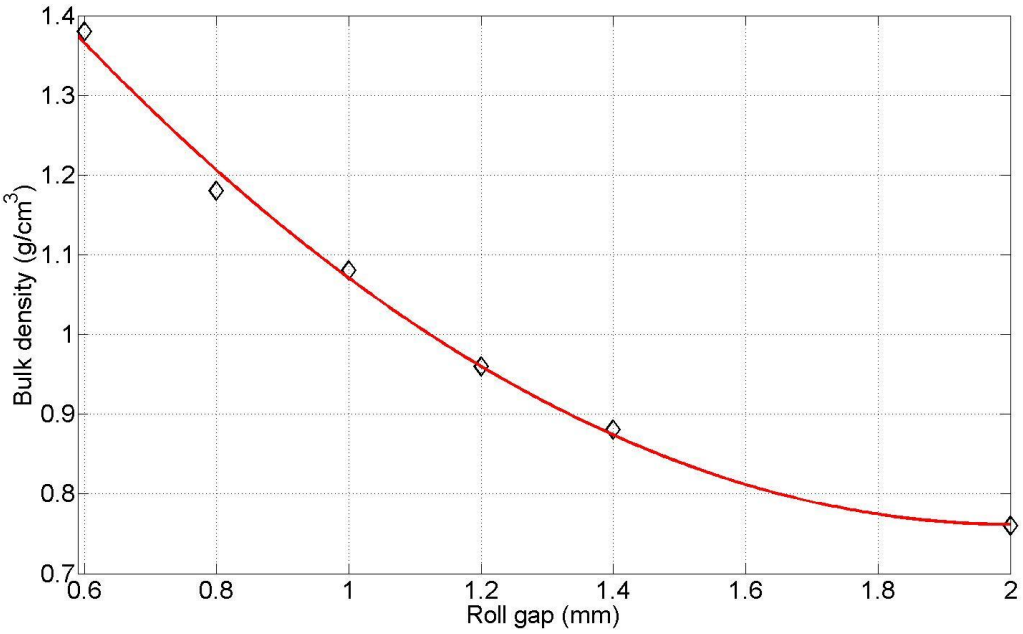

Figure 5.28 Bulk densities of the ribbons as a function of roll gap.

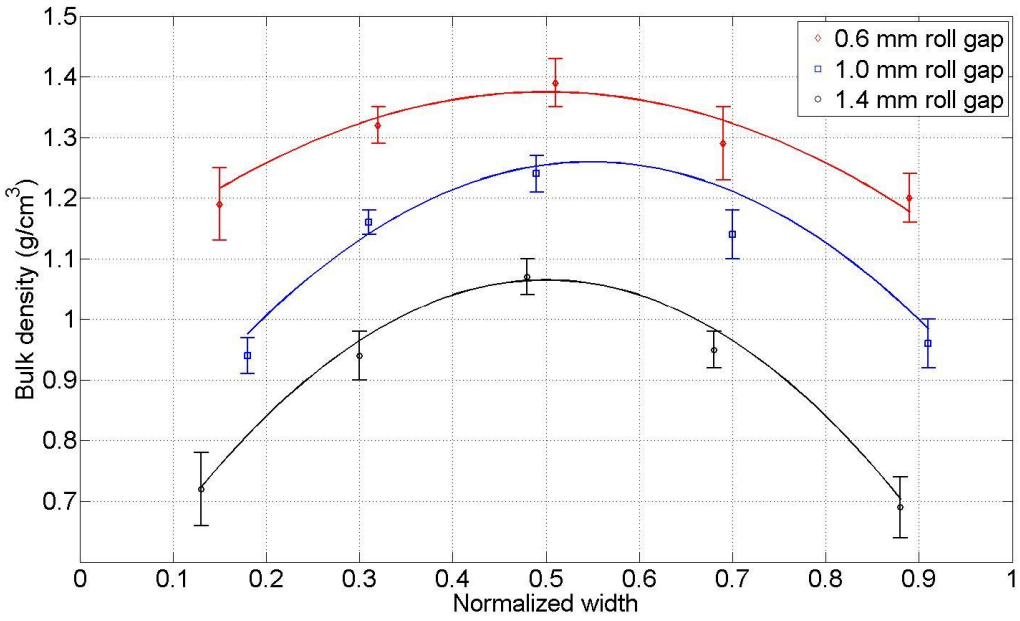

Figure 5.29 Bulk densities of sectioned ribbons as a function of normalized width for ribbons produced at various roll gaps.

Effects of roll speed

The effects of roll speed on ribbon properties are discussed in this section. The bulk densities (Fig. 5.30) and fracture energies (Fig. 5.31) decreased with increasing roll speed since the compression pressure applied decreased (Fig. 5.19). It may be noted that for the roll speeds considered, the bulk density and fracture energy are approximately constant when the roll speed is higher than 4 rpm. In order to study the effects of roll speed on the density distribution across the ribbon width, ribbons produced at roll speeds of 0.5, 2 and 5 rpm; the data are shown in Fig. 5.32. It can be seen that the density is more uniform across the ribbon width with increasing roll speed. However, the variation of the density uniformity is limited.

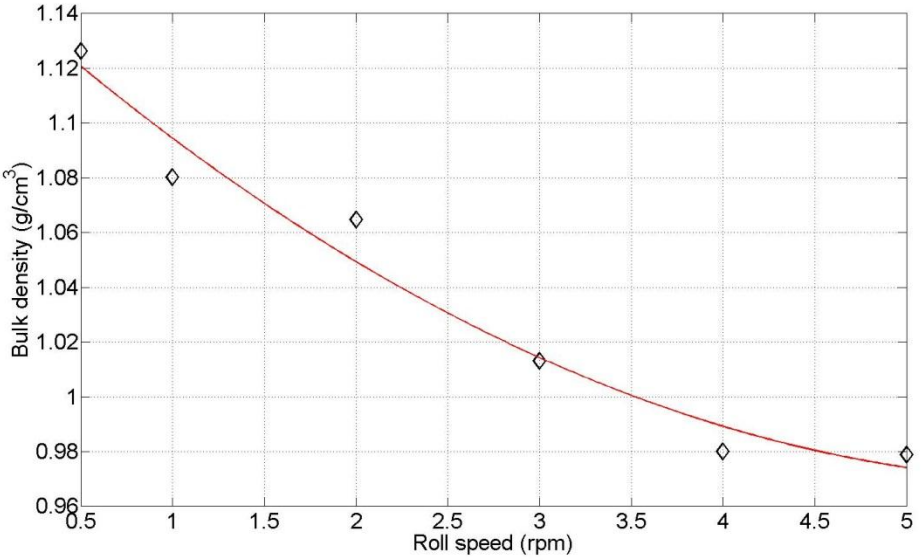

Figure 5.30 Bulk densities of the ribbons as a function of roll speed.

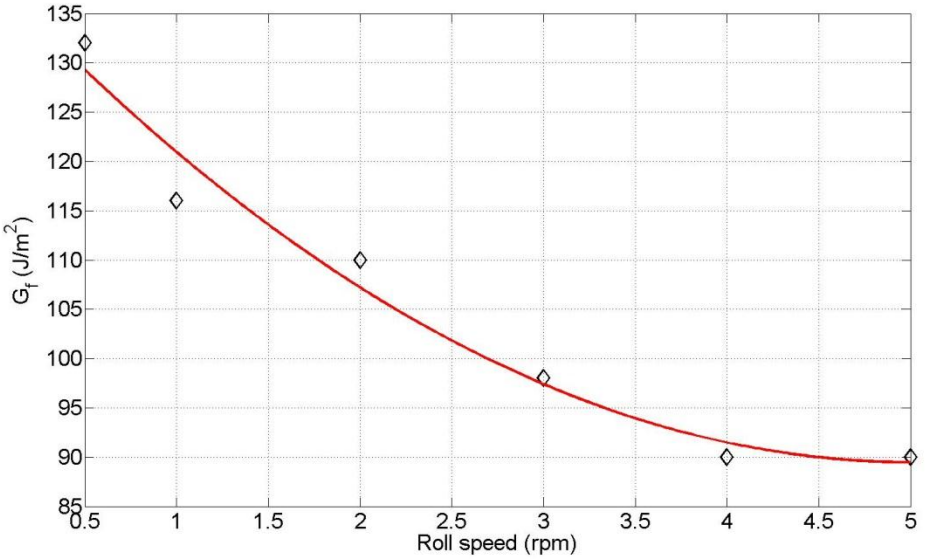

Figure 5.31 Fracture energy of the ribbons as a function of roll speed.

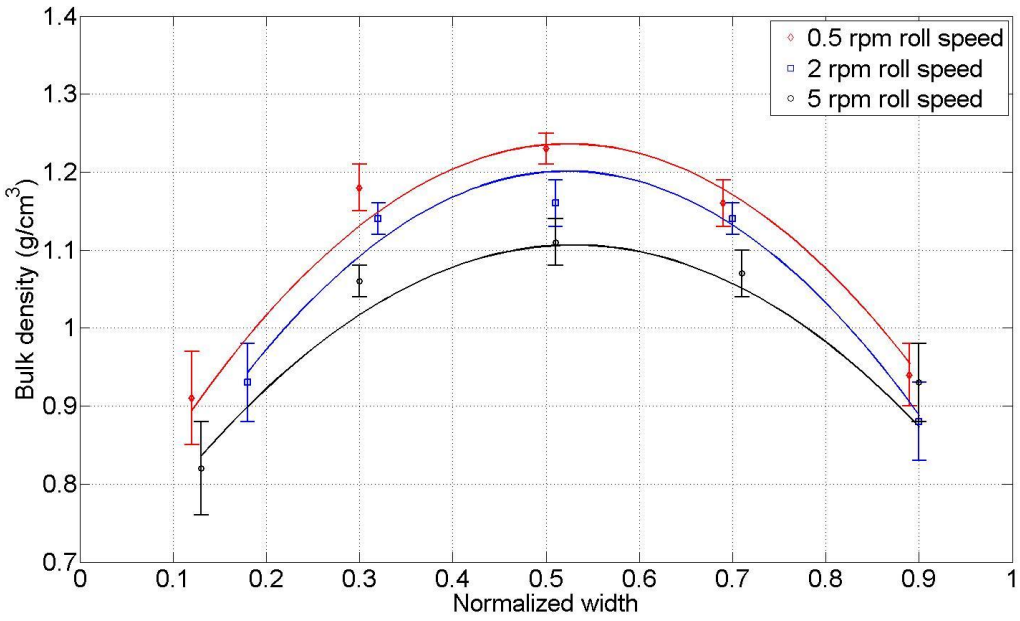

Figure 5.32 Bulk densities of sectioned ribbons as a function of normalized width for ribbons produced at various roll speeds.

Effects of lubrication

Table 5.5 lists the results for MCC (Avicel PH 102) ribbons produced with wall and bulk lubrication (0.25 and 1% MgSt w/w). By comparing the results with the values for unlubricated powders, it was found that bulk lubrication results in a decrease in the binding between the particles, and hence a decrease in the bulk density and fracture energy. However, there are no significant changes observed when wall lubrication was applied.

The density distribution results (Fig. 5.33) indicate that an enhanced uniformity is achieved in the case of wall lubrication. On the other hand, bulk lubrication leads to a reduction in the bulk density but shows no significant effect on the ribbon density distribution across the width.

Table 5.5 Bulk densities and fracture energies of MCC (Avicel PH 102) ribbons under various lubrication conditions (S =1.0 mm, u =1.0 rpm).

	Bulk density (g/cm^3)	Fracture energy (J/m^2)
No Lubrication	1.072 ±0.055	112 ±3
0.25 % MgSt (wall lubrication)	1.048 ±0.028	112 ±4
1% of MgSt (wall lubrication)	1.010 ±0.038	109 ±3
0.25 % MgSt (bulk lubrication)	0.843 ±0.020	69 ±1
1% of MgSt (bulk lubrication)	0.745 ±0.000	52 ±3

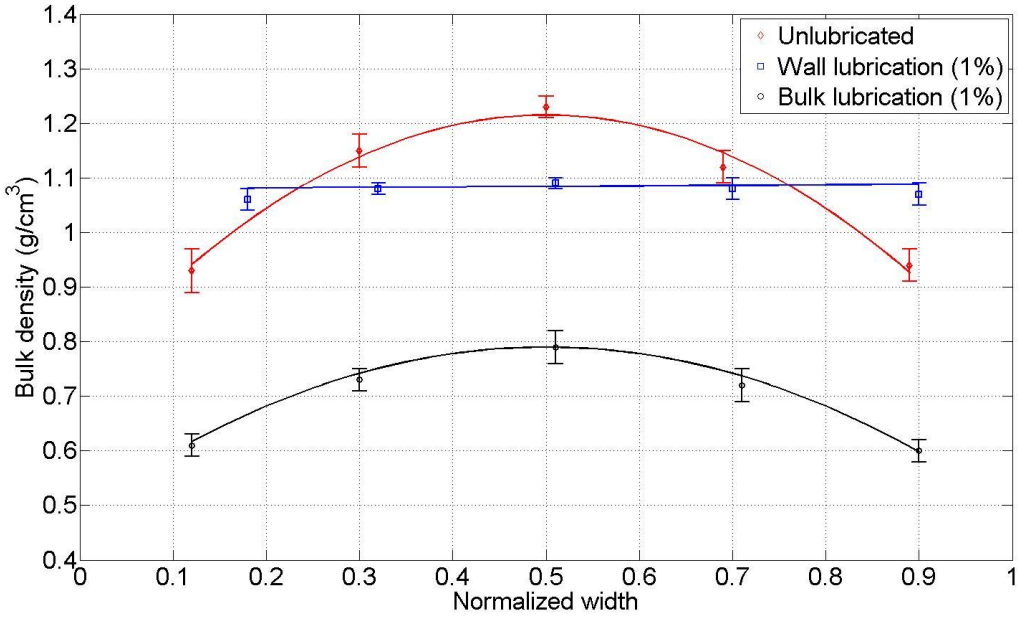

Figure 5.33 Bulk densities of sectioned ribbons as a function of normalized width for ribbons produced at under lubricated conditions.

Effects of moisture content

As shown in Fig. 5.34, the bulk density and fracture energy of ribbons made from moist powders were constant initially with an increase in the amount of additional water (2.5% w/w), but then the values increase with increasing moisture content, which is consistent with the variation of the maximum compression pressure (Fig. 5.23). It should be emphasised that the variations in both bulk density and fracture energy of the ribbons are not significant. There are no data collected for the ribbons produced from powders with more than 10% (w/w) added water. Due to cracking, which occurred along the central axis of the ribbons, as observation reported previously (Wu *et al.*, 2010b), accurate ribbon strength and bulk densities cannot be measured.

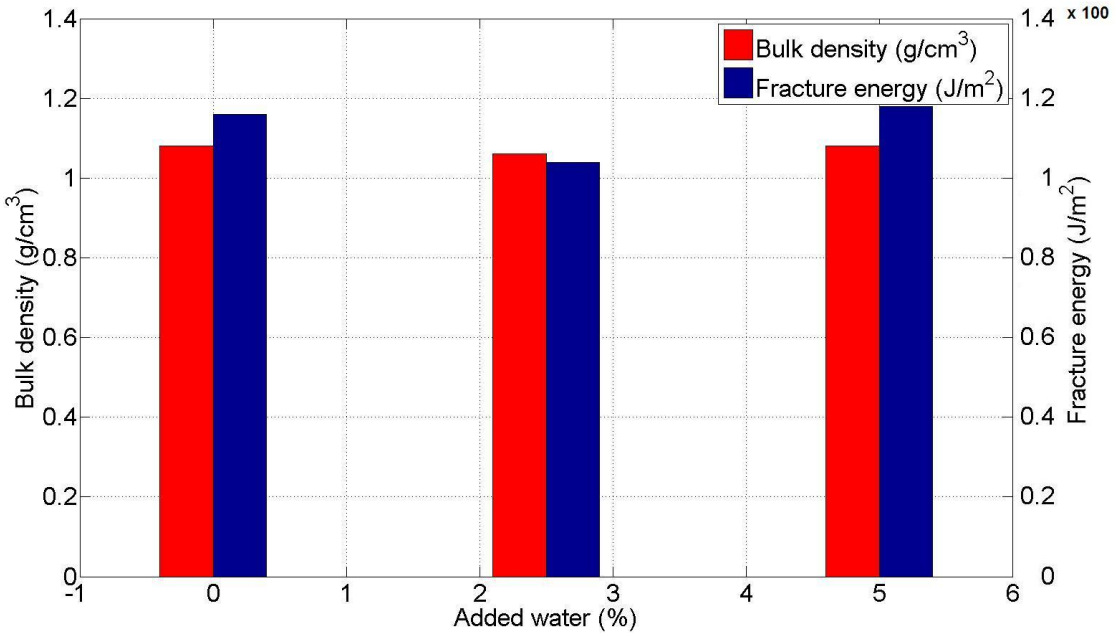

Figure 5.34 Bulk densities and fracture energies of the ribbons as a function of added water.

Surface topography

Typical surface topographies of the central part (1.27 x 1.71 mm) of the ribbons obtained by white light scanning are shown in Fig 5.35, and compared with SEM images. The roughness

of the ribbon is also accessible by combining the scan results of different section area of the ribbons. The bulk densities and the 3D surface roughness of the ribbons with various strengths may be fitted to an exponential relationship (Fig 5.36). In this thesis, arithmetic average 3D roughness S_a is used to describe the tomography of the ribbons, which was calculated from the average value of the heights integrated along a sampling area to a selected reference plane. This suggests another convenient approach for measuring the ribbon density, especially for the density measurement of isolated sections of the ribbons.

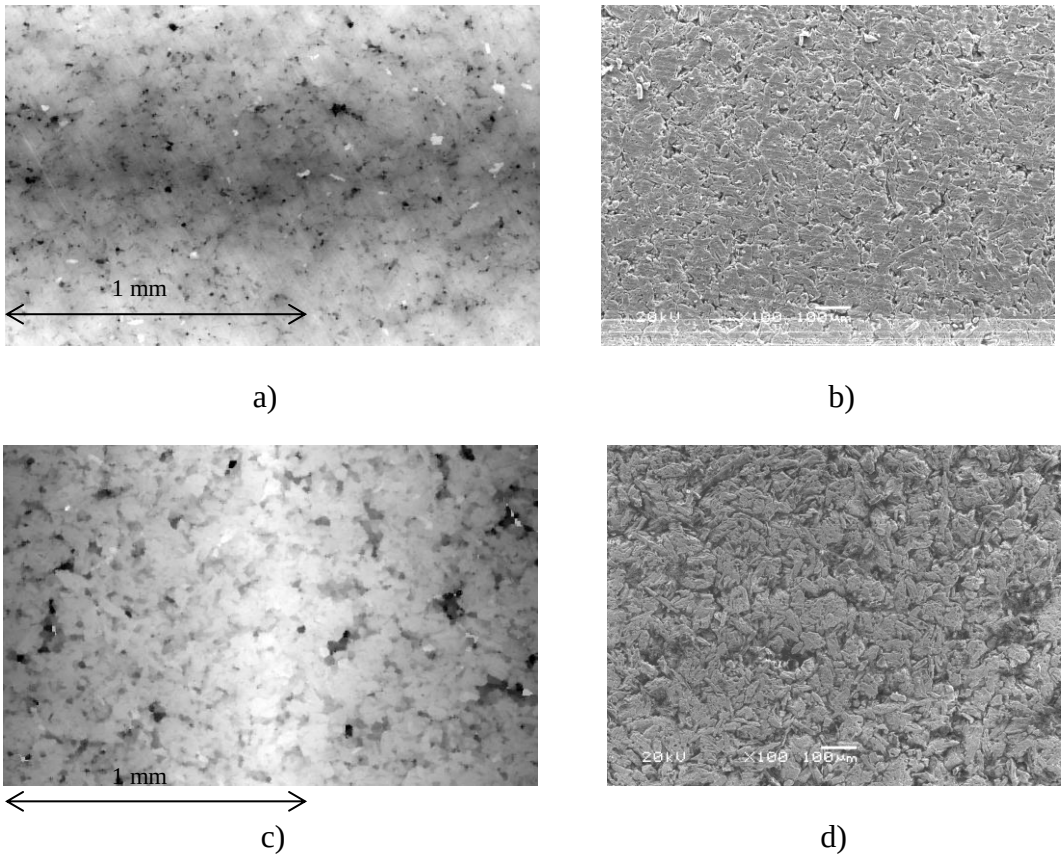

Figure 5.35 Interferometer surface image and SEM image of MCC ribbon with fracture energies of 116 J/m^2 $S_a = 5.78\mu m$ (a, b) and 22 J/m^2 $S_a = 2.68\mu m$ (c, d).

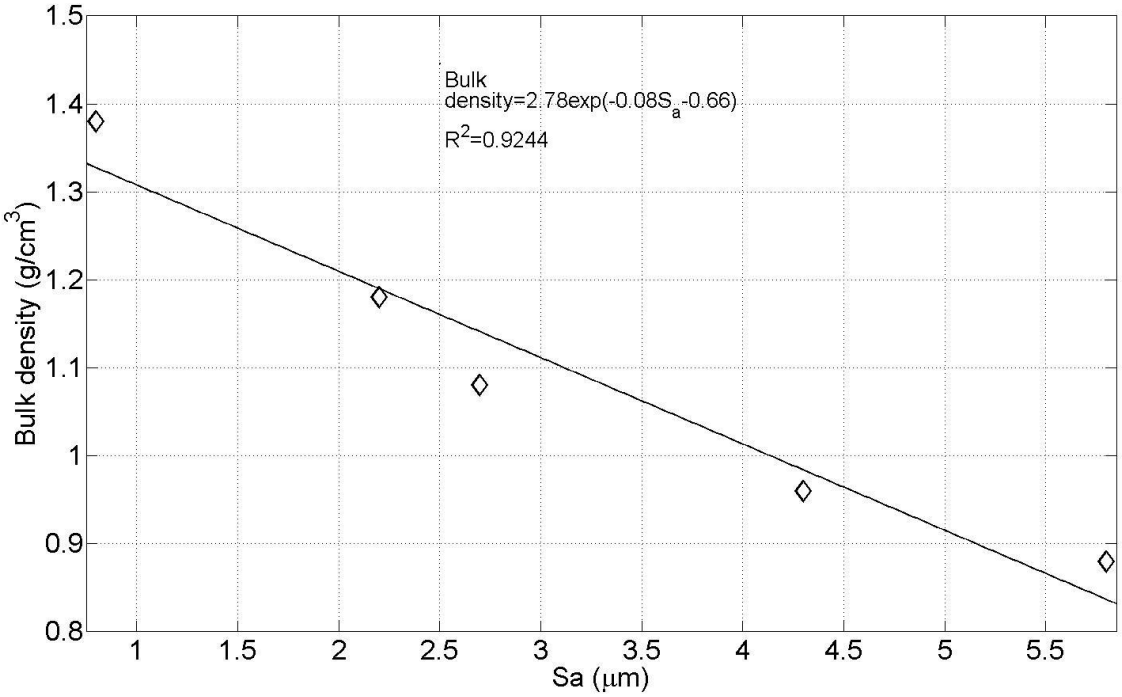

Figure 5.36 Bulk densities of the ribbons as a function of the surface roughness.

5.3 Conclusions

In this chapter, the characteristics of the primary powders are presented. The effects of flow and frictional properties of the powders on roll compaction behaviour are explored by investigating the behaviour of powders with distinctive properties. Lubricated, moist powders and binary mixtures are also considered to explore the influence of powder condition on roll compaction. The ribbons are characterised by bulk density, fracture energy and density distribution. The results highlight the correlation between ribbon properties and process parameters, and the domination of the properties of the feeding powder. Generally, high values of the flow function, internal and wall friction angle of the feeding powder results in a greater pressure in roll compaction and therefore corresponding stronger and denser ribbons. For a given feed powder, high compaction pressures and large nip angles are only achievable at small roll gaps and roll speeds. The detailed discussion and the mechanisms will be given in Chapter 8.

CHAPTER 6 MILLING RESULTS

In the pharmaceutical industry, milling processes are employed to fragment roll compacted ribbons in order to produce granules of the specified size for tabletting. In this study, experiments have been carried out to investigate the process and explore the influence of the properties of roll compacted ribbons. Milling experiments were performed using an oscillating graulator. The effects of process parameters (*i.e.* the screen mesh size of the mill which indicates the size of the openings on the screen mesh, and the milling frequency) and the properties of the ribbons (*i.e.* the fracture energy) are explored in this chapter.

6.1. First order kinetic model for milling

Figure 4.18 shows a typical variation of the mass throughput as a function of the number of milling cycles. The mass throughput increases with the number of cycles, but with a decreasing rate. It is possible to describe the data using first order kinetics (Largergren, 1898):

$$\frac{dm}{dN} = k\,(m_\infty - m) \qquad \text{Eq (6.1)}$$

where N is the number of cycles, and m and m_∞ are the current mass of granules and that at the end of the milling process. Integrating Eq. (6.1) with the limits m = 0 at N = 0 and $m = m_\infty$ at $N = N_\infty$ gives an expression that may be written in the following form (detailed derivation is shown in Appendix 2):

$$\frac{m_\infty - m}{m_\infty} = \exp\left(-\frac{N}{N_c}\right) \qquad \text{Eq (6.2)}$$

where N_c is the characteristic number of milling cycles at which $m = 1 - e^{-1}$. Thus N_c can be used to describe the mass throughput of the milling process (Fig. 6.1): a smaller value of N_c corresponds to more rapid breakdown of the ribbons, and a larger value corresponds to a lower fracture rate of the ribbons. Eq. (6.2) can be re-arranged as:

$$m = m_{\infty}\left[1 - \exp\left(-\frac{N}{N_c}\right)\right] \qquad \text{Eq (6.3)}$$

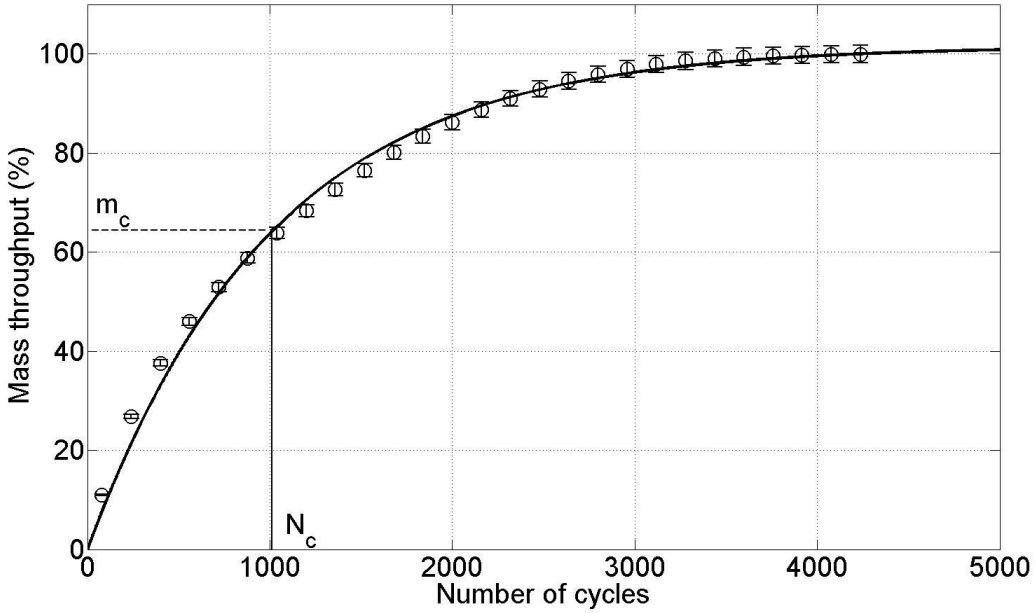

Figure 6.1Typical milling results for roll compacted ribbons made from unlubricated MCC powders at a roll gap of 1.0 mm and a roll speed of 1.0 rpm. The line is the best fit to Eq. (6.3).

The capability of the first order kinetic model was evaluated for various milling parameters (*i.e.* milling frequency and screen size), as shown in Fig. 6.2. For all the milling conditions, a full granulation (100% percentage mass throughput for the granules) could be attained. However, the value of N_c increases with decreasing screen mesh size (Fig. 6.2a) and milling frequency (Fig. 6.2b) which indicated a reducing mass throughput in unit time. The first order

kinetics model shows good agreement with the experimental results (Fig. 6.2), indicating that the milling processes are well described using the model.

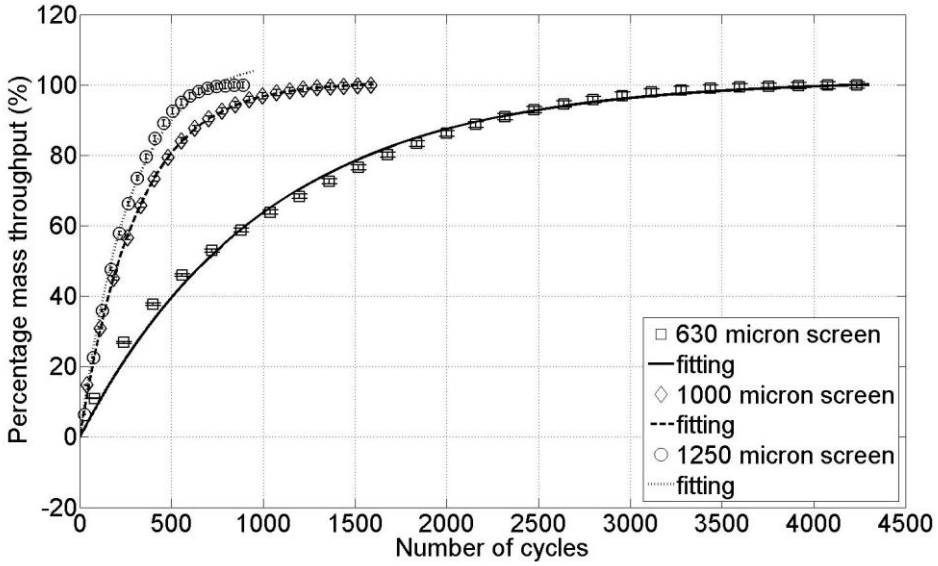

a)

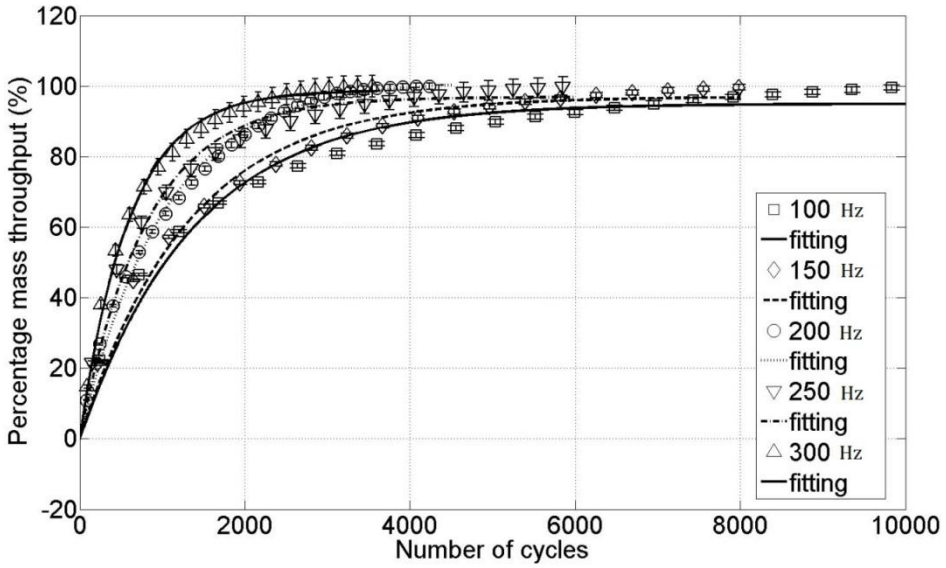

b)

Figure 6.2 Variation of mass throughput with the number of cycles for milling processes with a) various screen mesh sizes and b) various milling frequencies. The lines are the best fits to Eq. (6.3).

6.2 Influence of realtive density of the ribbons and milling parameters

The mass throughput and mean particle of the milled granules were measured. The effects of the ribbon relative density, and milling parameters (screen mesh size and milling frequency) were evaluated. Figures 6.3 and 6.4 show the reciprocal of N_c and mean granule size as a function of the ribbon relative density, respectively. It can be seen that mean size of the granules increases with the relative density of the ribbons while the mass throughput decreases. This indicates that the milling of denser and stronger ribbons is more time consumed, and the granules produced are larger in size.

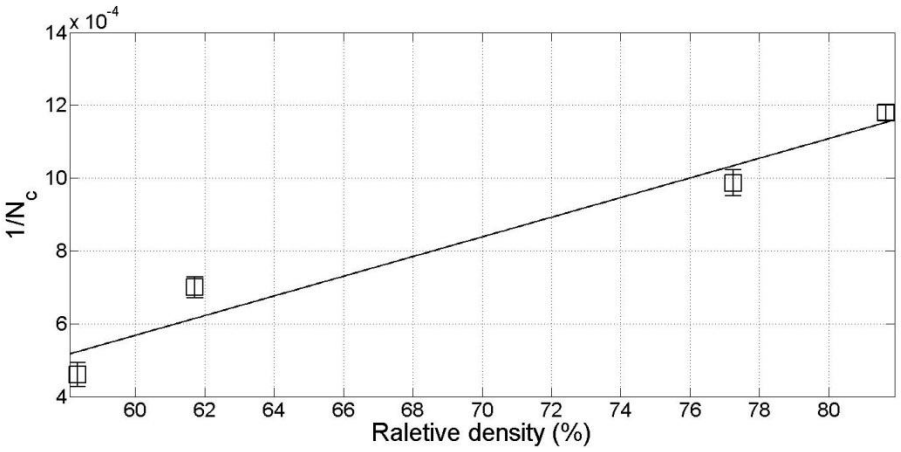

Figure 6.3 Reciprocal of N_c as a function of ribbon relative density (milled with a 630 µm screen at 200 Hz).

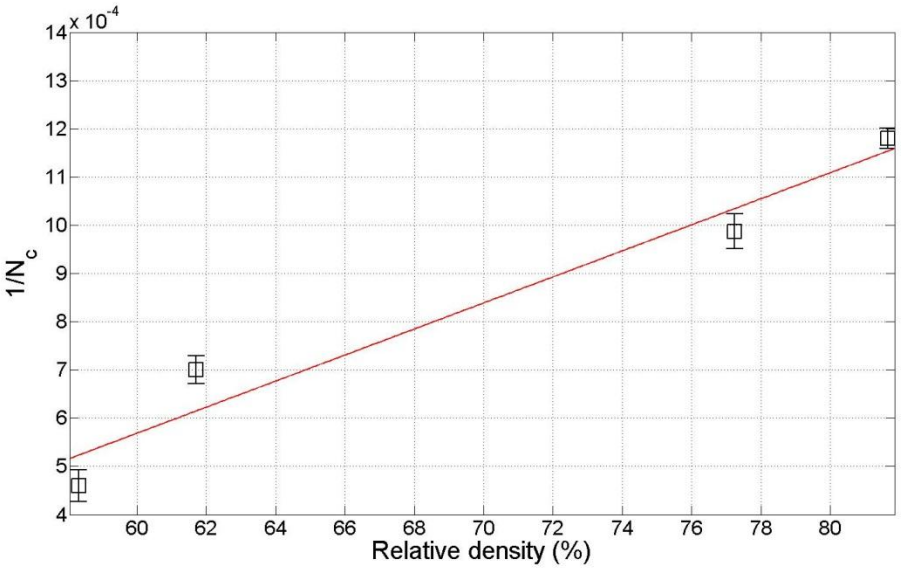

Figure 6.4 Mean granule size as a function of ribbon relative density (milled with a 630 µm screen at 200 Hz).

Fig. 6.5 shows that the variation of the reciprocal of N_c is increases with increasing screen size. It can be seen that the mass throughput of the milling process increases with the screen mesh size as expected, since the energy required to break the ribbons to a size that is sufficiently small to pass through the screen decreases with increasing mesh size. The variation of the mean particle size of the granules produced with increasing screen size is shown in Fig. 6.6. It is interesting to note that the mean granule size shows a linear relationship with the screen size (Fig. 6.6) for the current system, which suggests that the mean size of the granules can be simply predicted as being approximately 69% of the screen mesh size.

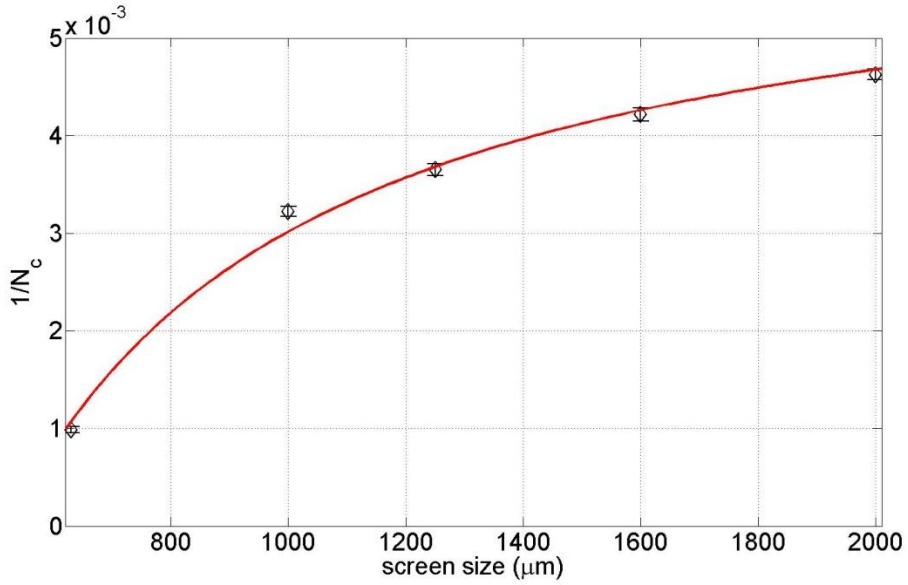

Figure 6.5 Reciprocal of N_c as a function of screen mesh size (ribbons with 112 J/m^2 fracture energy milled at 200 Hz milling frequency).

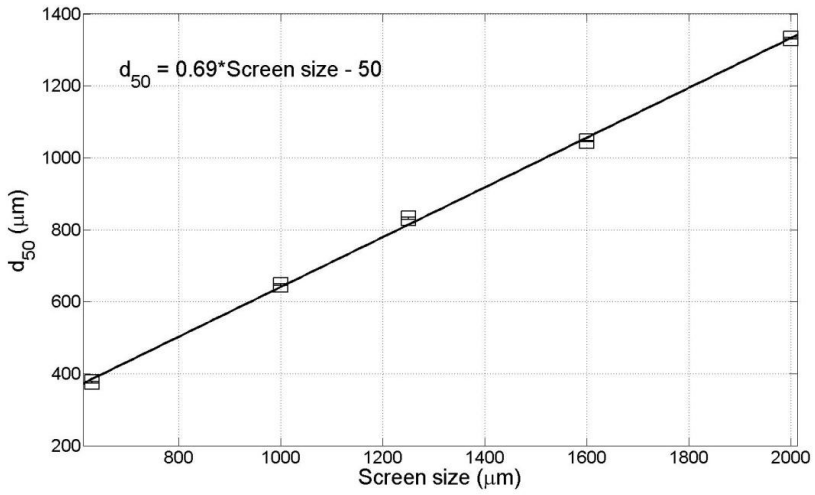

Figure 6.6 Mean granule size as a function of screen mesh size (ribbons with 112 J/m^2 fracture energy milled at 200 Hz milling frequency).

With increasing milling frequency, when other parameters were fixed, the mass throughputs of the granules were relatively constant at relatively low milling frequencies (*i.e.* < 200 Hz) but increase sharply at higher milling frequencies (*i.e.* ≥ 200 Hz) (Fig. 6.7). Thus, the data can be divided into two distinct regions implying that different milling mechanisms are involved.

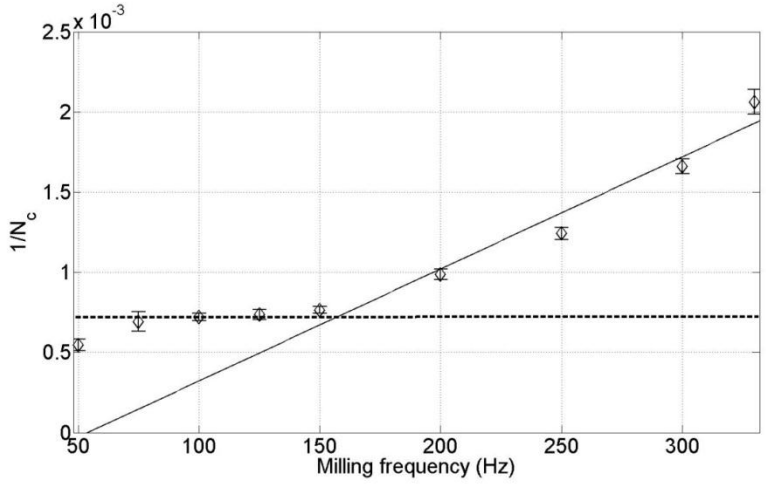

Figure 6.7 Reciprocal of N_c as a function of milling frequency (ribbons with 112 J/m^2 fracture energy milled at 630 µm screen).

Figure 6.8 shows the variation of the mean granule size with the increasing milling frequency. It can be seen that the mean granule size decreases with the increasing milling frequency. The mean granule sizes were 446 and 333 µm for 50 and 330 Hz milling frequencys, respectively. A difference of over 25% is induced by only changing the milling frequency.

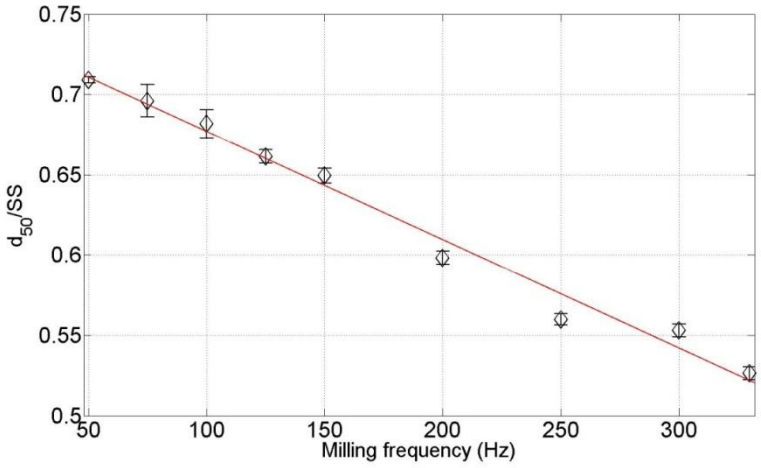

Figure 6.8 Mean granule size as a function of milling frequency (ribbons with 112 J/m^2 fracture energy milled at 630 µm screen).

The granule size distributions of the products from various conditions are presented in Fig 6.9. All the granules were milled from the ribbons produced at 1 mm roll gap and 1 rpm roll speed. It can be seen that the granule sizes for DCPD, which is more fragile and cannot form solid compacts during roll compaction, is much smaller than those for MCC. 'MCC Granule 0.8mm1rpm …' and 'MCC Granule 1.4mm5rpm…' were labelled by the roll compactor conditions used to produce the ribbons, representing the strongest and weakest ribbons used in this measurement, respectively. The detailed information of d_{10}, d_{50}, and d_{90} of the MCC granules are shown in Table 6.1. It can be seen that the value of both d_{10} and d_{90} of the granules increases with the ribbons strength and screen mesh size. However, the variation of d_{90} is much larger than that of d_{10}. It may also be observed that the value of d_{90} is larger than the corresponding screen mesh size. This might be caused by the granules with sides longer than the screen mesh size.

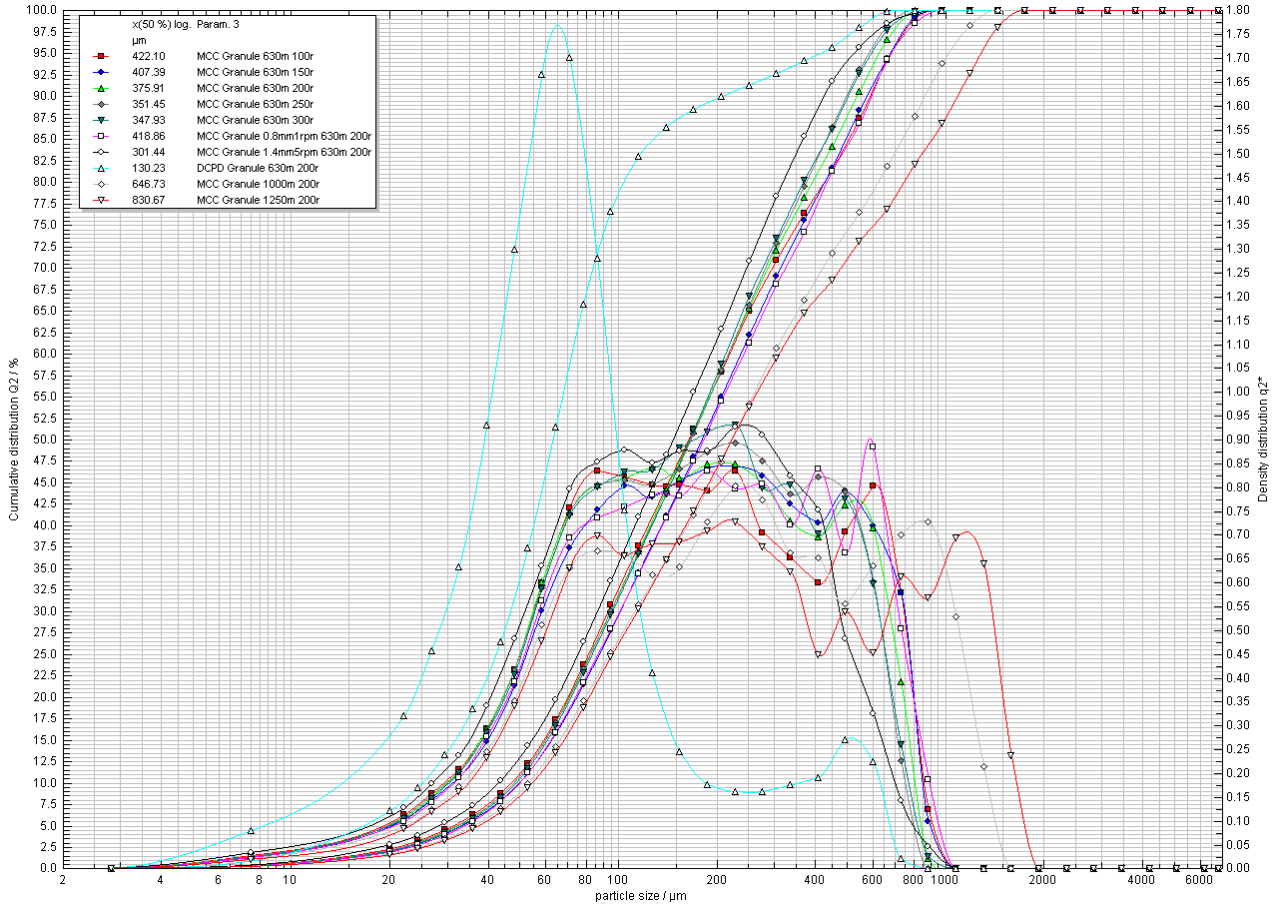

Figure 6.9 Granule size distributions obtained from various conditions.

Table 6.1 Size of the MCC granules (derived from Fig 6.9).

Granule			d_{10} (μm)	d_{50} (μm)	d_{90} (μm)
Ribbon fracture energy (J/m^2)	Screen mesh size (μm)	Milling frequency (Hz)			
52	630	200	102	301	562
212		200	131	419	740
112		100	113	422	732
		150	121	407	727
		200	111	376	686
		250	109	351	626
		300	109	348	634
	1000	200	148	647	1180
	1250	200	149	831	1400

6.3 Fracture mechanisms

As reported in section 6.2, the experimental results suggested that there are two milling regimes. The sets of data obtained from the milling processes for the MCC ribbons with constant strength (112 J/m^2 fracture energy), which were milled at various milling frequencies but with a fixed screen mesh of 630 μm, were employed to investigate the relationship between the energy input and mass throughput of the granules. The instantaneous mass of the ribbons in the milling chamber was multiplied by the velocity of the blade to determine the kinetic energy input. Thus, the mass throughput of the process can be plotted as a function of the kinetic energy (see in Fig. 6.10). Two regions were also observed in this case. With a lower kinetic energy input, (< 0.16 J) the reciprocal of N_c is almost constant. By contrast, the reciprocal of N_c increases linearly with the input kinetic energy for higher kinetic energies (≥ 0.16 J). This might be ascribed to two possible mechanisms for the fracture of the ribbons: 1) abrasive fracture in which fragments are produced by the scratching of the objectives (*i.e.* ribbons and the mesh screen; and 2) impact fracture in which the ribbons are broken by the large forces at a collision of the ribbons with a blade.

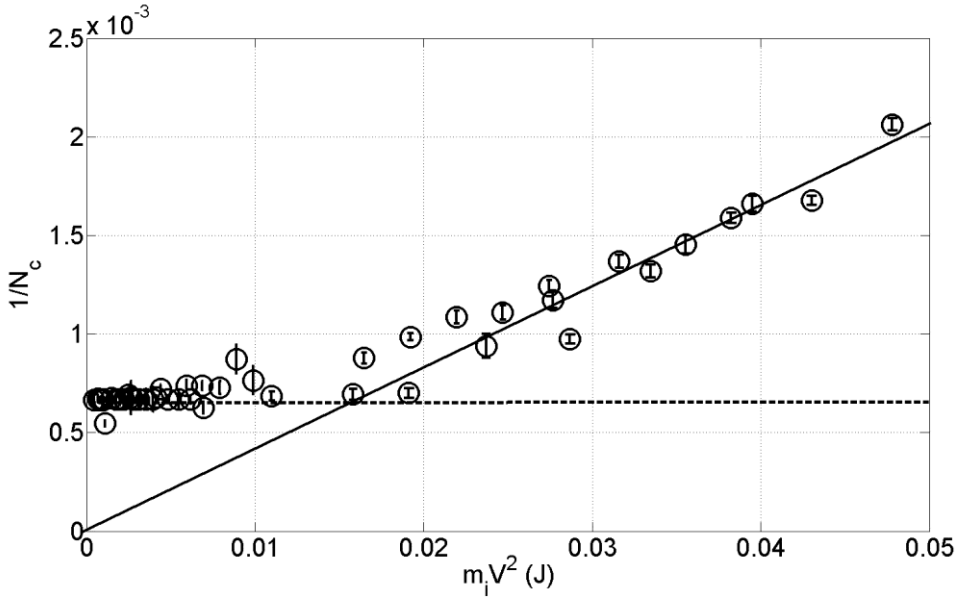

Figure 6.10 Reciprocal of N_c as a function of kinetic energy (ribbons with 112 J/m^2 fracture energy milled at 630 µm screen).

6.4 PEPT analysis

Positron emission tomography (PET) was firstly applied in medicine, and treated as one of the most powerful functional imaging modality in the field. In order to study engineering processes, positron emission particle tracking (PEPT) has been developed by adapting the PET technique (Parker *et al*., 2008). In the current work, PEPT has been employed to record the motion of the ribbons in the milling processes. The influence of material properties (*i.e.* ribbons made from different powders and ribbons with distinct strengths) and process parameters (*i.e.* screen mesh size and milling frequency) were examined. The velocity and occupancy of the ribbons were calculated to attain further understanding of the fracture mechanisms in the oscillating granulation system.

6.4.1 Single tracer experiments

By adding a radioactive tracer into a ribbon during roll compaction, the motion of the ribbons during the milling was recorded. Relative velocity mapping and the speed distribution of the

ribbons were obtained numerically to evaluate the influence of the ribbon fracture energy and the most dominating milling parameter – milling frequency. The occupancies of the ribbons were also evaluated to investigate the milling mechanisms.

Influence of ribbon fracture energy

In order to evaluate how the milling behaviour is affected by the strength of the ribbons, MCC ribbons with various fracture energies were milled with a screen mesh size of 1 mm and milling frequency of 200 Hz. Figure 6.11 shows the velocity mapping of the ribbons during the milling. In the milling process, the region in which the ribbon specimen moves vortically around a centre location where the instantaneous velocity is almost zero is defined as a 'vortex'. It can be seen that for all the ribbons, three vortices occur. With an increase in the ribbon strength, the vortices are more prominent, which suggests increasing circulating motion of the ribbons.

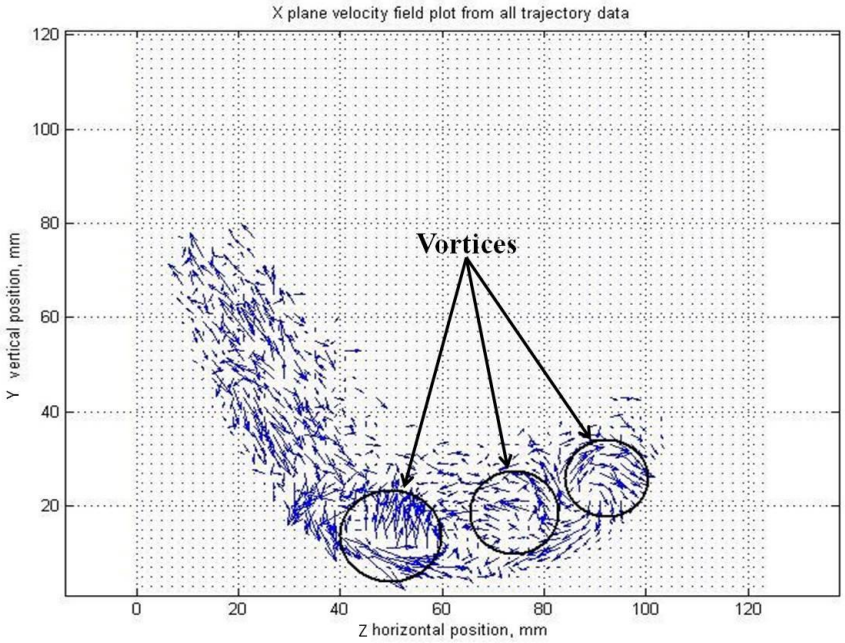

a)

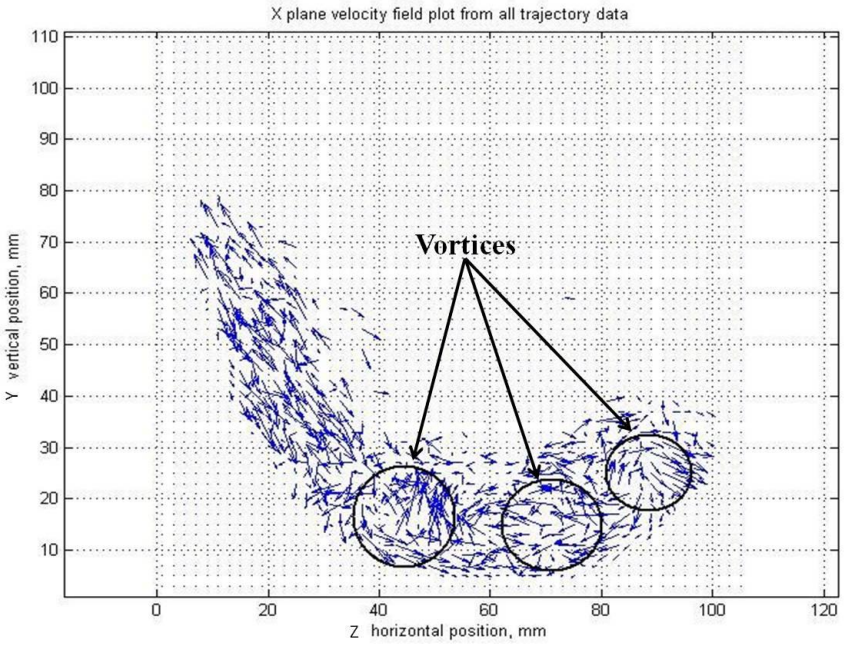

b)

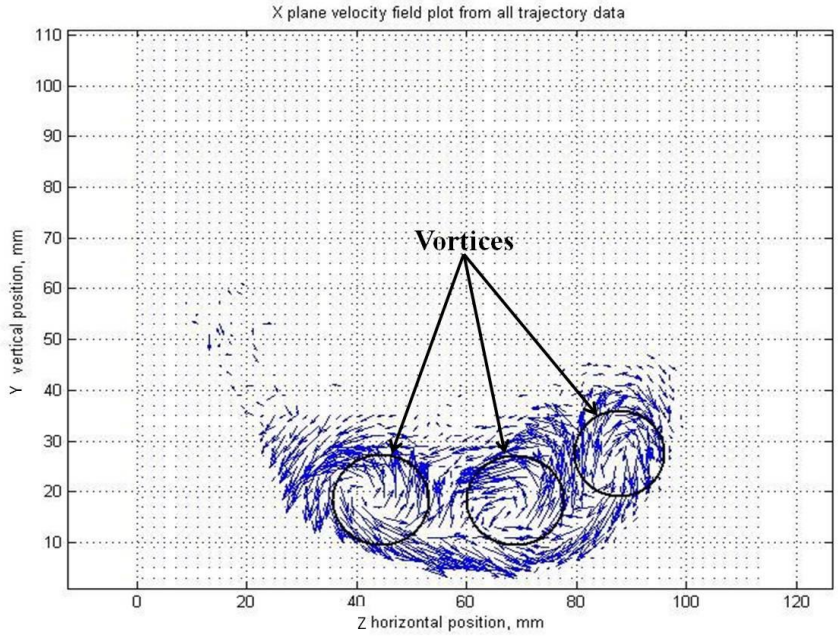

c)

Figure 6.11 Velocity mapping on the y-z plane for MCC ribbons with a) 52, b) 112 , c) 369 J/m^2 fracture energy.

The distributions of the relative speed of the ribbons during the milling are shown in Fig 6.12. The relative speed is defined as the ratio of ribbon speed to the blade speed, which is a dimensionless value of the speed of the ribbons. The blade speed is calculated in terms of the milling rotational speed and radius of the impeller. Since the rotation angle of the impellor is 90 º, the following relationship was adopted:

$$V_{Blade} = f_{mill} \times \pi \times R_{Blade} \qquad \text{Eq (6.4)}$$

where V_{blade} is the speed of the blade, f_{mill} is the milling frequency, R_{Blade} is the radius of the impeller.

It is clear that the speed of the ribbons decreases with increasing ribbon strength, since larger remains of the stronger ribbon hindered the motion of the ribbon specimens. The relative speed of the ribbon to the blade was calculated according to the instantaneous direction and values of the ribbon speed and blade speed It is found that the fracture energy of the ribbon increases from 52 to 369 J/m^2, the average relative speed decreases from 0.08 to 0.04, and the peak value decreases from 0.95 to 0.45.

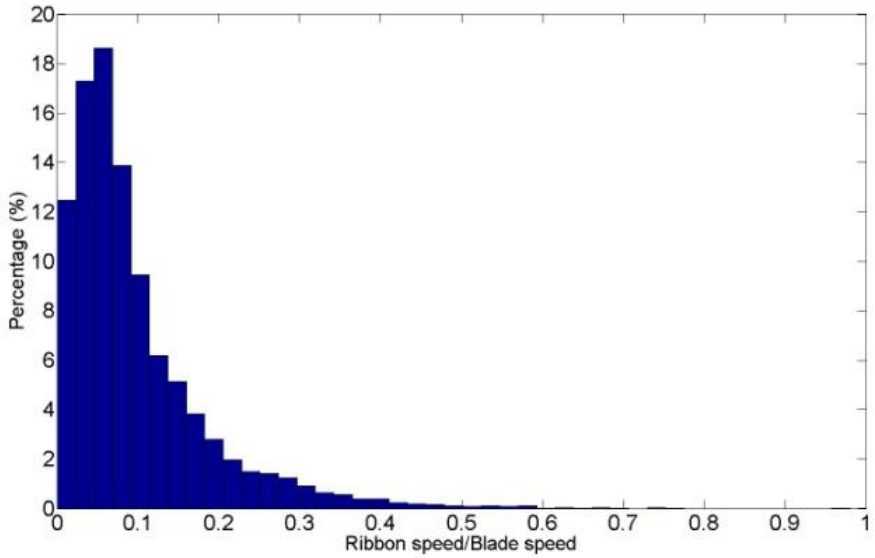

a)

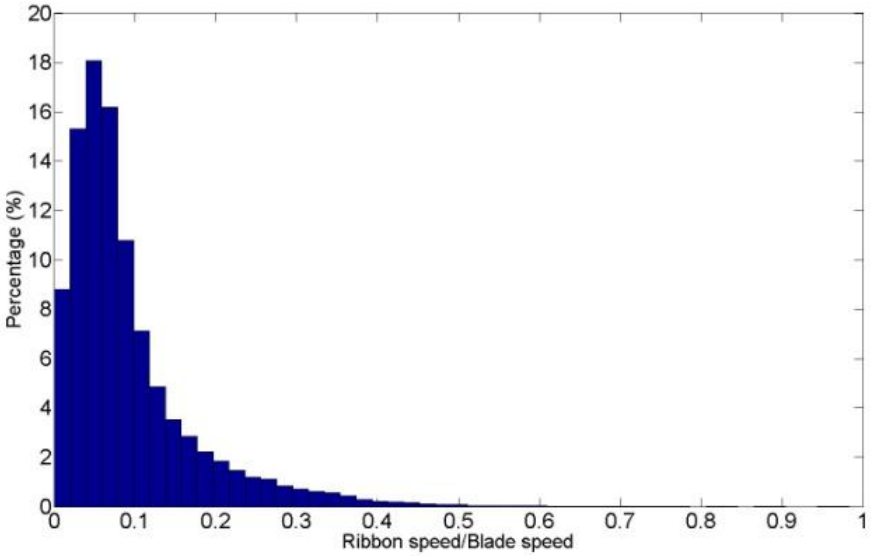

b)

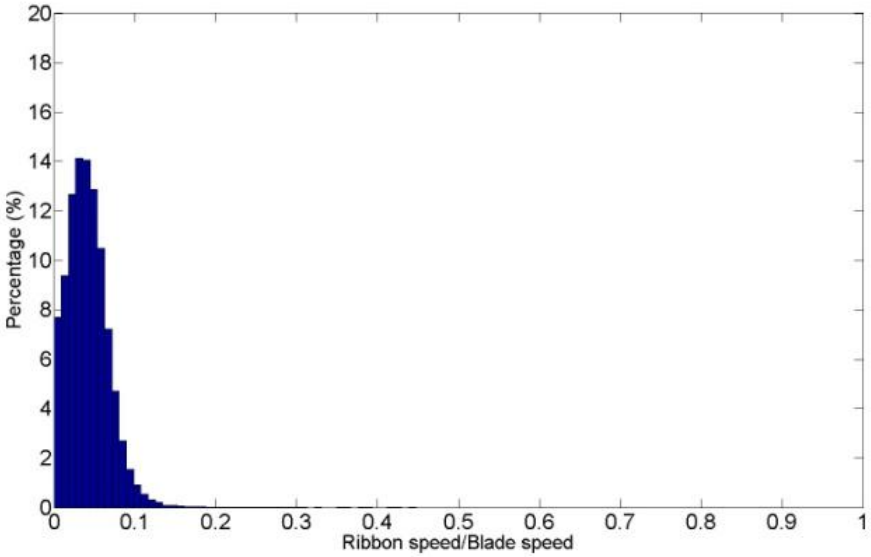

c)

Figure 6.12 Relative speed distribution on the y-z plane for MCC ribbons with a) 52, b) 112 , c) 369 J/m^2 fracture energy.

Influence of milling frequency

The velocity fields for various milling frequencys are shown in Fig. 6.13. It can be seen that the typical circulating motion, which is significant at the milling frequency of 200 Hz, does not occur at low or high milling frequency (50 and 300 Hz). This circulating motion is ascribed to the rotation of the ribbon specimens, which does not occur at the low milling frequency (*i.e.* 50 Hz) where plug flow dominates, or at high milling frequency (*i.e.* 300 Hz) where the momentum is high enough for the ribbon specimens to move to the upper part of the milling chamber. Additionally, the ribbons occupy more space in the milling chamber with increasing milling frequency.

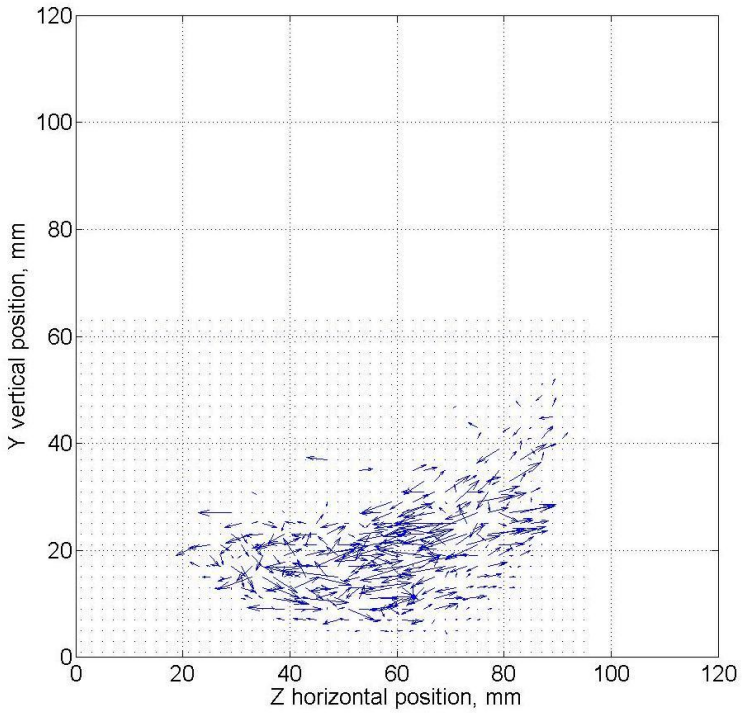

a)

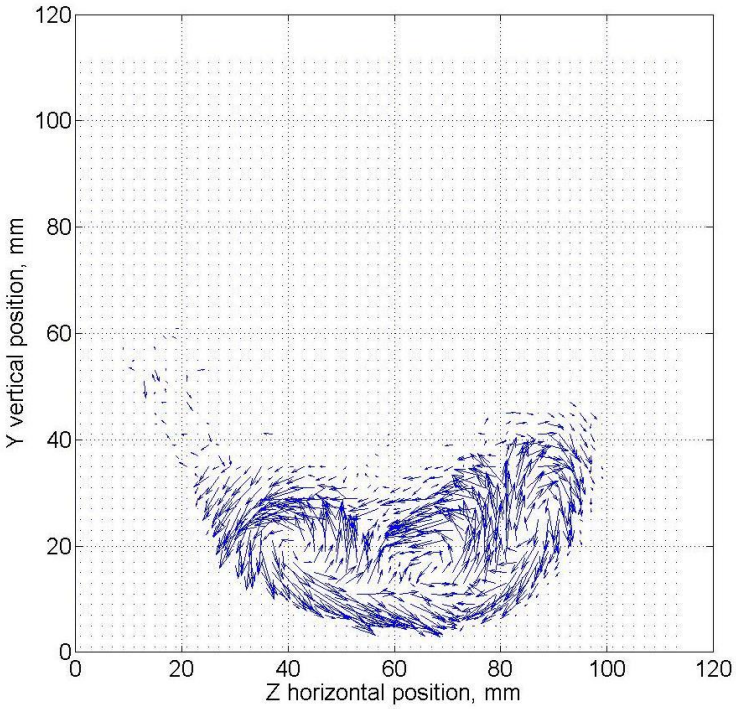

b)

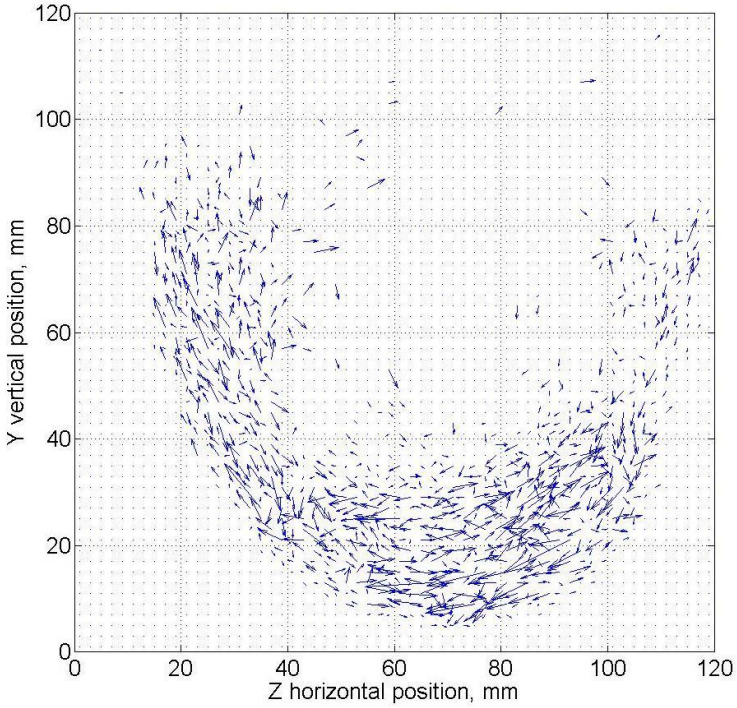

c)

Figure 6.13 Velocity mapping on y-z plane for MCC ribbons with 112 J/m^2 fracture energy milled at a) 50, b) 200 and c) 300 rpm milling frequency.

The speed distributions of the ribbons at various milling frequencies (*i.e.* 50, 200, 300 Hz) are presented in Fig. 6.14. A significant increase in the speed of the ribbons is observed with increase in the milling frequency due to the momentum balance. The peak velocity of the ribbons was almost twice that of the blade when 300 Hz milling frequency was applied.

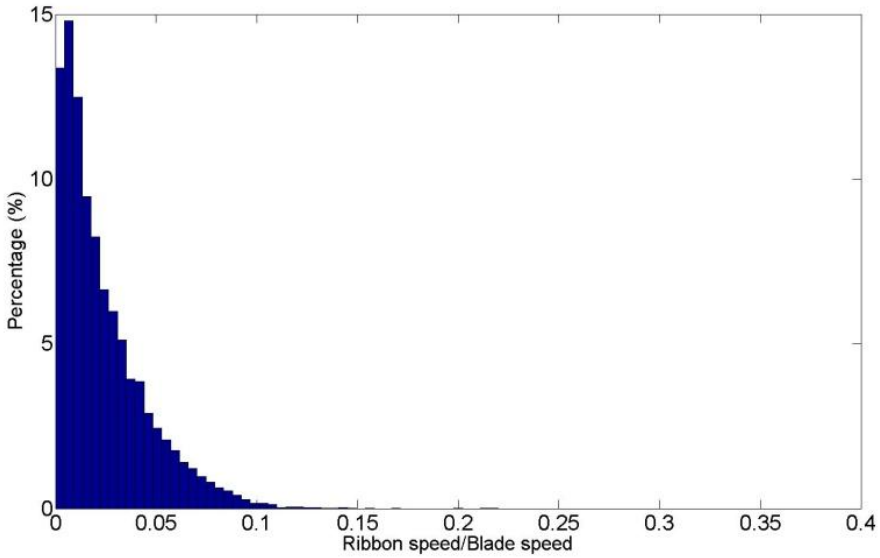

a)

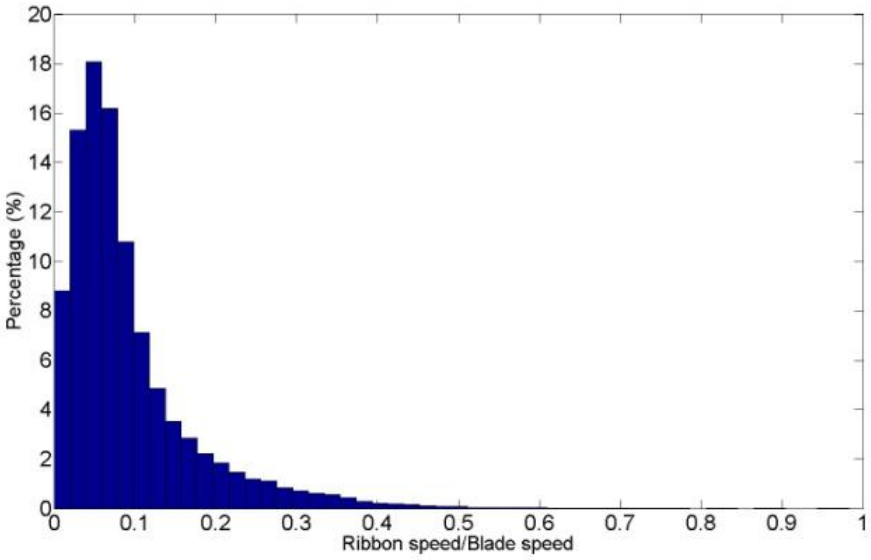

b)

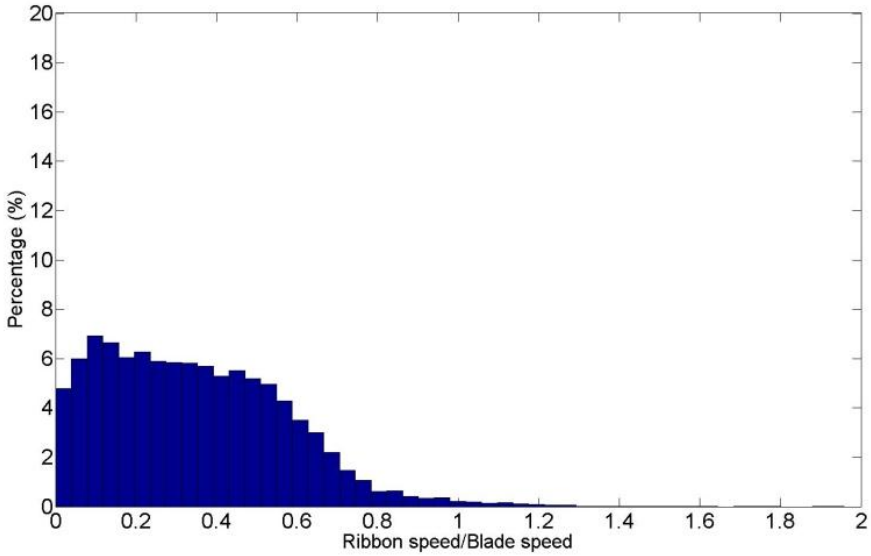

c)

Figure 6.14 Relative velocity mapping on the y-z plane for MCC ribbons with 112 J/m^2 fracture energy milled at a) 50, b) 200 and c) 300 Hz milling frequency.

Milling regions

The numbers of appearance of the ribbons within cells of 1 x 1 mm were examined to determine the occupancies, as shown in Fig. 6.15. The velocities of the ribbons were superimposed. It is found that the velocities of the ribbons increased sharply with increasing milling frequency, especially in the high milling frequency region (say > 200 Hz). In addition, the motion of the ribbons concentrated in the lower part of the milling chamber at lower milling frequency (50 Hz), had spread to upper part of the milling chamber with increasing milling frequency (200, 300 Hz). It is also remarkable that the ribbons moved at a relatively low velocity in the lower part but at a higher velocity in upper part in the milling chamber. This suggests that the motion of the ribbons (both trace and velocity) at low milling frequency (≤ 200 Hz) and high milling frequency (> 200 Hz) are similar to the observations in Section 6.3. In both cases, the partition of the two regions is dominated by the milling frequency, or in other words, the kinetic energy input.

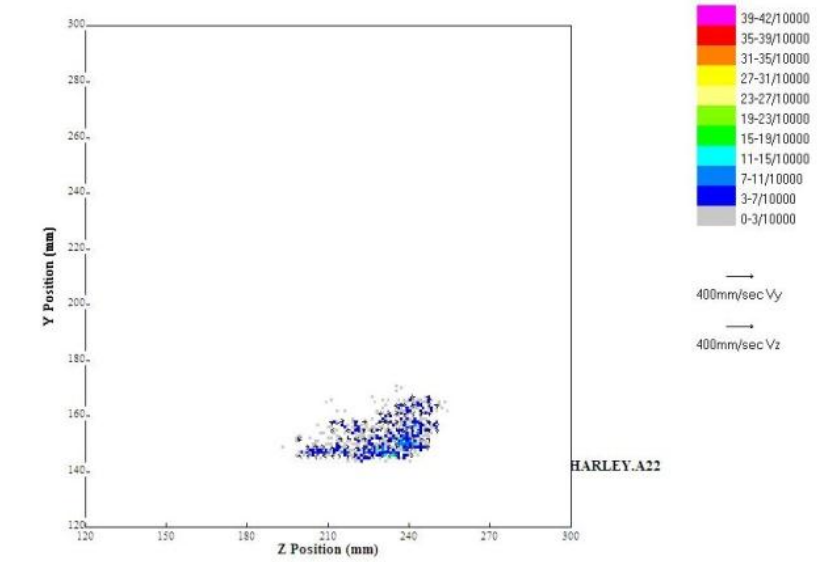
39-42/10000
35-39/10000
31-35/10000
27-31/10000
23-27/10000
19-23/10000
15-19/10000
11-15/10000
7-11/10000
3-7/10000
0-3/10000
400mm/sec Vy
400mm/sec Vz
Y Position (mm)
Z Position (mm)
HARLEY.A22

a)

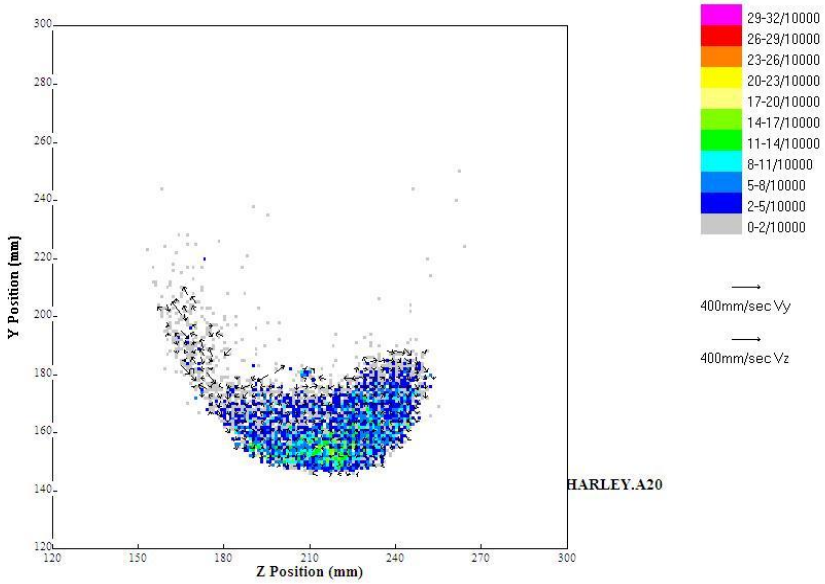
29-32/10000
26-29/10000
23-26/10000
20-23/10000
17-20/10000
14-17/10000
11-14/10000
8-11/10000
5-8/10000
2-5/10000
0-2/10000
400mm/sec Vy
400mm/sec Vz
Y Position (mm)
Z Position (mm)
HARLEY.A20

b)

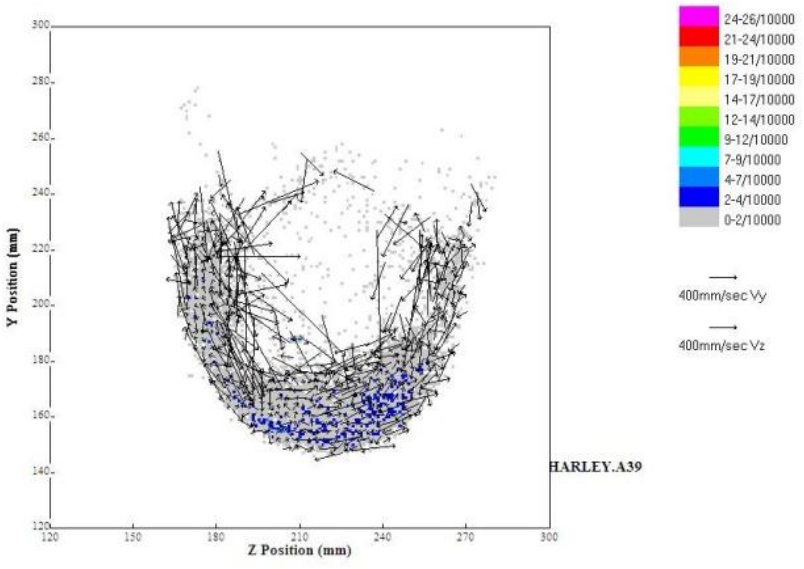

c)

Figure 6.15 Occupancy mapping on the y-z plane for MCC ribbons with 112 J/m^2 fracture energy milled at a) 50, b) 200 and c) 300 Hz milling frequency, recording to the results shown in Fig. 6.14.

6.4.2 Double tracer experiments

In order to obtain a better understanding of the ribbon motion during the milling process, double-tracer tracking experiments were carried out. Two cases were considered: 1) one tracer in the ribbon and the other on the arm of the blade; 2) two tracers located at different position of the tracer ribbon. The effects of the milling frequencies on the motion and breakage of the ribbons were studied.

Ribbon-blade tracking

The mapping of the relative velocities of the ribbons at various milling frequency are shown in Fig. 6.16, in which the vectors in red colour represent the motion of the blade. The positions of the vectors were normalized to ensure that the origin represent the centre of the impeller. In this case, the relative velocity of the ribbon was calculated from the difference

between the instantaneous velocity of the ribbon and blade. Thus, the results should be more reliable and accurate compared to those obtained using single tracer. Additionally, the location of the blade can be determined in a way that is not affected by the fluctuation of the system. Similar to the results reported in 6.4.1, the ribbons occupy more space at larger milling frequencies. It may also be observed that at 50 and 200 Hz, the relative velocity of the ribbons close to the blade radius tends to zero, indicating that plug flow dominates. However, the value and direction of the velocity at 300 Hz are very random in the milling chamber.

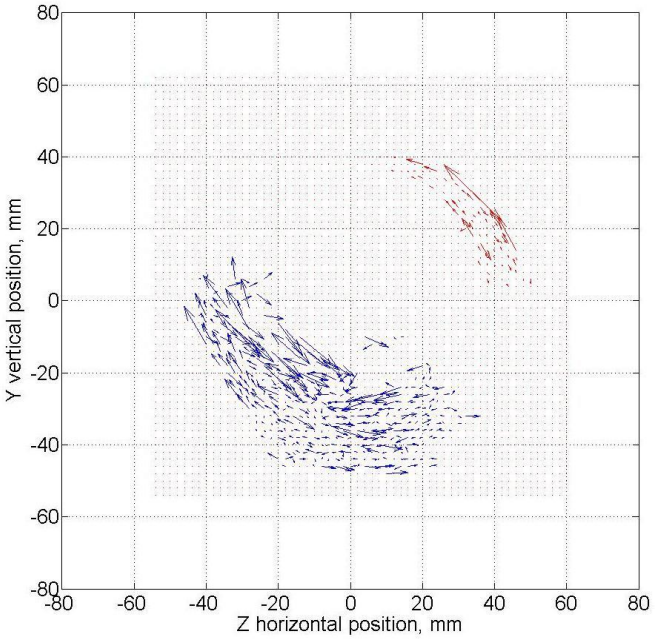

a)

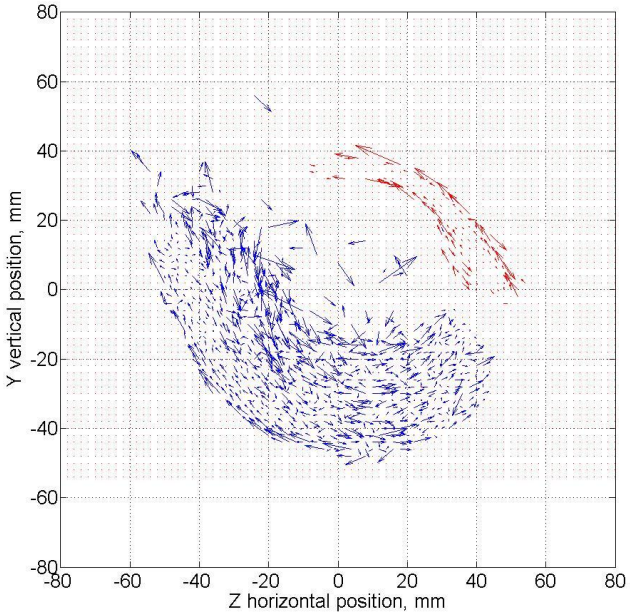

b)

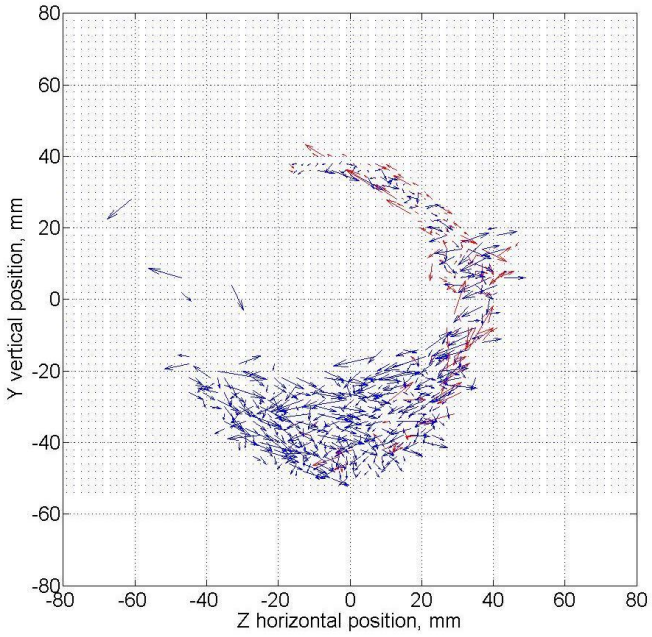

c)

Figure 6.16 Relative velocity mapping on the y-z plane for MCC ribbons with 112 J/m^2 fracture energy milled at a) 50, b) 200 and c) 300 Hz milling frequency, solid black circle presents the milling blade.

Ribbon-ribbon tracking

By adding two tracers in a single piece of ribbon, it is possible to determine the breakage of the ribbon by the separation of the two tracers. To be specific, the distance between the tracers was measured and recorded before the milling. A term 'number of milling cycles for breakage' N_b was defined as the number of the milling cycles at which the difference from the actual distance of the tracers to the original value is larger than 10%. The variation of the reciprocal of N_b with the milling time is shown in Fig. 6.17. It can be seen that the value of the reciprocal of the term is almost constant from 50 to 200 Hz milling frequency, but increases sharply in the region from 200 to 300 Hz. Generally, a larger value of the reciprocal of N_b indicates that the ribbons are more likely to break during the milling processes. Therefore, a conclusion can be drawn that there are two regions in which the breakage behaviour of the ribbons are distinct, consistent with the observations in Section 6.3 and 6.4.1. The milling regions are dominated mainly by the milling frequency.

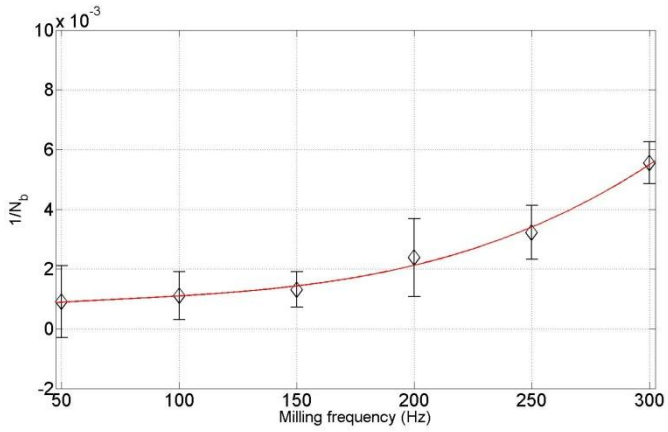

Figure 6.17 Reciprocal of N_b as a function of milling frequency (ribbons with 112 J/m^2 fracture energy milled at 1 mm screen).

6.5 Conclusions

This chapter introduced an experimental study of the milling process for MCC 102 ribbon specimens (22 X 22 mm) which attempted to obtain a better understanding of the influence of the ribbon properties and milling parameters. A first order kinetics model was introduced to describe the mass throughput during the milling process. The results revealed the relationship between milling mass throughput with the ribbon relative density, screen mesh size and milling frequency. Generally, the mass throughput of the granules can be improved by increasing screen mesh size and milling frequency. On the other hand, increasing ribbon relative densityfracture energy results in decreasing mass throughput. There are two regions dominated by the milling frequency that might be ascribed to distinct fracture mechanisms. The motion of the ribbons in the milling chamber and detailed velocity fields were measured using the PEPT technique. The results revealed that the behaviour of the ribbons were greatly affected by the milling frequency and showed further evidences of two regions of granule breakdown, in which the fracture of the ribbons was dominated by abrasion and impact, respectively.

CHAPTER 7 TABLETTING RESULTS

In this chapter, the experimental work carried out to examine the behaviour of the feed powders and roll compacted granules during tabletting is presented. Compressibility, compactibility and pressure-density relationship are considered. The results for feed powders with distinct properties are compared to explore the influence of their properties. Compression of the roll compacted granules under various lubrication conditions are also described to investigate the effect of the powder conditioning.

7.1 Compressibility analysis

Four approaches were used to analyse the compressibility and porosity-pressure behaviour of the powders: (i) the Heckel equation (Heckel, 1961), (ii) the Kawakita equation (Kawakita and Lüdde, 1970), (iii) calculating the compressibility factor using Johanson theory (Johanson, 1965), (iv) calculating the compressibility factor using the Adams equation (Adams *et al*., 1994).

7.1.1 Heckel analysis

The reciprocals of the porosity of the powders obtained during uniaxial compression are plotted as a function of the normal pressure. Heckel equation (Eq (2.7)) is used to analyse the results. Figure 7.1 shows typical Heckel fitting for various powders, the slope of the regression line presents the value of the constant *k*. Referring to the physical meaning of the constants in the Heckel equation, *k* can be considered as the compressing behaviour of the substances. Larger value of *k* indicates better compressibility of the powder. The fitting results imply that MCC powder is most compressible powder, while DCPD has the smallest compressibility.

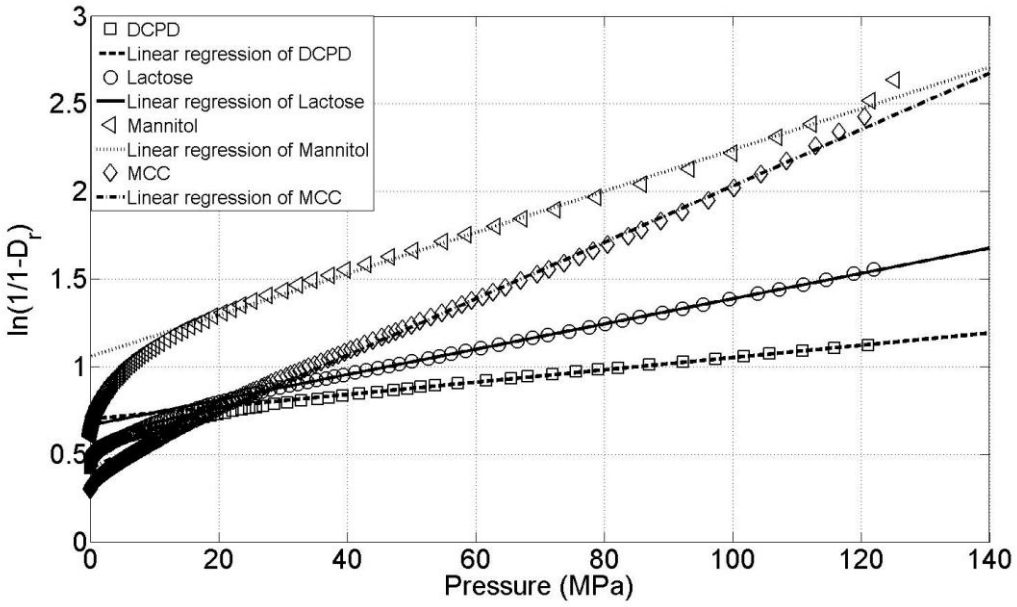

Figure 7.1 Heckel plots for powders under a maximum force of 16 kN.

7.1.2 Kawakita analysis

In the current work, the bulk density in tabletting die at the initial state ρ_0 (at zero pressure) was calculated from the following expression:

$$\rho_{ini} = \frac{4m_{powder}}{\pi d_{die}^{2} h_i} \qquad \text{Eq (7.1)}$$

where m_{powder} is the mass of powder, ρ_{ini} is the bulk density of the powder at the initial height h_i, d_{die} is the internal diameter of the die. Thus, Eq (2.10) can be written as:

$$C_K = 1 - \frac{\rho_p}{\rho_{ini}} = 1 - \frac{h_i}{h_p} \qquad \text{Eq (7.2)}$$

With the measured current height of the powder bed, h_p, the degree of volume reduction C_K can be calculated. Typical Kawakita plots (see Eq. (2.9)) for the data presented in Fig. 7.1 are shown in Fig. 7.2. The slope of the regression line equals the reciprocal of the constant a_K, which describes the compressibility of the powder. Consistent with Heckel equation, Kawakita analysis reveals that MCC is most compressible and DCPD is most incompressible powder. However, it can be seen that the extent of the curved regions before the linear regions in Kawakita plots are smaller when compared to those in the Heckel plots. Thus, Kawakita fitting gives more reliable results comparing to Heckel fitting.

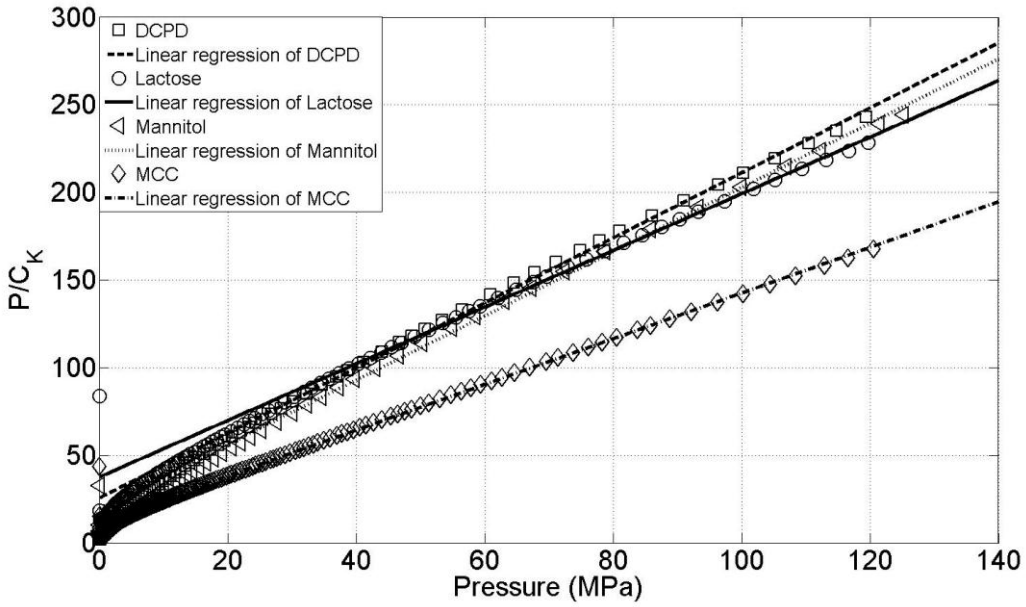

Figure 7.2 Kawakita plots of various powders under a maximum force of 16 kN.

7.1.3 Johanson's approach

The value of the compressibility factor κ can be obtained from the reciprocal of the slope of the log-log plot for the variation of density with normal pressure using multivariate fitting. Eq (2.13) is used to fit the results obtained from uniaxial compression to evaluate the compressibility of the feed powders. The apparent density of the powder bed is calculated using the following expression, similar to the calculation of the initial bulk density shown in Eq (7.2):

$$\rho_p = \frac{4m_{powder}}{\pi d_{die}^{\ 2} h_p} \qquad \text{Eq (7.3)}$$

It may be noted that this linear relationship is not valid for the region in which the stress is smaller than σ_α. As shown in Fig. 7.3, the pressure-density relationship is not valid for $\log\sigma \leq 1$. Therefore, the data with normal stresses greater than 10 MPa were selected to analyse the compressibility (see Fig 7.4).

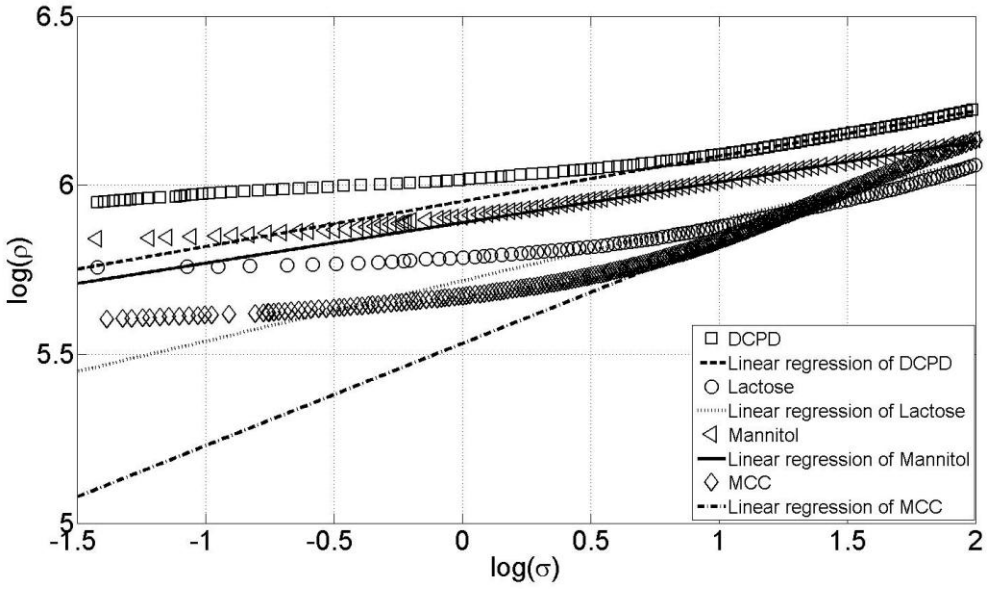

Figure 7.3 The log-log plot of density versus normal pressure of primary powders, under 16 kN maximum normal force.

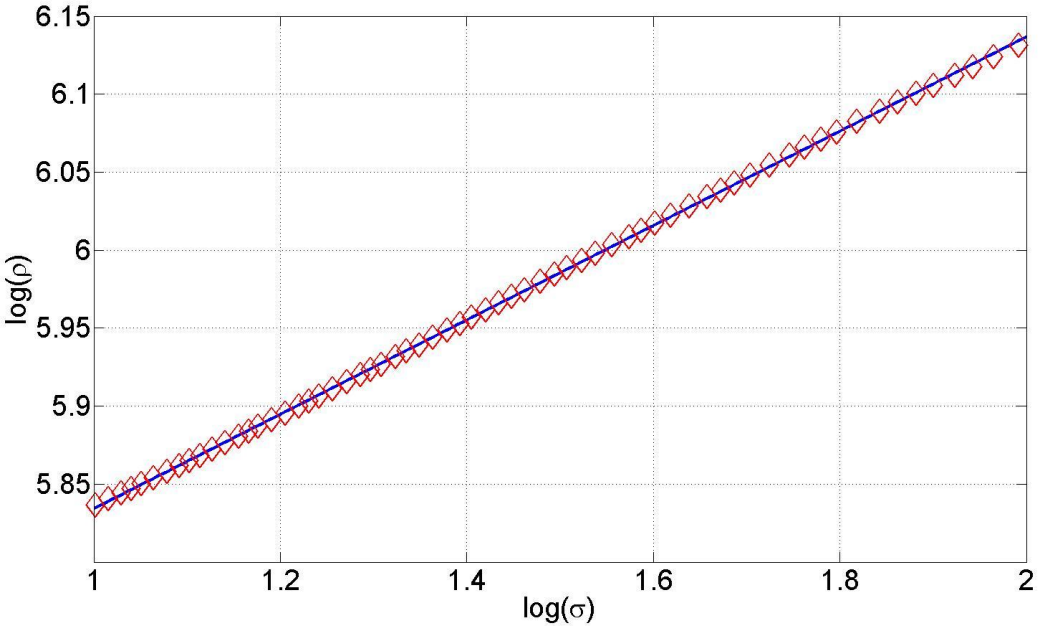

Figure 7.4 Typical fitting for the log-log relationship of the apparent density and normal stress during uniaxial compression for determining the compressibility factor (MCC Avicel PH 102, at maximum load of 16 kN).

7.1.4 Adams' equation

In terms of the Adams equation (1994), the compressibility factor describing the compression behaviour of the uniaxial compressed materials can be obtained from the multivariate fitting of Eq (2.14) (see in Fig 7.5). This approach shows a better reliability when fitting to the low pressure range (*i.e.* the curve part in the experimental data), comparing to Johanson's approach (1965).

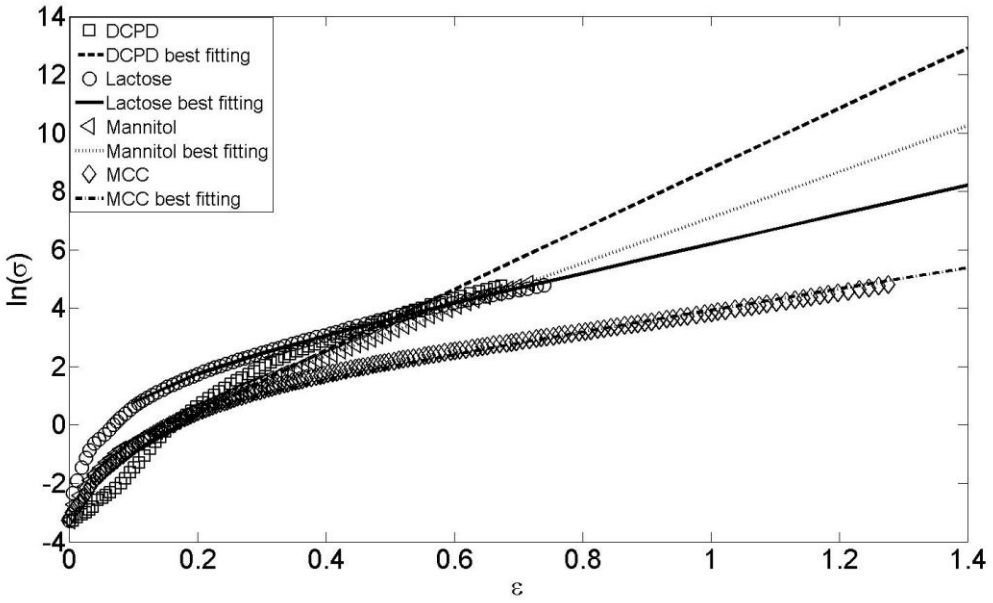

Figure 7.5 The plots for the best fits of the Adams equation (Eq (2.14)).

7.2 Compactibility

As introduced in Chapter 2, compactibility indicating the capability of a powder to form tablets under a certain compression pressure is also an important parameter to characterise the feed powders and granules. In this work, the dimensionless term 'compactibility parameter (C_p)' proposed by Sonnergaard (2006) is adopted (see Fig. 7.6).

The tensile strength (σ_t) derived from the maximum diametric fracture force, F_{crush}, for a cylindrical tablet is defined as (Fell and Newton, 1968):

$$\sigma_t = \frac{2F_{crush}}{\pi D_t h_t} \qquad \text{Eq (7.4)}$$

SCS deviates from the tensile strength (σ_t) by a factor of $2/\pi$, so that C_p can also be attained from the correlation between P_{mu} and σ_t which is more commonly used (Sonnergaard, 2006). The relationship between σ_t and C_p can be written as:

$$\sigma_t = \frac{2C_p P_{mu}}{\pi} + \frac{2b_c}{\pi} \qquad \text{Eq (7.5)}$$

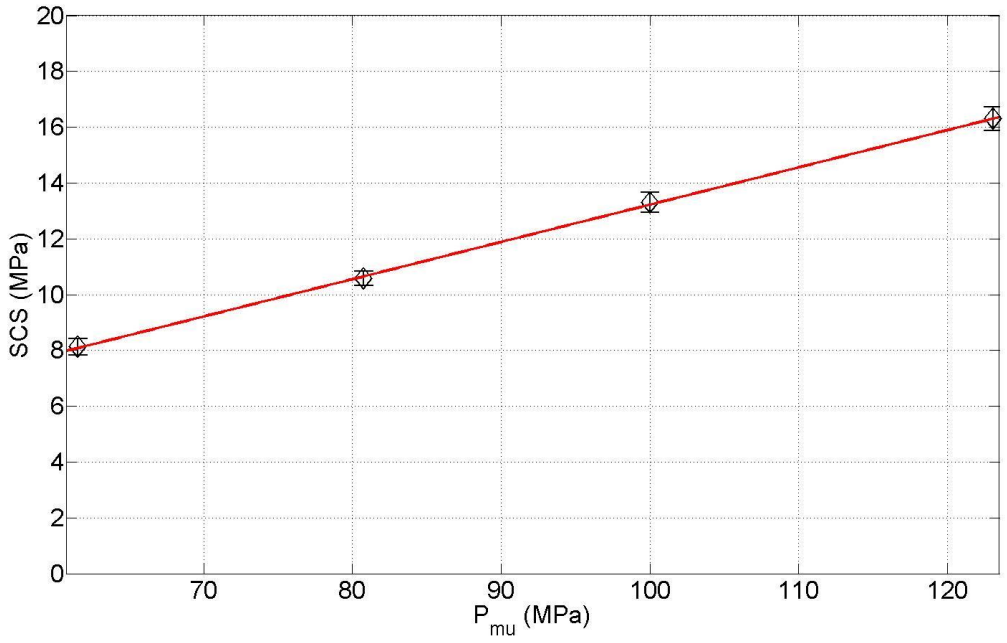

Figure 7.6 Typical fitting for determining the compactibility parameter (C_p) (MCC Avicel PH 102) according to the specific crushing strength (*SCS*) as a function of the maximum compression pressure, P_m

7. 3 Effects of the feed material properties on tabletting

The results obtained using the approaches introduced in the previous section are presented here to investigate the effect of the feed material properties on tabletting behaviour. The factor k_H in the Heckel equation (Eq (2.7)), a_K in Kawakita equation (Eq (2.9)),

compressibility factor κ in Johanson's approach (Eq (2.13)), parameter β in Adams equation (Eq (2.14)) and the compactibility parameter C_p (2006) have been selected as key parameters to describe the tabletting behaviour.

7.3.1 Compression behaviour of different primary powders

Table 7.1 gives the parameters described in the previous section. According to the definition of the parameters, the larger values of compressibility factor κ and β indicate powders with a smaller compressibility. In contrast, the larger values of the constants k_H and a_K indicate a high compressibility. C_p calculated from Eq (2.18) reflects the capability of powders to form tablet under a given maximum compression pressure viz., an indicator of the tablet strength produced under a certain compression pressure.

Table 7.1 The parameters describing the compression behaviour for the primary pharmaceutical excipients powders.

Powder	κ	β	k_H (x 10^{-3})	a_K	C_p
DCPD	7.82 ±0.65	10.62 ±0.87	3.79 ±0.44	0.52 ±0.08	0.039 ± 0.008
Lactose	5.62 ±0.23	4.40 ±1.22	7.29 ±0.54	0.58 ±0.06	0.068 ± 0.005
Mannitol	8.46 ±0.15	8.12 ±0.33	11.22 ±1.2	0.52 ±0.12	0.042 ± 0.009
MCC Avicel PH 101	2.98 ±0.21	3.06 ±0.18	17.33 ±0.42	0.81 ±0.09	0.146 ± 0.003
MCC Avicel PH 102	3.32 ±0.16	3.62 ±0.17	15.02 ±0.46	0.76 ±0.04	0.132 ± 0.006

It is clear that the nature of the feed powders greatly affects their compression behaviour. Organic polymers, such as MCC powders (both grade Avicel PH 101 and 102), show the greatest compressibility and considerable potential to produce tablets with high strength. DCPD and mannitol powders are relatively incompressible.

7.3.2 Effect of granule size on compression behaviour

In order to explore the influence of the size of the feed materials on the tabletting processes, compression experiments with the feed powders and granules with various sizes were performed. MCC Avicel PH 102 ribbons produced at a roll speed of 1 rpm and a roll gap of 1 mm were milled to granules with a screen size of 630 μm and milling frequency of 200 Hz and sieved to different size groups. Figs 7.7 and 7.8 show the variation of the compressibility factor and compactibility parameter as a function of the size of the feed powders and granules.

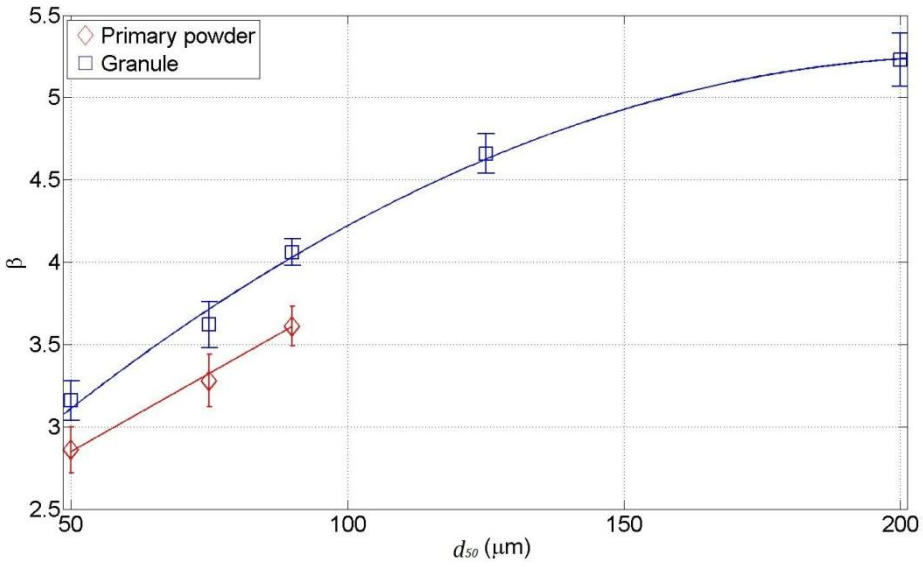

Figure 7.7 The variation of the compressibility factor as a function of particle size of the sieved feed powders and granules for MCC Avicel PH 102.

It is shown in Fig 7.7 that for the feed powders and granules, the value of the compressibility factor increases with the particle size. Moreover, the values of the compressibility factor for

the granules are larger than those for the primary powders. This indicates that 1) the powder and granules become more incompressible with increasing particle size; and 2) the granules lose compressibility in the roll compaction processes.

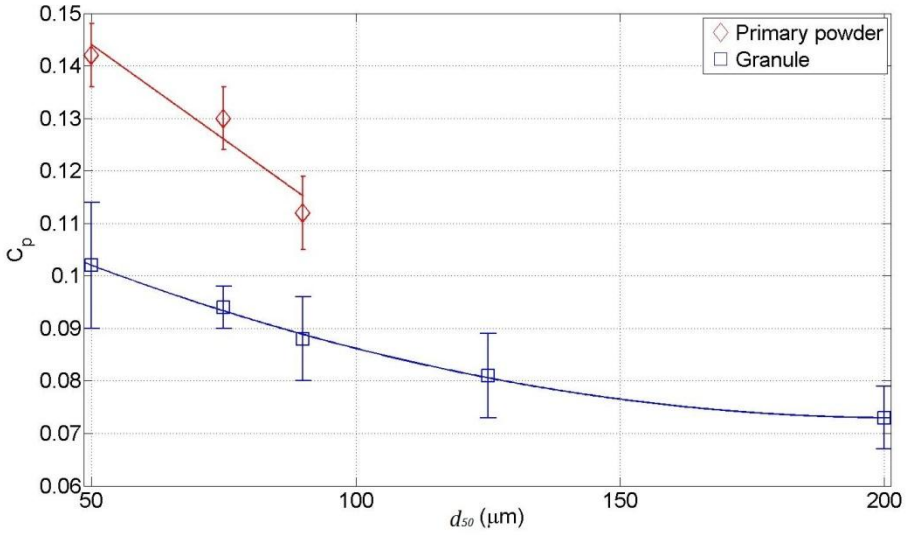

Figure 7.8 The variation of C_p as a function of particle size for the MCC (Avicel PH 102) powders and granules.

Fig. 7.8 presents the variation of the compactibility parameters as a function of the particle size for the MCC Avicel PH 102 feed powders and granules. It is clear that the compactibility decreases with increasing particle size. Furthermore, the compactibility is decreased in the roll compaction processes, similar to the tendency of the compressibility.

7.3.3 Effects of the roll compaction conditions

The influence of the roll compaction conditions (*i.e.* roll gap and roll speed) were investigated by examining the uniaxial compression behaviour of the granules made from MCC Avicel PH 102 at various roll gaps and roll speeds. The produced ribbons were then milled to granules at a milling frequency of 200 Hz and screen size of 630 μm. The compressibility and compactibility of the granules were examined and reported here.

In order to evaluate the effects of the roll gap, MCC powder (Avicel PH 102) was roll compacted with various roll gaps at a constant roll speed of 1 rpm. The ribbons were granulated by milling. The corresponding granules were compressed into tablets under a maximum load of 16 kN. The effects of the roll gap on the compression behaviour are shown in Figs 7.10 and 7.11. It is observed in Fig. 7.9 that the compressibility factor for the granules decreases with increasing roll gap, which indicates that increasing the roll gap results in less reduction in the compressibility of the produced granules. Fig. 7.10 shows the changing of the compactibility with increasing roll gap. It is clear that increasing roll gap results in an increase in the strength of the produced tablets.

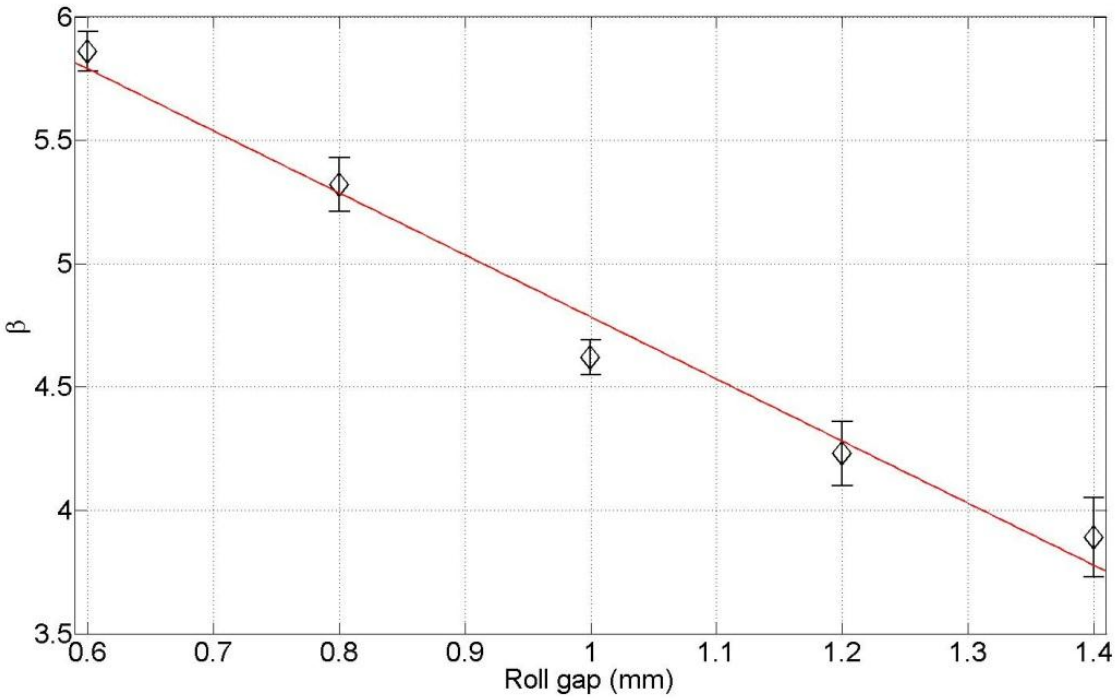

Figure 7.9 The variation of the compressibility factor of the granules as a function of the roll gap (at a constant roll speed of 1 rpm).

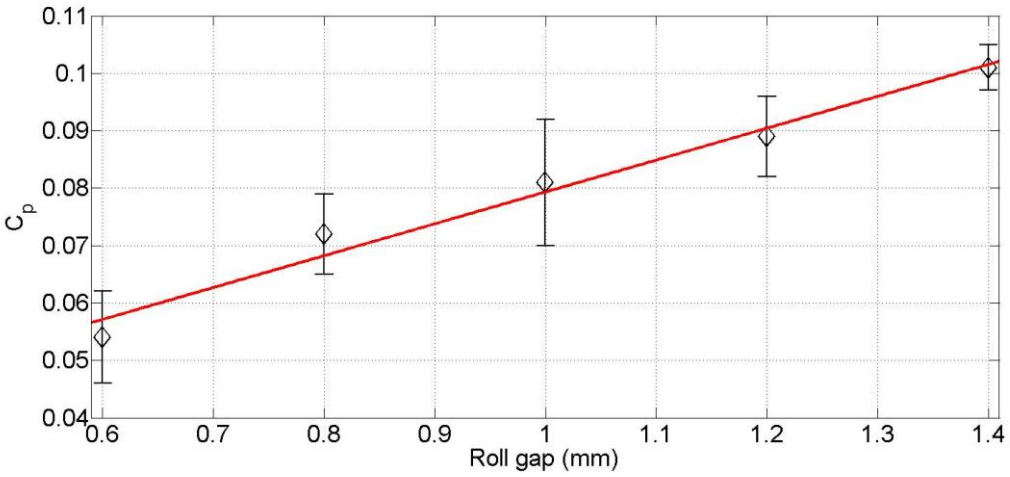

Figure 7.10 The variation of the compactibility parameter of the granules as a function of the roll gap (at a constant roll speed of 1 rpm).

MCC (Avicel PH 102) ribbons compacted at a constant roll gap (S =1.0 mm) with roll speeds in a range of 0.5 to 5 rpm were milled to granules at a milling frequency of 200 Hz and a screen size of 630 μm. The produced granules were then fed into the compression die for uniaxial compression. The results show that both compressibility and compactibility increase with increasing roll gap (see in Figs 7.12 and 7.13).

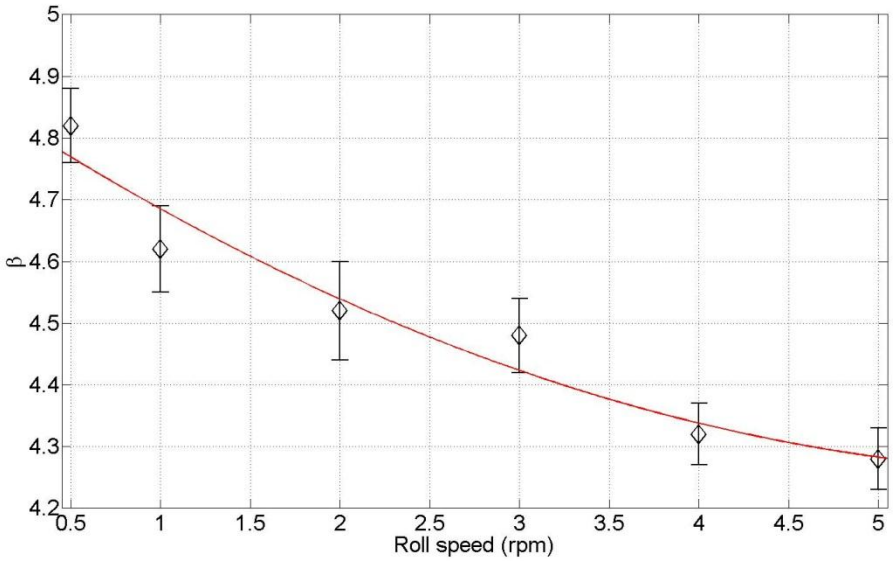

Figure 7.11 The variation of the compressibility factor of the granules as a function of the roll speed (at a constant roll gap of 1 mm).

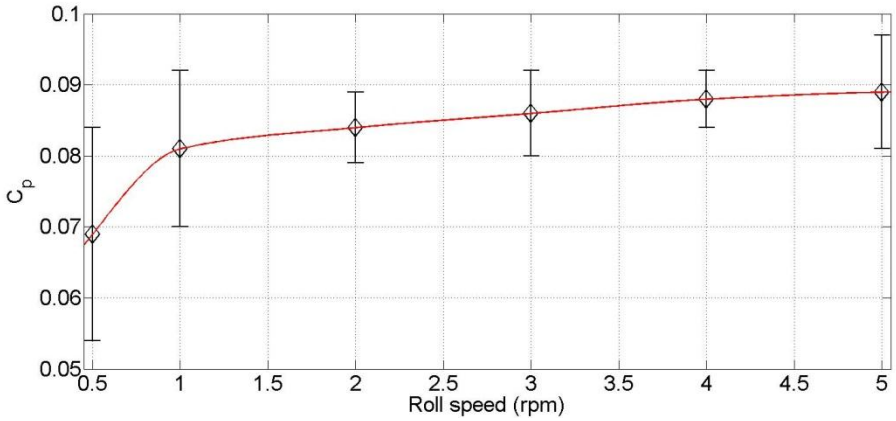

Figure 7.12 The variation of the compressibility factor of the granules as a function of the roll speed used to produce the ribbons (at a constant roll gap of 1 mm).

7.3.4 Effects of the milling frequency

MCC ribbons produced at fixed roll compaction conditions (S =1.0 mm, u =1.0 rpm) were milled at a constant screen size of 630 μm and milling frequencies in the range 50 to 300 Hz. The granules were compressed uniaxially to investigate the effects of the milling frequencies on the compression behaviour. The compressibility factors and compactibility parameters are shown in Figs 7.13 and 7.14. The compressibility factor decreases with increasing milling frequency (Fig. 7.13), which indicates that the granules produced at a higher milling frequency are more compressible. It is also found that the compactiblity of the granules increases with milling frequency (Fig. 7.14).

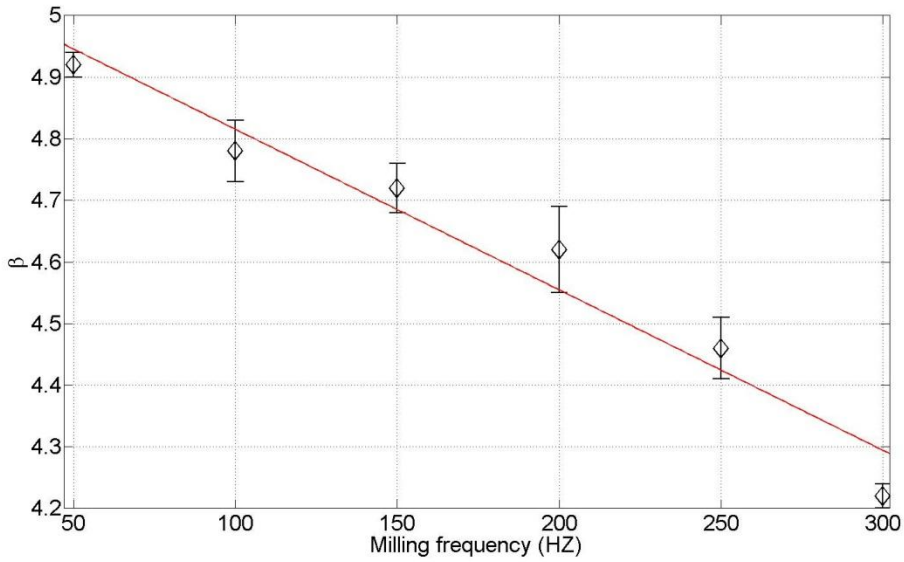

Figure 7.13 Effects of the milling frequency on the compressibility factor of the granules for MCC Avicel PH 102 (S =1.0 mm, u =1.0 rpm).

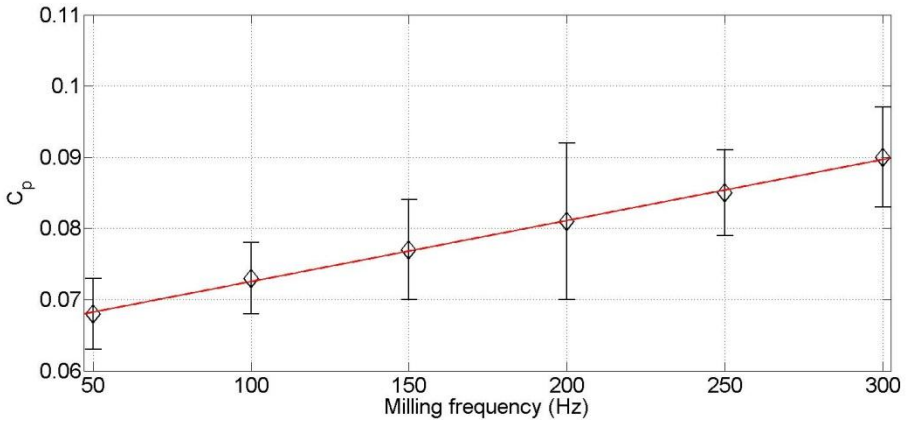

Figure 7.14 Effects of the milling frequency on the compressibility factor of the granules for MCC Avicel PH 102 (S =1.0 mm, u =1.0 rpm).

7.3.5 Effects of the lubrication

In order to investigate the effects of lubrication in the roll compaction process on the subsequent tabletting, ribbons produced with bulk lubrication with various concentrations of MgSt were milled and compressed uniaxially. The compression behaviour for lubricated MCC and DCPD were investigated using the compressibility factor (Fig. 7.15) and

compactibility parameter (Fig. 7.16). The compressibility was not affected by the addition of the lubricant (Fig. 7.15). The values of the compressibility factor of the granules were comparable to the granules produced without lubricant for both MCC and DCPD.

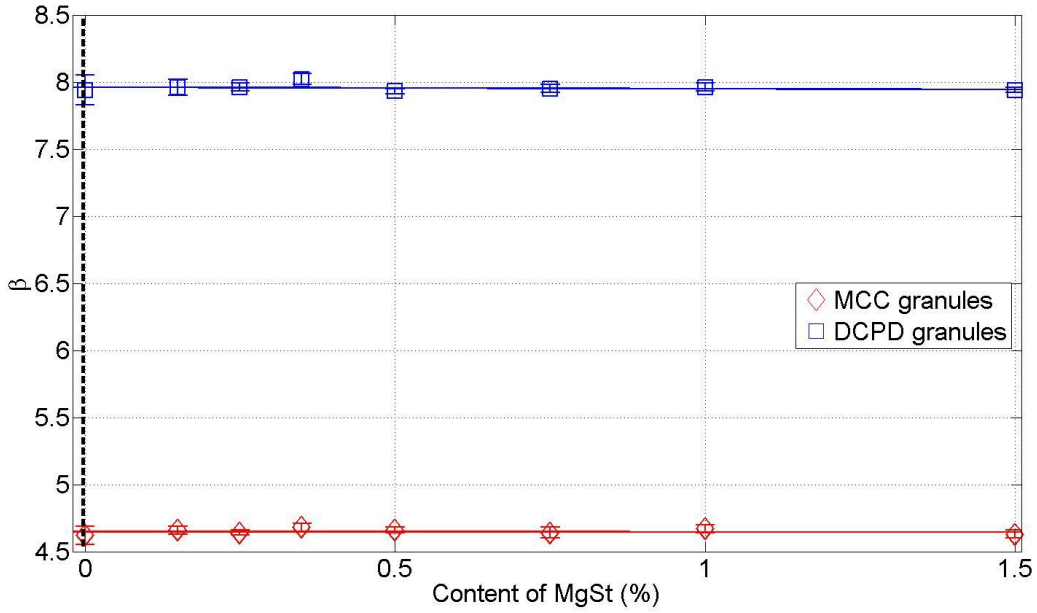

Figure 7.15 Effects of lubrication on the compressibility factor. The dashed line (x=0) represents the values for unlubricated cases.

The effects of the lubricant on the compactibility are shown in Fig 7.16. The compactibility of DCPD shows insensitivity to the lubricant. The value of the compactibility remains constant with additional MgSt up to 1.5 % (w/w). However, the compactibility parameter of MCC decreases sharply when a small amount of MgSt was added. It seems to reach a limited value and only changes slightly when the content of MgSt is more than 0.5 %.

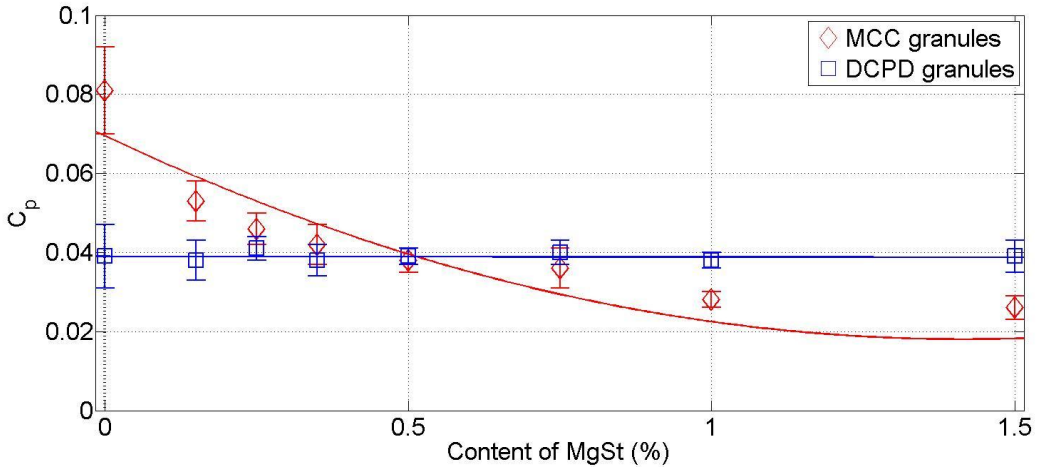

Figure 7.16 Effects of lubrication on the compactibility parameter. The dashed line (x=0) represents the values for unlubricated cases.

In order to obtain gain understanding of the effects of the lubrication on the uniaxial compression, additional experiments at a constant strain were performed. The masses of MCC and DCPD powders and granules used were 0.8 and 1.1 g, respectively. The corresponding initial powder heights at a pre-compression load of 5 N were 15.05 and 9.43 mm for MCC and DCPD, respectively. The samples were then compressed to uniaxial strains of 0.66 and 0.53, respectively, in order to produce tablets of similar thickness (ca. 5 mm).

Three cases were considered for the uniaxial compression of the feed powders: 1) unlubricated, 2) lubricated powder and 3) lubricated inner wall of the die. Once the tablets were ejected, the dimensions (*i.e.* diameter, thickness) and masses were measured so that the bulk densities could be determined. The tablets were then compressed diametrically to determine their tensile strength.

The tensile strengths of the produced granules were plotted as a function of the relative density (obtained using the method mentionedin Section 4.3.2), as shown in Fig. 7.18. The Ryshkewitch-Duckworth equation (Duckworth, 1953) was employed to fit the experimental data:

$$\sigma_t = \bar{\sigma} e^{-k_{RD}(1-D_r)} \qquad \text{Eq (7.6)}$$

where σ_t is the tensile strength of the compacts at a relative density of D_r, $\bar{\sigma}$ is the tensile strength for the same material at zero porosity, k_{RD} is a constant representing the bonding capacity of the material with a larger value of k_{RD} indicating weaker bonding capacity. Typical data fitting are shown in Fig. 13, and the values of the fitting parameters are listed in Table 7.2. For DCPD, the values of $\bar{\sigma}$ and k_{RD} for various cases considered are essentially identical. For MCC, granulation and lubrication lead to a reduction in the value of $\bar{\sigma}$, but an increase in the value of k_{RD}, indicating a reduction in bonding capacity.

The strength of the DCPD tablets is much less than those made from MCC (Fig. 7.18), which is analogous to data for the strength of the ribbons as indicated by the fracture energy shown in Chapter 5. Bulk lubrication causes a reduction in the strength of the MCC tablets (Figs 7.17 and 7.18b). Thus the influence of lubrication on both the DCPD and MCC tablets is also similar to the trends observed for the ribbons as described, in Chapter 5.

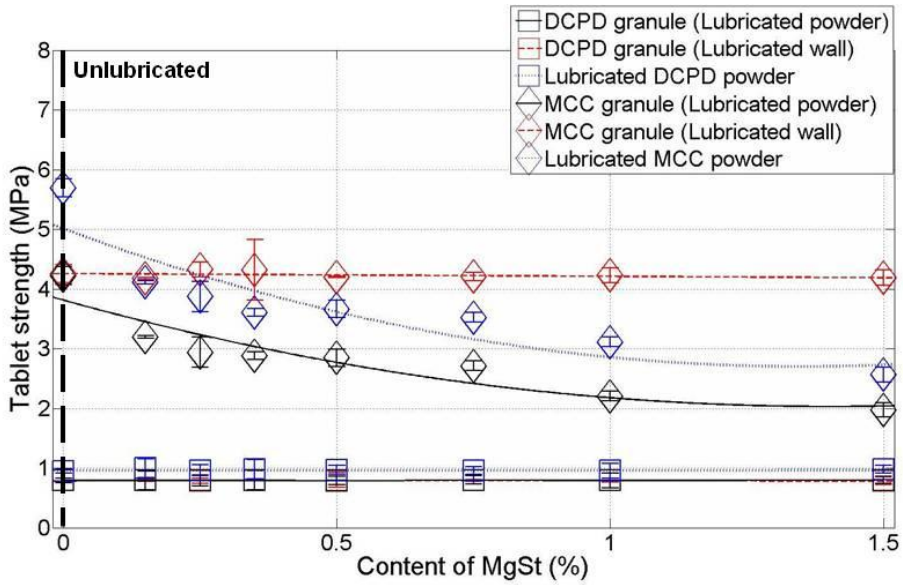

Figure 7.17 Effects of lubrication on the tablet strength. The dashed line (x=0) represents the values for unlubricated cases.

Table 7.2 The value of fitting parameters in Eq (6), obtained from multivariate fitting to experimental data.

Feeding material	$\overline{\sigma}$ (MPa)	k_{RD}
DCPD	924.2	19.1180
MCC Granule (bulk lubrication)	9.1	6.8998
MCC Granule (wall lubrication)	12.4	6.4918
MCC Granule (no lubridation)	12.1	6.3497
MCC powder (bulk lubrication)	11.8	6.5436
MCC powder (no lubrication)	15.9	5.7308

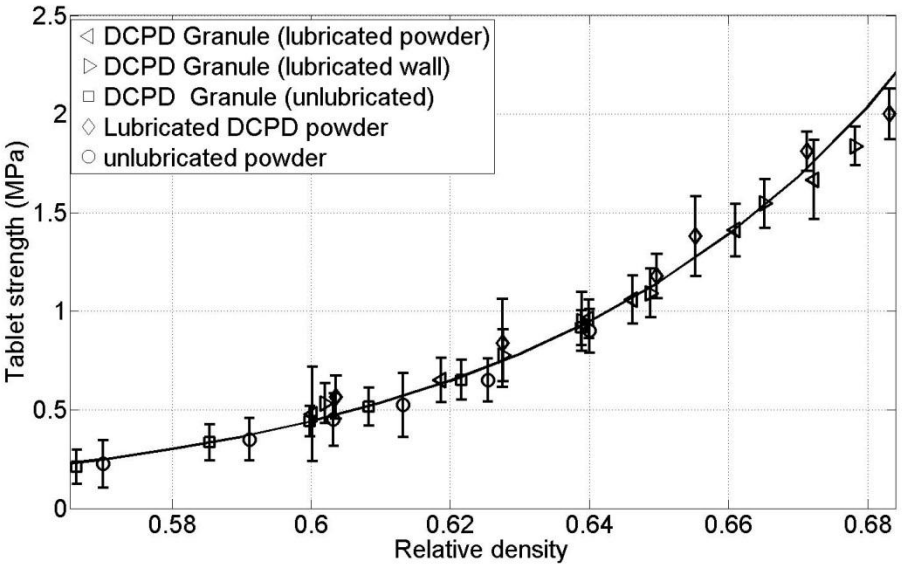

a)

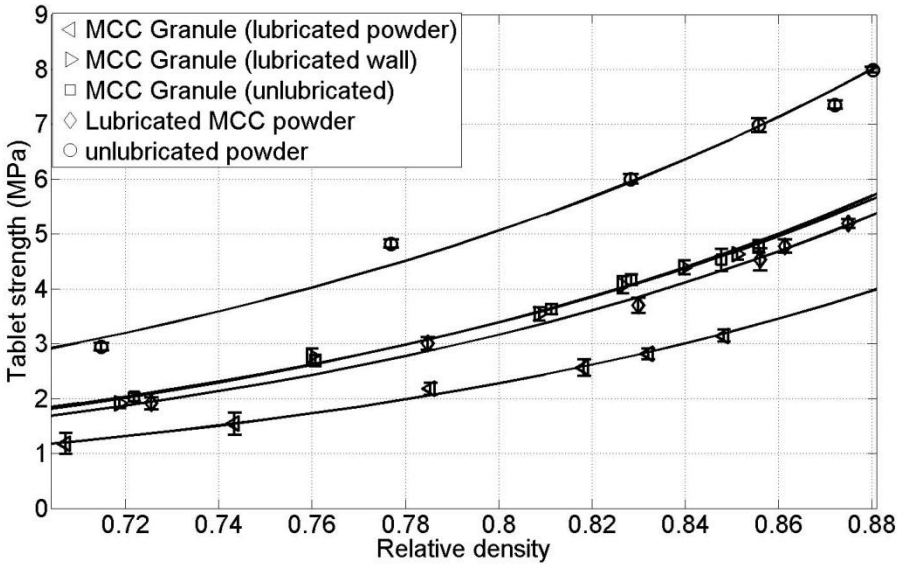

b)

Figure 7.18 The tensile strength as a function of relative density of the tablets produced under various lubricating conditions for a) DCPD and b) MCC.

7.4 Conclusions

This chapter presents the experimental investigation of uniaxial compression to investigate the compression behaviour of the feed powders and granules produced from roll compaction. The performances of the feed powders with distinct properties in the uniaxial compression were examined using various approaches to evaluate the pressure-density relationship. The correlation between the roll compacted granules and tabletting processes were also investigated. The factors affecting the compression behaviour such as particle size, roll compaction conditions, lubrication and milling conditions (*i.e.* milling frequency) were explored. The compressibility factors, which indicate the capability of a particle system to be compressed and the compactibility parameter, which refers to the strengths of the tablets produced at a given compression pressure, were evaluated to describe the compression behaviour. It was found that: 1) the compressibility and compactibility for granules are smaller than the values for corresponding feed powders; 2) the compressibility and compactibility of the feed powders and granules decrease with increasing particle size; 3) increasing roll gap and roll speed results in increases in the compressibility and compactibility of the granules; 4) an increase in the milling frequency leads to increases in compressibility and compactibility of the granules. An investigation of the effects of lubrication on the tabletting of DCPD and MCC granules revealed that the lubrication shows no significant influence on the compressibility. For DCPD, the compactibility remained constant with increasing concentration of MgSt. For MCC, the compactibility decreased with increasing concentration of MgSt. The constant strain experiments on the lubricated powders also implied that 1) DCPD was insensitive to lubrication and 2) the compactibility of MCC reduced with bulk lubrication.

CHAPTER 8 DISCUSSION

Measurements have been carried out to study the effects of the feed powder properties and process conditions on the roll compaction behaviour. The influences of the material properties and process parameters on the milling process were investigated. PEPT results were analysed to explore the fracture mechanisms involved. The compressibility and compactiblity of the feed powders and granules were studied to examine the influence of roll compaction and milling on uniaxial compression. The results obtained in the experiments are discussed in this chapter to understand the particular processes and the overall process of roll compaction-milling-tabletting used in the pharmaceutical sector.

8.1 Roll compaction

8.1.1 Effects of roll compaction parameters

Effects of roll gap

Experiments (Section 5.2.1) revealed the variation of the maximum pressure and nip angle for MCC and DCPD powder (Figs 5.17 and 5.18). The nip angle increases with increasing roll gap for MCC in the measured range, consistent with previous literature results (Bindhumadhavan, 2004, Bindhumadhavan *et al*., 2005). According to Johanson theory (Johanson, 1965), the nip angle is a function of the ratio of the roll gap to the roll diameter for a given powder. The value of the nip angle can be determined by using Eqs (3.6) and (3.8). As shown in Fig. 8.1, the nip angle predicted using Johanson theory increases with the roll gap. However, the variation of the predicted nip angle is much less than the measured values. On the other hand, the nip angle decreases with the roll gap for DCPD, contrary to the predicted trend. This can be attributed to insufficient feeding and aeration caused by the small particle size of DCPD (Spinov and Vinogradov, 1967, von Eggelkraut-Gottanka *et al*., 2002).

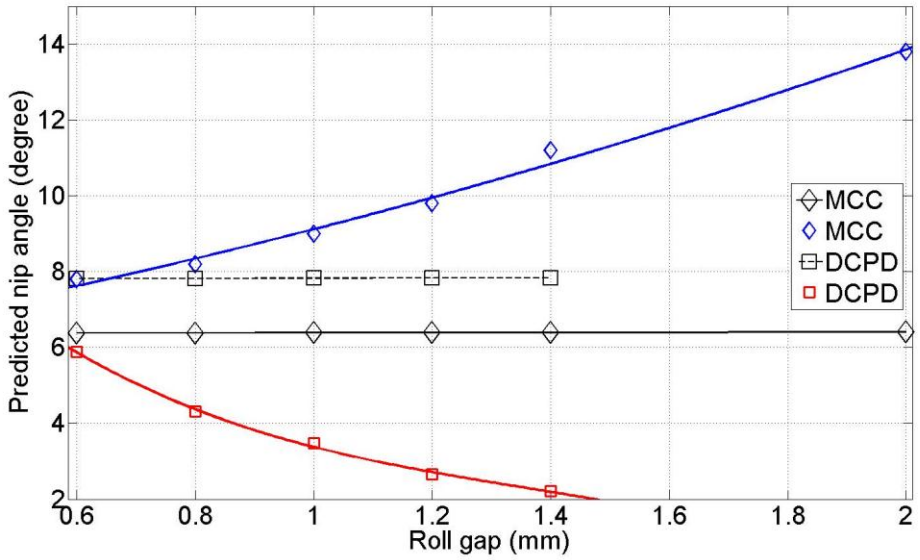

Figure 8.1 The variation of nip angle with roll gap at a fixed roll speed ($u = 1.0$ mm).

A reduction in the maximum pressure with the increasing roll gap was observed for both MCC and DCPD powders (Fig. 5.17). As introduced in Chapter 3, the pressure distribution in roll compaction can be predicted by adopting the expression suggested by Johanson (1965) (Eq (3.4)), which assumes that the nip pressure is kept constant for a change in the roll gap. The maximum pressure occurs at the minimum roll gap ($\theta = 0$) in Johanson theory. Thus, the maximum pressure can be determined from the pressure distribution, provided that the nip angle, nip pressure and compressibility factor are known:

$$\sigma_\theta = \sigma_\alpha \left[\frac{\left(1 + \frac{S}{D} - \cos\alpha\right)\cos\alpha}{1 + \frac{S}{D}} \right]^\kappa \quad \text{for } \theta \le \alpha \qquad \text{Eq (8.1)}$$

Assuming that the nip pressure is dominated by the feed pressure which does not vary much in the gravity feeding roll compactor used in this work, it can be concluded that the maximum pressure is dominated by $\left[\left(1 + \frac{S}{D} - \cos\alpha\right)\cos\alpha \Big/ 1 + \frac{S}{D}\right]^\kappa$, which is a dimensionless factor

indicating the dependency of the maximum pressure to the roll gap and powder properties (*i.e.* compressibility). The values for this term were calculated adopting the predicted nip angles and measured compressibility factors. It can be seen that this factor decreases with roll gap for MCC and DCPD powders, giving a reasonable prediction of the trend of the variation of the maximum pressure with the roll gap.

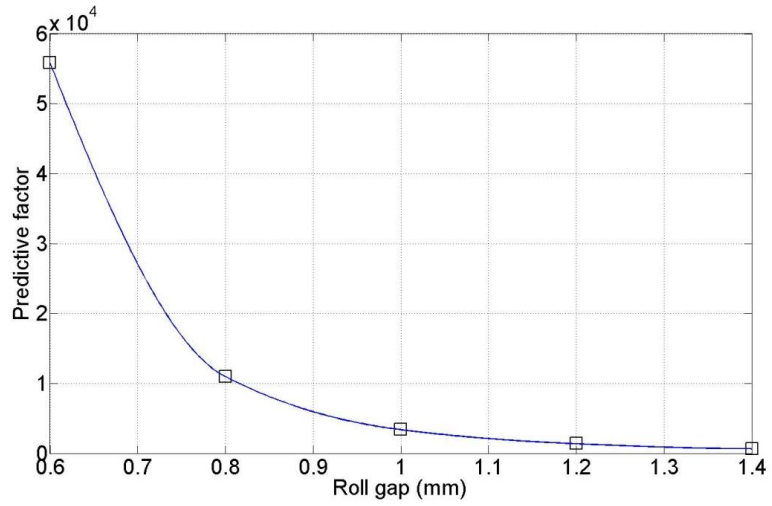

a)

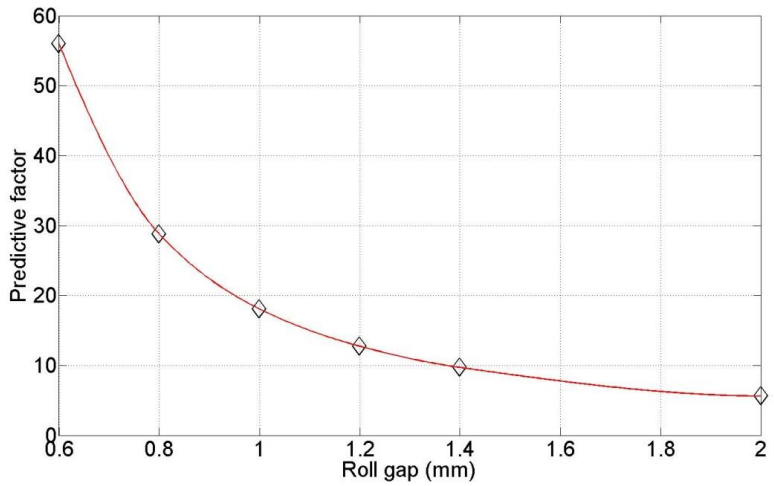

b)

Figure 8.2 The variation of the predictive factor (Eq. (8.1) with increasing roll gap for a) DCPD and b) MCC.

As expected, the fracture energy (Fig. 5.27) and the bulk density (Fig. 5.28) of MCC ribbons decrease with increasing roll gap, since the compaction pressure decreases. It is also observed that the density is more uniform across the ribbon width at smaller roll gaps (Fig. 5.29). This might be attributed to the frictional force (*i.e.* powder-powder friction, powder- roll friction forces), which is directly proportional to the normal force in the nip region. At the edges of the roll, higher frictional forces overcome the frictional force on the side plate at smaller roll gaps, and therefore drag a larger amount of powder to the minimum gap. Thus, the variation of the density across the width is smaller.

Effects of roll speed

Generally, the maximum pressure and nip angle decreases with increasing roll speed for MCC and DCPD. These observations agree with previous published experimental work (Bindhumadhavan, 2004, Bindhumadhavan *et al*., 2005, Inghelbrecht and Remon, 1998, Mansa, 2006, Petit-Renaud *et al*., 1998). These previous investigations suggested that these observations are ascribed to insufficient feeding (Lecompte *et al*., 2005, von Eggelkraut-Gottanka *et al*., 2002). The compaction is performed under the normal stress acting on the powder-roll surface, and can only be achieved when the gap between the rolls is fully occupied by the powder. With increasing roll speed, a larger amount of powder is fed into the system. Thus the nip angle, which indicates the extent of the compaction region, and the maximum pressure decreases with increasing roll speed if the amount of powder fed is not sufficient. In addition, there are another two problems leading to the reduction of the maximum pressure and nip angle: 1) air aeration (Spinov and Vinogradov, 1967, von Eggelkraut-Gottanka *et al*., 2002) and 2) inhomogeneous feeding through the thickness of the compacts (see Fig. 3.5) (John C. Cunningham *et al*., 2010, Nesarikar *et al*., 2012).

8.1.2 Effects of powder properties

The experimental results obtained using DCPD and MCC with distinctive material properties (friction, compressibility and flowability, see Chapter 5) reveal that a number of factors

contribute to the roll compaction performance in a much more complicated manner than that suggested in previous studies (Bindhumadhavan *et al*., 2005, Johanson, 1965), in which the frictional properties of the feed powder were regarded as the dominant parameters in roll compaction. Previous theoretical analysis (Johanson, 1965) and experimental investigation (Bindhumadhavan, 2004, Mansa, 2006) concluded that the nip angle and maximum pressure increase as the values of effective friction coefficient and wall friction coefficient of the feed powders increase, when other parameters are kept constant. The experimental work on the roll compaction of lubricated MCC powders by Bindhumadhavan *et al.* (2005) showed that the maximum compression pressure increased substantially with increasing wall friction. Compressibility of the feed powders also plays an important role in roll compaction. Johanson (1965) found that as the value of the compressibility factor increases, the nip angle decreases but the maximum pressure increases. This explains why DCPD has a larger maximum pressure (Fig. 5.19) but a smaller nip angle (Fig. 5.20) compared to MCC at small roll speed (*i.e.* $u = 0.5$ rpm). The observation is ascribed to the fact that the compressibility factor of DCPD is much greater than that of MCC (Table 7.1).

However, the actual compaction behaviour for DCPD (*i.e.* maximum pressure and nip angle) is different from the prediction using the Johanson theory (1965), as discussed in Section 8.1.1. This is believed to be attributed to the efficiency of the feeding process, which is dominated by the flowability of the feeding powder since a gravity feeding system is used in this work. In addition, the feeding of the powder is greatly affected by the aeration that is largely depending upon the particle size. According to a previous study of the aeration during roll compaction (Spinov and Vinogradov, 1967), two types of air flow – 1) flowing passing between the particles and 2) flow passing along the powder-roll interface – are involved. DCPD is greatly affected by aeration due to its small particle size (Figs 5.1 and 5.2). The first type of air flow limits the amount of powder fed, and thus results in a sharp reduction in maximum pressure (Figs 5.17 and 5.19). The second type of air flow reduces the wall friction on the powder-roll interface. According to the theoretical model of roll compaction (Johanson, 1965), it is assumed that the powder feeding is uniform and the powder mass is dragged primarily by frictional forces. Thus, the air flow induces a decrease in the nip angle (Figs 5.18 and 5.20), and hence further reduction in the maximum pressure.

Due to its dynamic nature, roll compaction can also be affected by the flowability of the feeding powder, which may determine the efficiency of the powder feeding and therefore the compression pressure induced, especially for a gravity feeding system. It is clear that a larger compaction region (*i.e.* nip angle) and a greater maximum compression pressure is obtained for MCC with better flowability at larger roll gap (Figs 5.17 and 5.18) and higher roll speed (Figs 5.19 and 5.20). On the other hand, poorer flowability of DCPD can result in an insufficient feeding and a fluctuation in powder filling, as reported by von Eggelkraut-Gottanka *et al.* (2002), and therefore a reduction in the process efficiency. In order to systematically explore the effects of the flowability, the nip angle for MCC/DCPD binary mixture is studied. As shown in Fig. 8.3, the nip angle for the binary mixture obtained at fixed roll compaction conditions (S =1.0 mm, u =1.0 rpm) is plotted as a function of the MCC content. The predicted values using Johanson theory (1965) are superimposed for comparison. It can be seen that the nip angle increases with the MCC content, which optimize the flowability of the mixture (Fig. 5.16), even though both the internal and wall friction angle decrease (Figs 5.14 and 5.15). It is also observed that Johanson theory (1965) overestimates the nip angle for DCPD and DCPD-MCC mixtures with concentrations of MCC <50% that have relatively poor flowability, but underestimated the nip angle when the concentration of MCC is sufficiently high (≥ 50%) and the formulation has acceptable flowability (*i.e.* $ff_c > 4$). The maximum pressure for the mixture is determined by the extent of the compaction region, which is characterised by the nip angle and compressibility of the feeding powders. It is clear that a steady increase in maximum pressure with MCC content is observed (Fig. 5.25), as a result of the increase in nip angle and compressibility.

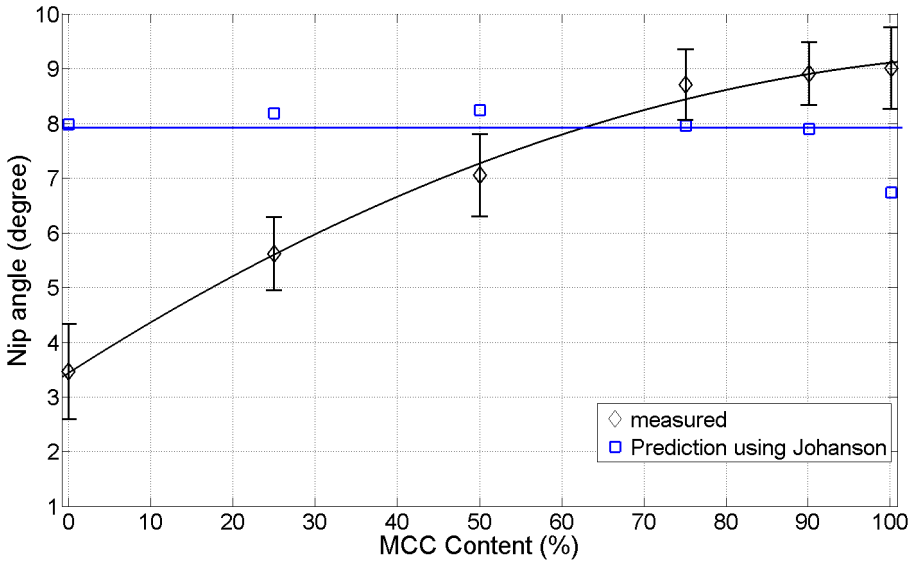

Figure 8.3 Comparison of measured and predicted (Johanson theory (1965)) nip angle values for MCC-DCPD mixtures as a function of MCC content (S =1.0 mm, u =1.0 rpm).

8.1.3 Effects of lubrication

The coefficient of wall friction for unlubricated DCPD is about a factor of 5 greater than that for MCC (Fig. 5.10). This arises from the smaller interfacial shear strength of organic compared with inorganic materials. Boundary lubricants provide a weak interfacial layer with coefficients of friction being typically ~ 0.1 (Bowden and Tabor, 1950), which represents the minimum value that can generally be achieved. This is similar to that measured for unlubricated MCC and consequently boundary lubrication was ineffective at reducing the friction. Organic polymers are generally difficult to boundary lubricate since they typically have similar interfacial shear strengths to boundary lubricants because both are organic in nature. However, the coefficient of friction for unlubricated DCPD was ~ 0.5 and therefore it could be effectively reduced by the application of MgSt to the observed minimum value of ~ 0.1. There is clearly a minimum amount of MgSt (0.75 % w/w) required to achieve a uniform and robust surface layer on the processing tool surfaces.

The effective angles of internal friction for the two unlubricated powders are relatively similar despite the evident large differences in their wall frictional characteristics (Fig. 5.10). However, other factors, such as particle shape and size distribution, are important that may account for this observation. There is no reduction in ϕ_e when the DCPD is lubricated in the bulk. This suggests that there is shear induced fracture of the particles that exposes fresh unlubricated surfaces, which is consistent with their brittle nature. Clearly, this mechanism does not operate for the MCC. Wall lubrication causes a small reduction in the coefficient of wall friction and this must account for the relatively large reduction in ϕ_e with a considerable scaling effect from single particles to assemblies.

For MCC, lubricating the rolls does not affect either the nip angle (Fig. 5.22) or the maximum roll pressure (Fig. 5.21), which is consistent with the insensitivity of the friction to wall lubrication. However, there is a reduction in both parameters for bulk lubrication that increases with the amount of MgSt. This is reflected in the reduction in the density and strength of the ribbons (Table 5.3). As discussed above, it is difficult to boundary lubricate MCC. However, the bulk lubrication reduces the internal friction and increases the overall powder flowability. Therefore, the nip angle and the maximum pressure are reduced.

For DCPD, unlike MCC, the nip angle (Fig. 5.22), maximum pressure (Fig. 5.21) and also the density of the ribbons are all reduced by lubricating the rolls. The much greater sensitivity of the wall friction to boundary lubrication is a possible explanation since the values for the nip angle and maximum pressure are similar to those for critically bulk lubricated DCPD. That is, the bulk lubrication is again providing an internal source of the lubricant.

8.1.4 Effects of moisture

In this work, a reduction in nip angle (Fig. 5.24) and an increase in maximum pressure (Fig. 5.25) are observed with an increase in the amount of the added water. These observations agreed with the general tendency of the maximum pressure and nip angle reported in a previous work in roll compaction of moist MCC powder (Wu *et al*., 2010b) using a similar approach. Wu *et al.* (2010b) showed that the nip angle decreases with the moisture content

while the maximum pressure increases until reaching a critical point of 10 % moisture content and argued that the observations were caused by the reduction in cohesion and increase in the flowability of the powders with high moisture. Thus, the powders passed through the roll gap without being compacted. However, such critical point of moisture content is not observed in the current work. The experimental results showed that the water acting as a binder for all moist MCC powder (with moisture content from 6.3 to 16.4 %).

In addition, the results shown in Section 5.2.1 reveal that a small amount of additional moisture (say $\leqslant$ 2.5 % w/w) results in a reduction in the maximum pressure (Fig 5.23) but an increase in the nip angle (5.24). On the other hand, more water added into the system causes an increase in the maximum pressure but a decrease in the nip angle. This suggests that small amounts of moisture act as a lubricant, while large amounts of moisture act as binder, which enhances the binding of the MCC powder. The bulk densities and fracture energies of the ribbons produced from moist MCC (Figs 5.36 and 5.37) decrease at small amounts of additional water but then increase. The reduction of the bulk densities and fracture energies at 2.5% (w/w) moisture show similarity to those for lubricated ribbons (Table 5.3), which also indicates that small amount of additional water acts as a lubricant.

8.2 Milling

8.2.1 Influence of material properties and milling parameters on milling behaviour

In terms of the first order kinetics proposed to describe the milling process (Eq 6.1), the reciprocal of the characteristic number of milling cycles $\frac{1}{N_c}$ can be used to define the time required for the milling processes under given milling conditions. The milling results show that:

- Increasing ribbon relative density leads to increasing milling time and increasing mean granule size (Figs 6.3 and 6.4).

- Increasing screen size leads to decreasing milling time and increasing mean granule size (Figs 6.5 and 6.6).
- Increasing milling frequency leads to decreasing milling time and decreasing mean granule size (Fig 6.7 and 6.8).

The experimental results suggest that the dominating factor for the granule size is the screen size, followed by the milling frequency, which is consistent with the literature (Lantz, 1990). On the other hand, the ribbon properties (*i.e.* relative density, fracture energy) also affect the granule size.

The milling time is generally determined by the energy input, which is calculated from the mass and velocity of the blade and energy requirement for ribbon fracture. Since the granulation is driven by the kinetic energy of the milling blades, the energy input is dominated by the milling frequency. The energy requirement is determined by the fracture energy of the ribbons and the mesh size (see Appendix 3). The results showed that increasing milling frequency, decreasing ribbon strength and increasing screen size led to a decrease in the milling time, as expected. In order to get better understanding of the milling behaviour and energy consumption during the process, the reciprocal of N_c is plotted against the ratio of input energy to the energy requirement for fracture, $M_{blade}V^2/G_f A_f$, for ribbons with various fracture energies, as shown in Fig. 8.4.

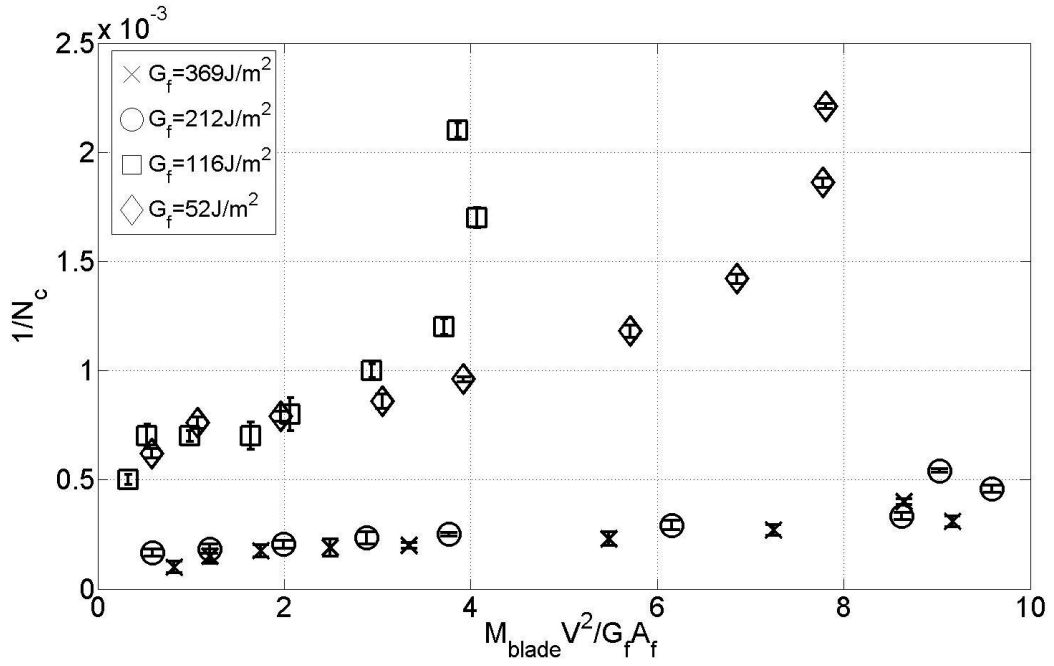

Figure 8.4 Reciprocal of N_c as a function of the ratio of input energy to the energy requirement for fracture (milled with a 630 µm screen at 200 rpm).

It is seen that the reciprocal of N_c increases with increasing energy input for all the fracture energies considered, which indicates a reduction in the of milling time. For ribbons with a smaller fracture energy (*i.e.* 52 and 116 J/m^2), there is a sharp increase of the reciprocal of N_c, which suggests the process is dominated by impact mechanisms. However, the variation of the reciprocal of N_c is not remarkable for those ribbons with high fracture energy (*i.e.* 212 and 369 J/m^2). This suggests that a major part of the input energy transfer involves heating for the strong ribbons. These observations are also supported by the PEPT results (Fig. 6.12), which showed that the ribbon speed is much larger for those with smaller fracture energies. Conclusively, the efficiency of the milling process (*i.e.* the reciprocal of N_c) depends on the milling frequency and screen size, and can be greatly affected by the fracture energy of the ribbons.

8.2.2 Fracture mechanisms dominated by milling frequency

As introduced in Section 6.3, there are two regions in which two distinct fracture mechanisms are involved 1) abrasion and 2) impact, indicated by the two regression lines shown in Fig. 6.10. PEPT experiments were carried out to obtain detailed information on the ribbon motion to achieve better understanding of the milling mechanics (Section 6.4). The PEPT results on the effects of milling frequency show that:

- The ribbons only occupy a small region of the milling chamber at smaller milling frequencies (≤ 200 Hz). The ribbons occupy a larger area of the milling chamber at higher milling frequencys (*i.e.* 300 Hz) (Figs 6.13, 6.15 and 6.17).
- Ribbons move at relatively small speed (< blade speed) when smaller milling frequencies are applied (≤ 200 Hz) (Fig. 6.14). The velocity of the ribbons is comparable to the blade speed, which indicates a plug flow (Fig. 6.15).
- The speed of the ribbons increases with the milling frequency (Fig. 6.14). The ribbons move at velocities much higher than that of the blade in the upper region of the milling chamber at higher milling frequencies (*i.e.* 300 rpm) (Fig. 6.15). However, the velocities of the ribbons located in the smaller region of the milling chamber remain comparable to those of the blade (Fig. 6.15).

By adopting the speed and velocities of the ribbons as indicators of the milling mechanics, it is straightforward to achieve a determination of the abrasion and impact regions. As shown in Fig. 8.5, an abrasion region can be found in the smaller region of the milling chamber (*i.e.* under the milling blade) in which ribbons move at velocities comparable or smaller than the blade speed, at all milling frequencies considered. In this region, the fracture of the ribbon is mainly caused by the abrasion between the ribbons and mesh. Additionally, an impact region occurs in the upper region of the milling chamber when the milling frequency (*i.e.* input energy) is sufficiently high. The impact of the ribbons moving at velocities more than a factor of 10 greater than those in the abrasion region induces fragmentation. The results obtained from multi-tracer experiments, which suggest that the number of milling cycles required to break a ribbon specimen (approximately 22 x 22 mm) remains constant at smaller milling frequencies (≤ 200 Hz), but decreases sharply with further increasing milling frequency. This is additional evidence supporting the milling mechanics discussed above.

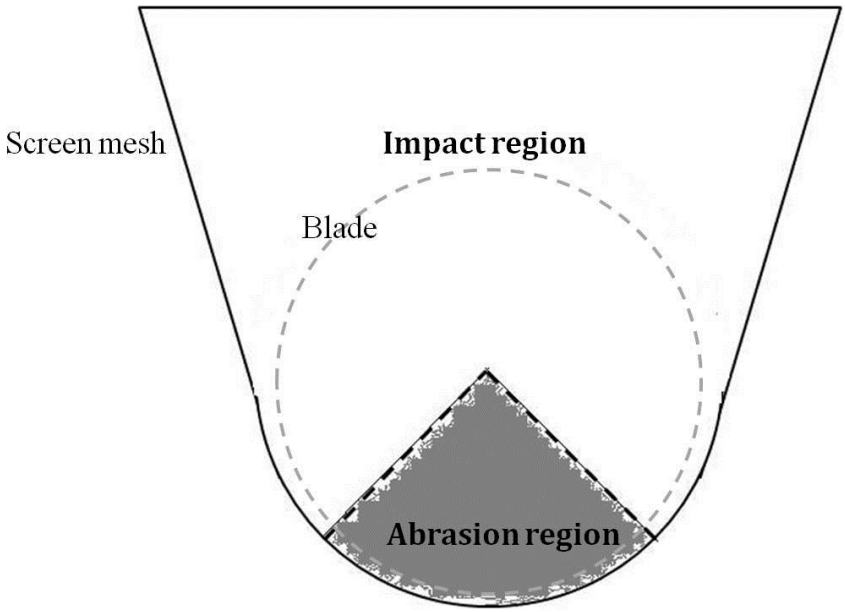

Figure 8.5 Schematic diagram of the abrasion region and impact region in the milling chamber.

It should be emphasised that no significant variation in the fine and coarse fractions of the granules produced at various milling frequencies was observed (Table 6.1). The granule size distribution may primarily be determined by the screen size, while the energy input does not contribute to the final products (*i.e.* granules) as it mostly occurs in the upper region of the milling chamber. The abrasion taking place in the smaller region of the milling chamber dominates the size distribution of the granules.

8.3 Tabletting

8.3.1 Compressibility and compactibility

As represented in Chapter 7, the compressibility of powder materials may be obtained using various approaches such as that of Johanson's (1965), Adams Adams, 1994), Heckel (1961) and Kawakita (1970). According to definition of the compressibility factor, a large value of κ and β refers to a small compressibility. Due to the lower stress limit for Johanson's

theory (1965), the pressure-density relationship is only applicable when a linear relationship is obtained for a logarithm plot of the normal stress and apparent density. In practice, the relationship cannot be used to examine the data in the region where the strain is small (Fig. 7.3). the Adams equation (Adams and McKeown, 1996, Patel *et al.*, 2010) shows advantages in evaluating the data points in all strain ranges (Fig. 7.5). It shows better reliability for evaluating the compression behaviour of a powder in the whole compression process. It is noted that the values for the two compressibility factors (*i.e.* κ and β) are considerably different for the brittle materials (*i.e.* DCPD and mannitol) that experience possible fragmentation of the feed powders and re-arrangement at relatively small normal stresses, as happens at the beginning of the compression.

In addition to the compressibility factor κ (Eq (2.13)) and β (Eq (2.14)), the constants k (Eq (2.7)) and a (Eq (2.9)) can also be used to describe the ability of a powder material to be compressed. For these two factors, the values are proportional to the compressibility. Similar to the pressure-density relationship adopted by Johanson (1965), the Heckel and Kawakita equations are only valid for linear region (Figs 7.1 and 7.2).

In summary, the Adams equation is most appropriate for examining the compressibility of powders. It is better than other relationships for the examination of brittle materials, which are likely to experience plastic deformation at relatively small stresses and then fragment. The Heckel and Kawakita equations can be used for the estimation of the compressibility. However, the accuracy of the results obtained is not reliable due to the limitation of the linear regression methods used, as is the case for the Johanson's equation (1965).

Compactibility, which is another important parameter to describe the compression behaviour of a powder, is defined as the ability of a powder to form compacts in tablet form under a given normal stress. In the current work, the dimensionless compactiblity parameter, C_p, is determined from the slope of the specific crushing strength as a function of the compression pressure. As introduced in Chapter 7, C_p can be determined from the commonly used tensile strength as well (Eq (7.5)).

8.3.2 Effects of the roll compaction conditions

The experiments on the effects of the roll compaction conditions on the uniaxial compression of the subsequent granules were evaluated using compressibility and compactibility. The results show that:

- Compressibility of the granules increases with increasing roll gap and roll speed (Figs 7.9 and 7.11);
- Compactibility of the granules increases with increasing roll gap and roll speed (Figs 7.10 and 7.12.

By integrating the results with the effects of roll compaction conditions on the maximum pressure (Figs 5.17 and 5.19), it is found that the compressibility and compactibility is inversely proportional to the maximum pressure generated in roll compaction. This is attributed to the work hardening and the production of robust granules with increasing resistance to deformation (Malkowska and Khan, 1983). The experimental results agree with the investigation of the re-compression of MCC by Malkowska and Khan (1983), showing that the reduction of the compressibility and compactibility is more significant when higher pressures are generated in roll compaction.

8.3.3 Effects of the lubrication

The experimental results imply that the lubrication in roll compaction does not affect the compressibility of the granules (Fig 7.15). Since the amount of MgSt added to the system is limited, the volume reduction under pressure for the sample materials does not vary significantly with the content of MgSt. On the other hand, the compactibility of MCC decreases with the amount of MgSt (Fig. 7.16). The commonly accepted model of MgSt is a Langmuir monolayer-film with preferential location of the stearate in the cavities (Roblot-Treupel and Puisieux, 1986). MCC powder consists of needle shaped particles with a porous structure on the particle surface (Fig. 4.1). Therefore, the MCC particles are covered by monomolecular films of MgSt (Tawashi, 1963), which weakens the binding property of the host particles. In addition, the cavities on the host particles are filled by MgSt when bulk

lubrication applied (Bolhuis *et al.*, 1980), and hence obstruct the inter-locking between the particles. Thus, the MCC covered by MgSt shows a decrease in binding and hence in the crushing strength of the subsequent tablets. DCPD, which is a fragmenting material, was reported to be very insensitive to MgSt mixing. Due to the fragile nature of DCPD, new surfaces without lubricant were generated during compression (Vromans *et al.*, 1988). Therefore, no significant changes in the compactibility are observed for DCPD (Fig. 7.16).

The strength of the DCPD tablets is much less than those formed from MCC (Fig. 7.17), which is analogous to data for the strength of the ribbons as indicated by the fracture energy shown in Table 5.3. The relative values of the stored elastic strains are probably again the main governing factor. The insensitivity of the strength of the DCPD tablets to lubrication (Figs 7.16 and 7.17a) may be attributed to the fragmentation characteristics of the powder particles and grains that cause fresh surfaces to be exposed and thus inhibit any potential binding by MgSt. Bulk lubrication causes a reduction in the strength of the MCC tablets (Table 3, Figs 7.16 and 7.17b), which suggests that the MgSt is acting as a weak boundary layer (*i.e.* a lubricant film) between the particles (Zuurman *et al.*, 1999), that reduces the bonding strength. Thus the influence of lubrication on both the DCPD and MCC tablets is also similar to the trends observed for the ribbons as shown in Table 5.3.

8.3.4 Effects of granule size and milling frequency

Figure 7.7 shows that the compressibility decreases with particle size for MCC powder and consequent granules. At the same time, the compactibility of the feed powders and granules also decreases (Fig. 7.8), which is consistent with the literature (M. G. Herting and Kleinebudde, 2007, C. Q. Sun and Himmelspach, 2006). This can be attributed to a decrease in the surface area of the particles, which leads to a reduction of the inter-particle bonding. It is noticeable that the compactibility of the granules is smaller than the feed particles with comparable size (Fig. 7.8), which is consistent with the results reported by (M. G. Herting and Kleinebudde, 2008). It is suggested that this loss of compactibility after roll compaction may be attributed to work hardening, and a combination of particle size enlargement and hardening of the material.

For the granules granulated from ribbons produced under exactly same conditions but at various milling frequencies, the compressibility and compactibility are directly proportional to the milling frequency. It is believed that the variation of the compressibility and compactibility are caused by the different sizes of the granules (Table 6.1 and Fig 6.9). The granules produced at high milling frequencies have better compactibility due to their small sizes, which is consistent with the results obtained from the experiments for particles and granules with various particle sizes (Fig 7.7 and 7.8).

8.4 Roll compaction-milling-tabletting process

In this section, the roll compaction, milling and tabletting processes are combined in order to achieve a clear understanding of the factors that will affect the specification of a process line. In pharmaceutical manufacturing, the final goal of the whole process is to produce tablet dosage with desired properties (*i.e.* dissolution rate, uniformity, tensile strength). On the basis of the experimental results and process understanding, attempts are made here to provide a rough guidance on the manufacturing of tablets with greater densities and tensile strengths.

According to the experimental investigations carried out in this work and a review of the literature, the requirement of the granule properties for successful tabletting can be summarised as follows:

- The density of the granules needs to be large enough to avoid segregation and corresponding inhomogeneity in the die filling (Xie and Puri, 2012).
- Good flowability (*i.e.* easy flowing, with $ff_c > 4$) of the granular material is required to achieve sufficient and uniform filling to the compression die (Felton *et al*., 2002, Xie and Puri, 2012, Yaginuma *et al*., 2007).
- A decrease of the particle size leads to increasing compression pressure and hence a higher relative density of the produced tablets, provided that the flowability of the powders is good enough (Section 7.3.2).

- The compressibility and compactibility of the granule is sufficiently high to ensure a high degree of densification in compression, and the tensile strength of the final products (*i.e* .tablets). This requires small pressures to be generated in roll compaction, according to the theory of the work hardening (Malkowska and Khan, 1983).

In the current work, the experimental investigation has been carried out using a instrumented roll compactor with adjustable roll gap and roll speed, with a gravity feeding system. Assuming that a powder is suitable to be roll compacted using the current system, the following smalling properties should be fulfilled as revealed in the experiments:

- The flowability of the powders is good enough.
- The particle size is sufficiently large to minimise aeration.
- The adhesion of the powder is not too high, which might result in jamming during roll compaction.

In this work, granules are produced using an oscillating mill. The flowability of the granules is directly proportional to the granule size, which increases with increasing screen size and decreasing milling frequency. In order to obtain a baseline of the flowability of the granules, the flowabilities of the granules were examined, which shows that the granules produced are at least free-flowing (Appendix 4).

Thus, the process conditions required for successful tabletting with high density and tensile strength can be obtained from the analysis of the roll compaction and milling process conditions, as shown in Fig. 8.6. Since the variations of the compressibility and compactibility show similar tendency to the material properties and changing process conditions (Section 7.3), a term ‘reworkability’, which represents the compressibility and compactibility, is introduced to describe the tabletting potential of granules.

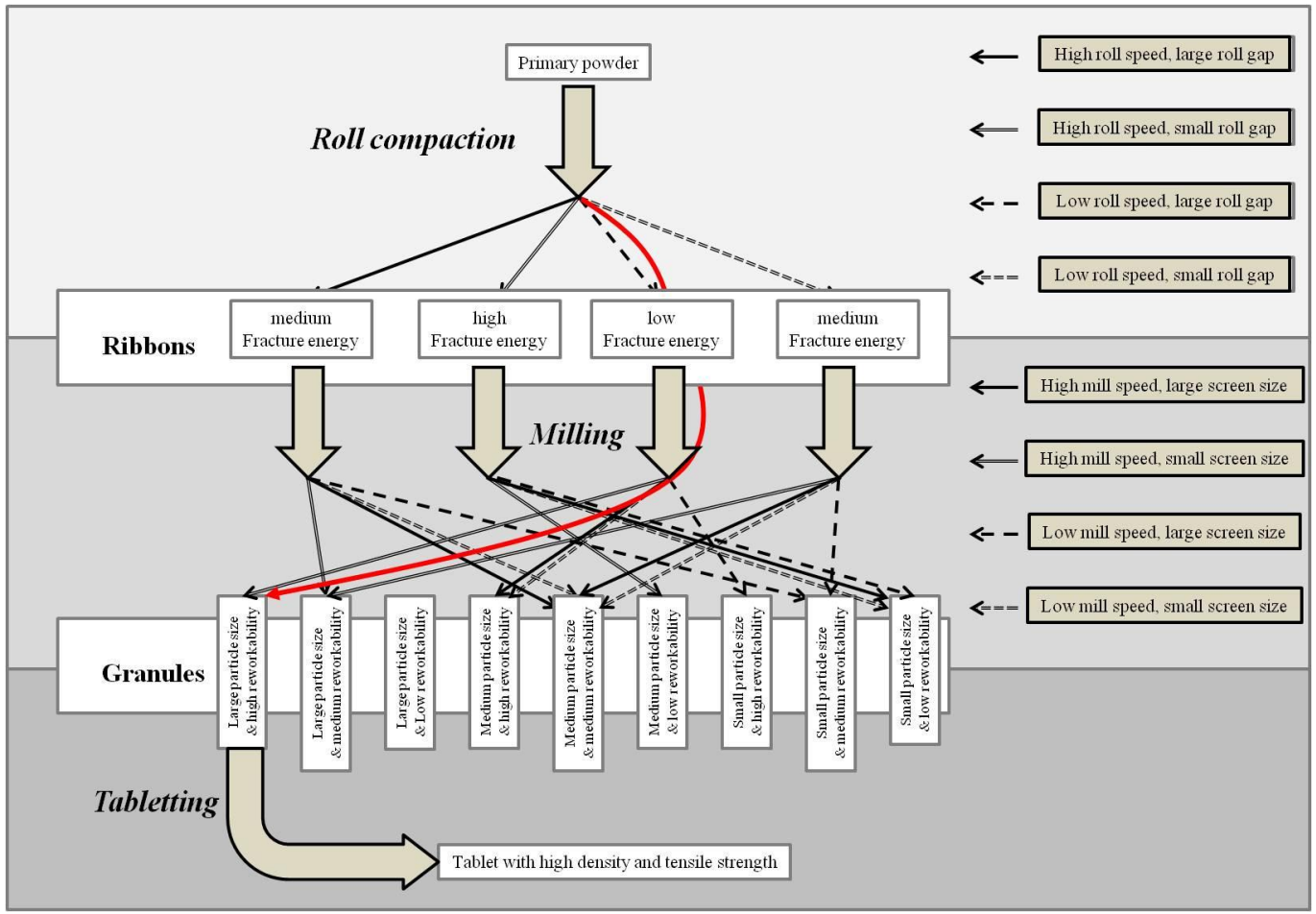

Figure 8.6 The schematic diagram for the required process conditions of the practical processes (*i.e.* roll compaction, milling) to produced desired tablets, the red curved line represents the conditions producing granules best for tableting, for MCC Avicel PH 102 powder using current experimental settings.

The optimized processing conditions are highlighted by the red line. It can be seen that granules, which is ready produce the target tablets, can be obtained under the following roll compaction and milling process conditions:

- Small roll speed in roll compaction.
- Large roll gap in roll compaction.
- High milling frequency in milling.
- Small screen size in milling.

The current results are only valid for the system layout used in this thesis. However, the methodology can be extended to other specific equipment. Despite the complex nature of the roll compaction process, the process conditions required for optimizing the manufacturing can be achieved with an explicit understanding on the granules required for tabletting to produce desired products.

8.5 Conclusions

This chapter discussed the experimental results obtained in the current work. The effects of the roll compaction parameters were evaluated. The influence of the material properties was studied. The roll compaction behaviour of lubricated and moist powders were analysed to achieve better understanding of the process. The subsequent milling and tabletting processes were studied to understand the whole manufacturing line in the pharmaceutical industry. The dominating factors in the milling processes were evaluated. The fracture mechanisms involved were studied. The performances of the feed powders and granules in the uniaxial compression were studied to attain the dependence of the tabletting process. The major findings can be summarised as:

- The maximum pressure generated in roll compaction decreases with the roll gap, which can be explained by Johanson theory (1965).

- The nip angle for powders with sufficient flowability (*i.e.* easy flowing, ff_c > 4) increases with the roll gap. However, the nip angle decreases with the roll gap for the poor flow powder consisting of small size particles due to the aeration.

- The compaction behavior (*i.e.* maximum pressure and nip angle) varies slightly with changing roll speed when the powder is sufficiently fed into the system.

- The poor flowability and small particle size of the feed powder result in a sharp decrease of the maximum pressure and nip angle, which is attributed to insufficient feeding.

- The properties of the powder greatly affect the roll compaction behaviour: greater internal and wall friction leads to greater nip angle and maximum pressure. An increasing compressibility factor results in decreasing in the nip angle, but increasing maximum pressure. However, all these effects might be dominated by the affects of powder feeding when a gravity feeding system is used.

- The effects of lubrication are different for powders with distinctive properties. The results reveal that bulk lubrication mainly affects the internal friction and bonding properties for MCC. Thus, the roll compaction behavior of MCC is not affected significantly by wall lubrication. On the other hand, bulk lubrication greatly affects the roll compaction of MCC.

- The internal friction and binding properties of DCPD are not affected by bulk lubrication using MgSt due to the fragile nature of the material. On the other hand, the wall lubricant results in sharp reduction in the nip angle and maximum pressure during roll compaction. A critical amount of MgSt (0.75 % w/w) is required to achieve a uniform and robust surface layer.

- The roll compaction experiments of moist MCC powder indicate that the water added acts as a lubricant at relatively small moisture contents (~2.5 %) and as a binder at larger moisture contents.

- A first order kinetics equation is introduced to describe the milling behavior. The model can successfully express the mass throughput of the granules during the milling.

- The milling time required for sufficient granulation increases with increasing relative density, decreasing screen size and decreasing milling time. The size of the granules

produced is dominated by the screen size, followed by the ribbons relative density and milling frequency.

- It is found that there are two regions involved in the milling, namely an abrasion region and impact region. The abrasion region is located in the smaller part of the milling chamber in which the ribbon moves at velocities comparable to the blade or even smaller. In this region, the fracture of the ribbons is mainly caused by the friction. The impact region, which is located in the upper part of the milling chamber, occurs at high milling frequencies, in which the ribbons move at velocities much larger than the blade. In this region, the fracture of the ribbons is dominated by impact.

- Work hardening leads to a reduction in reworkability (*i.e.* compressibility and compactibility) of the granules. This is a combination of the hardening of the material and particle size enlargement.

- The reworkability of the granules is directly proportional to the milling frequency, which can be attributed to the effects of granule size.

- Bulk lubrication shows slight effects on the compressibility of the granules, while the compactibility of the granules is determined by the formation of an MgSt layer on the host particles. For MCC with cavities on the surface, the bonding potential greatly reduces due to the weak binding properties of the monomolecular layer of MgSt. In the other hand, the brittle/ductile nature of the powder material might affect its performances with lubrication. According to the Young's modulus which can be used as an indicator for the brittleness, DCPD (with Young's modulus of 47.8 GPa) is more brittle than MCC (with Young's modulus of 8.2 GPa). Therefore, , new surfaces without MgSt are likely to be generated for DCPD whose main deformation mechanism is brittle fracture (Almaya and Aburub, 2008). Therefore, the binding properties of DCPD which is brittle are insensitive to bulk lubrication.

- With an explicit understanding in the requirement of granule properties for successful tabletting, required roll compaction and milling process conditions can be derived by integrating the effects of process parameters in particular processes (*i.e.* roll compaction, milling).

CHAPTER 9 CONCLUSIONS AND FUTURE WORK

9.1 Conclusions

The roll compaction of pharmaceutical excipients was experimentally carried out to investigate the influence of the material properties of the feed powders on the performance of the process. Key findings can be summarised as follows:

- The effects of lubrication depend on the type of feed powder. The effects of wall lubrication and bulk lubrication are significantly different for MCC and DCPD due to their frictional properties and the way in which DCPD fragments unlike MCC. In addition, wall lubrication results in a more uniform density distribution of the roll compacted ribbons.

- A small amount of additional water does not affect the roll compaction behaviour for MCC (Avicel PH 102) powder . A large amount of added water acts as binder which increases the maximum pressure during roll compaction and thus increases the density and the strength of the ribbons.
- The roll compaction behaviour of the binary mixtures depends on the composition of the mixtures. The roll compaction performances were dominated by the major component of the mixture.

Milling of the roll compacted ribbons was explored using an oscillating mill. The PEPT technique was used to investigate the kinematics in the milling process. It was found that:

- First order kinetics can be used to describe the milling process. The model fits the mass throughput of the produced granules well and introduces a term of characteristic number of cycles describing the process.

- The required milling time increases with increasing relative density of the ribbon, decreasing screen size and milling frequency.

- The particle size of the granules from the mill increases with increasing ribbon relative density, increasing screen size and decreasing milling frequency.

- There are two regions that control the milling behaviour. The first is the area under the milling blade in which abrasion dominates, and the second is the upper part of the milling chamber in which impact occur.

The results of the uniaxial compression experiments of the feed powders and granules revealed that:

- The feed powders and granules with small particle sizes show better reworkability (*i.e.* compressibility and compactibility).

- The reduction in the reworkability of the granules was mainly caused by the work hardening of the materials, a combination of the hardening of the material and size enlargement.

- Increasing the roll gap and roll speed results in less reduction in reworkability.

- Neither bulk lubrication of the feeding powder nor wall lubrication on the roll surfaces during roll compaction affects the compressibility of the granules. However, the compactibility might vary, depending on the properties of the feed powder.

- Increasing the milling frequency leads to an improved tabletablity of the granules. This is believed to be ascribed to the reduction in the granule sizes with the increasing kinetic energy, which result in the tablets with enhanced tensile strength yield in die compression.

9.2 Future work

- Work has been done to explore the effects of particle size distribution on the roll compaction performances of the feed powders. However, the relationship between the particle size/roll gap ratio and the compaction behaviour has not been investigated. It is worthy to carry out such experiments on powders of a narrow particle size distribution at various roll gaps to explore the potential correlation between the particle size and roll gap. This might assist in gaining a more detailed understanding of the process and hence specifying the optimal operating parameters for specific powders.

- The feeding system combined with the roll compactor determines the amount of powder fed, and the initial pressure prior to the roll compaction, and thus greatly affects the process. Previous work has highlighted the importance of the feed pressure (Guigon and Simon, 2003, Johanson, 1965) and the feed rate of the screw system (Lecompte *et al*., 2005, Simon and Guigon, 2003). Since the current industrial screw feeder – roll compactor system is actually a combination of an extruder and a roll compactor, problems such as inhomogeneous feeding and work hardening caused by densification in feeding system at high feeding speed may result. It might be interesting to explore the boundary of the feeding speed/pressure to achieve a target roll compaction pressure for powders with various flow and mechanical properties using a screw feeding system. Additionally, work should be done to explore the roll compaction behaviour using an alternative feeding system such as hydraulic feeding.

- The current work on the granulation process using the milling technique is based on a batch system. The investigation should be extended to continuous systems which are employed in practical industrial manufacturing in order to explore the kinematics and determine the guidelines for the milling parameters.

- Abrasion is one essential mechanism in the milling process. Thus, the investigation of the thermal conditions in the milling chamber should be investigated for a better understanding of the process.

APPENDIX 1 Determination of adhesion

In ring shear cell tests, the normal stress σ and shear stress τ are obtained from wall friction measurements. With the cross section area of the powder bed, A_R, the normal force F_{NR} and friction force F_{SR} can be determined from:

$$F_{NR} = \sigma A_R$$

$$F_{SR} = \tau A_R$$

Thus, the $F_{SR} - F_{NR}$ plot for the tested powder can be obtained, as shown in the following figure:

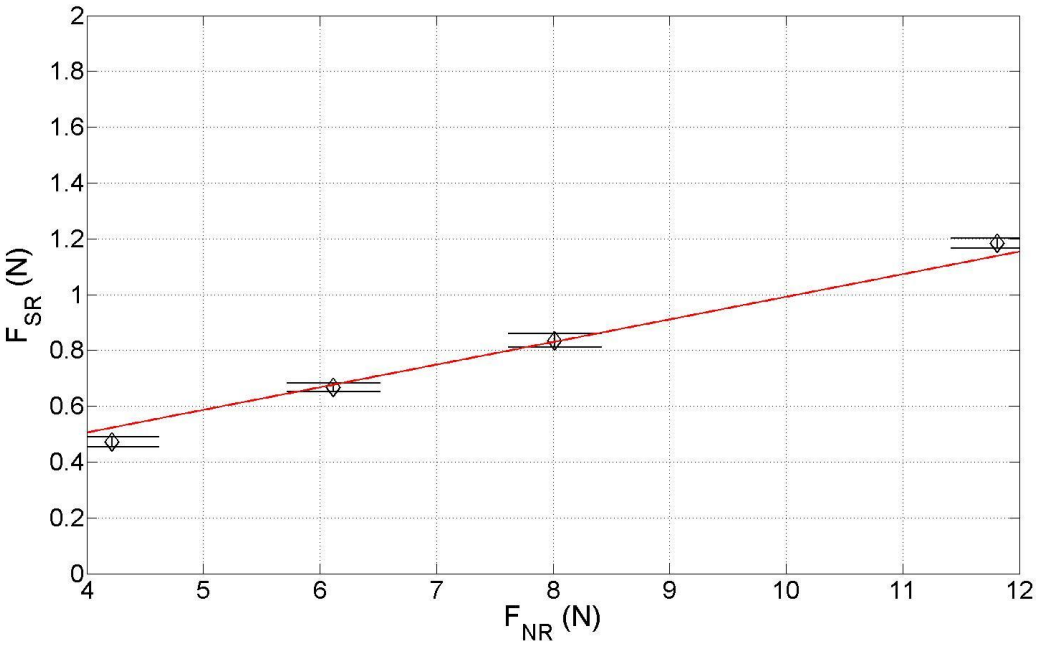

Figure A.1.1 Variation of friction force as a function of normal force.

The adhesion of a powder against the wall material equals to the negative value of the intercept on the x-axis.

APPENDIX 2 Detailed derivation of the first order kinetic for milling

The first order kinetic for milling process is written as:

$$\frac{dm}{dN} = k\,(m_\infty - m) \qquad \text{Eq (A.2.1)}$$

which can be reformed to:

$$\frac{dm}{m_\infty - m} = k\,dN \qquad \text{Eq (A.2.2)}$$

Integrating Eq (A.2.2) to $m = 0$ at $N = 0$ gives

$$-\ln\left(m_\infty - m\right) = kN + c \qquad \text{Eq (A.2.3)}$$

where $c = \ln m_\infty$.

In order to solve the equation, a term 'characterised number of milling cycles', N_c, which is defined as the number of milling cycles at which the granule mass fraction is $1 - \exp(-1)$.

If $k = 1/N_c$, Eq (A.2.3) is solved, giving following relationship:

$$\frac{m_\infty - m}{m_\infty} = \exp\left(-\frac{N}{N_c}\right) \qquad \text{Eq (A.2.4)}$$

APPENDIX 3 Calculation of the energy requirement for ribbon fracture

As discussed in Section 4.3.4, the fracture energy G_f of the ribbons is obtained using three point bending tests. Thus, the energy requirement for ribbon fracture can be expressed $G_f A_f$, provided that the surface area generated by fracture A_f is known.

With measured dimensions (*i.e.* width w_r, length l_r, and thickness h_r) of the ribbon specimens, the surface area of the ribbons A_r before the milling can be obtained by:

$$A_r = 2 \times \left(w_r l_r + w_r h_r + h_r l_r \right) \quad \text{Eq (A.3.1)}$$

Assumed the ribbons are granulated into equivalent squares with side lengths equalling to the operated screen size d_s, the number of the granules n_g and the surface area of an individual granule A_g is given by:

$$n_g = \frac{w_r l_r h_r}{d_s^3} \quad \text{Eq (A.3.2)}$$

$$A_g = 6 d_s^2 \quad \text{Eq (A.3.3)}$$

Combining Eq (A.3.1), (A.3.2) and (A.3.3) gives that:

$$A_f = n_g A_g - A_r = \frac{6 w_r l_r h_r}{d_s} - 2 \times \left(w_r l_r + w_r h_r + h_r l_r \right) \quad \text{Eq (A.3.4)}$$

APPENDIX 4 Correlation between the properties of products obtained from unit processes and process conditions

Table A.4.1 Correlation between the properties of products obtained from unit process and process conditions

Primary powder	Roll compaction conditions	G_f (J/m^2)	Milling conditions	ff_c for granules	**Tablet strength (MPa)
*MCC	u = 0.5 rpm, S = 0.6 mm	412	ω = 50 rpm, d_s = 630 μm	12.6	3.9
			ω = 50 rpm, d_s = 2000 μm	28.6	1.1
			ω = 300 rpm, d_s = 630 μm	8.8	5.2
			ω = 300 rpm, d_s = 2000 μm	21.6	1.8
	u = 0.5 rpm, S = 2 mm	32	ω = 50 rpm, d_s = 630 μm	15.6	5.3
			ω = 50 rpm, d_s = 2000 μm	35.3	2.1
			ω = 300 rpm, d_s = 630 μm	9.8	7.2
			ω = 300 rpm, d_s = 2000 μm	24.2	2.6
	u = 5 rpm, S = 0.6 mm	262	ω = 50 rpm, d_s = 630 μm	16.4	4.3
			ω = 50 rpm, d_s = 2000 μm	30.2	1.4
			ω = 300 rpm, d_s = 630 μm	8.8	5.7
			ω = 300 rpm, d_s = 2000 μm	23.2	2.1
	u = 5 rpm, S = 2 mm	14	ω = 50 rpm, d_s = 630 μm	17.6	6.2
			ω = 50 rpm, d_s = 2000 μm	38.2	2.3
			ω = 300 rpm, d_s = 630 μm	11.6	7.6
			ω = 300 rpm, d_s = 2000 μm	25.4	3.0

*MCC (Avicel PH 102) was used as sample powder for success roll compaction.

** Tablets were produced under a maximum compression force of 16 kN.

APPENDIX 5 List of publications

Andrews, J., Yu, S., Gururajan, B., Reynolds, G., Roberts, R., Wu, C.Y. and Adams, M. (2010) Analytical solutions for roll compaction of pharmaceutical powders. *Journal of Pharmacy and Pharmacology*, 62: (10): 1403-1404.

Yu, S., Adams, M., Gururajan, B., Reynolds, G., Roberts, R. and Wu, C.-Y. The effects of lubrication on roll compaction, ribbon milling and tabletting. (accepted for publication in *Chemical Engineering Science*).

Yu, S., Gururajan, B., Reynolds, G., Roberts, R., Adams, M.J. and Wu, C.Y., Determining the nip angle during roll compaction of pharmaceutical excipients, *World Congress on Particle Technology 6*, 26-29 April 2010, Nuremberg, Germany.

Yu, S., Gururajan, B., Reynolds, G., Roberts, R., Adams, M.J. and Wu, C.Y. (2012) A comparative study of roll compaction of free-flowing and cohesive pharmaceutical powders. *International Journal of Pharmaceutics*, 428: (1-2): 39-47.

Yu, S., Gururajan, B., Reynolds, G., Roberts, R., Wu, C.Y. and Adams, M. (2010), Exploring roll compaction of two commonly used pharmaceutical powders. *Journal of Pharmacy and Pharmacology*, 62: (10): 1434-1435.

Yu, S., Gururajan, B., Reynolds, G., Roberts, R., Wu, C.Y. and Adams, M., Effects of lubrication on roll compaction, ribbon milling and tabletting, *UK-China Particle Technology Forum III*, 3-6 July 2011, Birmingham, UK.

Yu, S., Gururajan, B., Reynolds, G., Roberts, R., Wu, C.Y. and Adams, M., Experimental Investigation of milling of roll compacted ribbons, *UK-China Particle Technology Forum III*, 3-6 July 2011, Birmingham, UK.

Yu, S., Gururajan, B., Reynolds, G., Roberts, R., Wu, C.Y. and Adams, M., Milling of roll compacted pharmaceutical ribbons, *UK-PharmSci Conference 2011*, 31 August-2 September 2011, Nottingham, UK.

REFERENCES

(EFCE), E.F.o.C.E. (1989) Standard shear testing technique for particulate solids using the Jenike shear cell. **IChemE.**

Abraham, B. and Cunningham, J. (2008) **Method are provided for dry granulation processing of a pharmaceutical composition to provide granulated pharmaceutical compositions with improved flow characteristics and reduced amounts of fine particles**. US, Janssen Pharmaceutica NV.

Adams, M.J. and McKeown, R. (1996) Micromechanical analyses of the pressure-volume relationships for powders under confined uniaxial compression. **Powder Technology**, 88: (2): 155-163.

Adams, M.J., Mullier, M.A. and Seville, J.P.K. (1994) Agglomerate strength measurement using a uniaxial confined compression test. **Powder Technology**, 78: (1): 5-13.

Agatonovic-Kustrin, S. and Beresford, R. (2000) Basic concepts of artificial neural network (ANN) modeling and its application in pharmaceutical research. **Journal of Pharmaceutical and Biomedical Analysis**, 22: 717-727.

Almaya, A. and Aburub, A. (2008) Effect of particle size on compaction of materials with different deformation mechanisms with and without lubricants. **AAPS PharmSciTech**, 9: (2): 414-418.

Bacher, C., Olsen, P.M., Bertelsen, P., *et al*. (2008) Compressibility and compactibility of granules produced by wet and dry granulation. **International Journal Pharmaceutics.** 358: (1-2):69-74.

Balicki, M. (2003) **Numerical methods for predicting roll press powder compaction parameters**. PhD thesis**,** École des Mines d'Albi-Carmaux.

Bennett, B. and Cole, G. (2003) Pharmaceutical production: An engineering guide. Institution of Chemical Engineers, UK.

Bindhumadhavan, G. (2004) **Roller compaction of pharmaceutical powders**. PhD thesis, University of Birmingham.

Bindhumadhavan, G., Seville, J.P.K., Adams, M.J., *et al*. (2005) Roll compaction of a pharmaceutical excipient: Experimental validation of rolling theory for granular solids. **Chemical Engineering Science**, 60: (14): 3891-3897.

Bolhuis, G.K., Lerk, C.F. and Broersma, P. (1980) Mixing Action and Evaluation of Tablet Lubricants in Direct Compression. **Drug Development and Industrial Pharmacy**, 6: (1): 15 - 33.

Bourquin, J., Schmidli, H., van Hoogevest, P., *et al*. (1997) Application of Artificial Neural Networks (ANN) in the Devlopment of Solid Dosage Forms. **Pharmaceutical Development and Technology**, 2: (2): 111-121.

Bowden, F.P. and Tabor, D. (1950) **The Friction and Lubrication of Solids**. New York: Oxford University Press.

Caillard, R. and Subirade, M. (2011) Quantification of the compactibility of several protein isolates: Relationship between isolate physical-chemical properties and compaction properties. **Food Research International**, 44: (4): 917-924.

Chekmarev, A.P. and Vinogradov, G.A. (1963) Investigation on specific pressure, specific friction, and the coefficient of friction during metal powder rolling. **Soviet Powder Metal Ceram**, 112-115.

Cohn, R., Heiling, H. and Delorimier, A. (1966) A Critical Evaluation of the Compactor. **Journal of Pharmaceutical Sciences**, 55: 328-331.

Coulomb, C. A. (1776) Sur une application des re ́gles de maximis &minimis a` quelques proble`ms de statique, reltifs a` l'architecture, in *Me ́moires de Mathe ́matique et de Physique, Presented at the Royal Academy of Sciences*. **Imp. R. Acad. Sci., Paris**, 343–384.

Cunningham, J.C. (2005) **Experimental Studies and Modelling of the Roller Compaction of Pharmaceutical Powders**. PhD thesis, Drexel University.

Cunningham, J.C., Winstead, D. and Zavaliangos, A. (2010) Understanding variation in roller compaction through finite element-based process modeling. **Computers & Chemical Engineering**, 34: (7): 1058-1071.

Dec, R.T., Zavaliangos, A. and Cunningham, J.C. (2003) Comparison of various modeling methods for analysis of powder compaction in roller press. **Powder Technology**, 130: 265-271.

Duckworth, W. (1953) Discussion of Ryshkewitch paper. **Journal of the American Ceramic Society**, 36: (2): 68-68.

Fell, J.T. and Newton, J.M. (1968) The tensile strength of lactose tablets. **The Journal of pharmacy and pharmacology**, 20: (8): 657-659.

Felton, L.A., Garcia, D.I. and Farmer, R. (2002) Weight and Weight Uniformity of Hard Gelatin Capsules Filled with Microcrystalline Cellulose and Silicified Microcrystalline Cellulose. **Drug Development and Industrial Pharmacy**, 28: (4): 467-472. 19 : (4): 281-289.

Feritag, F. and Kleinebudde, P. (2003) How do roll compaction/dry granulation affect the tableting behaviour of inorganic materials? Comparison of four magnesium carbonates. **European Journal of Pharmaceutical Sciences**,

Funakoshi, Y., Asogawa, T. and Satake, E. (1977) The use of a novel roller compactor with a concavo-convex roller pair to obtain uniform compacting pressure. **Drug Development and Industrial Pharmacy**, 3: (6): 555-573.

Guigon, P. and Simon, O. (2003) Roll press design--influence of force feed systems on compaction. **Powder Technology**, 130: 41-48.

Guo, Y., Kafui, K.D., Wu, C.Y., *et al*. (2009) A Coupled DEM/CFD Analysis of the Effect of Air on Powder Flow During Die Filling. **Aiche Journal**, 55: (1): 49-62.

Guo, Y., Wu, C.Y., Kafui, K.D., *et al*. (2010) Numerical analysis of density-induced segregation during die filling. **Powder Technology**, 197: (1-2): 111-119.

Hebb, D. (1949) **The Organization of Behaviour**. New York: Wiley.

Heckel, R.W. (1961) Density-Pressure relationship in powder compaction. **Trans. Metal. Soc. AIME**, 221: (4): 671-675.

Herting, M.G. and Kleinebudde, P. (2007) Roll compaction/dry granulation: Effect of raw material particle size on granule and tablet properties. **International Journal of Pharmaceutics**, 338: (1-2): 110-118.

Herting, M.G. and Kleinebudde, P. (2008) Studies on the reduction of tensile strength of tablets after roll compaction/dry granulation. **European Journal of Pharmaceutics and Biopharmaceutics**, 70: (1): 372-379.

Hertz, H. (1881) On the contact of elastic solids. **J. reine angew. Math**, 92: (156-171): 110.

Inghelbrecht, S. and Remon, J.P. (1998) The roller compaction of different types of lactose. **International Journal of Pharmaceutics**, 166: (2): 135-144.

Inghelbrecht, S., Remon, J.P., deAguiar, P.F., *et al*. (1997) Instrumentation of a roll compactor and the evaluation of the parameter settings by neural networks. **International Journal of Pharmaceutics**, 148: (1): 103-115.

Jaminet, F. and Hess, H. (1966) Studies on compacting and dry granulation. **Untersuchungen uber Kompaktierung und Trockengranulierung.**, 41: (1): 39-58.

Jenike, A. W. (1961) **Gravity flow of bulk solids.** University of Utah Engineering Experiment Station, No. 8.

Jenike, A. W. (1967) Quantitative design of mass-flow bins, **Powder Technology**, 1: (4): 237-244.

Jenike, A.W. (1964) **Storage and flow of solids** Salt Lake City, Utah : University of Utah.

Jenike, A.W. and Shield, R.T. (1959) On the plastic flow of Coulomb solids beyond original failure. **Journal of Applied Mechanics**, 81: 599-602.

Jivraj, M., Martini, L. G., Thomson, C. M. (2000) An overview of the different excipients useful for the direct compression of tablets, **Pharmaceutical Science & Technology Today**, 3: (2): 58-63.

Johanson, J.R. (1965) A rolling theory for granular solids. **Journal of Applied Mechanics**, 32: (4): 842-848.

Katashinskii, V.P. (1966) Analytical determination of specific pressure during the rolling of metal powders. **Powder Metallurgy and Metal Ceramics**, 5: (10): 765-772.

Kawakita, K. and Lüdde, K.-H. (1970) Some considerations on powder compression equations. **Powder Technology**, 4: 61-68.

Kleinebudde, P. (2004) Roll compaction/dry granulation: pharmaceutical applications. **European Journal of Pharmaceutics and Biopharmaceutics**, 58: (2): 317-326.

Kuhn, H.A. and Downey, C.L. (1971) Deformation characteristics and plasticity theory of sintered powder materials. **International Journal of Powder Metallurgy**, 7: 15-25.

Kuntz, T., Schubert, M.A. and Kleinebudde, P. (2011) Increased compactibility of acetames after roll compaction. **European Journal of Pharmaceutics and Biopharmaceutics**, 77: (1): 164-169.

Lagergren, S. (1898), Zur theorie der sogenannten adsorption gel öster stoffe, **Kungliga Svenska Vetenskapsakademiens. Handlingar**, 24: (4) : 1-39.

Lantz, R.J. (1990) "Size Reduction". In Lieberman, H.A. & Schwartz, J.B. (Eds.) **Pharmaceutical Dosage Forms: Tablets**. 2nd ed. New York, Marcel Dekker 107-200.

Lecompte, T., Doremus, P., Thomas, G., *et al*. (2005) Dry granulation of organic powders - dependence of pressure 2D-distribution on different process parameters. **Chemical Engineering Science**, 60: (14): 39933-33940.

Leuenberger, H. (1982) The compressibility and compactibility of powder systems. **International Journal of Pharmaceutics**, 12: (1): 41-55.

Leuenberger, H. and Jetzer, W. (1984) The compactibility of powder systems - a novel approach. **Powder Technology**, 37: (1): 209-218.

Malkowska, S. and Khan, K.A. (1983) Effect of Re-Conpression on the Properties of Tablets Prepared by Dry Granulation. **Drug Development and Industrial Pharmacy**, 9: (3): 331-347.

Mansa, R.F. (2006) **Roller compaction of pharmaceutical excipients and predictiopn using intelligent software**. PhD thesis, University of Birmingham.

Mansa, R.F., Bridson, R.H., Greenwood, R.W., *et al*. (2008) Using intelligent software to predict the effects of formulation and processing parameters on roller compaction. **Powder Technology**, 181: 217-225.

McCulloch, W.S. and Pitts, W. (1943) A logical calculus of the ideas imminent in nervous activity. **Bulletin of Mathematical Biophysics**, 5: 115-153.

Michel, B. (1994) **Compactage en presse a rouleaux de poudres minerales**. PhD thesis, Universit é de Compi ègne.

Michrafy, A., Diarra, H., Dodds, J.A., *et al*. (2011a) Experimental and numerical analyses of homogeneity over strip width in roll compaction. **Powder Technology**, 206: (1-2): 154-160.

Michrafy, A., Diarra, H., Dodds, J.A., *et al*. (2011b) Analysis of strain stress state in roller compaction process. **Powder Technology**, 208: (2): 417-422.

Miguélez-Morán, A.M., Wu, C.Y., Dong, H., *et al*. (2009) Characterisation of density distributions in roller-compacted ribbons using micro-indentation and X-ray micro-computed tomography. **European Journal of Pharmaceutics and Biopharmaceutics**, 72: (1): 173-182.

Miguélez-Morán, A.M., Wu, C.Y. and Seville, J.P.K. (2008) The effect of lubrication on density distributions of roller compacted ribbons. **International Journal of Pharmaceutics**, 362: (1-2): 52-59.

Miller, R.W. (1994) Advances in Pharmaceutical Roller Compactor Feed System Designs. **Pharmaceutical Technology**, 18: (3): 154-162.

Miller, R.W. (1997) "Roller compaction technology". In Parikh, D.M. (Ed.) **Handbook of Pharmaceutical Granulation Technology**. New York, Marcel Dekker 99-149.

Mindlin, R.D. and Deresiewicz, H. (1953), Elastic Spheres in Contact under Varying Oblique Forces. **Trans. ASME, Series E, J. Appl. Mech**, 20: 327-353.

Mohr, O. (1900) Welche Umstände bedingen die Elastizitätsgrenze und den Bruch eines Materials? **Zeitschrift des vereins deutscher Ingenieure**, 44: 1524-1530, 1572-1577.

Muliadi, A.R., Litster, J.D. and Wassgren, C.R. (2012) Modeling the powder roll compaction process: Comparison of 2-D finite element method and the rolling theory for granular solids (Johanson's model). **Powder Technology**, 221: (0): 90-100.

Nesarikar, V.V., Vatsaraj, N., Patel, C., *et al*. (2012) Instrumented roll technology for the design space development of roller compaction process. **International Journal of Pharmaceutics**, 426: (1-2): 116-131.

Odagi, K., Tanaka, T. and Tsuji, Y. (2001) Compressive flow property of powder in roll-type presses—Numerical simulation by discrete element method (in Japanese). **Journal of the Society of Powder Technology, Japan**, 38: 150-159.

Parikh, D.B. (1997) **Handbook of pharmaceutical granulation technology**. Marcel Dekker.

Parker, D.J., Broadbent, C.J., Fowles, P., *et al*. (1993) Positron emission particle tracking - a technique for studying flow within engineering equipment. **Nuclear Instruments and Methods in Physics Research Section A: Accelerators, Spectrometers, Detectors and Associated Equipment**, 326: (3): 592-607.

Parker, D.J., Leadbeater, T.W., Fan, X., *et al*. (2008) Positron imaging techniques for process engineering: recent developments at Birmingham. **Measurement Science and Technology**, 19: (9): 094004.

Parrot, E.L. (1981) Densification of powders by concavo-convex roller compactor. **Journal of Pharmaceutical Sciences**, 70: 288-291.

Patel, B.A., Adams, M.J., Turnbull, N., *et al*. (2010) Predicting the pressure distribution during roll compaction from uniaxial compaction measurements. **Chemical Engineering Journal**, 164: 410-417.

Petit-Renaud, A., Laroche, C. and Guigon, P. (1998) "Experimental Study of the Roll Compaction of Powders". **World Congress on Particle Technology 3**. Brighton, UK.

Radchenko, K.M. (1974) Neutral angle in the densification rolling of sintered materials. **Powder Metallurgy and Metal Ceramics**, 13: (4): 266-270.

Roblot-Treupel, L. and Puisieux, F. (1986) Distribution of magnesium stearate on the surface of lubricated particles. **International Journal of Pharmaceutics**, 31: (1-2): 131-136.

Rosenblatt, F. (1958) The Perceptron: A Probabilistic Model for Information Storage and Organization in the Brain. **Pyschological Review**, 65: 386-408.

Rowe, R.C. and Roberts, R.J. (1996) "Mechanical Properties". In Alderborn, G. & Nyström, C. (Eds.) **Pharmaceutical Powder Compaction Technology**. New York, Marcel Dekker 283-322.

Rumpf, H.C.H. (1970) Zur Theorie der Zugfestigkeit von Agglomeraten bei Kraftübertragung an Kontaktpunkten. **Chemie Ingenieur Technik**, 42: (8): 538-540.

Sakwanichol, J., Puttipipatkhachorn, S., Ingenerf, G., *et al*. (2012) Roll compaction/dry granulation: Comparison between roll mill and oscillating granulator in dry granulation. **Pharm Dev Technol**. 17: (1): 30-39.

Schönert, K. and Sander, U. (2002) Shear stresses and material slip in high pressure roller mills. **Powder Technology**, 122: (2-3): 136-144.

Schulze, D. (2006) **Flow Properties of Powders and Bulk Solids.** Berlin: Springer.

Schulze, D. (2008) **Powders and Bulk Solids: Behavior, Characterization, Storage and Flow** New York: Springer.

Shlieout, G., Lammens, R.F. and Kleinebudde, P. (2000) Dry granulation with a roller compactor. Part I: The functional units and operation modes. **Pharmaceutical Technology Europe**, 12: (11): 24-35.

Simon, O. and Guigon, P. (2000) Interaction between feeding and compaction during lactose compaction in a laboratory roll press. **Kona**, 18: 131-138.

Simon, O. and Guigon, P. (2003) Correlation between powder-packing properties and roll press compact heterogeneity. **Powder Technology**, 130: 257-264.

Sinka, I.C., Cunningham, J.C. and Zavaliangos, A. (2003) The effect of wall friction in the compaction of pharmaceutical tablets with curved faces: a validation study of the Drucker-Prager Cap model. **Powder Technology**, 133: (1-3): 33-43.

Sonnergaard, J.M. (2006) Quantification of the compactibility of pharmaceutical powders. **European Journal of Pharmaceutics and Biopharmaceutics**, 63: (3): 270-277.

Spinov, V.A. and Vinogradov, G.A. (1967) Influence of Air on the Rolling of Powders (in Russian). **Poroskaya Metallurgyia**, 8: (56): 96-99.

Strickland., W.A.J., Nelson., E., Busse, L.W., *et al*. (1956) The physics of tablet compression IX. Fundamental aspects of tablet lubrication. **Journal of the American Pharmaceutical Association**, 45: (1): 51-55.

Sun, C.Q. and Himmelspach, M.W. (2006) Reduced tabletability of roller compacted granules as a result of granule size enlargement. **Journal of Pharmaceutical Sciences**, 95: (1): 200-206.

Sun, C.Q.C. (2008) On the mechanism of reduced tabletability of granules prepared by roller compaction. **International Journal of Pharmaceutics**, 347: (1-2): 171-172.

Tawashi, R. (1963) Der Einfluss von Aerosil auf die Packungseigenschaften von pulvern. **Pharmaceutical Industry**, 25: 655-658.

Tsuji, Y., Tanaka, T. and Ishida, T. (1992) Lagrangian numerical simulation of pulg flow of cohesionless particles in a horizontal pipe. **Powder Technology**, 71: 239-250.

Turkoglu, M., Aydin, I., Murray, M., *et al*. (1999) Modeling of a roller-compaction process using neural networks and genetic algorithms. **European Journal of Pharmaceutics and Biopharmaceutics**, 48: (3): 239-245.

Vendola, T.A. and Hancock, B.C. (2008) The Effect of Mill Type on Two Dry-Granulated Placebo Formulations. **Pharmaceutical Technology**, 32: (11): 72-86.

Vinogradov, G.A., Semenov, Y.N., Katrus, O.A., *et al*. (1970) Rolling of metal powders. **Powder Metallurgy and Metal Ceramics**, 9: (6): 515-516.

von Eggelkraut-Gottanka, S.G., Abu Abed, S., Muller, W., *et al*. (2002) Roller compaction and tabletting of St. John's wort plant dry extract using a gap width and force controlled roller compactor. I. Granulation and tabletting of eight different extract batches. **Pharmaceutical Development and Technology**, 7: (4): 433-445.

Vromans, H., Bolhuis, G.K. and Lerk, C.F. (1988) Magnesium stearate susceptibility of directly compressible materials as an indication of fragmentation properties. **Powder Technology**, 54: (1): 39-44.

Willshaw, D.J. and von der Marlsburg, C. (1976) How Patterned Neural Connections can be set up by Self-Organization. **Proceeding of the Royal Society of London. Series B, Biological Sciences**, 194: 431-445.

Wong, L. W. and Pilpel, N. (1990) The effect of particle shape on the mechanical properties of powders. **International Journal of Pharmaceutics**, 59: (2): 145-154.

Wu, C.Y., Fan, X.F., Motazedian, F., *et al*. (2010a) Quantitative investigation of powder flow during die filling using positron emission particle tracking. **Proceedings of the Institution of Mechanical Engineers Part E-Journal of Process Mechanical Engineering**, 224: (E3): 169-175.

Wu, C.Y., Hung, W.L., Miguélez-Morán, A.M., *et al*. (2010b) Roller compaction of moist pharmaceutical powders. **International Journal of Pharmaceutics**, 391: (1-2): 90-97.

Xie, X. and Puri, V.M. (2012) Powder deposition in three parallel-oriented dies of cylindrical and E shapes. **Advanced Powder Technology**, 23: (1): 1-7.

Yaginuma, Y., Ozeki, Y., Kakizawa, M., *et al*. (2007) Effects of powder flowability on die-fill properties in rotary compression. **Journal of Drug Delivery Science and Technology**, 17: (3): 205-210.

Yang, Z., Parker, D.J., Fryer, P.J., *et al*. (2006) Multiple-particle tracking -- an improvement for positron particle tracking. **Nuclear Instruments and Methods in Physics Research Section A: Accelerators, Spectrometers, Detectors and Associated Equipment**, 564: (1): 332-338.

Yusof, Y.A., Smith, A.C. and Briscoe, B.J. (2005) Roll compaction of maize powder. **Chemical Engineering Science**, 60: (14): 3919-3931.

Zinchuk, A.V., Mullarney, M.P. and Hancock, B.C. (2004) Simulation of roller compaction using a laboratory scale compaction simulator. **International Journal of Pharmaceutics**, 269: (2): 403-415.

Zuurman, K., Van der Voort Maarschalk, K. and Bolhuis, G.K. (1999) Effect of magnesium stearate on bonding and porosity expansion of tablets produced from materials with different consolidation properties. **International Journal of Pharmaceutics**, 179: (1): 107-115.